BIOMECHANICS OF CARTILAGE-BONE CROSSTALK IN LOAD-INDUCED OSTEOARTHRITIS

A Dissertation

Presented to the Faculty of the Graduate School

of Cornell University

In Partial Fulfillment of the Requirements for the Degree of

Doctor of Philosophy

by

Olufunmilayo Olatokunbo Adebayo

August 2017

BIOMECHANICS OF CARTILAGE-BONE CROSSTALK IN LOAD-INDUCED OSTEOARTHRITIS

Olufunmilayo Olatokunbo Adebayo, Ph. D.

Cornell University 2017

Osteoarthritis (OA), a degenerative disease affecting approximately 27 million Americans, is characterized by cartilage degradation, subchondral bone changes, and joint pain and discomfort. Although OA is hypothesized to occur due to joint instability that stimulates cell-mediated pathologies, the mechanical environment associated with the disease is unknown. In this thesis, a load-induced model of OA was used to elucidate the mechanical environment associated with OA development.

To examine the mechanical nature of joint instabilities in which OA develops in load-induced and other injury models, we conducted a quasi-static kinematic analysis on cadaver mice. Labeled adult male right joints were subjected to destabilization of the medial meniscus (DMM) or anterior cruciate ligament transection (ACLT). Left knees remained intact. Roentgen stereophotogrammetric analysis (RSA) was conducted on each joint during loading from 0 to 9N. Intact and DMM joints exhibited consistent and similar kinematics, with the tibia translating proximally and anteriorly, and knee flexion increasing with load. ACLT knees dislocated at 0N, suggesting that OA development in this model may be induced by severe joint instabilities.

Because bone is the primary load-bearing tissue in the joint, we examined the role of subchondral bone properties and remodeling in load-induced OA development. Adult male C57Bl/6 (low bone mass) and FVB (high bone mass) mice were treated with alendronate (ALN) to inhibit bone remodeling or vehicle treatment, and subjected to tibial loading for 1, 2, or 6

weeks. OA was attenuated in FVB mice compared to B6. ALN generally prevented the age-related cancellous bone mass reduction, but had no effect on load-induced bone changes. ALN treatment attenuated cartilage damage only in FVB mice.

Finally, discrete element analysis was used to characterize the stresses associated with intact joint kinematics from 0-9N. Areas of highest cartilage stresses strongly correlated with locations of most severe tissue damage. To determine the role tissue properties on cartilage stresses, parametric analyses were conducted on a FE contact model. Unlike cartilage properties, modulating bone properties in this model did not significantly affect stresses induced on the cartilage surface. In summary, this thesis characterized the mechanical environment, and changes thereof, associated with load-induced OA pathology.

BIOGRAPHICAL SKETCH

Olufunmilayo (Funmi) Olatokunbo Adebayo was born in Berlin, Germany, and moved to Nigeria at the age of 4. In 2000, her family immigrated to the United States. After graduating with honors from Medfield High School, Funmi attended Worcester Polytechnic Institute (WPI) where she graduated with high distinction in 2011. At WPI, she was a thrower and served as the captain for the women's varsity track and field team. She also served as the president of the Omicron Iota Chapter of Alpha Phi Omega, a community service co-ed fraternity, and a peer tutor for math and science courses. In addition, she participated in vascular tissue engineering research and received a Sigma Xi Grant-In-Aid of Research Award to fund her project. In 2015, she received her Master of Science degree in Biomedical Engineering at Cornell University. While at Cornell, she was a graduate coordinator for the Louis Stokes Alliance for Minority Participation (LSAMP) program through Diversity Programs in Engineering (DPE), a Graduate Resident Fellow (GRF) for Carl Becker house, and a fitness instructor for Cornell Fitness Centers. In August 2017, she received her Doctor of Philosophy degree in Biomedical Engineering. During her time at Cornell, she was awarded the Zellman Warhaft Commitment to Diversity Award, the Diversity Programs Graduate Student of the Year Award, and a Teagle Teaching-as-Research Fellowship. She was funded by an NSF Graduate Research Fellowship, a Sloan Graduate Fellowship, and the Robert and Helen Appel Fellowship for Biomedical Research, and received an AAOS/ORS Young Investigator Travel Award.

I dedicate this work to my mom, my biggest role model

ACKNOWLEDGMENTS

I would like to acknowledge the following funding sources, people and organizations that have provided support and allowed me to pursue this work. I would like acknowledge the National Science Foundation and the Sloan Foundation who provided funding for my graduate studies. I also acknowledge the NIH (R21-AR064034), the Robert & Helen Appel Fellowship, and the NSF ENGAGE program for their research support, and travel grants from Cornell Graduate School, Diversity Programs in Engineering and an AAOS/ORS Young Investigator Travel Award.

I would like to thank my committee members whose guidance and support have been invaluable throughout my graduate career. Thank you to the chair of my committee, Dr. Marjolein van der Meulen whose mentorship, passion for research and compassionate support has allowed me to not only grow as an independent scientific researcher, but also pursue my passions inside and outside the lab. She has continuously inspired me to think critically and creatively about research questions in the field of orthopedic biomechanics. I would also like to thank my committee members Dr. Timothy Wright and Dr. Alan Nixon. Thank you both for the insight, knowledge and the biomechanics and clinical perspectives you have provided throughout my graduate studies.

I thank my mentors and collaborators who have provided valuable advice and input during my research studies, including Dr. Steve Goldring, Dr. Mary Goldring, Dr. Frank Ko, Dr. Suzanne Maher, Dr. Hongsheng Wang, Dr. Cecilia Dragomir and Kirk Gunsallus. I am also grateful for the research mentors I met during my time here, who always had a listening ear whether for research advice or moral support, especially Dr. Natalie Kelly.

My work would certainly not be possible if not for the countless hours and effort by the

students and colleagues who assisted in experiments. I would like to thank Hyun Jong (Elliott) Kim, Allison Hsia, Philip Wan, Naa Shidaa Armar and Dan Loeffler for their assistance in this work. I also thank Lyudmila Lukashova, Glenn Swan, Mary Lou Norman, the Cornell CARE staff and the Cornell Statistical Consulting Unit and for all their help with this work. I could not have made it through graduate school without Judy Thoroughman, Marcia Sawyer and Belinda Floyd, and I thank them.

I also thank my lab mates, past and present, for all their feedback and support, including Dr. Frank Ko, Dr. Garry Brock, Dr. Katie Melville, Dr. Natalie Kelly, Julia Chen, Derek Holyoak, Mandy Rooney, Sophia Zeiman, Carolyn Chlebek and Tibra Wheeler.

I would like to acknowledge the several groups without which, I would not have gained valuable feedback on abstracts, presentations and research ideas. I would like to thank Dr. Mathias Bostrom and his lab group, Dr. Chris Hernandez, Dr. Eve Donnelly and the Bone Labs group, and the faculty and students in the Cornell Biomechanics group.

During my time at Cornell, I was fortunate to be involved in several organizations, and develop lasting relationships with mentors and people outside of research and I am incredibly grateful for their support. First, I would like to thank Jami Joyner and Sara Hernandez for welcoming me into the DPE family. I would not have made it through without their support and encouragement, and definitely would not have found friends who have now become family. I would also like to thank Dr. Traci Nathans-Kelly, Dr. Rick Evans and Cornell Center for Teaching Excellence for igniting my passion for teaching and teaching-as-research. Thank you to Amanda Carreiro, Dr. Ed Baptist, Donnette Baptist and all the staff and students at Becker House, who never made a day boring during my time as a Graduate Resident Fellow. Thank you to Emily Ellison and Cornell Fitness Centers, for allowing me to pursue my passion for teaching

fitness.

I would especially like to thank my family and friends. I would like to thank my mom, who has been my biggest support since day one. Thank you so much for all your sacrifice, encouragement, prayers and love. I honestly cannot thank you enough. Thank you to my siblings, Bukky, Ife, and Laniyi who have continuously been a source of joy throughout my time here. Thank you to my friends from home, Laura-Ashley, Amira and Skyler, and all the friends I've met here. I especially could not imagine my life in graduate school without Dr. Malika Grayson, Cassi Norgaisse and Ashley Torres. The outpouring of love and support from these three women has been incredible, and more than I can put into words. Thank you for everything.

I am grateful to have met everyone during my time here. You all have enriched my life and graduate experience and for that, I say thank you.

TABLE OF CONTENTS

LIST OF FIGURES

LIST OF TABLES

CHAPTER 1

INTRODUCTION

The following chapter is adapted, with permission, from a chapter that will be submitted as a part of a book entitled *Mechanomedicine*. The anticipated reference to this work will be:

Adebayo OO*, Holyoak DT*, van der Meulen MCH. (2017) Mechanobiological Mechanisms of Load-Induced Osteoarthritis. In *Mechanomedicine.* New York, NY: Springer.

**Authors contributed equally to this chapter*

1.1 Osteoarthritis

Osteoarthritis (OA) is a degenerative joint disease that affects approximately 27 million people in the United States, and is predicted to affect 25% of the adult population by 2030[1,2]. With highest prevalence in the knee[3], OA is characterized by cartilage degradation, subchondral bone changes, and osteophyte formation[4] (Figure 1.1). The disease clinically presents as radiographic narrowing of the joint space, debilitating pain and stiffness, and loss of joint function[5]. Based on clinical evidence, a wide range of risk factors have been identified, including obesity[6,7], aging[8], excessive mechanical loading during occupational activities[9,10], prior joint injuries[11,12], and genetic abnormalities[11]. While mechanical forces play a major role in OA initiation[11,13,14], the exact disease etiology is unknown, thus limiting effective preventative measures and clinical treatment options prior to surgical intervention.

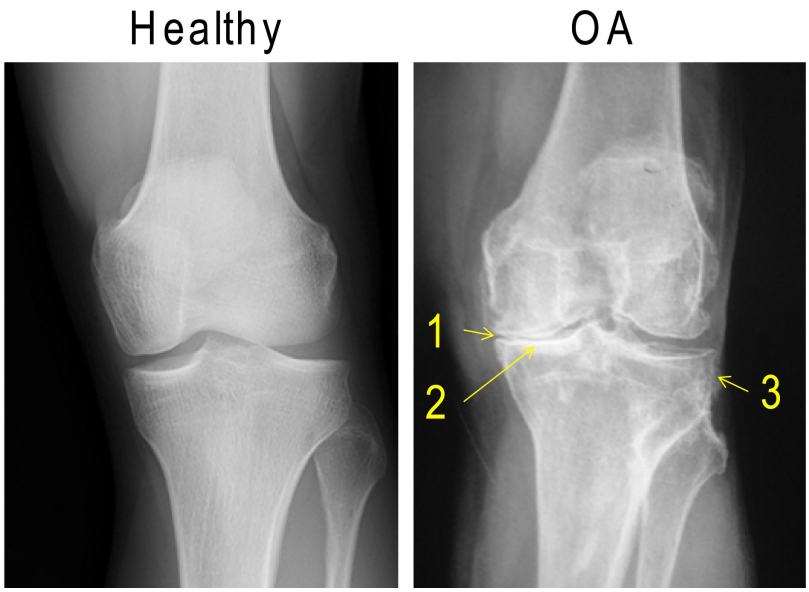

Figure 1.1 X-ray images of human knee joints depicting healthy and OA conditions. Compared to the healthy knee, the image of the OA knee shows (1) cartilage thinning based on the narrower joint space, (2) subchondral bone sclerosis on the medial tibial plateau and femoral condyle indicated by the brighter, thicker bone, and (3) osteophyte formation on the lateral side of the tibia (Image courtesy: Dr. Mathias P. Bostrom at the Hospital for Special Surgery, New York).

1.2 Pathophysiology of Osteoarthritis

1.2.1 The Healthy Joint

Several tissue types contribute biomechanically within the healthy diarthrodial joint including articular cartilage, subchondral bone, menisci, and ligaments. Articular cartilage is composed primarily of water and Type II collagen fibers interlinked with proteoglycans in which chondrocytes reside[15]. The tissue consists of 4 distinct zones, the superficial, middle, deep, and calcified cartilage zones, where zone-specific fiber alignments account for its compressive and shear properties[16]. Located at the end of long bones, cartilage allows for low-friction articulation and transfer of loads[16].

The subchondral bone consists of a cortical plate in direct contact with the calcified cartilage and the cancellous epiphyseal bone[17]. Composed of Type I collagen, hydroxyapatite and non-collagenous proteins, the subchondral bone is the major load-bearing tissue in the joint.

Bone cells, including osteoblasts that form bone, osteoclasts that resorb bone, and osteocytes that act as mechanosensors, drive bone remodeling and rapid adaption to changes in mechanical stimulus[18,19].

The menisci, fibrocartilageous tissues that lies on the perimeter of the cartilage on the medial and lateral plateaus of the knee, participates in the distribution of loads during articulation between cartilage surfaces[20–22]. Predominantly acting to redistribute joint forces, the menisci are important in reducing stresses induced in the cartilage during excessive physical activity. Unlike the menisci, ligaments act primarily in tension. Ligaments, such as the anterior cruciate ligament or the medial collateral ligament stabilize the joint and prevent excessive translations or rotations between the articulating bones.

Osteoarthritis has been shown to initiate via damage to any of the aforementioned tissues. Direct mechanical or chemical change to the cartilage[23–27], bone[28], menisci[29–31] and ligaments[29,32–34] have been implicated in the onset of OA in both clinical and preclinical models. Regardless of in which tissue the injury originates, disease progression affects all tissues in the joints, particularly the cartilage, but also the synovium[35] (Figure 1.2). Although the pathology of OA has been debated, many hypothesize that since most tissues in the joints are mechanically active, disease may be initiated, or at least progressed, by changes in mechanical forces in the joint[36].

1.2.2 Mechanical Forces and OA Initiation

Osteoarthritis is hypothesized to initiate from abnormal mechanical forces due to joint instability or injury. Increased or abnormal mechanical loading of the joint, as reflected with obesity[37,38], prior joint injury[39–41], or occupational activities such as military service, farming,

and intensive sports[9,10,42] have been associated with an increased risk for OA development. Conversely, weight loss and moderate exercise has been suggested to attenuate OA progression, clinically[7,43,44]. While the etiology of OA progression and its relation to mechanical forces is unknown, abnormal mechanical forces are hypothesized to initiate a cascade of cellular and molecular events leading to a feed-forward cycle of cartilage degeneration. Specifically, abnormal mechanical forces initiate fibrillations in the cartilage surface, leading to the production of enzymes such as matrix metalloproteinase (MMPs) and ADAMTS. These enzymes induce the recruitment of synovial fibroblasts and macrophages leading to stress-induced production of cytokines and a subsequent feed-forward production of degenerative enzymes[36] (Figure 1.3).

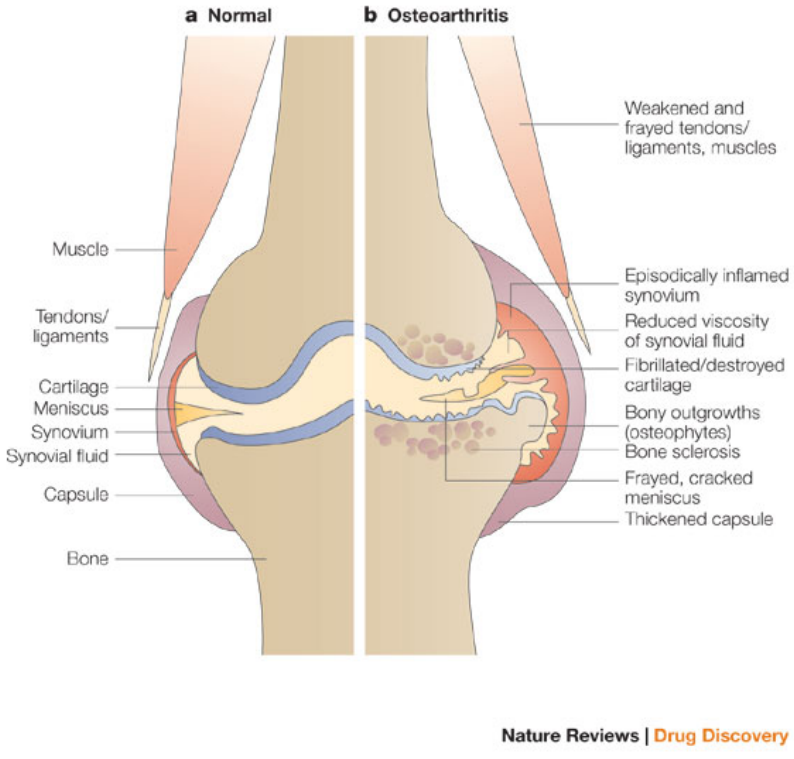

Figure 1.2 A) Healthy tissue is shown: normal cartilage without any fissures, or signs of synovial inflammation. B) Early focal degenerate lesion and 'fibrillated' cartilage, as well as remodeling of bone, is observed in osteoarthritis. This can lead to bony outgrowth and subchondral sclerosis.[45]

Mechanical forces also play an important role in bone remodeling in an osteoarthritic joint. Abnormal loading is hypothesized to generate microdamage in the subchondral bone, leading to increased osteoclast production and a decoupling of healthy bone remodeling. In addition, osteophyte formation occurs at the joint margins. Changes in the underlying bone leads to sclerosis, or a stiffening and thickening of the subchondral, and is hypothesized to increase the stresses engendered on the cartilage, thus exacerbating cartilage breakdown.

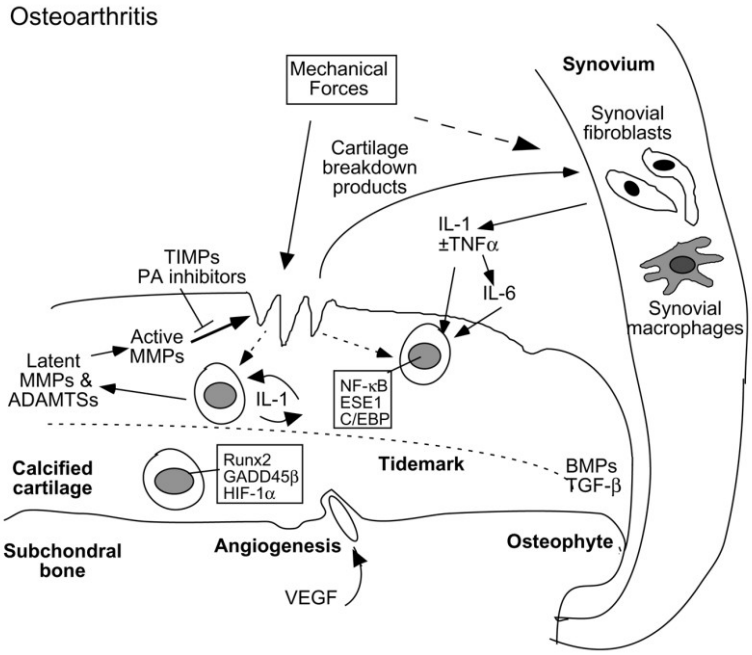

Figure 1.3 Role of mechanical forces in cartilage, bone, and synovium during OA initiation[36]

1.2.3 Cartilage-Bone Crosstalk in OA Development and Progression

While osteoarthritis affects several tissues in the joints, bone changes during disease progression have been of great interest as they present a potential target for treatment. As a major load-bearing and mechanically-adapting tissue in the joint, OA is hypothesized to initiate with changes in bone remodeling and accompanying property changes[17,46–51]. Clinical evidence

such as subchondral bone sclerosis and osteophyte formation in patients with late-stage OA, implicate bone remodeling as an integral feature of disease progression[1,45]. In addition, preclinical studies have demonstrated an initial loss of subchondral bone followed by an increase in bone mass during disease progression[34,52]. Thus, clinical studies have examined the effect of inhibiting bone remodeling on OA initiation and progression[53,54]. Specifically, patients in these studies have been treated with bisphosphonates to attenuate bone remodeling. Bisphosphonates, drugs used primarily as treatments for osteoporosis, embed into the bone matrix where they are uptaken by osteoclasts, and result in osteoclast apoptosis and inhibition of subsequent bone resorption[55,56]. Patients with osteoarthritis were treated with risedronate, a type of bisphosphonate. While the treatment reduced bone remodeling as indicated by lower levels of subchondral bone sclerosis, the treatment had varied results in attenuated cartilage degradation as reflected in radiographic joint space narrowing.

In addition to clinical studies, preclinical studies have also have investigated the role of bone remodeling on OA progression[57–60]. These studies have been conducted on many species subjected to traumatic joint injury such as ligament transections and chemical degradation to induce OA initiation. Animals have then been treated with bisphosphonates, including zoledronic acid and alendronate, or other drugs to inhibit bone remodeling. Results demonstrated that inhibiting bone remodeling via bisphosphonate treatment in post-traumatic OA attenuated both bone changes and cartilage degeneration. Although these studies show promising results for clinical treatment, distinguishing the effect of the treatment on bone from its effect on cartilage and post-traumatic inflammation is a limitation.

Furthermore, other studies have investigated the role of subchondral bone properties on OA initiation. Given the clinical evidence of subchondral bone stiffening, it has been

hypothesized that while bone changes contribute to disease progression, bone stiffness plays a significant role in disease initiation[46–48]. Stiffer subchondral bone could to lead high stresses being induced in the cartilage during articulation, thus leading to mechanical failure in the form of fibrillations on the cartilage surface. Experimental and computational studies have investigated the role of inherent subchondral bone stiffness on OA initiation. Studies by Burr et al.[19,61] placed mechanical rods in the subchondral bone of sheep and examined the propensity towards OA initiation. The results of these studies suggested that increased bone stiffness by itself may not be sufficient to initiate OA. Instead, bone changes may indeed be the catalyst for OA initiation and progression; however, confounding factors of inflammation due to surgery need to be addressed. Thus, the roles of bone remodeling and bone structural and tissue properties need to be investigated in a controlled mechanical environment without these confounding factors.

1.3 Preclinical Animal Models of OA

To better understand disease mechanism, preclinical animal models have been developed to recapitulate OA progression, and they can be classified under invasive and non-invasive categories (Figure. 1.4). Invasive models primarily use chemically-induced cartilage degeneration or surgical injuries, while non-invasive models involve repetitive joint loading, load-induced impact injury, or spontaneously occurring OA progression[62–64].

1.3.1 Invasive Preclinical OA Models

Under the invasive models, chemically-induced cartilage degeneration approaches involve intra-articular injection of collagenase[23–25], TGF-β[26], monosodium iodoacetate[65–69], or

papain[27,70,71]. These methods have provided critical knowledge about key molecular and cellular pathways during disease initiation. However, these models do not fully recapitulate human OA progression, limiting their use in understanding clinical scenarios[62,63].

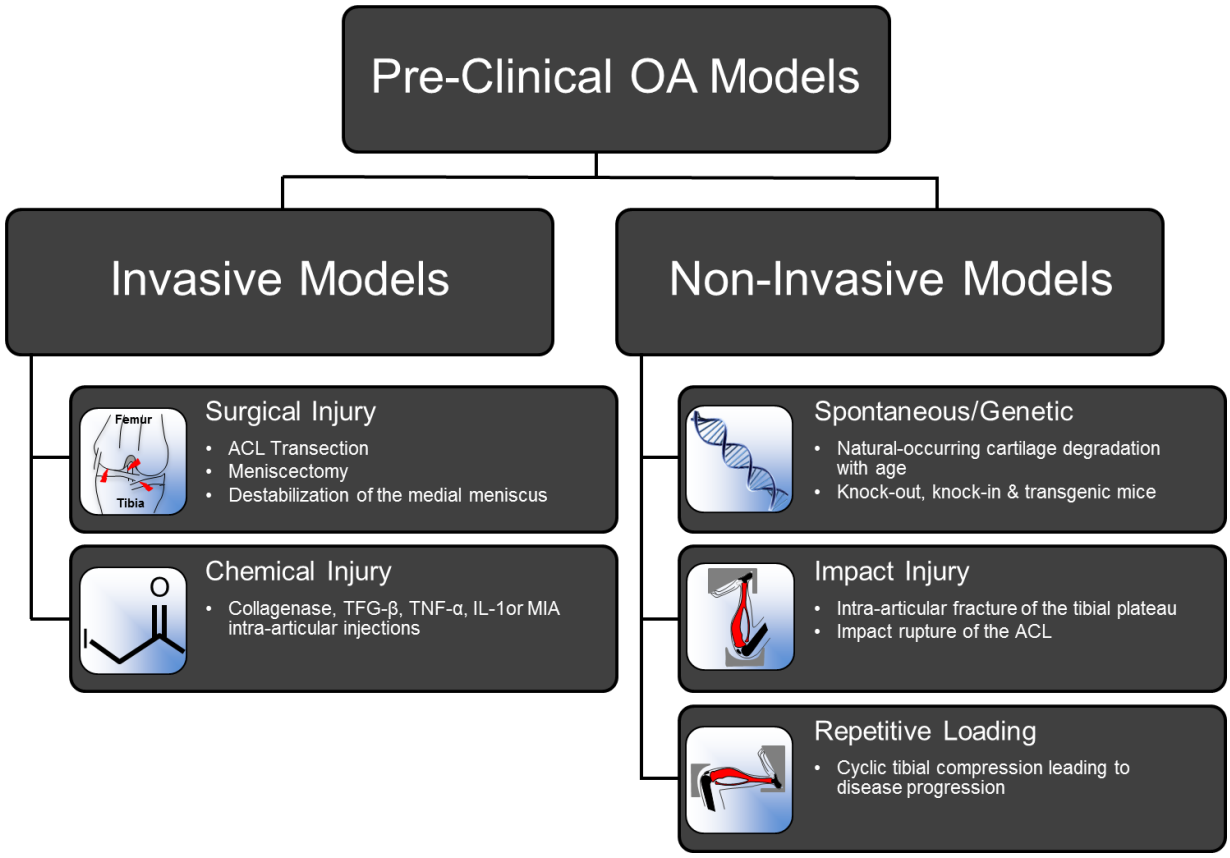

Figure 1.4 Overview of invasive and non-invasive pre-clinical OA models.

Post-surgical models of OA better mimic clinical injuries and subsequent OA progression. Models, such as the anterior cruciate ligament transection (ACLT)[29,32–34], meniscectomy[33,34], and the destabilization of the medial meniscus (DMM),[30,31] involve the use of surgical methods to disrupt or transect stabilizing ligaments, leading to alterations in joint mechanics. With surgical trauma, OA develops over time, enabling the investigation of the full time-course of post-traumatic OA progression. Surgical injury models have been applied to a

variety of animals[62], and have significantly contributed to our knowledge of post-traumatic OA progression. However, a major limitation of these models is the difficulty in differentiating the surgical inflammatory and healing response from the progression of OA, which confounds the understanding of disease etiology.

1.3.2 Non-Invasive Preclinical OA models

Non-invasive models of osteoarthritis have been developed to elucidate the mechanism of OA progression without the confounding effects of surgical intervention[72]. These models include genetic/spontaneous OA development[73,74], non-invasive impact injury models[28,75–77], and the recently-developed cyclic load-induced model[78,79]. Genetic/spontaneous models involve the use of animals, such as the guinea pig[74], certain strains of mice (e.g. C57Bl/6 and BALB/c)[80], or mice that have been genetically manipulated and develop the disease throughout their lifespan. Such studies allow for understanding OA pathology without external intervention and exploring genetic pathways for potential therapeutic targets. However, many forms of spontaneous OA can take months or even years to develop, limiting their use in laboratory settings.

Non-invasive impact injury models utilize high compressive loads to induce an intra-articular fracture of the tibial plateau[28] or a rupture of the ACL[76], both leading to OA initiation and progression. Each of these models provides key advantages in understanding OA pathology, particularly in recapitulating the clinical scenario without invasive measures. However, the exact mechanical environment of the joint within these models is unknown, and thus the relationship between mechanical forces and OA progression is difficult to understand.

The cyclic load-induced model offers a unique platform to specifically elucidate the relationship between mechanical forces and disease initiation. Primarily used in mice, the load-

induced model applies controlled, cyclic compressive loading to the tibia and results in predictable OA progression in the knee joint[78,79]. In the rest of this chapter, the focus is on this load-induced mouse model, highlighting its development, characterization, and aims to study the link between mechanical and cellular pathways, and thus the biomechanical mechanism of load-induced OA initiation and progression (Figure 1.5).

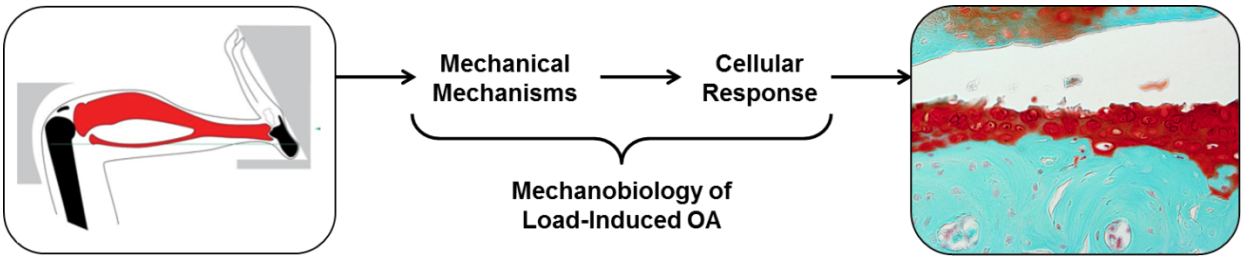

Figure 1.5 Overview of Load-Induced OA model.

1.4 Development of the Load-Induced OA Model

1.4.1 Cyclic Tibial Compression: From Bone Adaptation to OA Model

Although cyclic tibial compression is a novel technique for recapitulating OA in mice[78,79], this model has been used extensively to study bone response to load[81,82]. Adapted from the ulna-loading model[83], cyclic tibial compression applies repetitive axial loading at the ankle and the knee joint, and reliably induces anabolic responses in the tibial cancellous metaphysis and cortex[81,84,85]. Specifically, the cyclic tibial compression model involves the use of a loading system or a loading device, which consists of an electromagnetic actuator and a load cell, attached to either a foot or knee holder. The actuator applies cyclic loads according to voltage outputs from an amplifier, and the load cell provides force feedback control (Figure 1.6). The system delivers controlled compressive forces to the tibia without dislocation of the knee or ankle joints. Detailed instructions on using the system are available[86].

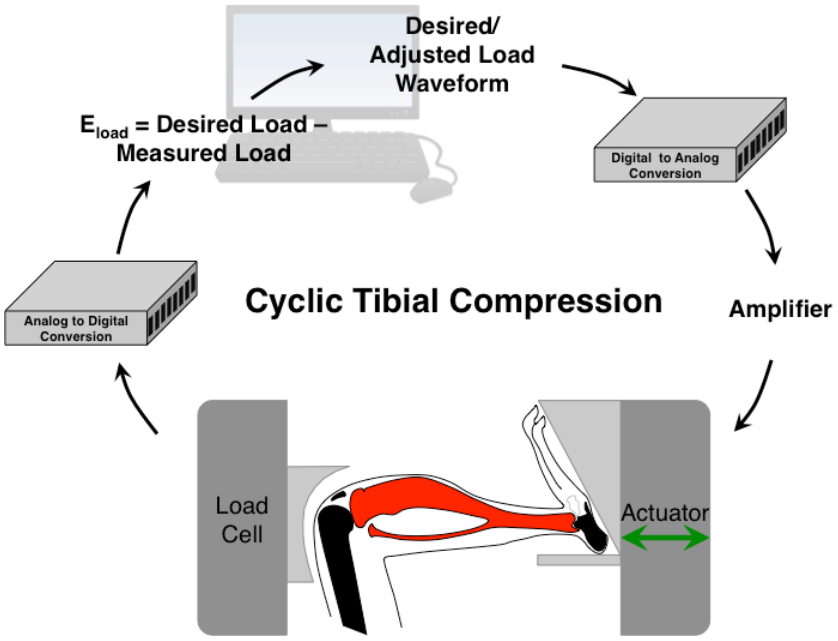

Figure 1.6 Schematic of a mouse limb mounted in the loading device. The foot holder is attached to an electromagnetic actuator that applies cyclic compression to the tibia according to voltage output from a LabVIEW-controlled amplifier. The knee holder is attached to a load cell that measures the applied compressive force and sends feedback to the LabVIEW program to adjust the output voltage accordingly.

Cyclic tibial compression enables simultaneous and specific examination of cancellous and cortical bone responses to mechanical forces in osteoporosis and fracture healing models. These advantages also render the model appropriate for examining cartilage changes with loading, allowing for non-invasive, controlled compression of the articular cartilage in the knee without ligament rupture. Additionally, the model permits analyses of temporal changes in both bone and cartilage, and potential investigation of the crosstalk between the two tissues (and others) in response to repetitive mechanical loading.

1.4.2 Metrics for Analyzing Bone and Cartilage Morphology

To examine the relationship between mechanical forces and OA progression, studies report bone morphology, cartilage degradation, and other joint tissue changes with cyclic

loading. Upon completion of loading, mice are euthanized, and the knee joints are harvested, fixed, scanned using microcomputed tomography (microCT), and processed for paraffin embedding and histology. MicroCT scans are taken of the knee joints to assess cortical and trabecular bone morphology. Specifically, the thickness and tissue mineral density of the subchondral bone plate (Figure 1.7A) can be determined. The underlying cancellous bone morphology in the epiphysis (distal to the subchondral bone plate and proximal to the growth plate, Figure 1.7B) and metaphysis (distal to the growth plate, Figure 1.7C) can also be analyzed for bone volume fraction, trabecular thickness and separation, and tissue mineral density.

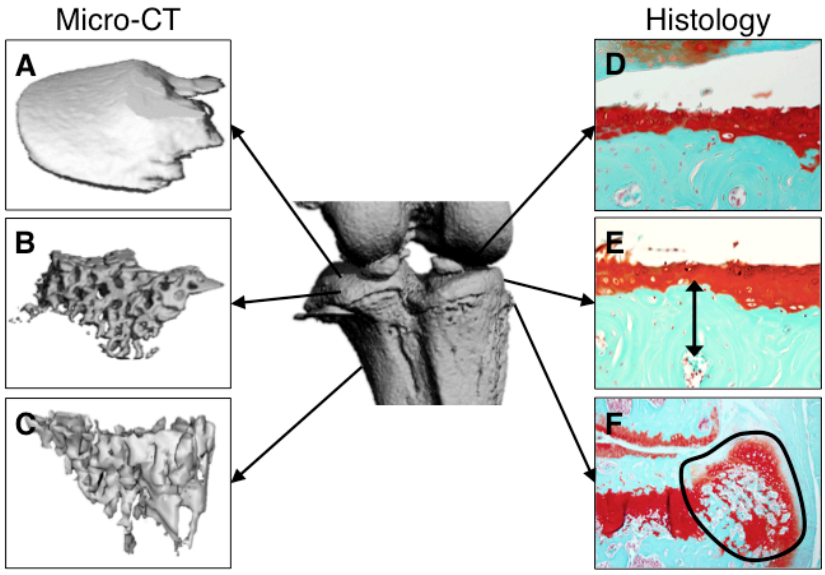

Figure 1.7 Analysis of bone and cartilage in the load-induced OA model. MicroCT analyses include A) subchondral bone thickness, B) epiphyseal cancellous morphology, and C) metaphyseal cancellous morphology. Histological analyses include D) cartilage morphology, E) local subchondral bone thickness, and F) osteophyte size and maturity.

The histological analysis seeks to measure the severity of load-induced articular cartilage damage using a histological scoring method. Thin sections are typically stained with Safranin O or Toluidine blue, and examined for structural and cellular changes in the cartilage (Figure 1.7D). In general, normal healthy cartilage is scored low (0) and the score increases to represent

damaged cartilage. For example, with the recommended OARSI modified murine scoring system[87], normal articular cartilage scores a 0, proteoglycan loss is 0.5, small fibrillations on the cartilage surface is 1, vertical clefts down to immediately below the superficial layer is 2, and vertical clefts/erosion to the calcified cartilage extending <25%, 25-50%, 50-75%, and 75-100% of the articular surface are 3, 4, 5, and 6, respectively. Scoring is generally performed across the entire joint, and scores are then averaged, summed, or the maximum is taken to assess OA severity. Additional histological outcomes include local subchondral bone thickness (Figure 1.7E), osteophyte severity (Figure 1.7F) and changes in the synovial lining, meniscus, and ligaments.

More recently, efforts have increased to understand the cellular pathways within the load-induced OA model. To this end, immunohistochemistry (IHC) has been implemented to further analyze bone, cartilage, synovial and meniscal changes on the protein level[77,88]. Briefly, tissue sections are incubated with a primary antibody for the protein of choice, and then with a secondary antibody and substrate for appropriate visualization. Positive staining in the joint tissues is then quantified and compared to contralateral control joints, thus expanding our understanding of load-OA progression from the cellular to the tissue scale.

1.4.3 Load-Induced OA Model

Using the aforementioned metrics, load-induced OA models were recently developed and described in two labs, with slightly different device setups and loading regimens[78,79]. The first of these setups involves the tibia horizontally positioned between knee and foot holders, allows for normal knee flexion, and loads the joint through the foot holder (Figure 1.8A)[79]. This setup will be referred to as the "normal flexion" model henceforth. The second of these setups involves

positioning the tibia vertically between custom-made cups attached to the actuator and load cell, with both the knee and ankle joints in deep flexion, and joint loading from the knee holder (Figure 1.8A)[78]. This setup will be referred to as the "deep flexion" model for the remainder of the chapter. These setups involve different loading regimens and experimental parameters, which allows a unique opportunity to compare the effects of age, mouse strain, load magnitude, and loading frequency and duration on the knee joint.

Development of the normal flexion setup used 10- and 26-week old male C57Bl/6 mice to investigate the effects of age and load-magnitude on OA progression[79]. The loading consisted of a triangular waveform with 9.0N peak loads, applied for 1200 cycles per day at a 4Hz frequency for durations of 1, 2, and 6 weeks for 5 days per week (Figure 1.8B). The initial study using the deep flexion setup[78] involved eight-week old male CBA mice, with waveforms consisting of 9.0N-peak loads applied 40 times, 3 days/week with durations of 1 day, 2 weeks, and 5 weeks (Figure 1.8B).

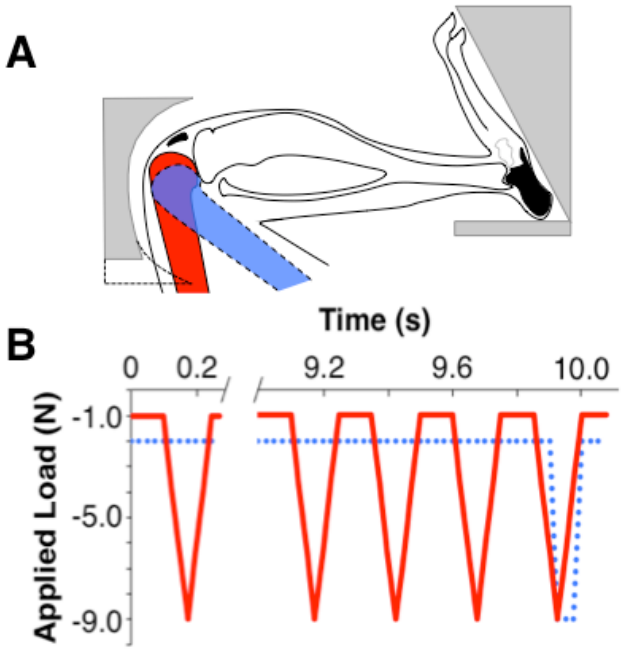

Figure 1.8 Schematic of a mouse limb in the A) deep flexion (blue) and normal flexion (red)

loading devices. The loading device applies compression, with waveforms of cyclic tibial loading for the B) deep flexion (blue) and normal flexion (red) set-ups, respectively. Figure adapted from Poulet et al. 2011and Ko et al. 2013[78,79].

After loading, bone and cartilage morphological examination demonstrated that non-invasive mechanical loading was indeed capable of recapitulating OA-like symptoms. Specifically, loading produced lesions and erosion of the cartilage that progressed with duration of loading, as indicated by histological analysis (Figure 1.9). Osteophyte formation also occurred with both loading regimens (Figure 1.9). Furthermore, 9.0N loading induced posterior subchondral bone plate thickening in the normal and deep flexion setups. Thus, cyclic tibial compression recapitulated key features of human OA in both studies.

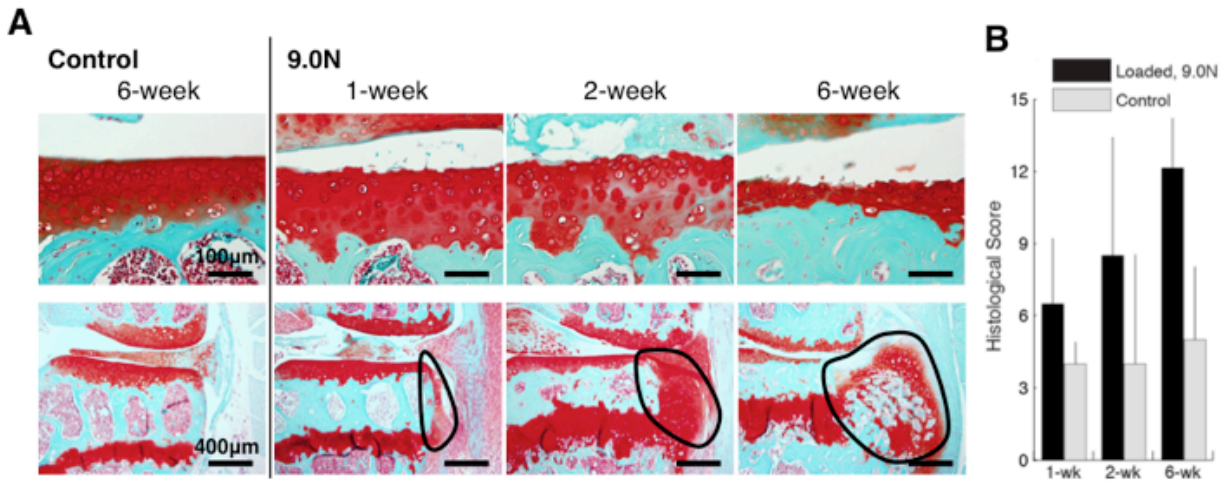

Figure 1.9 A) Cartilage matrix and osteophyte changes in the tibia after cyclic tibial compression loading. The left tibiae of adult mice were loaded for 1, 2, and 6 weeks. The nonloaded contralateral limb at 6 weeks load duration served as control. B) Quantification of Safranin O–fast green staining of the medial articular cartilage revealed that damage to the cartilage matrix occurred following mechanical loading and was exacerbated with longer durations. Figure from Ko et al. 2013[79].

Further analyses demonstrated decreased epiphyseal and unchanged metaphyseal trabecular bone volume fraction with loading in normal flexion[79]. In contrast, both epiphyseal

and metaphyseal trabecular bone changed in the deep flexion model[89]. After 5 weeks of repetitive loading using the deep flexion setup, epiphyseal trabecular bone volume fraction and thickness increased in lateral compartments of both loaded and non-loaded contralateral limbs. Loading in the deep flexion model also induced meniscal chondroplasia, synovial lining thickening, increased hypertrophy in the anterior cruciate ligament insertion points[78], and gait changes[89]. Interestingly, gait patterns changed only in the non-loaded contralateral limbs. Specifically, stance time, stride length, and paw area all increased in contralateral limbs after loading, while these characteristics of gait were unchanged in loaded limbs. Therefore, cyclic tibial compression not only mimics the hallmarks of OA, but also leads to other important changes in the tissues surrounding the joint. Ultimately, the models are excellent tools to study the biomechanical pathology of the bone and cartilage, and their interactions in OA development under controlled mechanical environment.

1.4.4 Elucidating Cellular Mechanisms of Load-Induced OA

While cyclic loading induces OA initiation and progression at the tissue level in both the normal and deep flexion setups, the complete mechanobiological response of the knee joint remains unknown if the cellular activity within the tissues is not understood. To this end, critical cellular responses to mechanical loading in these models have been characterized[77,78,88]. Specifically, the cellular and tissue response to a single bout of loading have been examined to elucidate the mechanism by which OA initiates in these models. The normal flexion model utilized the aforementioned loading protocol for a single bout of 1200 cycles of compressive loading; the single bout did not induce spontaneous cartilage lesions (Figure 1.10 top panel), but rather initiated cell-mediated processes that led to OA without additional loading[88]. Immediately

after loading, cartilage appeared normal in both control and loaded limbs. However, after 1 and 2 weeks of normal activity, cartilage damage, cartilage thinning, and pre-osteophyte formation were present at the medial aspect of the tibia plateau. In addition, loading induced thinning of the subchondral bone plate in loaded limbs 1 and 2 weeks after the loading bout. Immunohistochemistry analyses indicated that chondrocyte apoptosis was the same between control and loaded limbs, suggesting loading had no acute effects on chondrocyte viability. Furthermore, no sign of synovial hyperplasia was evident after the single loading bout. However, osteoclast activity in the underlying subchondral bone increased after loading, which explained the decreased subchondral bone plate thickness. Ultimately, because hyperplasia and chondrocyte apoptosis did not change with loading, the tissue response to loading was most likely mediated by resident cells in the bone, cartilage, and other surrounding tissues.

In contrast to the normal flexion setup, a single bout of loading in the deep flexion setup initiated spontaneous lesions and clefts in the articular cartilage surface (Figure 1.10 bottom panel)[78]. If left alone, the lesion remained, but did not progress further; however, if loading continued after the single bout, the cartilage lesions grew, subsequently leading to more severe OA.

Another deep flexion model investigated OA severity in 8-week old C57Bl/6 mice after single loading bouts of 60 cycles with magnitudes of 3N, 6N, and 9N at 5, 9, or 14 days post-loading[77]. Interestingly, the 9N load level resulted in rupture of the ACL, dissimilar to previous studies with the same load magnitude; therefore, this chapter will focus on results from 3N and 6N loads. The traumatic event at 9N emphasizes how even a slight variation in body position (i.e., joint angle) or loading regimen can play a significant role in the mechanical response of the joint tissues. Nonetheless, articular cartilage lesions occurred primarily on the lateral condyle of

the femur. Lesion size increased with loads of greater magnitude, but did not increase with time, maintaining their size between 5 and 14 days after the loading bout.

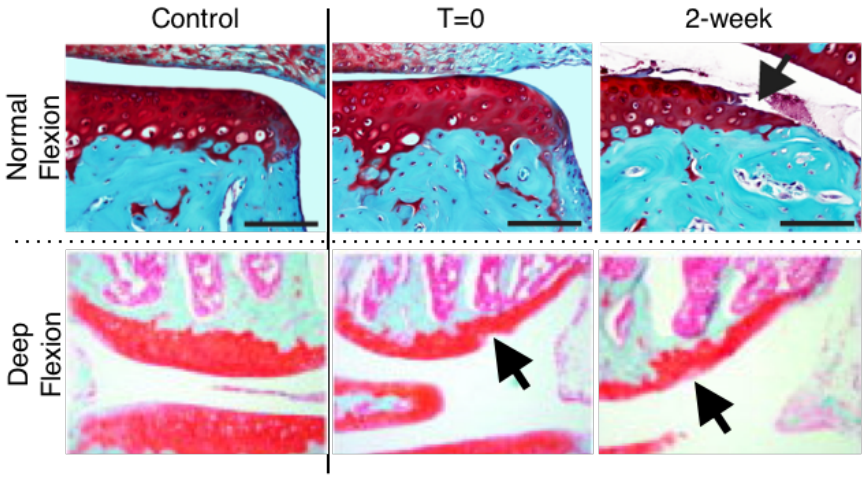

Figure 1.10 A single loading bout with the deep flexion set-up initiated spontaneous cartilage lesions immediately after loading. In contrast, no cartilage damage was observed immediately following a single loading session using the normal flexion set-up, but was seen 2 weeks post-loading. Figure adapted from Ko et al. 2016 and Poulet et al. 2011[78,88].

In addition to examining the morphological changes that occurred in the cartilage in response to loading, a few key cellular factors were related to cartilage degradation in the study performed by Wu and colleagues[77]. Chondrocyte apoptosis increased with loading and was localized to the surface of the location with the cartilage lesion. In addition, loaded limbs at 6N had higher synovitis scores compared to control limbs. On the protein level, the amount of type II collagen did not change in response to loading and was uniformly distributed throughout the entire cartilage region. Aggrecan fragments were internalized by apoptotic chondrocytes due to an activation of ADAMTS-5 from the surface of dying cells. Overall, loading had little to no effect on type II collagen, but significantly changed the amount and distribution of aggrecan (Figure 1.11). In addition, the distribution of COMP extended to the middle zone of the cartilage

in loaded limbs, but was only present in the superficial zone in control limbs. Chondrocytes in deeper zones and synovial cells produced COMP in response to mechanical stress, suggesting that COMP plays an important role in load-induced cartilage degradation.

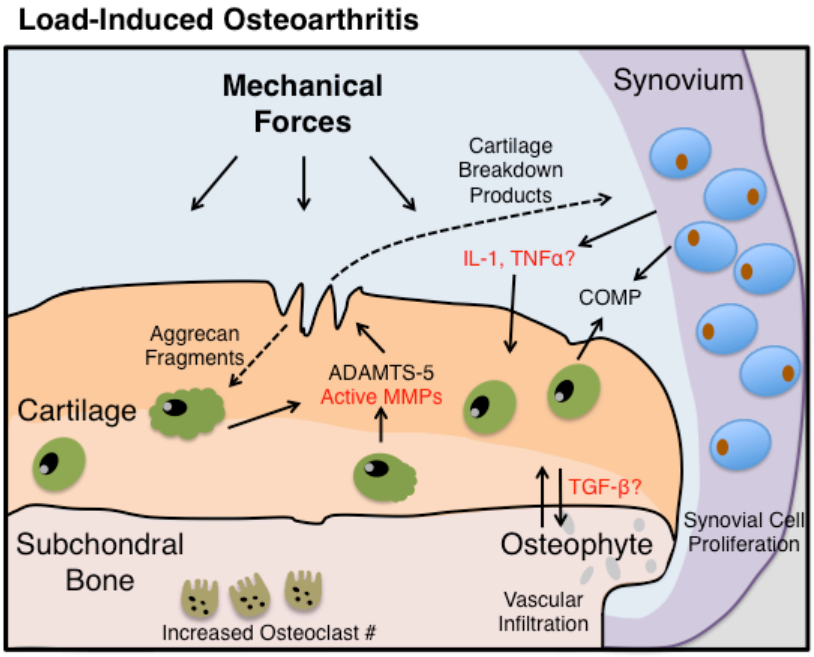

Figure 1.11. Schematic of cellular and molecular changes in load-induced OA progression. Tibial cyclic compression induces a cascade of destructive events including active aggrecanases (ADAMTS-4 & 5) and collagenases that break down key components of the cartilage matrix. Changes in the subchondral bone and synovium have also been shown to play a role in load-induced OA. Indicated in red are key proteins involved in OA initiation and progression, but this finding has not been confirmed in the load-induced OA model. Figure adapted from Goldring et al 2009.[36]

The tissue-level and cellular responses from the aforementioned studies provide us with large amounts of information on how the knee joint responds to damaging mechanical loads. Load-induced OA models allow us to directly relate areas of acute cartilage damage to specific cellular signaling in response to loading (Figure 1.11). Continuing to study this relationship, particularly from a mechanical perspective, is integral to understanding the mechanobiological mechanisms of OA.

1.5 Thesis Aims

OA pathology has been studied in several invasive and non-invasive models including surgical injury, chemical injection, spontaneous OA, impact injury, and load-induced OA models. While each model has key advantages, the load-induced OA model provides a controlled means of exploring the relationship between mechanical forces and OA progression, without confounding invasive surgeries. Using cyclic tibial compression, the load-induced OA model provides controlled mechanical forces to the joint that lead to cellular responses and subsequent OA progression. Since the model is relatively new, few studies have characterized the full mechanobiology of load-induced OA progression, and thus knowledge is limited. Understanding the exact biomechanical pathogenesis of the mouse tibial-loading OA model will strengthen the interpretation of pre-clinical results in the context of clinical human OA, enabling improved translation to the human case. Using both experimental and computational techniques, this thesis aims to better understand the relationship between joint mechanics and the progression of load-induced osteoarthritis with the normal-flexion set-up.

1.5.1 Aim 1: Kinematics of Meniscal- and ACL-Transected Mouse Knees during Controlled Tibial Compressive Loading Captured Using Roentgen Stereophotogrammetry

Although the tibial loading model recapitulates features of OA in the mouse knee, the joint kinematics related to this loading protocol is unknown. Understanding the relationship between joint kinematics and OA pathology is a key step to elucidating the role of joint instability and the biomechanical interaction of bone and cartilage in disease progression. To this end, we examined the kinematics of injured and intact joints subjected to controlled tibial compressive loading[90]. We hypothesized that injuries such as the destabilization of the medial

meniscus (DMM)[30] and anterior cruciate ligament transection (ACLT)[34] models result in uncontrolled joint instability and greater variability compared to intact joints, in which the timing of tissue changes in relation to joint mechanics may be more precisely measured. 32-week-old C57Bl/6 cadaver male mice right joints were subjected to DMM or ACLT. Left knee joints remained intact. Using a modified single-plane roentgen stereophotogrammetric analysis (RSA), the bone kinematics of each limb was examined during compressive loading from 0-9N. The translation and rotation of the tibia and the relative translation and rotation of the femur to the tibia about the proximal-distal (X), medial-lateral (Y), and anterior-posterior (Z) axes were analyzed using the Eulerian method for rigid body kinematics.

1.5.2 Aim 2: Role of Subchondral Bone Properties and Changes in Development of Load-Induced Osteoarthritis in Mice

As subchondral bone is a significant load-bearing tissue in the joint, understanding its biomechanical role in load-induced OA initiation and progression is critical to elucidating the etiology of OA in this model. We aimed to understand the role of subchondral bone properties and remodeling in OA initiation using the tibial loading mouse model. We hypothesized that OA initiation would be attenuated in mice with low subchondral bone mass compared to mice with high bone mass, and in mice treated with alendronate (ALN), a bisphosphonate that inhibits bone remodeling. Adult male C57Bl/6 (B6, low bone mass) and FVB (high bone mass) mice were treated with ALN or vehicle (VEH) treatment with left limbs loaded for 1, 2, or 6 weeks. Subchondral bone plate and epiphyseal cancellous bone morphology were examined using microCT, and cartilage damage and joint changes were quantified using summed histological scores, cartilage thickness measurements, and osteophyte measurements.

1.5.3 Aim 3: Computational Models for the Analysis of Load-Induced Osteoarthritis

Although the cellular and molecular mechanisms of load-induced OA have been investigated, only two studies have examined the mechanical environment that lead to disease progression in this model[78,90]. Quantifying the stresses in the cartilage and bone and how changes to these tissues affect mechanical stresses in the joint is important to understanding the mechanobiology of the tibial loading model. Specifically, we aimed to characterize the stresses and strains in the joint and hypothesized that locations of highest mechanical stresses would correlate with areas of highest cartilage damage. To this end, two computational models were developed to 1) quantify the magnitude and location of contact stresses in the cartilage under tibial compression and 2) to examine the effects of changing material properties of different tissues in the joint on cartilage surface stresses. Using a discrete element model (DEA)[91] in conjunction with joint kinematics data, contact stresses in tibial cartilage during compressive loading were quantified from 0-9N at every 1N increment. Further, a simplified finite element (FEA) contact model was developed to simulate the knee joint, and a parametric analysis was conducted to investigate the effects of altering material properties on joint stresses.

1.5.4 Aim 4: Empowering Early Mastery of Spatial Visualization Skills in Underrepresented Minority Engineering Students

In addition to the three aims listed above, a fourth aim is included in this thesis. Although not directly related to the field of biomechanics research, this aim is important in the field of engineering education. Spatial visualization (SV), defined as the "ability to mentally manipulate, rotate, twist, invert pictorially presented stimuli"[92], has been suggested to predict student success in engineering[93]. While correlations exist between SV skills and engineering retention, studies

have suggested evidence of different SV skills in female and underrepresented minority students, which may account for the lower retention and success rates of these groups[94–96]. We aimed to explore the correlation between SV skills and success in engineering, with the intention of examining the exact mechanism of this correlation and its discrepancies among female and minority student groups. The Cornell University Engineering Success (CUES) program used the NSF ENGAGE curriculum to introduce SV basic skills to a select group of first year students, through a project-based course. Student teams worked with biomedical faculty researchers and were tasked to produce professional-level visualizations of real-world research projects. We employed action research/grounded theory methodologies (observations, instructor journals, expert responses, and e-portfolios) to track their skill development of spatial concepts, representations and critical stances, and the application of their skills to their projects.

1.6 REFERENCES

1. Lawrence RC, Felson DT, Helmick CG, Arnold LM, Choi H, Deyo RA, Gabriel S, Hirsch R, Hochberg MC, Hunder GG, Jordan JM, Katz JN, Kremers HM, Wolfe F, National Arthritis Data Workgroup. Estimates of the prevalence of arthritis and other rheumatic conditions in the United States. Part II. *Arthritis Rheum*. 2008;58(1):26-35. doi:10.1002/art.23176.
2. Hootman JM, Helmick CG. Projections of US prevalence of arthritis and associated activity limitations. *Arthritis Rheum*. 2006;54(1):226-229. doi:10.1002/art.21562.
3. Felson DT. Epidemiology of hip and knee osteoarthritis. *Epidemiol Rev*. 1988;10:1-28.
4. Wieland HA, Michaelis M, Kirschbaum BJ, Rudolphi KA. Osteoarthritis - an untreatable disease? *Nat Rev Drug Discov*. 2005;4(4):331-344. doi:10.1038/nrd1693.
5. Hunter DJ, Felson DT. Osteoarthritis. *BMJ*. 2006;332(7542):639-642. doi:10.1136/bmj.332.7542.639.
6. Felson DT, Anderson JJ, Naimark A, Walker AM, Meenan RF. Obesity and Knee Osteoarthritis. *Ann Intern Med*. 1988;109(1):18. doi:10.7326/0003-4819-109-1-18.
7. Messier SP, Loeser RF, Miller GD, Morgan TM, Rejeski WJ, Sevick MA, Ettinger WH, Pahor M, Williamson JD. Exercise and dietary weight loss in overweight and obese older adults with knee osteoarthritis: the Arthritis, Diet, and Activity Promotion Trial. *Arthritis Rheum*. 2004;50(5):1501-1510. doi:10.1002/art.20256.
8. Buckwalter JA, Saltzman C, Brown T. The impact of osteoarthritis: implications for research. *Clin Orthop Relat Res*. 2004;(427 Suppl):S6-15.
9. Kaila-Kangas L, Arokoski J, Impivaara O, Viikari-Juntura E, Leino-Arjas P, Luukkonen R, Heliövaara M. Associations of hip osteoarthritis with history of recurrent exposure to manual handling of loads over 20 kg and work participation: a population-based study of men and women. *Occup Environ Med*. 2011;68(10):734-738. doi:10.1136/oem.2010.061390.
10. Cameron KL, Hsiao MS, Owens BD, Burks R, Svoboda SJ. Incidence of physician-diagnosed osteoarthritis among active duty United States military service members. *Arthritis Rheum*. 2011;63(10):2974-2982. doi:10.1002/art.30498.
11. Felson DT. Osteoarthritis: New Insights. Part 1: The Disease and Its Risk Factors. *Ann Intern Med*. 2000;133(8):635. doi:10.7326/0003-4819-133-8-200010170-00016.
12. Lohmander LS, Englund PM, Dahl LL, Roos EM. The long-term consequence of anterior cruciate ligament and meniscus injuries: osteoarthritis. *Am J Sports Med*. 2007;35(10):1756-1769. doi:10.1177/0363546507307396.
13. Arokoski J, Kiviranta I, Jurvelin J, Tammi M, Helminen HJ. Long-distance running causes site-dependent decrease of cartilage glycosaminoglycan content in the knee joints of beagle dogs. *Arthritis Rheum*. 1993;36(10):1451-1459. doi:10.1002/art.1780361018.
14. Lapveteläinen T, Nevalainen T, Parkkinen JJ, Arokoski J, Kiraly K, Hyttinen M, Halonen P, Helminen HJ. Lifelong moderate running training increases the incidence and severity

of osteoarthritis in the knee joint of C57BL mice. *Anat Rec*. 1995;242(2):159-165. doi:10.1002/ar.1092420204.

15. Dudhia J. Aggrecan, aging and assembly in articular cartilage. *Cell Mol Life Sci*. 2005;62(19-20):2241-2256. doi:10.1007/s00018-005-5217-x.

16. Sophia Fox AJ, Bedi A, Rodeo SA. The basic science of articular cartilage: structure, composition, and function. *Sports Health*. 2009;1(6):461-468. doi:10.1177/1941738109350438.

17. Li G, Yin J, Gao J, Cheng TS, Pavlos NJ, Zhang C, Zheng MH, Grynpas M, Alpert B, Katz I, Lieberman I, Pritzker K, Suri S, Walsh D, Madry H, Dijk C van, Mueller-Gerbl M, Burr D, et al. Subchondral bone in osteoarthritis: insight into risk factors and microstructural changes. *Arthritis Res Ther*. 2013;15(6):223. doi:10.1186/ar4405.

18. Goldring MB, Goldring SR. Articular cartilage and subchondral bone in the pathogenesis of osteoarthritis. *Ann N Y Acad Sci*. 2010;1192(1):230-237. doi:10.1111/j.1749-6632.2009.05240.x.

19. Burr DB. The importance of subchondral bone in osteoarthrosis. *Curr Opin Rheumatol*. 1998;10(3):256-262.

20. Makris EA, Hadidi P, Athanasiou KA. The knee meniscus: Structure–function, pathophysiology, current repair techniques, and prospects for regeneration. *Biomaterials*. 2011;32(30):7411-7431. doi:10.1016/j.biomaterials.2011.06.037.

21. Cameron H, Macnab I. The Structure of the Meniscus of the Human Knee Joint. : Clinical Orthopaedics and Related Research. *Clin Orthop Relat Res*. 1972;89:215-219.

22. Proctor CS, Schmidt MB, Whipple RR, Kelly MA, Mow VC. Material Properties of the Normal Medial Bovine Meniscus. *J Orthop Res*. 1989;7:771-782.

23. van der Kraan PM, Vitters EL, van de Putte LB, van den Berg WB. Development of osteoarthritic lesions in mice by metabolic and mechanical alterations in the knee joints. *Am J Pathol*. 1989;135(6):1001-1014.

24. Kikuchi T, Sakuta T, Yamaguchi T. Intra-articular injection of collagenase induces experimental osteoarthritis in mature rabbits. *Osteoarthr Cartil*. 1998;6(3):177-186. doi:10.1053/joca.1998.0110.

25. van der Kraan PM, Vitters EL, van Beuningen HM, van de Putte LB, van den Berg WB. Degenerative knee joint lesions in mice after a single intra-articular collagenase injection. A new model of osteoarthritis. *J Exp Pathol (Oxford)*. 1990;71(1):19-31.

26. van Beuningen H., Glansbeek H., van der Kraan P., van den Berg W. Osteoarthritis-like changes in the murine knee joint resulting from intra-articular transforming growth factor-β injections. *Osteoarthr Cartil*. 2000;8(1):25-33. doi:10.1053/joca.1999.0267.

27. Inoue S, Glimcher MJ. The reaction of cartilage and osteophyte formation after the intraarticular injection of papain. *Nihon Seikeigeka Gakkai Zasshi*. 1982;56(5):415-430.

28. Furman BD, Strand J, Hembree WC, Ward BD, Guilak F, Olson SA. Joint degeneration following closed intraarticular fracture in the mouse knee: a model of posttraumatic arthritis. *J Orthop Res*. 2007;25(5):578-592. doi:10.1002/jor.20331.

29. McErlain DD, Appleton CTG, Litchfield RB, Pitelka V, Henry JL, Bernier SM, Beier F, Holdsworth DW. Study of subchondral bone adaptations in a rodent surgical model of OA using in vivo micro-computed tomography. *Osteoarthr Cartil*. 2008;16(4):458-469. doi:10.1016/j.joca.2007.08.006.

30. Glasson SS, Blanchet TJ, Morris EA. The surgical destabilization of the medial meniscus (DMM) model of osteoarthritis in the 129/SvEv mouse. *Osteoarthritis Cartilage*. 2007;15(9):1061-1069. doi:10.1016/j.joca.2007.03.006.

31. Culley KL, Dragomir CL, Chang J, Wondimu EB, Coico J, Plumb DA, Otero M, Goldring MB. Mouse models of osteoarthritis: surgical model of posttraumatic osteoarthritis induced by destabilization of the medial meniscus. *Methods Mol Biol*. 2015;1226:143-173. doi:10.1007/978-1-4939-1619-1_12.

32. Pond MJ, Nuki G. Experimentally-induced osteoarthritis in the dog. *Ann Rheum Dis*. 1973;32(4):387-388.

33. Kamekura S, Hoshi K, Shimoaka T, Chung U, Chikuda H, Yamada T, Uchida M, Ogata N, Seichi A, Nakamura K, Kawaguchi H. Osteoarthritis development in novel experimental mouse models induced by knee joint instability. *Osteoarthritis Cartilage*. 2005;13(7):632-641. doi:10.1016/j.joca.2005.03.004.

34. Hayami T, Pickarski M, Zhuo Y, Wesolowski GA, Rodan GA, Duong LT. Characterization of articular cartilage and subchondral bone changes in the rat anterior cruciate ligament transection and meniscectomized models of osteoarthritis. *Bone*. 2006;38(2):234-243. doi:10.1016/j.bone.2005.08.007.

35. Scanzello CR, Goldring SR. The role of synovitis in osteoarthritis pathogenesis. *Bone*. 2012;51(2):249-257. doi:10.1016/j.bone.2012.02.012.

36. Goldring MB, Marcu KB. Cartilage homeostasis in health and rheumatic diseases. *Arthritis Res Ther*. 2009;11(3):224. doi:10.1186/ar2592.

37. Felson DT, Zhang Y, Hannan MT, Naimark A, Weissman B, Aliabadi P, Levy D. Risk Factors for Incident Radiographic Knee Osteoarthritis in the Elderly The Framingham Study. 1997;40(4):728-733.

38. Schouten JS, van den Ouweland FA, Valkenburg HA. A 12 year follow up study in the general population on prognostic factors of cartilage loss in osteoarthritis of the knee. *Ann Rheum Dis*. 1992;51(8):932-937.

39. Buckwalter JA, Lane NE. Athletics and osteoarthritis. *JA Buckwalter, NE Lane 1998 Athl osteoarthritis Occup Heal Ind Med 38 98*. 1998;2(38):98.

40. Lohmander LS, Felson D. Can we identify a “high risk” patient profile to determine who will experience rapid progression of osteoarthritis?11Supported by the Swedish Research Council (Medicine) and NIH AR47785. *Osteoarthr Cartil*. 2004;12:49-52. doi:10.1016/j.joca.2003.09.004.

41. Lohmander LS, Ostenberg A, Englund M, Roos H. High prevalence of knee osteoarthritis, pain, and functional limitations in female soccer players twelve years after anterior cruciate ligament injury. *Arthritis Rheum*. 2004;50(10):3145-3152. doi:10.1002/art.20589.

42. Cogon D, Kellingray S, Inskip H, Croft P, Campbell L, Cooper C. Osteoarthritis of the

Hip and Occupational Lifting. *Am J Epidemiol*. 1998;147(6):523-528. doi:10.1093/oxfordjournals.aje.a009483.

43. Felson DT. Weight Loss Reduces the Risk for Symptomatic Knee Osteoarthritis in Women. *Ann Intern Med*. 1992;116(7):535. doi:10.7326/0003-4819-116-7-535.

44. Hochberg MC, Altman RD, April KT, Benkhalti M, Guyatt G, McGowan J, Towheed T, Welch V, Wells G, Tugwell P. American College of Rheumatology 2012 recommendations for the use of nonpharmacologic and pharmacologic therapies in osteoarthritis of the hand, hip, and knee. *Arthritis Care Res (Hoboken)*. 2012;64(4):465-474. doi:10.1002/acr.21596.

45. Wieland HA, Michaelis M, Kirschbaum BJ, Rudolphi KA. Osteoarthritis - an untreatable disease? *Nat Rev Drug Discov*. 2005;4(4):331-344. doi:10.1038/nrd1693.

46. Radin E, Paul I, Rose R. Role of mechanical factors in pathogenesis of primary osteoarthritis. *Lancet*. 1972;299(7749):519-522. doi:10.1016/S0140-6736(72)90179-1.

47. Radin EL, Rose RM. Role of subchondral bone in the initiation and progression of cartilage damage. *Clin Orthop Relat Res*. 1986;(213):34-40.

48. Radin EL, Martin RB, Burr DB, Caterson B, Boyd RD, Goodwin C. Effects of mechanical loading on the tissues of the rabbit knee. *J Orthop Res*. 1984;2(3):221-234. doi:10.1002/jor.1100020303.

49. Burr DB, Schaffler MB. The Involvement of Subchondral Mineralized Tissues in Osteoarthrosis : Quantitative Microscopic Evidence. *Microsc Res Tech*. 1997;37:343-357. doi:10.1002/(SICI)1097-0029(19970515)37:4<343::AID-JEMT9>3.0.CO;2-L.

50. Burr DB. The importance of subchondral bone in the progression of osteoarthritis. *J Rheumatol Suppl*. 2004;70:77-80.

51. Kawcak CE, McIlwraith CW, Norrdin RW, Park RD, James SP. The role of subchondral bone in joint disease: a review. *Equine Vet J*. 2010;33(2):120-126. doi:10.1111/j.2042-3306.2001.tb00589.x.

52. Botter SM, Van Osch GJVM, Clockaerts S, Waarsing JH, Weinans H, Van Leeuwen JPTM. Osteoarthritis induction leads to early and temporal subchondral plate porosity in the tibial plateau of mice: An in vivo microfocal computed tomography study. *Arthritis Rheum*. 2011;63(9):2690-2699. doi:10.1002/art.30307.

53. Spector TD, Conaghan PG, Buckland-Wright JC, Garnero P, Cline GA, Beary JF, Valent DJ, Meyer JM, Dixon T, Shaw M, Ebrahim S, Dieppe P, Millar W, Melzer D, Guralnik J, Brock D, Quam J, Michet C, et al. Effect of risedronate on joint structure and symptoms of knee osteoarthritis: results of the BRISK randomized, controlled trial [ISRCTN01928173]. *Arthritis Res Ther*. 2005;7(3):R625. doi:10.1186/ar1716.

54. Bingham CO, Buckland-Wright JC, Garnero P, Cohen SB, Dougados M, Adami S, Clauw DJ, Spector TD, Pelletier JP, Raynauld JP, Strand V, Simon LS, Meyer JM, Cline GA, Beary JF. Risedronate decreases biochemical markers of cartilage degradation but does not decrease symptoms or slow radiographic progression in patients with medial compartment osteoarthritis of the knee: Results of the two-year multinational knee osteoarthritis st. *Arthritis Rheum*. 2006;54(11):3494-3507. doi:10.1002/art.22160.

55. Fleisch H. Bisphosphonates: Mechanisms of Action. *Endocr Rev*. 1998;19(1):80-100. doi:10.1210/edrv.19.1.0325.

56. Russell RGG, Watts NB, Ebetino FH, Rogers MJ. Mechanisms of action of bisphosphonates: similarities and differences and their potential influence on clinical efficacy. *Osteoporos Int*. 2008;19(6):733-759. doi:10.1007/s00198-007-0540-8.

57. Muehleman C, Green J, Williams JM, Kuettner KE, Thonar EJ-MA, Sumner DR. The effect of bone remodeling inhibition by zoledronic acid in an animal model of cartilage matrix damage. *Osteoarthr Cartil*. 2002;10(3):226-233. doi:10.1053/joca.2001.0506.

58. Hayami T, Pickarski M, Wesolowski GA, Mclane J, Bone A, Destefano J, Rodan GA, Duong LT. The role of subchondral bone remodeling in osteoarthritis: Reduction of cartilage degeneration and prevention of osteophyte formation by alendronate in the rat anterior cruciate ligament transection model. *Arthritis Rheum*. 2004;50(4):1193-1206. doi:10.1002/art.20124.

59. Myers SL, Brandt KD, Burr DB, O'Connor BL, Albrecht M. Effects of a bisphosphonate on bone histomorphometry and dynamics in the canine cruciate deficiency model of osteoarthritis. *J Rheumatol*. 1999;26(12):2645-2653.

60. Siebelt M, Waarsing JH, Groen HC, Müller C, Koelewijn SJ, de Blois E, Verhaar JAN, de Jong M, Weinans H. Inhibited osteoclastic bone resorption through alendronate treatment in rats reduces severe osteoarthritis progression. *Bone*. 2014;66:163-170. doi:10.1016/j.bone.2014.06.009.

61. Brown TD, Radin EL, Martin RB, Burr DB. Finite element studies of some juxtarticular stress changes due to localized subchondral stiffening. *J Biomech*. 1984;17(1):11-24.

62. Christiansen BA, Guilak F, Lockwood KA, Olson SA, Pitsillides AA, Sandell LJ, Silva MJ, van der Meulen MCH, Haudenschild DR. Non-invasive mouse models of post-traumatic osteoarthritis. *Osteoarthr Cartil*. 2015;23(10):1627-1638. doi:10.1016/j.joca.2015.05.009.

63. Holyoak DT, Tian YF, van der Meulen MCH, Singh A. Osteoarthritis: Pathology, Mouse Models, and Nanoparticle Injectable Systems for Targeted Treatment. *Ann Biomed Eng*. 2016;44(6):2062-2075. doi:10.1007/s10439-016-1600-z.

64. Bendele AM. Animal models of osteoarthritis. *J Musculoskelet Neuronal Interact*. 2001;1(4):363-376.

65. Clements KM, Ball AD, Jones HB, Brinckmann S, Read SJ, Murray F. Cellular and histopathological changes in the infrapatellar fat pad in the monoiodoacetate model of osteoarthritis pain. *Osteoarthr Cartil*. 2009;17(6):805-812. doi:10.1016/j.joca.2008.11.002.

66. Guzman RE, Evans MG, Bove S, Morenko B, Kilgore K. Mono-iodoacetate-induced histologic changes in subchondral bone and articular cartilage of rat femorotibial joints: an animal model of osteoarthritis. *Toxicol Pathol*. 31(6):619-624.

67. Little C, Zaki yz Raymond S. What constitutes an animal model of osteoarthritis, the need for consensus? 2012. doi:10.1016/j.joca.2012.01.017.

68. Bove S., Calcaterra S., Brooker R., Huber C., Guzman R., Juneau P., Schrier D., Kilgore

K. Weight bearing as a measure of disease progression and efficacy of anti-inflammatory compounds in a model of monosodium iodoacetate-induced osteoarthritis. *Osteoarthr Cartil*. 2003;11(11):821-830. doi:10.1016/S1063-4584(03)00163-8.

69. Combe R, Bramwell S, Field MJ. *The Monosodium Iodoacetate Model of Osteoarthritis: A Model of Chronic Nociceptive Pain in Rats?* Vol 370.; 2004. doi:10.1016/j.neulet.2004.08.023.

70. Murat N, Karadam B, Ozkal S, Karatosun V, Gidener S. Quantification of papain-induced rat osteoarthritis in relation to time with the Mankin score. *Acta Orthop Traumatol Turc*. 2007;41(3):233-237.

71. Bentley G. Papain-induced degenerative arthritis of the hip in rabbits. *J Bone Joint Surg Br*. 1971;53(2):324-337.

72. Poulet B. Non-invasive Loading Model of Murine Osteoarthritis. *Curr Rheumatol Rep*. 2016;18(7):40. doi:10.1007/s11926-016-0590-z.

73. McCoy AM. Animal Models of Osteoarthritis: Comparisons and Key Considerations. *Vet Pathol*. 2015;52(5):803-818. doi:10.1177/0300985815588611.

74. Jimenez PA, Glasson SS, Trubetskoy O V, Haimes HB. Spontaneous osteoarthritis in Dunkin Hartley guinea pigs: histologic, radiologic, and biochemical changes. *Lab Anim Sci*. 1997;47(6):598-601.

75. Lewis JS, Hembree WC, Furman BD, Tippets L, Cattel D, Huebner JL, Little D, DeFrate LE, Kraus VB, Guilak F, Olson SA. Acute joint pathology and synovial inflammation is associated with increased intra-articular fracture severity in the mouse knee. *Osteoarthr Cartil*. 2011;19(7):864-873. doi:10.1016/j.joca.2011.04.011.

76. Christiansen BA, Anderson MJ, Lee CA, Williams JC, Yik JHN, Haudenschild DR. Musculoskeletal changes following non-invasive knee injury using a novel mouse model of post-traumatic osteoarthritis. *Osteoarthr Cartil*. 2012;20(7):773-782. doi:10.1016/j.joca.2012.04.014.

77. Wu P, Holguin N, Silva MJ, Fu M, Liao W, Sandell LJ. Early response of mouse joint tissue to noninvasive knee injury suggests treatment targets. *Arthritis Rheumatol (Hoboken, NJ)*. 2014;66(5):1256-1265. doi:10.1002/art.38375.

78. Poulet B, Hamilton RW, Shefelbine S, Pitsillides AA. Characterizing a novel and adjustable noninvasive murine joint loading model. *Arthritis Rheum*. 2011;63(1):137-147. doi:10.1002/art.27765.

79. Ko FC, Dragomir C, Plumb DA, Goldring SR, Wright TM, Goldring MB, van der Meulen MCH. In vivo cyclic compression causes cartilage degeneration and subchondral bone changes in mouse tibiae. *Arthritis Rheum*. 2013;65(6):1569-1578. doi:10.1002/art.37906.

80. Stoop R, Van Der Kraan PM, Buma P, Hollander AP, Billinghurst RC, Poole AR, Van Den Berg WB. Type II collagen degradation in spontaneous osteoarthritis in C57BL/6 and BALB/c mice. *Arthritis Rheum*. 1999;42(11):2381-2389. doi:10.1002/1529-0131(199911)42:11<2381::AID-ANR17>3.0.CO;2-E.

81. Fritton J, Myers E, Wright T, van der Meulen M. Loading induces site-specific increases in mineral content assessed by microcomputed tomography of the mouse tibia. *Bone*.

2005;36(6):1030-1038. doi:10.1016/j.bone.2005.02.013.

82. De Souza RL, Matsuura M, Eckstein F, Rawlinson SCF, Lanyon LE, Pitsillides AA. Non-invasive axial loading of mouse tibiae increases cortical bone formation and modifies trabecular organization: a new model to study cortical and cancellous compartments in a single loaded element. *Bone*. 2005;37(6):810-818. doi:10.1016/j.bone.2005.07.022.

83. Lee KC., Maxwell A, Lanyon L. Validation of a technique for studying functional adaptation of the mouse ulna in response to mechanical loading. *Bone*. 2002;31(3):407-412. doi:10.1016/S8756-3282(02)00842-6.

84. Lynch ME, Main RP, Xu Q, Schmicker TL, Schaffler MB, Wright TM, van der Meulen MCH. Tibial compression is anabolic in the adult mouse skeleton despite reduced responsiveness with aging. *Bone*. 2011;49(3):439-446. doi:10.1016/j.bone.2011.05.017.

85. Sugiyama T, Saxon LK, Zaman G, Moustafa A, Sunters A, Price JS, Lanyon LE. Mechanical loading enhances the anabolic effects of intermittent parathyroid hormone (1–34) on trabecular and cortical bone in mice. *Bone*. 2008;43(2):238-248. doi:10.1016/j.bone.2008.04.012.

86. Melville KM, Robling AG, van der Meulen MCH. In vivo axial loading of the mouse tibia. *Methods Mol Biol*. 2015;1226:99-115. doi:10.1007/978-1-4939-1619-1_9.

87. Glasson SS, Chambers MG, Van Den Berg WB, Little CB. The OARSI histopathology initiative – recommendations for histological assessments of osteoarthritis in the mouse. *Osteoarthr Cartil*. 2010;18:S17-S23. doi:10.1016/j.joca.2010.05.025.

88. Ko FC, Dragomir CL, Plumb DA, Hsia AW, Adebayo OO, Goldring SR, Wright TM, Goldring MB, van der Meulen MCH. Progressive cell-mediated changes in articular cartilage and bone in mice are initiated by a single session of controlled cyclic compressive loading. *J Orthop Res*. 2016;(October 2015):n/a-n/a. doi:10.1002/jor.23204.

89. Poulet B, de Souza R, Kent a. V, Saxon L, Barker O, Wilson a., Chang Y-M, Cake M, Pitsillides a. a. Intermittent applied mechanical loading induces subchondral bone thickening that may be intensified locally by contiguous articular cartilage lesions. *Osteoarthr Cartil*. 2015;23(6):940-948. doi:10.1016/j.joca.2015.01.012.

90. Adebayo OO, Ko FC, Goldring SR, Goldring MB, Wright TM, van der Meulen MCH. Kinematics of meniscal- and ACL-transected mouse knees during controlled tibial compressive loading captured using roentgen stereophotogrammetry. *J Orthop Res*. 2016;(April 2016):1-23. doi:10.1002/jor.23285.

91. Volokh KY, Chao EYS, Armand M. On foundations of discrete element analysis of contact in diarthrodial joints. *Mol Cell Biomech*. 2007;4(2):67-73.

92. McGee MG. Human spatial abilities: Psychometric studies and environmental, genetic, hormonal, and neurological influences. *Psychol Bull*. 1979;86:889-918.

93. Program NE, Metz S, Sorby S. *Spatial Skills & Persistence in Engineering: A Critical Link*.; 2014.

94. Linn MC, Petersen A. Emergence and characterization of gender differences in spatial abilities: A meta-analysis. *Child Dev*. 1985;56:1479-1498.

95. Council NR. *Learning to Think Spatially*.; 2006.

96. Lieu D, Sorby SA. *The Fundamentals of Visualization, Modeling, and Graphics for Engineering Design*. New York: Cengage Learning; 2009.

CHAPTER 2

KINEMATICS OF MENISCAL- AND ACL-TRANSECTED MOUSE KNEES DURING CONTROLLED TIBIAL COMPRESSIVE LOADING CAPTURED USING ROENTGEN STEREOPHOTOGRAMMETRY

The following chapter is published in the *Journal of Orthopaedic Reserach* and reprinted here with permission. The reference to the published work is:

Adebayo O, Ko F, Goldring S, Goldring M, Wright T, van der Meulen M. (2017) Kinematics of Meniscal- and ACL-Transected Mouse Knees during Controlled Tibial Compressive Loading Captured using Roentgen Stereophotogrammetry. *Journal of Orthopaedic Research* 35(2): 353-360.

2.1 Introduction

Osteoarthritis (OA) is characterized clinically by cartilage degradation, subchondral bone changes, joint pain and impaired joint function[1,2]. Tissue alterations in OA joints extend beyond cartilage and bone to include changes in the menisci, ligaments and other peri-articular soft tissues[3]. Epidemiological studies indicate that abnormal biomechanical loading and joint instability from injury are important etiological factors in the pathogenesis of OA[1,4]. This concept is substantiated by observations that certain occupational activities[5–7], obesity[8,9], and joint laxity and injury[10–12] are correlated with an increased risk of OA, while reduction in body weight[13] and mild to moderate exercise[14,15] may slow disease progression. Although epidemiological and clinical studies of OA suggest a strong relationship between the joint mechanical environment and the incidence of the disease, the exact ways in which changes in the mechanical environment influence OA initiation and progression are not well defined[16].

Pre-clinical studies in murine species using surgical models, such as the destabilization of the medial meniscus (DMM)[17,18] and anterior cruciate ligament transection (ACLT)[17,19], have examined the structural changes and biological pathways that lead to OA disease initiation after joint injury. These models induce moderate to severe OA pathology characterized by cartilage degradation and subchondral bone changes, and provide insights into the morphological and biochemical changes in joint tissues during OA disease progression[17–20]. Furthermore, while several studies demonstrated that these injuries affect joint stability in large vertebrates[21–24], the relationship between altered joint kinematics and the initiation of OA has not been fully characterized in murine models due to their small size. Measurements of joint kinematics in murine models have been limited to using weight bearing and ground reaction forces as metrics for instability[25,26]. While these data provide information on the functionality of the joint, they do not describe joint instability or the mechanical environment associated with the injury. Thus, these studies have provided little insight into how these joint injuries affect joint stability and how the altered joint kinematics relates to OA initiation. Characterization of joint kinematics in the DMM and ACLT models would provide valuable insights into the influence of instability on the local mechanical environment during the initiation and progression of OA, strengthening their use as small-animal models of post-traumatic OA.

Our group and others have previously presented a non-invasive tibial loading model in mice for bone adaptation studies[27,28]. The loading device in this model allows for normal flexion of the knee, while applying a controlled axial compressive load to the tibia through the femoral condyles. Adapted from the mouse ulna loading model[30], the tibial loading model has been used extensively in orthopaedics to study bone adaptation and is a widely accepted platform to recapitulate physiological mechanical forces during mouse gait[27–29], with a 9N compressive load

creating 1200με at the mid-shaft of the tibia[29]. This strain value is well within the normal range of functional strains during locomotion in mice and most vertebrates[31–34]. Recently, our group and others used this model on intact joints to recapitulate major features of OA after 1, 2, and 6 weeks of loading[35–37], with similar results to those induced by long-term treadmill running in mice[38]. To date, however, the tibial compressive loading model has not been applied to DMM and ACLT injured mouse knees.

With the understanding that mechanical forces play a key role in OA, we aimed to characterize the effects of the joint injuries in the DMM and ACLT models on joint kinematics under loading conditions. We hypothesized that the DMM and ACLT models would alter stability compared to intact joints, thus enabling future experiments to explore the effects of joint instability on patterns of OA initiation and severity in these mouse models under controlled loading. Our loading device, which permits controlled application of compressive loads to the tibia, was used as a tool to quantify and compare joint kinematics of intact, DMM and ACLT joints under a controlled loading regime. Due to the orientation and range of motion of the knee under our loading conditions, our results directly measured bone kinematics, rather than joint kinematics. Our results provide insights into the effects of these joint injuries on bone kinematics and associated joint motions in the context of defined compressive loading and demonstrate the importance of rigorous kinematic analysis to better understand disease progression in murine models of OA.

2.2 Methods

2.2.1 Animal Models

Eight 32-week old freshly frozen C57BL/6 male mice (Jackson Laboratories, Bar Harbor,

ME) were obtained and thawed at room temperature. The right knee joint of each mouse was subjected to either DMM or ACLT (n=4/group). Following previously established protocols[17], a longitudinal incision was performed from the distal patella to the proximal tibia. The joint capsule was exposed, and the fat pad was dissected, allowing visualization of the medial meniscotibial ligament (MMTL) and the anterior cruciate ligament (ACL). Using a #11 blade, either the MMTL or the ACL was transected. Care was taken to ensure that all other ligaments remained intact. The joint capsule was then closed with a continuous cutting suture (4-0 Sofsilk, Covidien, Minneapolis, MN). The left knee joints remained as intact controls.

2.2.2 Fiducial Marker Placement

To place the fiducial makers on the joint for use in kinematics measurements, two small incisions were created, one on the medial proximal region of each tibia and the other on the anterior distal region of each femur. The muscle and skin were retracted using blunt dissection techniques, and a periosteal elevator was used to remove the periosteum. The exposed bone was degreased with methyl ethyl ketone. At least 3 100μm tin/lead solder spheres (Caplinq Co., Ottawa ON, Canada) were affixed to a 2mm x 2mm flexible adhesive plastic to serve as fiducial bone markers. The bone markers were adhered onto the exposed regions of the tibia and femur using cyanoacrylate. Care was taken to ensure that the markers adhered firmly to the bone, and that the joint capsule remained intact.

2.2.3 Mechanical Loading & Imaging Protocol

All limbs were loaded from 0 to 9N compression at 1N increments using the tibial compressive loading device[35] (Figure 2.1A). The loading device is equipped with a feedback

control loop (National Instruments, Labview v8.2) that allows the user to set a constant compressive force at each load step (Figure 2.1B), using an in-line force transducer (ELPF-T2E-10L, Measurement Specialties). Medial-lateral radiographs were obtained at each stepped load using a single dental x-ray (VetVision DC, Progeny Dental, Lincolnshire, IL), with a resolution of 28μm. The stepped loading protocol was then repeated to obtain anterior-posterior radiographs (Figure 2.1C). This loading and imaging scheme was repeated for 3 trials per joint.

Compressive loading was applied through an actuator affixed to a foot-holder in the loading device, while the force transducer was attached to the knee-holder (Figure 2.1A). With each progressive load step, the foot-holder applied compression through proximal translation along the X-axis, towards the knee joint (Figure 2.1C). A prior kinematic analysis identified that this translation was associated with a slight positive rotation (1.4±1.3°) about the Z-axis at 9N. Thus, any positive rotations about the Z-axis resulting in adduction or abduction within this angular range were regarded as a function of the loading device for the right and left knee, respectively.

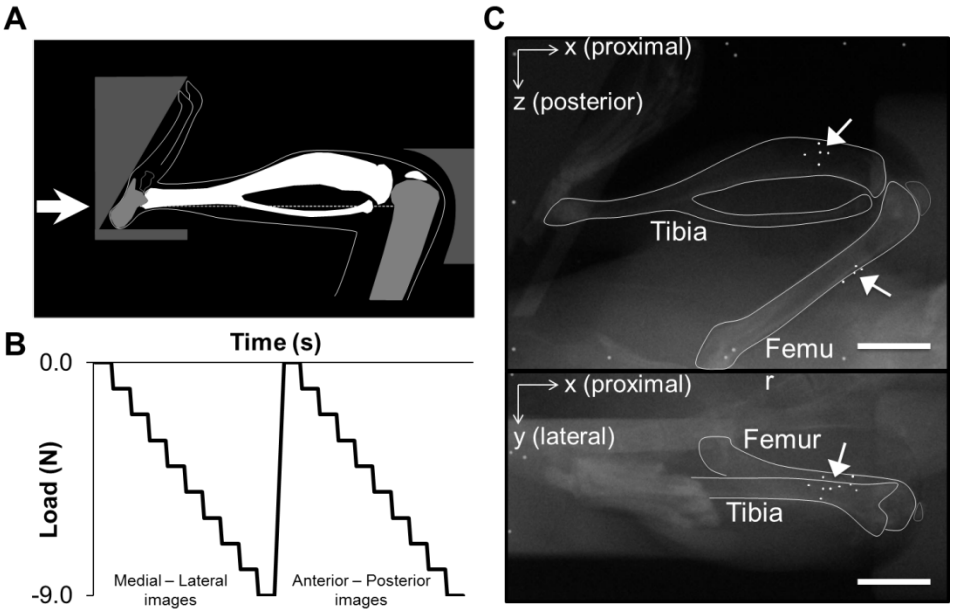

Figure 2.1 (A) Schematic of the mouse tibial loading device, (B) the loading configuration for each stepped loading trial applied to the joint, and (C) radiographs of an intact joint in the loading device from 2 imaging planes, with the tibial, femoral, and bone markers outlined. Arrows indicate bone markers. Scale bar = 5.0mm

2.2.4 Roentgen Stereophotogrammetry

Roentgen stereophotogrammetry (RSA) examination was performed using a custom-made calibration cage and previously-established protocols [39–41]. The calibration cage consisted of 2 orthogonal planes, one for each x-ray position, containing sets of tantalum markers with known locations. One set of markers defined the 3D global fiducial coordinate system, while the other set was used to determine the exact location of the dental x-ray. Error analysis was performed on the system using a phantom consisting of 2 wooden rods (2.2mm diameter, 15cm length), each labeled with at least 4 fiducial markers. To measure both the precision and accuracy of the system, we conducted 9 double examinations of the phantom with no relative motion between rods, similar to previous protocols[40]. Radiographs were taken at the 2 planes of the calibration cage, and used to determine each fiducial marker location, rigid-body fitting, and subsequent calculation of motion.

The relative motion calculated by the RSA set-up for the 9 examinations was averaged as the error of the system, and the standard deviation of these motions was the precision. The error and precision (mean ± standard deviation) associated with zero motion of the phantom were 0.03±0.25mm, -0.01±0.08mm, and -0.16±0.37mm in translation along the X-, Y-, and Z- axes, respectively, and -0.9±2.2°, 0.8±1.4°, and 1.3±1.3° in rotation about the X-, Y-, and Z- axes, respectively. These values were interpreted as the systematic error associated with calculations of rigid body motion using this RSA set-up, and any motions within the bounds of our error values were deemed negligible.

Furthermore, the use of a single dental x-ray for imaging two planes introduced an inherent error in joint positioning because the loading protocols were performed sequentially. We defined this error as the average error in determining the exact 3D location of the fiducial markers. The position of each marker was calculated as the intersection between the position vectors from each imaging focus point. However, due to both a systematic error from the lack of exact alignment of the two orthogonal planes of the calibration cage, and the irreproducibility of the joint positioning with a sequential loading protocol, the position vectors did not intersect in 3D space. Therefore, the position of each bone marker was calculated as the midpoint of the shortest line connecting the two vectors, with the error defined as half the length of the line along each axis. Using data from a previous kinematic analysis in which five mouse joints were placed under the same protocol for 15 loading/imaging protocols, we determined the average error of the system to be [±63μm, ±2.0μm, ±1.6μm] in the X-, Y- and Z-axes respectively.

2.2.5 Kinematics Analysis

All joints were placed in the loading device, with the tibial axis of loading aligned to the X-axis of the calibration cage (Figure 2.1), and RSA examination was performed. First, the initial, non-loaded position of the joint was examined qualitatively in the loading device. Due to the small size of the mouse joint, a reliable and consistent femoral coordinate system could not be established, thus all motions were described as translation and rotation from 0N load around the 3 axes in a tibial-oriented coordinate system. In accordance with RSA techniques, the tibial coordinate system was based on a reference alignment of the bone position in the loading device at 0N. Specifically, the tibial X-axis was defined as the axis at 0N in which the compressive load was applied, running from the tarsus to the intercondylar eminence, and was aligned to the global

X-axis. Furthermore, we assumed that the tibial Y-axis at the 0N position in the loading device intersected both the medial and lateral tibial plateaus, and was parallel to the global Y-axis. The tibial Z-axis, perpendicular to both the X- and Y-axes, thus paralleled the global Z-axis. To determine translation along each axis, the point of interest (POI) was defined as the geometric center of the tibial and femoral articulating surfaces for both the tibia and the femur (Figure 2.2). The location of the POI was defined and digitized manually as the midpoint of the overlapping surface of the tibia and femur in the 0N medial-lateral radiograph and the intercondylar eminence of the tibia in the 0N anterior-posterior radiograph.

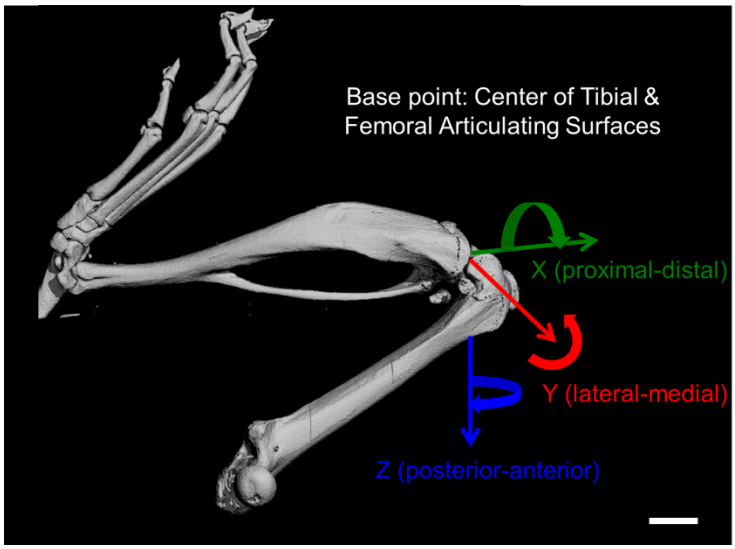

Figure 2.2 Schematic of the joint axes and coordinate system relative to the tibia used for the kinematics analysis. Straight arrows indicate the Superior-Inferior axis (green), Medial-Lateral axis (red) and Posterior-Anterior axis (blue), and curved arrows indicate Internal-External (green), Flexion-Extension (red) and Adduction-Abduction (blue) rotations. Scale bar = 2.0mm

To describe joint motions, tibial motion was first calculated at each stepped load as translation of the point of interest and Eulerian rotation of the bone about the body-oriented X-Y-Z axes relative to its position at 0N. These motions were thus interpreted as inferior-superior (IS), medial-lateral (ML), and anterior-posterior (AP) translations of the tibial plateau, and internal-external (IE), flexion-extension (FE), and abduction-adduction (AA) rotation of the

tibia. Then, the relative femur-to-tibia motion, interpreted as the motion of the knee joint, was determined using the tibia as the reference segment. Specifically, the motion of the tibia at each stepped load was first transformed back to its position at 0N, and then the relative motion of the femur was calculated in the tibial coordinate system. Relative translation in this case was calculated as the difference in the position of the point of interest due to femoral versus tibial motion from 0N to each stepped load. All coordinate system creations and kinematics calculations were completed in Matlab using a custom-written code.

2.2.6 Statistics

Statistical analysis was performed to compare the kinematics of intact and ligament-transected joints. All intact joints from both DMM and ACLT groups were pooled for statistical analysis with the exception of one intact joint that was dislocated due to an accidental initial overload in the loading device. The results of the kinematics trials for each joint were averaged and represented as descriptive data for statistical analysis. Due to the small sample size of each group, a Kruskal-Wallis test was then performed to compare the kinematics of intact and injured joints at each stepped load (JMP Pro 10.0, SAS Institute Inc). All data are shown as mean ± standard deviation, unless otherwise indicated. p-values of <0.05 indicate significance.

2.3 Results

2.3.1 Comparison of Joint Positions in the Loading Device

Changes in the joint position in the loading device were evident between the two models, even before the application of any compressive load (Figure 2.3). The DMM joints maintained positions similar to those of the intact joints in the loading device, with an apparent articulating

surface between the femur and tibia. However, all of the ACLT joints dislocated when placed in the loading device, even without compressive load. The dislocation resulted in the loss of an articulating surface between the femur and tibia, and thus further analysis of bone kinematics could not be performed accurately.

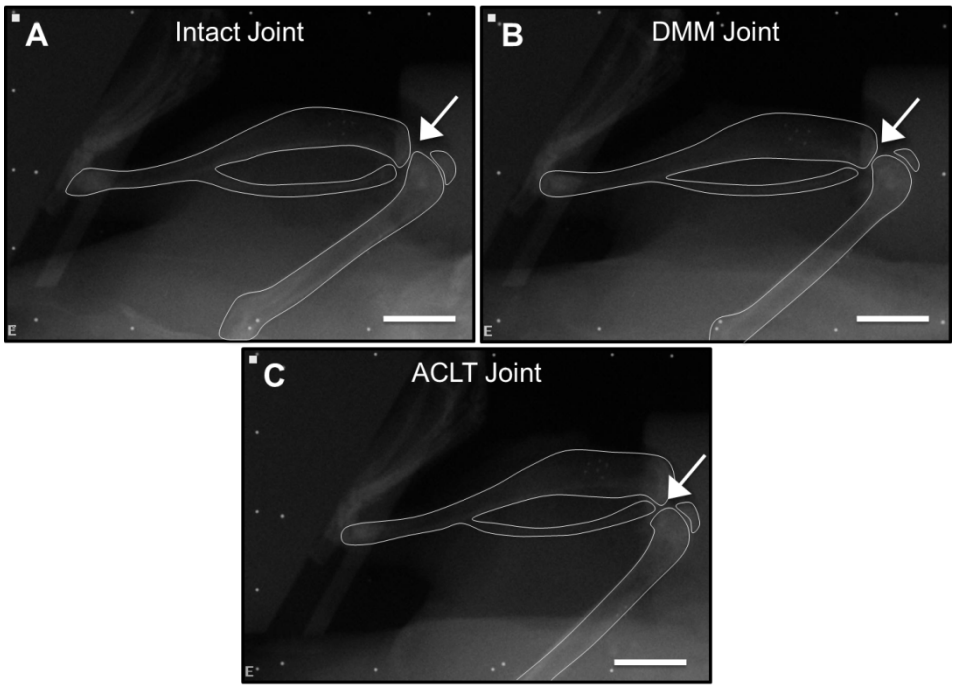

Figure 2.3 Medial-lateral radiographs of an (A) intact joint (n=7), (B) DMM joint (n=4), and (C) ACLT joint (n=4) in the loading device without load. Arrows indicate articular surface. Scale bar = 5.0mm

2.3.2 Tibial Motion Under Compression

The tibial motions of intact and DMM joints were similar at each stepped load relative to 0N. As the compressive load increased from 0 to 9N, both intact and DMM tibias exhibited superior translation, which peaked at 0.3±0.1mm and 0.2±0.0mm at 9N, respectively (Figure 2.4A). Additionally, both groups demonstrated minimal translation along the ML axis and AP motion of the tibia, which peaked at similar values for both intact and DMM joints (Figs. 2.4B-C). None of the translational motions of the tibia were significantly different at any of the loads

(p = 0.13 – 0.85). IE rotation was also minimal (p = 0.19 – 0.85) in all intact and DMM tibias, and the degree of tibial flexion was not different (p = 0.45 – 1.0) between intact and DMM groups (Figs. 2.4D-E). In contrast, the degree of tibial adduction at loads ≥ 4N was significantly different between the two groups (p<0.04, Figure 2.4F), although the differences were small (tibial adduction of 1.5±0.7° at 9N in intact joints and tibial abduction of 1.7±0.6° in DMM joints).

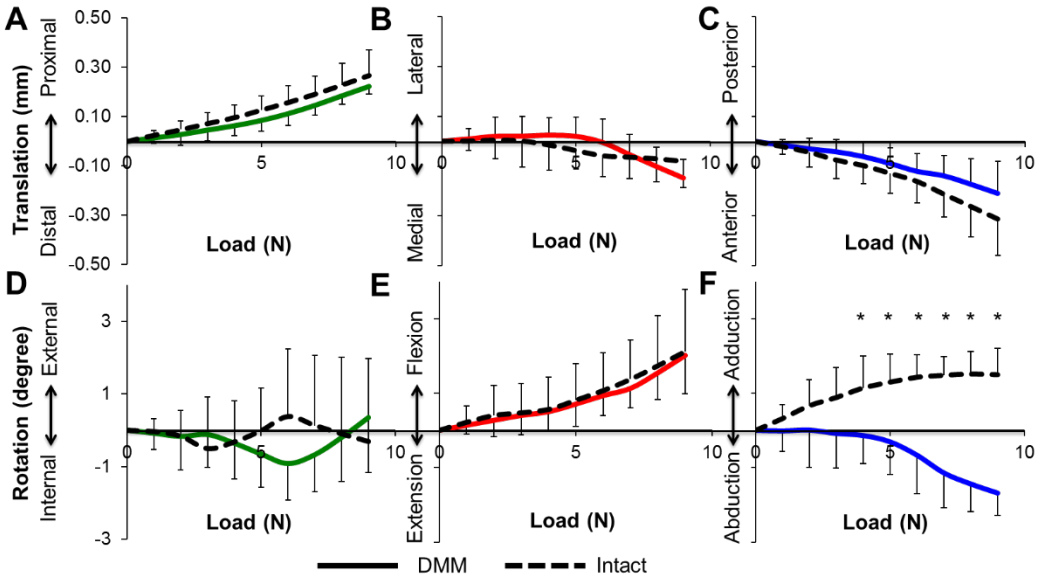

Figure 2.4 Tibial translations and rotations relative to the 0N position were not different between intact (n=7) and DMM (n=4) tibiae each stepped load, except for abduction-adduction at loads greater than 3N. Data are shown for translation along the (A) Superior-Inferior, (B) Lateral-Medial, and (C) Posterior-Anterior axes, and (D) Internal-External, (E) Flexion-Extension, and (F) Adduction-Abduction rotation. Data colors correspond to axis colors in Figure 2.2. *, p<0.05 by Kruskal-Wallis test.

2.3.3 Knee Joint Motion (Relative Femur to Tibia Motion) under Compression

Femur-to-tibia translations were minimal along the SI and AP axes (Figs. 2.5A,C). However, ML translation of the femur to tibia was significantly different between intact and DMM joints at 8N and 9N loads (p < 0.01, Figure 2.5B). Intact joints exhibited little motion (0.1±0.1mm) along the ML axis; however, in DMM joints, we observed lateral translation of the

femur starting at 6N, which peaked at 0.2±0.1mm at the 9N load. In both DMM and intact joints, we observed minimal internal rotation and similar flexion of the femur at most loads (Figs. 2.5D-E). However, rotation about the tibial AP axis was significantly different between these groups with femoral abduction (with the knee moving into varus) occurring in DMM joints compared to intact joints at all compressive loads ($p = 0.0082$, Figure 2.5F).

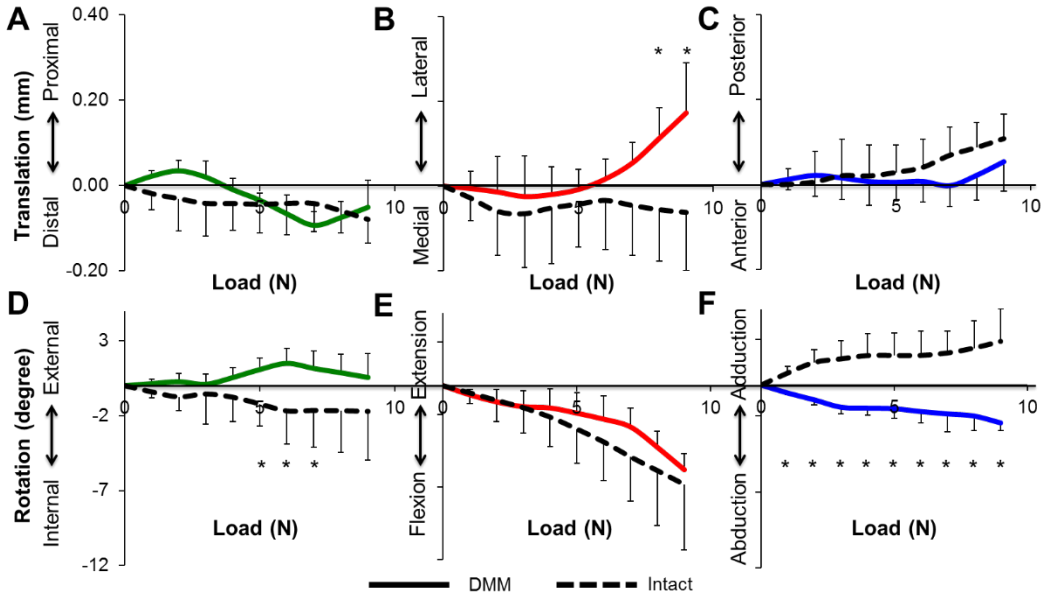

Figure 2.5 Most relative femur-to-tibia translations and rotations were not different between intact (n=7) and DMM (n=4) tibiae at each stepped load, except for translation along the medial-lateral axis at 8 and 9N and rotation about the anterior-posterior axis. Data are shown for translation along the (A) Superior-Inferior, (B) Lateral-Medial, and (C) Posterior-Anterior axes, and (D) Internal-External, (E) Flexion-Extension, and (F) Adduction-Abduction rotation. Data colors correspond to axis colors in Figure 2.2. *, $p<0.05$ by Kruskal-Wallis test.

2.4 Discussion

While pre-clinical models, such as DMM and ACLT, recapitulate features of post-traumatic OA[17–20], the exact mechanical environment associated with disease initiation and progression in these models is not understood completely. We sought to determine the kinematics of DMM and ACLT joints under a controlled loading environment, to gain insights into the impact of the injuries on joint stability. Our results demonstrate that bone kinematics

and, by extension, joint instability depend on the type of destabilization injury. Specifically, the initial dislocation of ACLT joints within the loading device, which allows for normal flexion, and the apparent loss of contact surface between the tibia and femur indicate that ACLT models of OA exhibit high levels of instability, with loading occurring at the edge of the injured joint[42]. In contrast, most measures of tibial and femoral motion were similar between DMM and intact joints, with only subtle differences in frontal plane rotations of the tibia and femur and greater relative lateral translation of the femur at higher compressive loads. While the differences in frontal rotations were significant, these small positive rotations about the AP-axis were within the range of the inherent motion of the foot-holder. Thus, the only significant, relevant difference between DMM and intact joints was in the slight lateral translation of the femur in the DMM group. Such similarities between kinematics in DMM and intact joints suggest that the induction of OA-like features in the DMM mouse model may not be due necessarily to extreme joint instability, but rather to a change in contact stresses as a result of an abnormal contact area[43–45].

Our study provides novel information about kinematics and instability of ACLT joints, specifically in murine models of OA, and such results are similar to those reported in other cadaveric studies. Bedi and colleagues reported kinematic changes in cadaveric human knees after an ACL injury, with significantly increased contract stress in the posterior-central aspect of the tibial plateau[46]. This finding is supported by other studies in mice, rabbits, sheep and humans, and is due to the increased anterior translation of the tibia as a result of the lack of the stabilizing constraint provided by the ACL[19,21,47–49]. In our study, the increased anterior translation of the tibia resulted in dislocation of the joint within the loading device, which may explain the rapid rate of OA progression present in murine ACLT models. *In vivo* murine joints subjected to ACLT demonstrate tibial anterior subluxation, marked degradation of the posterior aspect of the

tibial cartilage, erosion of the tibial posterior subchondral bone, and osteophyte formation at the joint margins[17,19]. These *in vivo* results indicate the presence of high joint instability and an abnormal anterior translation of the tibia during gait, consistent with the ACLT causing extreme joint motions, even in an otherwise well-controlled animal study[47]. While the ACLT mouse model is a relevant model of post-traumatic OA to understand pathologic joint tissue changes associated with such injuries, the kinematics of the model are extreme in the mouse. Thus, ACLT is unsuitable for mouse studies focused on elucidating the relationship between kinematics and subsequent joint injury and OA initiation.

To our knowledge, our study is the first to present the kinematics of DMM rodent joints under controlled mechanical loading. A previous study conducted by Allen and colleagues[25] focused on weight-bearing limb measurements in rats with medial collateral ligament (MCL) and medial meniscal transections, two more severe joint destabilization models. Significant differences were present in gait dynamics between injured and normal joints[25]. In contrast, our results suggest that the joint kinematics are generally unaffected by the DMM injury, which is much less destructive than a complete MCL or medial meniscal transection. Although we did not examine *in vivo* dynamic kinematics, our results are further substantiated by the slower rate of OA progression in DMM models compared to ACLT models *in vivo*[17,19,50]. Indeed, the progression of moderate OA in DMM and other meniscal injury situations has been attributed to the disruption of tibiofemoral contact mechanics, with damage to the meniscus causing decreased cartilage contact area[43–45,51]. Thus, higher stresses occur in the cartilage, particularly over the medial aspect of the tibia[17,50,52]. Although both the ACLT and the DMM mouse models develop OA-like features, the results of this study, along with evidence from *in vivo* studies, suggest that the joint mechanical environment associated with disease initiation differ. The

DMM model reflects increased contact stress due to a reduction of contact area. In contrast, the ACLT model resulted in tibial dislocation under normal flexion, suggesting extreme loading between any remaining articulating surfaces due to the injury compared to the DMM model. This finding, though obtained *ex vivo*, is supported by *in vivo* evidence, and leads to the likely conclusion that with tibial compressive loading during mouse gait, these differences in mechanical environment may play at least a partial role in the severity and progression of OA *in vivo*[53].

Our study has limitations. While we used a controlled mechanical platform to examine the kinematics of ACLT and DMM joints, strict axial compression of the tibia through the femoral condyles may not elicit the same motions that occur during gait. However, our intention was to examine bone kinematics using a controlled loading model that generates physiological mid-shaft strains and that recapitulates OA features[35]. This model induces OA by superimposing short cycles of controlled tibial loading over otherwise normal cage activity, and without the surgical disruption of the joint[35,36]. In contrast, DMM and ACLT models require invasive surgery, which induces inflammation that, in itself, may cause abnormal alterations in bone kinematics, thus confounding interpretation of the results. The compressive loading used in our study was done with little external constraint to the knee; the joint surfaces were free to move in any direction, though the motions of the tibia and femur were somewhat constrained to flexion-extension by the manner in which the tibia and femur were held in the loading fixture (Figure 2.1A). Furthermore, the applied loads were small and controlled compared to those applied by muscles and ligaments during normal cage activity. In addition, our approach did not account for tissue adaptation and muscle forces that may play a role *in vivo*. Nonetheless, we showed striking differences in bone kinematics following DMM and ACLT, even when our relatively mild

loading regime was applied. These differences in bone kinematics are likely exacerbated during normal cage activity, which may explain the differences in initiation and progression of OA pathology in the two models.

Additional considerations for our study are the use of a tibial-based coordinate system to describe knee joint kinematics, the small sample sizes, and the use of incremental static measurements of kinematics *ex vivo*. However, these points are offset by the fact that our study is the first to quantitatively characterize the bone kinematics associated with ACLT and DMM injuries in mice under controlled physiological tibial compressive loading. Thus, our results provide valuable insight into understanding the joint instability associated with these two commonly used OA mouse models *in vivo*.

In conclusion, we found marked differences in bone kinematics in the DMM and ACLT joints under controlled loading conditions. ACLT knees have extreme joint instability, which may explain the rapid progression of OA, particularly in the posterior aspect of the tibial plateau *in vivo*. In contrast, DMM joints exhibit kinematics similar to those in intact knees, suggesting that the progression of OA in this model reflects altered joint kinematics and contact mechanics, not a more extreme loading scenario. In summary, although both the ACLT and DMM mouse models have strengths and limitations with respect to elucidating the pathways associated with OA initiation and progression, the DMM model provides a more representative and relevant model of post-traumatic OA in terms of physiological bone kinematics.

2.5 REFERENCES

1. Felson DT, Lawrence RC, Dieppe PA, et al. 2000. Osteoarthritis: New Insights. Part 1: The Disease and Its Risk Factors. Ann. Intern. Med. 133(8):635-46.
2. Felson DT. 2006. Osteoarthritis of the knee. N. Engl. J. Med. 354(8):841–848.
3. Martel-Pelletier J. 2004. Pathophysiology of osteoarthritis. Osteoarthr. Cartil. 12:31–33.
4. Goldring MB, Marcu KB. 2009. Cartilage homeostasis in health and rheumatic diseases. Arthritis Res. Ther. 11(3):224.
5. Kaila-Kangas L, Arokoski J, Impivaara O, et al. 2011. Associations of hip osteoarthritis with history of recurrent exposure to manual handling of loads over 20 kg and work participation: a population-based study of men and women. Occup. Environ. Med. 68(10):734–8.
6. Cameron KL, Hsiao MS, Owens BD, et al. 2011. Incidence of physician-diagnosed osteoarthritis among active duty United States military service members. Arthritis Rheum. 63(10):2974–82.
7. Cogon D, Kellingray S, Inskip H, et al. 1998. Osteoarthritis of the Hip and Occupational Lifting. Am. J. Epidemiol. 147(6):523–528.
8. Felson DT, Zhang Y, Hannan MT, et al. 1997. Risk Factors For Incident Radiographic Knee Osteoarthritis In The Elderly: The Framingham Study. Arthrits Rheum. 40(4):728–733.
9. Schouten JS, van den Ouweland FA, Valkenburg HA. 1992. A 12 year follow up study in the general population on prognostic factors of cartilage loss in osteoarthritis of the knee. Ann. Rheum. Dis. 51(8):932–7.
10. Buckwalter JA, Lane NE. 1998. Athletics and osteoarthritis. Occup. Heal. Ind. Med. 38(2):98.
11. Lohmander LS, Felson D. 2004. Can we identify a “high risk” patient profile to determine who will experience rapid progression of osteoarthritis? Osteoarthr. Cartil. 12:49–52.
12. Lohmander LS, Ostenberg A, Englund M, Roos H. 2004. High prevalence of knee osteoarthritis, pain, and functional limitations in female soccer players twelve years after anterior cruciate ligament injury. Arthritis Rheum. 50(10):3145–52.
13. Felson DT, Zhang Y, Anthony JM, et al. 1992. Weight Loss Reduces the Risk for Symptomatic Knee Osteoarthritis in Women. Ann. Intern. Med. 116(7):535.
14. Messier SP, Loeser RF, Miller GD, et al. 2004. Exercise and dietary weight loss in overweight and obese older adults with knee osteoarthritis: the Arthritis, Diet, and Activity Promotion Trial. Arthritis Rheum. 50(5):1501–10.
15. Hochberg MC, Altman RD, April KT, et al. 2012. American College of Rheumatology 2012 recommendations for the use of nonpharmacologic and pharmacologic therapies in osteoarthritis of the hand, hip, and knee. Arthritis Care Res. 64(4):465–474.
16. Zhang Y, Jordan JM. 2010. Epidemiology of osteoarthritis. Clin. Geriatr. Med. 26(3):355–69.

17. Glasson SS, Blanchet TJ, Morris EA. 2007. The surgical destabilization of the medial meniscus (DMM) model of osteoarthritis in the 129/SvEv mouse. Osteoarthr. Cartil. 15(9):1061–9.

18. Culley KL, Dragomir CL, Chang J, et al. 2015. Mouse models of osteoarthritis: surgical model of posttraumatic osteoarthritis induced by destabilization of the medial meniscus. Methods Mol. Biol. 1226:143–73.

19. Kamekura S, Hoshi K, Shimoaka T, et al. 2005. Osteoarthritis development in novel experimental mouse models induced by knee joint instability. Osteoarthr. Cartil. 13(7):632–41.

20. Ma H-L, Blanchet TJ, Peluso D, et al. 2007. Osteoarthritis severity is sex dependent in a surgical mouse model. Osteoarthr. Cartil. 15(6):695–700.

21. Frank CB, Beveridge JE, Huebner KD, et al. 2012. Complete ACL/MCL deficiency induces variable degrees of instability in sheep with specific kinematic abnormalities correlating with degrees of early osteoarthritis. J. Orthop. Res. 30(3):384–92.

22. Tashman S. 2004. Abnormal Rotational Knee Motion During Running After Anterior Cruciate Ligament Reconstruction/ Am. J. Sports Med. 32(4):975–983.

23. Tashman S, Anderst W, Kolowich P, et al. 2004. Kinematics of the ACL-deficient canine knee during gait: serial changes over two years. J. Orthop. Res. 22(5):931–41.

24. Li G. 2005. In Vivo Articular Cartilage Contact Kinematics of the Knee: An Investigation Using Dual-Orthogonal Fluoroscopy and Magnetic Resonance Image-Based Computer Models. Am. J. Sports Med. 33(1):102–107.

25. Allen KD, Mata BA, Gabr MA, et al. 2012. Kinematic and dynamic gait compensations resulting from knee instability in a rat model of osteoarthritis. Arthritis Res. Ther. 14(2):R78.

26. Jay GD, Elsaid KA, Kelly KA, et al. 2012. Prevention of cartilage degeneration and gait asymmetry by lubricin tribosupplementation in the rat following anterior cruciate ligament transection. Arthritis Rheum. 64(4):1162–71.

27. Fritton J, Myers E, Wright T, van der Meulen M. 2005. Loading induces site-specific increases in mineral content assessed by microcomputed tomography of the mouse tibia. Bone 36(6):1030–1038.

28. De Souza RL, Matsuura M, Eckstein F, et al. 2005. Non-invasive axial loading of mouse tibiae increases cortical bone formation and modifies trabecular organization: a new model to study cortical and cancellous compartments in a single loaded element. Bone 37(6):810–8.

29. Lynch ME, Main RP, Xu Q, et al. 2010. Cancellous bone adaptation to tibial compression is not sex dependent in growing mice. J. Appl. Physiol. 109(3):685–91.

30. Torrance AG, Mosley JR, Suswillo RF, Lanyon LE. 1994. Noninvasive loading of the rat ulna in vivo induces a strain-related modeling response uncomplicated by trauma or periostal pressure. Calcif. Tissue Int. 54(3):241–7.

31. Mosley JR, March BM, Lynch J, Lanyon LE. 1997. Strain magnitude related changes in whole bone architecture in growing rats. Bone 20(3):191–198.

32. Lee KC., Maxwell A, Lanyon L. 2002. Validation of a technique for studying functional adaptation of the mouse ulna in response to mechanical loading. Bone 31(3):407–412.

33. Meakin LB, Price JS, Lanyon LE. 2014. The Contribution of Experimental in vivo Models to Understanding the Mechanisms of Adaptation to Mechanical Loading in Bone. Front. Endocrinol. 5:154.

34. Rubin C LL. 1985. Regulation of Bone Mass by Mechanical Strain Magnitude. Calcif. Tissue Int. :411–417.

35. Ko FC, Dragomir C, Plumb DA, et al. 2013. In vivo cyclic compression causes cartilage degeneration and subchondral bone changes in mouse tibiae. Arthritis Rheum. 65(6):1569–78.

36. Poulet B, Hamilton RW, Shefelbine S, Pitsillides AA. 2011. Characterizing a novel and adjustable noninvasive murine joint loading model. Arthritis Rheum. 63(1):137–47.

37. Christiansen BA, Guilak F, Lockwood KA, et al. 2015. Non-invasive mouse models of post-traumatic osteoarthritis. Osteoarthr. Cartil. 23(10):1627-38.

38. Lapveteläinen T, Nevalainen T, Parkkinen JJ, et al. 1995. Lifelong moderate running training increases the incidence and severity of osteoarthritis in the knee joint of C57BL mice. Anat. Rec. 242(2):159–65.

39. Selvik Gör. 1989. Roentgen stereophotogrammetry.Acta Orthop. 60(s232):1–51.

40. Valstar ER, Nelissen RGHH, Reiber JHC, Rozing PM. 2002. The use of Roentgen stereophotogrammetry to study micromotion of orthopaedic implants.ISPRS J. Photogramm. Remote Sens. 56(5-6):376–389.

41. Valstar ER, Gill R, Ryd L, et al. 2005. Guidelines for standardization of radiostereometry (RSA) of implants.Acta Orthop. 76(4):563–572.

42. Wright T, Maher S. 2015. Potential Mechanism of PTA: Alterations in Joint Loading. In: Olson S, Guilak F, editors. Post-Traumatic Arthritis. New York: Springer.

43. Fairbank TJ. 1948. Knee Joint Changes After Meniscectomy. J Bone Jt. Surg Br 30-B(4):664–670.

44. Messner K, Gao J. 1998. The menisci of the knee joint. Anatomical and functional characteristics, and a rationale for clinical treatment. J. Anat. 193 (Pt 2):161–78.

45. Lee SJ, Aadalen KJ, Malaviya P, et al. 2006. Tibiofemoral contact mechanics after serial medial meniscectomies in the human cadaveric knee. Am. J. Sports Med. 34(8):1334–44.

46. Bedi A, Chen T, Santner TJ, et al. 2013. Changes in dynamic medial tibiofemoral contact mechanics and kinematics after injury of the anterior cruciate ligament: a cadaveric model. Proc. Inst. Mech. Eng. H. 227(9):1027–37.

47. Tochigi Y, Vaseenon T, Heiner AD, et al. 2011. Instability dependency of osteoarthritis development in a rabbit model of graded anterior cruciate ligament transection. J. Bone Joint Surg. Am. 93(7):640–7.

48. Fukubayashi T, Torzilli PA, Sherman MF, Warren RF. 1982. An in vitro biomechanical evaluation of anterior-posterior motion of the knee. Tibial displacement, rotation, and torque. J. Bone Joint Surg. Am. 64(2):258–64.

49. Logan M. 2004. Tibiofemoral Kinematics of the Anterior Cruciate Ligament (ACL)-Deficient Weightbearing, Living Knee Employing Vertical Access Open “Interventional” Multiple Resonance Imaging. Am. J. Sports Med. 32(3):720–726.

50. Iijima H, Aoyama T, Ito A, et al. 2014. Destabilization of the medial meniscus leads to subchondral bone defects and site-specific cartilage degeneration in an experimental rat model. Osteoarthr. Cartil. 22(7):1036–1043.

51. Bedi A, Kelly NH, Baad M, et al. 2010. Dynamic contact mechanics of the medial meniscus as a function of radial tear, repair, and partial meniscectomy. J. Bone Joint Surg. Am. 92(6):1398–408.

52. Arunakul M, Tochigi Y, Goetz JE, et al. 2013. Replication of chronic abnormal cartilage loading by medial meniscus destabilization for modeling osteoarthritis in the rabbit knee in vivo. J. Orthop. Res. 31(10):1555–60.

53. Wright T. 2012. Biomechanical factors in osteoarthritis: the effects of joint instability. HSS J. 8(1):15–7.

CHAPTER 3

ROLE OF SUBCHONDRAL BONE PROPERTIES AND CHANGES IN DEVELOPMENT OF LOAD-INDUCED OSTEOARTHRITIS IN MICE

The following chapter is in review for publication in *Osteoarthritis and Cartilage* and reprinted here with permission. The anticipated reference to the work is:

> **Adebayo O,** Ko F, Wan P, Goldring S, Goldring M, Wright T, van der Meulen M. (2017) Role of Subchondral Bone Properties and Changes in Development of Load-Induced Osteoarthritis in Mice. *In review for publication in Osteoarthritis and Cartilage.*

3.1 Introduction

Osteoarthritis (OA) is a degenerative joint disease that clinically presents as radiographic narrowing of the joint space with accompanying subchondral bone (SCB) thickening and osteophyte formation[1,2]. Its exact etiology has been long debated, despite preclinical and clinical studies intended to elucidate the factors responsible for OA disease initiation and progression.[3–5]. Risk factors include traumatic injuries[5], occupational activities[6], and obesity[7], suggesting that mechanical loading plays a major role in OA initiation. An abnormal joint mechanical environment could initiate cell-mediated processes leading to both cartilage damage and SCB adaptation; however, the tissue in which the disease initiates is still controversial.

Given the clinical evidence of SCB thickening in OA patients, historically, the hypothesis has been that disease initiation is associated with increased mass and apparent stiffening of the SCB plate, diminishing its ability to act as an effective shock absorber for the cartilage[8–10]. However, recent studies suggest that SCB stiffening may not influence the stresses engendered on the cartilage surface[3,11] leading to the conclusion that OA joint pathology initiates in the

articular cartilage rather than the SCB. In more advanced stages of OA, abnormal mechanical forces can contribute to articular cartilage loss via the initiation of microcracks in the SCB plate that activate a bone remodeling response, leading to tidemark advancement and subsequent thinning of the cartilage[3,12–14]. These findings implicate a contributory role for bone remodeling in the pathogenesis of OA. Further evidence implicating bone remodeling in OA development is provided by the observation that in several animal models of OA, SCB mass is reduced at disease initiation, followed by thickening as the disease progresses[15,16]. Furthermore, in animal models, the inhibition of bone remodeling with pharmacological agents that impair osteoclast-mediated bone resorption attenuates the progression of OA[17–21].

The role of bisphosphonates, which inhibit osteoclast-mediated bone resorption, has been studied in multiple animal models of OA[17,18,20,21]. Bisphosphonates bind to the surface of mineralized bone and are metabolized by osteoclasts during bone remodeling, leading to impaired osteoclast activity and/or apoptosis[22,23]. Although bisphosphonates were effective in attenuating OA progression in preclinical post-traumatic OA models, clinical studies in human subjects failed to show attenuation of cartilage loss assessed radiographically, despite the evidence that the treatment inhibited bone remodeling[24,25]. The discrepancies in the efficacy of bisphosphonates between preclinical and clinical models could be due to multiple factors including the use of invasive injury to induce OA in the animal models and the diverse stages of OA progression in the patient cohorts at the time of treatment intervention[26]. Previous studies examining the effect of inhibiting bone remodeling with bisphosphonates on attenuating OA disease progression have not used a controlled, non-invasive, preclinical OA model.

We and others have recently developed a non-invasive load-induced model of OA in the mouse[27,28], based on controlled cyclic compression of the tibia and initially intended for bone

adaptation studies[29,30]. Using a peak load of 9N for 1200 cycles, this model induced controlled instabilities in the knee joint[31], and recapitulated OA pathology in the cartilage and SCB after 1, 2, and 6 weeks of daily loading in adult C57BL/6 mice[27,28]. A single bout of loading also induced disease initiation and progression, demonstrating that OA pathology in this model can be initiated by cell-mediated processes that are activated by mechanical loading[32].

In the present study, we sought to elucidate the role of SCB properties and remodeling on OA initiation and progression using our controlled, non-invasive, preclinical OA model. We utilized two mouse strains with different bone properties and used alendronate (ALN) treatment to inhibit bone remodeling to examine the respective roles of SCB properties and SCB remodeling on temporal changes in SCB plate and cartilage pathology. We hypothesized that mice with initially stiffer SCB would exhibit more severe disease and that the inhibition of bone remodeling using ALN would attenuate load-induced OA progression.

3.2 Methods

3.2.1 Mechanical Loading and Treatment Conditions

To examine the role of SCB properties on OA progression, we subjected two strains of mice with different bone mass and stiffness to compressive joint loading. We used 26-week-old male C57Bl/6 (B6) and FVB/NJ (FVB) mice, with FVB having higher bone mass and stiffness compared to B6 mice[33] (Figure 3.1A). To examine the role of SCB remodeling on OA, mice from both strains were randomly divided into 2 treatment groups: alendronate (ALN) to inhibit bone remodeling or vehicle saline control (VEH).

All mice were housed by strain in groups of four to five per cage with ad libitum access to food and water. At the start of the experiment, B6 and FVB mice weighed 30.7 ± 2.4g and

32.9 ± 2.6g, respectively. Body mass was measured 5 days/week to monitor the general health of each mouse over the duration of the experiment. A sample size of n = 6-7 was used per group based on a power analysis from previous data[27]. All experimental procedures occurred in the morning in a veterinary research facility. Mice were subjected to loading and treatment in random order within each cage. All procedures were approved by the Institutional Animal Care and Use Committee.

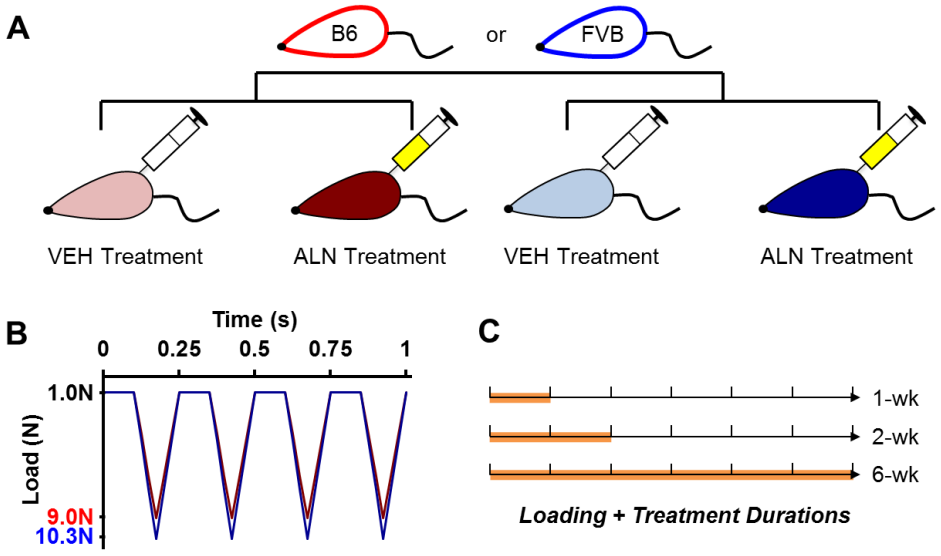

Figure 3.1 A) 26 week-old male C57Bl/6 (red) and FVB mice (blue) were administered alendronate (26μg/kg/day) or vehicle saline treatment for 1, 2, and 6 weeks (5 days/week). B) Concurrently, all mice were subjected to compressive tibial loading of the left limb at a peak load of 9N (B6) or 10.3N (FVB). The right limb served as the contralateral control. C) Mice were euthanized after 1, 2, and 6 weeks of loading and treatment (n = 5=7/group).

At 26 weeks, the left hindlimb of each mouse was subjected to *in vivo* cyclic compressive loading across the knee joint for 1, 2, or 6 weeks, 5 days/week (Figure 3.1B, C, n = 6-7/treatment/duration). Under general anesthesia (2% isoflurane, 1.0L/min, Webster, Devens, MA), B6 mice were loaded at 9.0N peak load, and FVB mice were loaded at 10.3N. These peak forces correspond to the loads required to generate 1200με of tension at the medial midshaft of

the tibia based on previous *in vivo* strain measurements with B6 mice[27,34] and a pilot strain gauge study with FVB mice. The loading protocol was applied for 1200 cycles (5 minutes) at a frequency of 4Hz based on previous studies[27]. The right limb served as a contralateral control. Concurrent with loading, each mouse was treated 5 days/week with ALN (26μg/kg/day ip, Sigma-Aldrich, St. Louis, MO) or VEH based on previous studies[35]. After 1, 2, or 6 weeks, the mice were euthanized. Both knee joints were dissected and fixed in 10% formalin overnight. One B6 mouse and three FVB mice were excluded, due to anesthesia-related death or excessive weight loss during loading.

3.2.2 Cartilage and Subchondral Bone Assessment

To assess bone morphological changes, intact joints were transferred to 70% ethanol after tissue fixation overnight, and scanned by microcomputed tomography (microCT) with a 10μm isotropic voxel resolution (μCT35, Scanco: 55kVp, 145μA, 600ms integration time). A 0.5mm aluminum filter was used to reduce the effects of beam hardening. In addition, with a scan resolution of 10μm, the voxel size is appropriately small relative to the cortical thickness, minimizing any error due to partial volume[36]. Knee joints were then decalcified in formic acid/sodium citrate for one week, dehydrated in an ethanol gradient, and embedded in paraffin. Serial coronal 6μm-thick sections were obtained (Leica RM2255, Germany). Safranin O/Fast green staining was performed on sections at 90μm intervals to assess cartilage morphology in the tibial plateau. Cartilage degradation was examined by a blinded observer using a modified murine cartilage histological scoring system[37] on the most posterior 180μm of the tibial plateau. Scores from the posterior medial and lateral plateaus were summed for our analyses, as these regions exhibited the most cartilage damage in previous studies[27,32].

Tibial SCB morphology was assessed using microCT in two volumes of interest (VOI): 1) the SCB plate, extending from the joint space to the epiphyseal cancellous bone, and 2) the epiphyseal cancellous bone. Mineralized tissue from the SCB plate and cancellous epiphysis were segmented using global thresholds. For the SCB plate VOI, cortical bone was manually contoured to assess average cortical plate thickness and tissue mineral density (TMD, mg HA/cm^3) in the medial and lateral tibial plateau. For the epiphyseal cancellous bone VOI, cancellous bone within the epiphysis was manually identified to measure cancellous bone volume fraction (BV/TV, mm^3/mm^3), trabecular thickness (Tb.Th, μm), trabecular separation (Tb.Sp, μm), and TMD.

We assessed localized cartilage and SCB plate thicknesses and osteophyte formation using sections stained with Safranin O/Fast green. The tibial plateau was divided into medial and lateral halves, and then further divided into anterior, middle, and posterior regions, resulting in six tibial plateau regions for evaluation. A single representative slide from each region was used to measure cartilage and local SCB plate thicknesses using previously established protocols[27]. In addition, osteophyte formation was examined at the margin of the posterior medial tibial plateau. Osteophyte maturity was measured based on previously established protocols[38] with scores of 0 (no osteophyte), 1 (mainly cartilaginous), 2 (cartilaginous/mineralized mixed tissue), and 3 (predominately mineralized osteophyte). Osteophyte size was measured as the maximum medial-lateral width of the tissue.

3.2.3 Statistical Analysis

All statistical analysis was performed using linear regression models (JMP Pro 10.0, SAS Institute Inc.). First, the effects of mouse strain and/or treatment were examined in the control

(right) limbs using a multiple linear regression model with fixed effects of mouse strain, treatment, duration, and their interactions. Then, to determine the effect of loading, differences between loaded and control limbs were calculated for each metric ([Loaded – Control] limb) and used in a multiple linear regression model with fixed effects as outlined above. In addition, a mixed multiple linear regression model was examined with fixed effects of limb, strain, treatment, duration, and interactions; a random mouse effect accounted for the repeated left-right limb measurement. Each model was optimized using backward elimination of interaction effects. For each linear regression model, we performed a residual analysis to ensure that the residuals were normally distributed and that the data exhibited homogenous variance. In the case of the bone morphology metrics (cancellous and cortical bone), one sample in the 1-week ALN-treated B6 group was an outlier, based on the residual analysis, and was excluded from all analyses of bone morphology. Tukey post-hoc comparisons were performed when interaction effects were significant. $p < 0.05$ indicated significance. All results presented are statistically significant unless otherwise stated.

3.3 Results

3.3.1 Intrinsic Differences in Bone and Cartilage due to Mouse Strain and Treatment

Control limbs of B6 and FVB mice had intrinsic differences in bone and cartilage morphology. FVB mice had significantly thicker SCB plates and higher epiphyseal cancellous bone mass than B6 mice due to thicker trabeculae and reduced Tb.Sp (Figure 3.2A-C, E). TMD was also higher in SCB and epiphyseal cancellous bone from FVB mice (Figure 3.2D, F). In both mouse strains, epiphyseal cancellous bone mass in control limbs decreased over time in VEH-treated mice. ALN treatment prevented age-related reductions in bone mass by increasing

Tb.Th and decreasing Tb.Sp (Figure 3.2A-C). ALN also significantly increased SCB plate and cancellous TMD over time (Figure 3.2D, F). SCB plate thickness increased with ALN only in control limbs of FVB mice, but not B6 control limbs (Figure 3.2E). Intrinsic cartilage properties differed in the mouse strains. Cartilage was thicker on the posterior, middle, and anterior aspects of the joint in FVB mice compared to B6 (Figure 3.3, middle & anterior data not shown). Based on average thickness values, ALN treatment had no effect on cartilage thickness in either mouse strain in this study. Generally, FVB mice had higher bone mass and thicker cartilage compared to B6 mice, and ALN prevented age-related cancellous bone loss in both mouse strains.

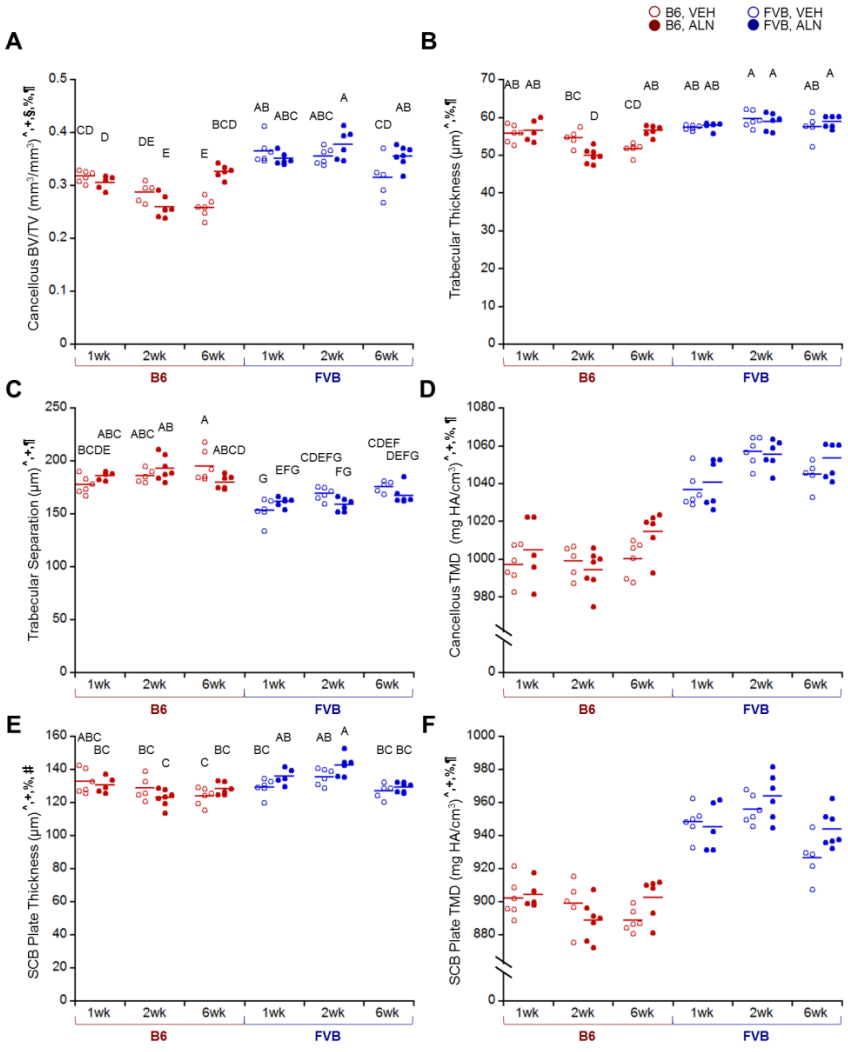

Figure 3.2 In control (right) limbs, FVB mice exhibited higher cancellous and cortical bone

mass than B6 mice, and ALN treatment inhibited bone remodeling. A) ALN prevented a decrease in BV/TV after 6 weeks, and FVB mice exhibited higher cancellous bone mass due to B) higher trabecular thickness and C) lower trabecular separation. FVB mice also had higher D) cancellous and F) cortical tissue mineral density and E) a thicker SCB plate, which was further increased with ALN treatment in FVB mice only. $p < 0.05$ for $^{\wedge}$strain, $^{+}$duration, §treatment, $^{\%}$strain*duration, $^{\sharp}$strain*treatment, ¶duration*treatment. Means sharing the same letter are not significantly different from each other by Tukey's HSD: A>B>C, $p<0.05$).

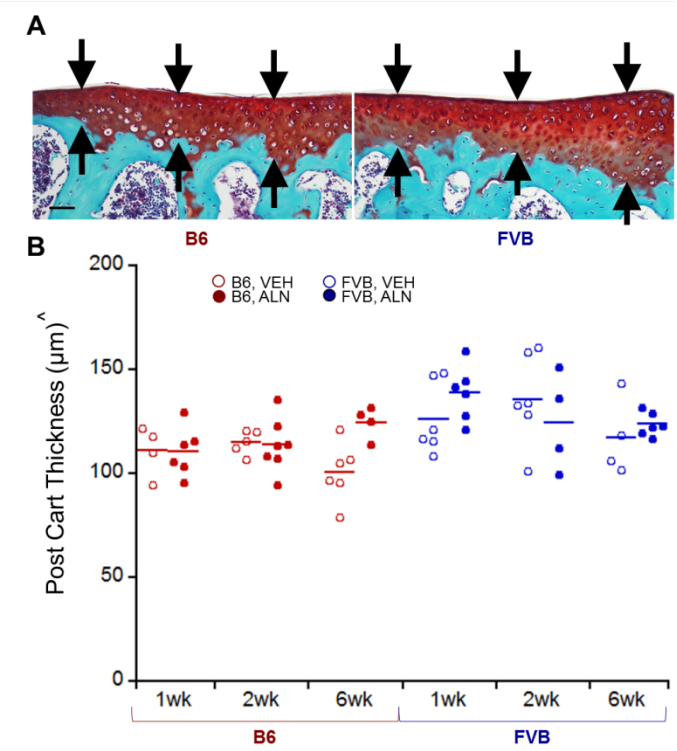

Figure 3.3 In control (right) limbs, cartilage was thicker in the posterior medial quadrant of FVB limbs than in the same region in B6 limbs. A) Representative posterior medial cartilage histology for B6 and FVB control limbs treated with VEH at 1 week, and B) quantitative cartilage thickness in B6 and FVB control limbs treated with VEH and ALN after 1, 2, and 6 weeks. Scale bar = 50μm. $p < 0.05$ for ^strain.

3.3.2 Load-Induced Subchondral Bone Adaptation was Mouse Strain-Specific

Loading and ALN treatment induced differential effects on SCB changes in the two mouse strains (Figure 3.4). Loading significantly thinned the SCB plate only in B6 mice after 6 weeks (Figure 3.4A), resulting in a 13% decrease in mean thickness regardless of treatment

based on microCT measurements (Table 3.1). Analysis of the local SCB plate thickness in B6 mice using histology showed a decrease in all aspects of the tibial plateau ranging from 2 – 50%, with the most thinning occurring in medial-middle and medial-anterior aspects. In contrast, SCB plate thickness was not altered with loading in FVB mice. Unlike SCB plate thickness, epiphyseal cancellous bone mass was not affected by loading in B6 mice; however, loading decreased cancellous bone mass in FVB mice regardless of treatment (Figure 3.5A). Cancellous and SCB plate TMD were also generally reduced in loaded limbs (Figure 3.5D, F). ALN treatment did not attenuate the load-induced reduction in SCB plate TMD in either strain. Loading decreased SCB plate TMD more over time in B6 compared to FVB limbs (Figure 3.5F). Loading affected only the SCB plate in B6 and only the cancellous bone in FVB mice. These load-induced responses were not attenuated by ALN treatment.

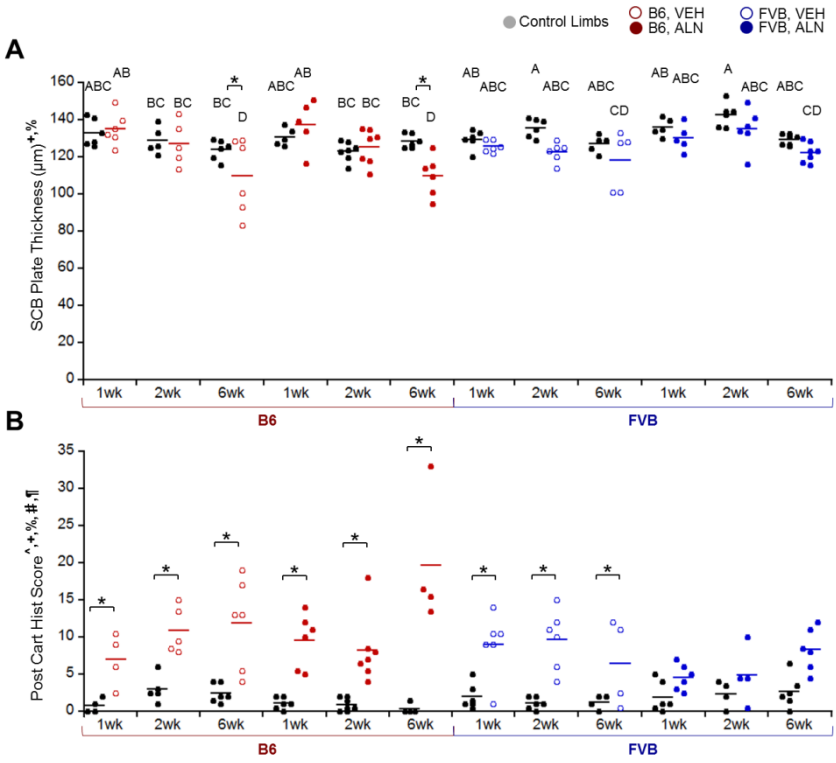

Figure 3.4 Control (right limb, black) and loaded (left limb) data shown. A) Loading thinned

SCB plate thickness at 6 weeks in B6 mice only. B) Loading damaged cartilage in most groups except the FVB, ALN group. $p < 0.05$ for ^strain, +duration, §treatment, %strain*duration, ♯strain*treatment, ¶duration*treatment, *load. Means sharing the same letter are not significantly different from each other by Tukey's HSD: A>B>C, $p<0.05$).

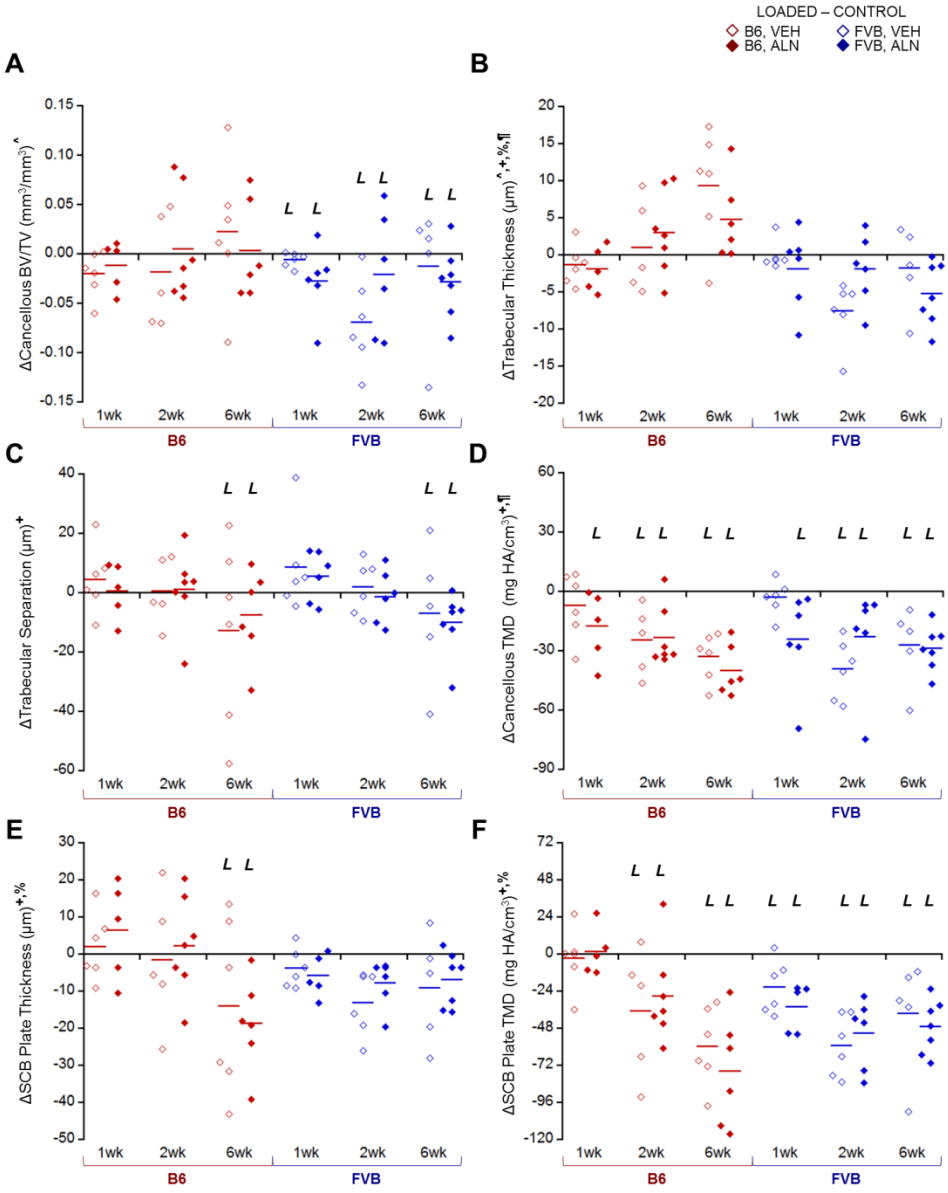

Figure 3.5 Loading affected cancellous and cortical SCB morphology in B6 and FVB mice treated with VEH and ALN after 1, 2, and 6 weeks. Δ = [Loaded – Control] (left – right limb) data shown. A) Loading decreased cancellous bone volume fraction in FVB mice only, due to combined effects in B) trabecular thickness and C) trabecular separation. D) Loading decreased cancellous TMD and E) SCB plate thickness more so in B6 mice than FVB. F) Cortical TMD was also generally decreased with loading. $p < 0.05$ for ^strain, +duration, §treatment, %strain*duration, ♯strain*treatment, ¶duration*treatment. ***L*** indicates load effect ($p<0.05$).

Table 3.1 Posterior, medial, and lateral cartilage score, thickness, and SCB plate measurements of control and loaded limbs in B6 and FVB mice treated with VEH and ALN after 1, 2, and 6 weeks of loading. $p<0.05$ for [a]strain, [b]limb, [c]strain*limb, [d]strain*treatment, [e]duration*treatment, [f]limb*duration, [g]strain*duration*limb [h]strain*treatment*limb, [i]strain*duration*treatment.

			Vehicle Treatment						Alendronate Treatment					
			1 week		2 week		6 week		1 week		2 week		6 week	
			Control	**Loaded**	Control	**Loaded**	Control	**Loaded**	Control	**Loaded**	Control	**Loaded**	Control	**Loaded**
Cartilage Score	B6	Medial[bcfg]	0.3±0.5	3.0±2.3	0.5±0.5	6.5±1.4	0.5±0.8	8.4±5.6	0.1±0.2	5.0±3.0	0.1±0.2	4.6±3.4	0.3±0.5	14.3±2.6
		Lateral[bcdhi]	0.5±1.0	4.0±1.8	2.5±2.0	4.4±1.9	1.9±1.1	3.5±1.4	1.0±0.8	4.5±1.2	0.9±0.9	3.6±2.9	0.1±0.3	2.2±2.1
	FVB	Medial[bcfg]	0.4±0.8	4.3±3.1	0.0±0.0	4.5±3.6	0.1±0.3	4.5±4.7	0.9±1.4	1.8±1.3	0.0±0.0	3.4±3.4	0.17±0.25	5.2±2.4
		Lateral[bcdhi]	1.6±1.2	4.7±1.9	1.1±0.8	5.2±2.9	1.1±0.9	2.0±1.5	1.0±0.8	2.8±1.5	2.4±1.8	1.5±0.9	2.5±2.1	3.2±1.2
Cartilage Thickness (μm)	B6	Medial[ab]	108±13	80±18	108±14	79±12	95±22	69±12	102±17	83±11	109±23	87±11	121±4	72±12
		Lateral[abefh]	114±23	101±11	122±6	86±13	107±14	87±11	119±10	93±15	119±18	93±16	129±10	79±28
	FVB	Medial[ab]	122±28	113±20	130±28	99±15	114±20	95±20	143±20	120±23	123±41	90±10	119±11	101±9
		Lateral[abefh]	130±15	109±26	141±23	98±6	121±18	94±19	134±14	132±24	127±15	93±17	129±11	112±15
SCB Plate Thickness (μm)	B6	Medial[b]	70±12	79±26	68±20	47±11	73±16	57±19	72±29	62±16	75±30	56±20	72±15	73±27
		Lateral[g]	71±9	64±11	53±10	49±14	52±21	58±12	56±18	53±14	51±15	54±24	56±21	62±7
	FVB	Medial[b]	84±23	57±17	74±15	55±13	62±32	59±38	68±9	62±11	70±18	54±17	56±33	61±26
		Lateral[g]	50±12	56±13	51±11	40±11	45±6	45±19	43±8	60±11	54±19	37±7	60±16	38±7

3.3.3 Articular Cartilage Pathology with Loading

Loading generally increased cartilage matrix loss and thinning over time. As in our previous study[27], cartilage damage was localized to the posterior aspect of the tibial plateau, with more damage occurring on the medial posterior aspect. The degree of cartilage pathology depended on mouse strain and treatment (Figure 3.6). Specifically, on the posterior aspect of the tibia, loading increased cartilage matrix loss compared to contralateral limbs in all groups except FVB mice treated with ALN (pooled across all treatment durations) (Figure 3.4B). FVB mice exhibited less cartilage pathology with loading compared to B6 mice (32% lower histological damage score). ALN-treated B6 mice had the most extensive cartilage matrix changes compared to all other groups after 6 weeks of loading. Local cartilage thinning also occurred with loading and increased with loading duration particularly on both the lateral and medial posterior joint aspects, regardless of mouse strain or treatment (Table 3.1). Cartilage thickness changes with loading ranged from a 21% decrease in the posterior medial aspect to a 23% increase in the anterior lateral aspect. While loading induced cartilage damage in both mouse strains, FVB mice exhibited less pathology compared to B6 mice.

3.3.4 Osteophyte Formation with In Vivo Loading

Loading induced pre-osteophyte or osteophyte formation in all but one mouse (FVB mouse, 1 week, VEH-treated). Osteophytes matured from primarily cartilaginous to mineralized tissue over longer load durations (Figure 3.7). Osteophytes in FVB mice were less mature, smaller, and slower growing compared to those in B6 mice (Figure 3.7B, C). ALN inhibited osteophyte maturation compared to VEH treatment, but did not affect osteophyte size. Osteophytes were absent in control limbs. Osteophytes occurred with loading, indicative of OA

pathology; however, osteophytes in loaded FVB limbs were less mature and smaller than those in B6 limbs.

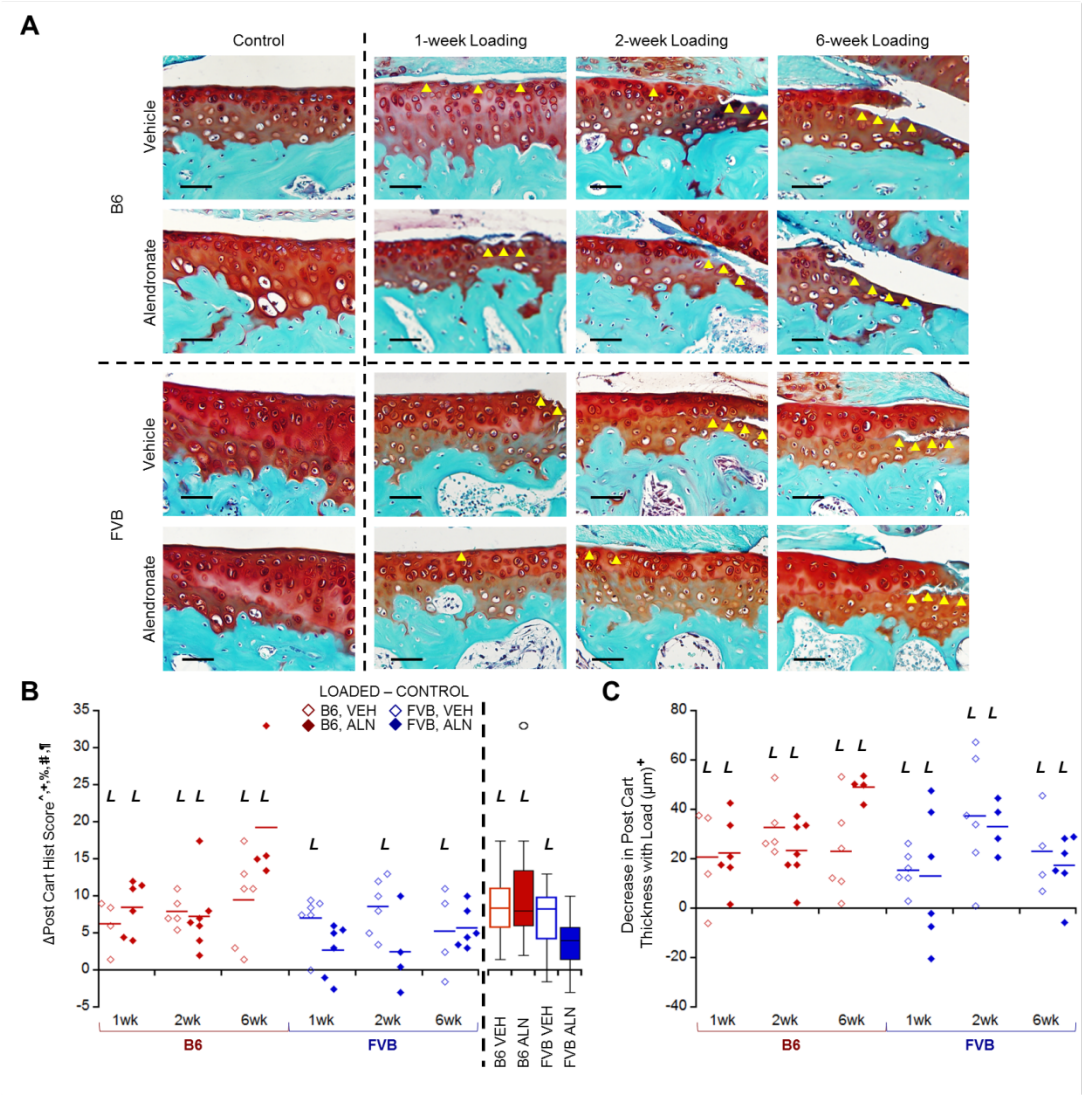

Figure 3.6 Loading damaged posterior cartilage matrix in B6 and FVB mice treated with VEH and ALN after 1, 2, and 6 weeks. Δ = [Loaded – Control] (left – right limb) data shown. (A) In most groups, loading created cartilage damage that increased over time as was reflected in the histological scores. (B) FVB mice treated with ALN did not exhibit cartilage damage with loading (pooled group means summarized in box plot). (C) Loading also decreased posterior cartilage thickness over time. Scale bar = 50μm. $p<0.05$ for ^strain, +duration, §treatment, %strain*duration, ♯strain*treatment, ¶duration*treatment. ***L*** indicates load effect ($p<0.05$). Yellow arrowheads indicate areas of cartilage damage.

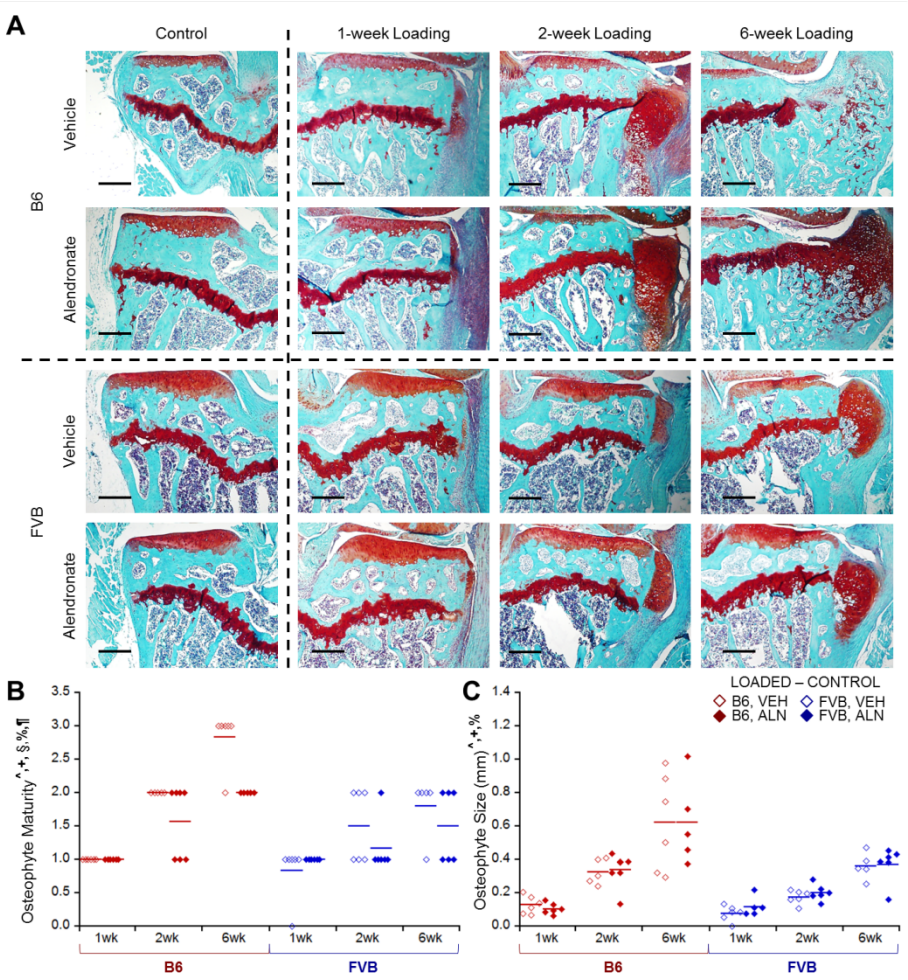

Figure 3.7 Loading induced osteophytes, which were smaller in FVB mice. A) Loading induced visible osteophytes that matured and grew over time. B) ALN treatment slowed maturation of osteophytes, which were also C) smaller in FVB mice. Scale bar = 250µm. $p<0.05$ for ^strain, +duration, §treatment, %strain*duration, ♯strain*treatment, ¶duration*treatment.

3.4 Discussion

In this study, we examined the role of SCB properties and changes in OA initiation and progression. We used two mouse strains with different bone properties and ALN treatment to inhibit bone changes, with the objective of examining OA pathology in both cartilage and SCB morphology. Our results confirmed the presence of significant intrinsic differences between FVB and B6 mouse strains in bone mass and stiffness and in responses to the inhibition of bone

remodeling with ALN treatment. In control limbs, FVB mice had a thicker SCB plate, higher epiphyseal cancellous bone mass, and higher bone mineral density than B6 mice. Furthermore, FVB mice had stiffer diaphyseal cortical bone as reflected by the higher load (10.3N) needed to engender +1200με at the mid-diaphysis of the tibia. While we did not directly measure SCB plate stiffness in this study, differences in cortical bone material properties between FVB and B6 mice were assessed by our strain calibration and have been assessed previously by mechanical loading[33]. Based on these diaphyseal data, we assume that FVB mice had stiffer SCB compared to B6 mice. Similar to previous preclinical studies[39], ALN prevented age-related reductions in cancellous bone mass. ALN treatment also increased the cancellous and SCB plate TMD over time in control limbs, indicating that the treatment was indeed effective in inhibiting bone remodeling in both cancellous and cortical bone[35,40]. These findings support the validity of our experimental approach to examine the role of intrinsic differences in bone properties and bone remodeling on the progression of load-induced OA joint pathology.

Non-invasive cyclic compression induced OA cartilage pathology and osteophyte formation in both mouse strains. We did not observe any ligament tears in this study. Similar to previous studies[27,28], loading generally led to reduced proteoglycan content, cartilage surface fibrillation, cartilage matrix thinning, osteophyte formation, and subchondral and epiphyseal cancellous bone adaptation, recapitulating OA progression. Lower initial SCB mass and stiffness in B6 mice did not attenuate load-induced OA severity compared to FVB mice. In fact, FVB mice exhibited less cartilage pathology and slower-growing and less mature osteophytes, consistent with diminished OA severity.

Cyclic loading induced differential effects on bone adaptation in the tibiae of B6 and FVB mice. In B6 mice, loading thinned the SCB plate, particularly after 6 weeks. In contrast,

loading decreased only the epiphyseal cancellous bone mass in FVB mice and did not affect SCB plate thickness. No increase in bone mass was detected in either strain over time. Ko *et al.*[27] reported a reduction in epiphyseal cancellous bone with daily loading in B6 mice, accompanied by localized thickening of the SCB plate. These contradictory outcomes could reflect the difficulty of distinguishing between calcified cartilage and SCB using microCT; however, localized SCB plate thickness measured by histology also did not increase with loading (Table 3.1). In several preclinical studies[15,16] SCB plate thickness decreased initially, followed by thickening as OA progressed. Thus, either our time points were too distant to detect subtle temporal changes in SCB plate thickness, or at 6 weeks post-loading the mice were still in the early stages of OA development.

Inhibiting bone remodeling had differential effects on cartilage and bone adaptation to loading in the two mouse strains. ALN treatment exacerbated cartilage pathology in B6 mice after 6 weeks of loading, but protected FVB limbs from load-induced cartilage changes. Unlike other preclinical studies[17–21], ALN treatment in our study did not consistently protect against cartilage pathology during OA progression. However, the lack of chondro-protection with ALN treatment is similar to the results found in a comprehensive clinical study[25]. Changes in cancellous and SCB plate bone mass and mineralization with loading depended on the mouse strain. Loading initially decreased cancellous TMD in both ALN- and VEH-treated groups; however, cancellous TMD was maintained without further loss thereafter with ALN treatment. Differences in these data compared to results obtained in post-traumatic injury models of OA may reflect the non-invasive nature of our model compared to the surgical intervention required in other models[32]. In this study, ALN generally did not inhibit load-induced changes in bone and had differential effects on cartilage changes depending on mouse strain. The limited effect of

ALN treatment on OA pathology could be due to the timing of treatment. Pre-treatment of bisphosphonates prior to OA induction may be more effective at attenuating bone changes and OA pathology[41]. Future studies could examine the use of higher doses or longer term ALN treatment to effectively inhibit load-induced changes in bone.

The results of our study do not support our initial hypothesis that intrinsically lower SCB mass and stiffness attenuate OA progression. Radin and Rose[9] first hypothesized that increased SCB mass and stiffness would diminish shock absorption by bone and increase stresses in the cartilage surface. However, Burr and others,[3,11] employing a model involving the insertion of a metal plug in the subchondral cancellous bone, demonstrated that increasing apparent SCB stiffness did not exacerbate cartilage damage. Our results using mice with intrinsically different SCB stiffness led to a similar conclusion.

The use of two mouse strains to test the contribution of intrinsic bone and cartilage physical properties to the development of OA joint pathology did not account for differences in intrinsic cartilage thickness and potential differences in bone and cartilage metabolism between the two strains. ALN treatment was chondro-protective in FVB mice as a group (all ALN treatment durations pooled), but exacerbated cartilage pathology in B6 mice. This seemingly contradictory result suggests that alternate factors determined the severity of OA progression in the different mouse strains, possibly related to differences in intrinsic strain, differences in cartilage thickness, or genetic variations in bone and cartilage homeostasis. Specifically, B6 mice with intrinsically thinner cartilage exhibited significant thinning of the SCB plate with loading, accompanied by severe cartilage pathology and osteophyte formation. In contrast, FVB mice with intrinsically thicker cartilage, when treated with ALN, did not display significant changes in SCB plate thickness or mineralization over time and exhibited diminished OA severity. Similar

findings were reported in another load-induced OA model in which intrinsically thicker cartilage in Str/ort mice correlated with diminished cartilage loss[42]. Based on FEA simulations in that prior study, increased cartilage thickness reduced the contact stresses, which accounted for the attenuated cartilage damage. Furthermore, genetic differences in bone remodeling between the two mouse strains were not examined and could play a significant role in our results. Future studies using mouse strains with established differences in cartilage thickness and/or differential patterns of bone and cartilage metabolism would permit assessment of these factors. Alternately, these factors could be minimized to eliminate their potential confounding contribution to load-induced OA.

While ALN treatment effectively reduced bone remodeling with age in control limbs, changes in bone with loading were still present. In addition, although we used ALN in our studies to target SCB remodeling, ALN treatment may not exclusively affect bone and may also directly affect cartilage metabolism[43]. We did not specifically examine the effect of ALN treatment on chondrocytes and macrophages, but we saw no effect of treatment on cartilage structure by histology. While ALN could affect chondrocytes and macrophages, these cells might not be involved in load-based adaptation, as is the case with the studies of Sugiyama *et al*.[44] in which they speculate that the increase in bone with loading was mediated by down-regulation of sclerostin in osteocytes, an effect that was not blocked by bisphosphonate treatment. Regardless of the ALN treatment effect on these cells, their role in load-induced tissue changes is unknown. Future studies should investigate the role of chondrocytes and macrophages on load-induced tissue adaptation. Although ALN effectively reduced bone remodeling by inhibiting bone resorption, alternate approaches for modulating SCB bone properties, for example by inhibiting sclerostin activity represent additional experimental approaches to test our hypothesis.

We used two different peak loads based on in vivo strain gauge data for B6 and FVB mice. Whereas the use of different peak loads for each mouse strain may appear to be a limitation, we intentionally controlled the strain induced on the bone. Bone surface strains during peak activity are remarkably well conserved across mammals[45]. Therefore, we used the loads to induce +1200 μstrain at the mid-diaphysis as a metric to equilibrate the applied loads across animals of different strains and ages. The body mass and skeleton of the FVB mouse are larger than those of the B6 mouse, suggesting that the loads engendered during normal activities would be higher and consistent with the higher loads needed to produce similar mechanical strains in the two mouse strains. Furthermore, we were interested in the effect of bone on OA progression in the cartilage, thus we controlled the stimulation (strain) engendered on the bone. Because we equalized the stimulation on the bone regardless of mouse strain, we can distinguish the role of bone mass/stiffness on cartilage degradation.

In conclusion, contrary to our prediction, we found that intrinsically lower SCB properties were not associated with attenuated load-induced cartilage pathology. This result may be related, in part, to intrinsic differences in cartilage thickness, although this hypothesis needs to be tested. Our findings that inhibition of bone remodeling produced differential patterns of OA pathology in animals with low or high SCB properties indicate that SCB properties and remodeling do affect the progression of load-induced OA cartilage pathology. These data support the utility of the compressive loading model for defining the roles of SCB plate properties and remodeling on the pathogenesis of OA.

3.5 REFERENCES

1. Lawrence RC, Felson DT, Helmick CG, Arnold LM, Choi H, Deyo RA, Gabriel S, Hirsch R, Hochberg MC, Hunder GG, Jordan JM, Katz JN, Kremers HM, Wolfe F, National Arthritis Data Workgroup. Estimates of the prevalence of arthritis and other rheumatic conditions in the United States. Part II. *Arthritis Rheum*. 2008;58(1):26-35. doi:10.1002/art.23176.
2. Wieland HA, Michaelis M, Kirschbaum BJ, Rudolphi KA. Osteoarthritis - an untreatable disease? *Nat Rev Drug Discov*. 2005;4(4):331-344. doi:10.1038/nrd1693.
3. Burr DB, Schaffler MB. The Involvement of Subchondral Mineralized Tissues in Osteoarthrosis : Quantitative Microscopic Evidence. *Microsc Res Tech*. 1997;37:343-357. doi:10.1002/(SICI)1097-0029(19970515)37:4<343::AID-JEMT9>3.0.CO;2-L.
4. Culley KL, Dragomir CL, Chang J, Wondimu EB, Coico J, Plumb DA, Otero M, Goldring MB. Mouse models of osteoarthritis: surgical model of posttraumatic osteoarthritis induced by destabilization of the medial meniscus. *Methods Mol Biol*. 2015;1226:143-173. doi:10.1007/978-1-4939-1619-1_12.
5. Felson DT. Osteoarthritis: New Insights. Part 1: The Disease and Its Risk Factors. *Ann Intern Med*. 2000;133(8):635. doi:10.7326/0003-4819-133-8-200010170-00016.
6. Cameron KL, Hsiao MS, Owens BD, Burks R, Svoboda SJ. Incidence of physician-diagnosed osteoarthritis among active duty United States military service members. *Arthritis Rheum*. 2011;63(10):2974-2982. doi:10.1002/art.30498.
7. Lohmander LS, Gerhardsson de Verdier M, Rollof J, Nilsson PM, Engström G. Incidence of severe knee and hip osteoarthritis in relation to different measures of body mass: a population-based prospective cohort study. *Ann Rheum Dis*. 2009;68(4):490-496. doi:10.1136/ard.2008.089748.
8. Radin E, Paul I, Rose R. Role of mechanical factors in pathogenesis of primary osteoarthritis. *Lancet*. 1972;299(7749):519-522. doi:10.1016/S0140-6736(72)90179-1.
9. Radin EL, Rose RM. Role of subchondral bone in the initiation and progression of cartilage damage. *Clin Orthop Relat Res*. 1986;(213):34-40.
10. Radin EL, Martin RB, Burr DB, Caterson B, Boyd RD, Goodwin C. Effects of mechanical loading on the tissues of the rabbit knee. *J Orthop Res*. 1984;2(3):221-234. doi:10.1002/jor.1100020303.
11. Brown TD, Radin EL, Martin RB, Burr DB. Finite element studies of some juxtarticular stress changes due to localized subchondral stiffening. *J Biomech*. 1984;17(1):11-24.
12. Burr DB. The importance of subchondral bone in the progression of osteoarthritis. *J Rheumatol Suppl*. 2004;70:77-80.
13. Li G, Yin J, Gao J, Cheng TS, Pavlos NJ, Zhang C, Zheng MH, Grynpas M, Alpert B, Katz I, Lieberman I, Pritzker K, Suri S, Walsh D, Madry H, Dijk C van, Mueller-Gerbl M, Burr D, et al. Subchondral bone in osteoarthritis: insight into risk factors and microstructural changes. *Arthritis Res Ther*. 2013;15(6):223. doi:10.1186/ar4405.
14. Kawcak CE, McIlwraith CW, Norrdin RW, Park RD, James SP. The role of subchondral bone in joint disease: a review. *Equine Vet J*. 2010;33(2):120-126. doi:10.1111/j.2042-3306.2001.tb00589.x.
15. Hayami T, Pickarski M, Zhuo Y, Wesolowski GA, Rodan GA, Duong LT. Characterization of articular cartilage and subchondral bone changes in the rat anterior cruciate ligament transection and meniscectomized models of osteoarthritis. *Bone*.

2006;38(2):234-243. doi:10.1016/j.bone.2005.08.007.
16. Botter SM, Van Osch GJVM, Clockaerts S, Waarsing JH, Weinans H, Van Leeuwen JPTM. Osteoarthritis induction leads to early and temporal subchondral plate porosity in the tibial plateau of mice: An in vivo microfocal computed tomography study. *Arthritis Rheum*. 2011;63(9):2690-2699. doi:10.1002/art.30307.
17. Muehleman C, Green J, Williams JM, Kuettner KE, Thonar EJ-MA, Sumner DR. The effect of bone remodeling inhibition by zoledronic acid in an animal model of cartilage matrix damage. *Osteoarthr Cartil*. 2002;10(3):226-233. doi:10.1053/joca.2001.0506.
18. Hayami T, Pickarski M, Wesolowski GA, Mclane J, Bone A, Destefano J, Rodan GA, Duong LT. The role of subchondral bone remodeling in osteoarthritis: Reduction of cartilage degeneration and prevention of osteophyte formation by alendronate in the rat anterior cruciate ligament transection model. *Arthritis Rheum*. 2004;50(4):1193-1206. doi:10.1002/art.20124.
19. Hayami T, Zhuo Y, Wesolowski GA, Pickarski M, Duong LT. Inhibition of cathepsin K reduces cartilage degeneration in the anterior cruciate ligament transection rabbit and murine models of osteoarthritis. *Bone*. 2012;50(6):1250-1259. doi:10.1016/j.bone.2012.03.025.
20. Myers SL, Brandt KD, Burr DB, O'Connor BL, Albrecht M. Effects of a bisphosphonate on bone histomorphometry and dynamics in the canine cruciate deficiency model of osteoarthritis. *J Rheumatol*. 1999;26(12):2645-2653.
21. Siebelt M, Waarsing JH, Groen HC, Müller C, Koelewijn SJ, de Blois E, Verhaar JAN, de Jong M, Weinans H. Inhibited osteoclastic bone resorption through alendronate treatment in rats reduces severe osteoarthritis progression. *Bone*. 2014;66:163-170. doi:10.1016/j.bone.2014.06.009.
22. Fleisch H. Bisphosphonates: Mechanisms of Action. *Endocr Rev*. 1998;19(1):80-100. doi:10.1210/edrv.19.1.0325.
23. Russell RGG, Watts NB, Ebetino FH, Rogers MJ. Mechanisms of action of bisphosphonates: similarities and differences and their potential influence on clinical efficacy. *Osteoporos Int*. 2008;19(6):733-759. doi:10.1007/s00198-007-0540-8.
24. Spector TD, Conaghan PG, Buckland-Wright JC, Garnero P, Cline GA, Beary JF, Valent DJ, Meyer JM, Dixon T, Shaw M, Ebrahim S, Dieppe P, Millar W, Melzer D, Guralnik J, Brock D, Quam J, Michet C, et al. Effect of risedronate on joint structure and symptoms of knee osteoarthritis: results of the BRISK randomized, controlled trial [ISRCTN01928173]. *Arthritis Res Ther*. 2005;7(3):R625. doi:10.1186/ar1716.
25. Bingham CO, Buckland-Wright JC, Garnero P, Cohen SB, Dougados M, Adami S, Clauw DJ, Spector TD, Pelletier JP, Raynauld JP, Strand V, Simon LS, Meyer JM, Cline GA, Beary JF. Risedronate decreases biochemical markers of cartilage degradation but does not decrease symptoms or slow radiographic progression in patients with medial compartment osteoarthritis of the knee: Results of the two-year multinational knee osteoarthritis st. *Arthritis Rheum*. 2006;54(11):3494-3507. doi:10.1002/art.22160.
26. Holyoak DT, Tian YF, van der Meulen MCH, Singh A. Osteoarthritis: Pathology, Mouse Models, and Nanoparticle Injectable Systems for Targeted Treatment. *Ann Biomed Eng*. 2016;44(6):2062-2075. doi:10.1007/s10439-016-1600-z.
27. Ko FC, Dragomir C, Plumb DA, Goldring SR, Wright TM, Goldring MB, van der Meulen MCH. In vivo cyclic compression causes cartilage degeneration and subchondral bone changes in mouse tibiae. *Arthritis Rheum*. 2013;65(6):1569-1578. doi:10.1002/art.37906.

28. Poulet B, Hamilton RW, Shefelbine S, Pitsillides AA. Characterizing a novel and adjustable noninvasive murine joint loading model. *Arthritis Rheum*. 2011;63(1):137-147. doi:10.1002/art.27765.
29. Turner CH, Akhter MP, Raab DM, Kimmel DB, Recker RR. A noninvasive, in vivo model for studying strain adaptive bone modeling. *Bone*. 1991;12(2):73-79. doi:10.1016/8756-3282(91)90003-2.
30. Fritton J, Myers E, Wright T, van der Meulen M. Loading induces site-specific increases in mineral content assessed by microcomputed tomography of the mouse tibia. *Bone*. 2005;36(6):1030-1038. doi:10.1016/j.bone.2005.02.013.
31. Adebayo OO, Ko FC, Goldring SR, Goldring MB, Wright TM, van der Meulen MCH. Kinematics of meniscal- and ACL-transected mouse knees during controlled tibial compressive loading captured using roentgen stereophotogrammetry. *J Orthop Res*. 2016;(April 2016):1-23. doi:10.1002/jor.23285.
32. Ko FC, Dragomir CL, Plumb DA, Hsia AW, Adebayo OO, Goldring SR, Wright TM, Goldring MB, van der Meulen MCH. Progressive cell-mediated changes in articular cartilage and bone in mice are initiated by a single session of controlled cyclic compressive loading. *J Orthop Res*. 2016;(October 2015):n/a-n/a. doi:10.1002/jor.23204.
33. Wergedal JE, Sheng MH-C, Ackert-Bicknell CL, Beamer WG, Baylink DJ. Genetic variation in femur extrinsic strength in 29 different inbred strains of mice is dependent on variations in femur cross-sectional geometry and bone density. *Bone*. 2005;36(1):111-122. doi:10.1016/j.bone.2004.09.012.
34. Lynch ME, Main RP, Xu Q, Schmicker TL, Schaffler MB, Wright TM, van der Meulen MCH. Tibial compression is anabolic in the adult mouse skeleton despite reduced responsiveness with aging. *Bone*. 2011;49(3):439-446. doi:10.1016/j.bone.2011.05.017.
35. Misof BM, Roschger P, Baldini T, Raggio CL, Zraick V, Root L, Boskey AL, Klaushofer K, Fratzl P, Camacho NP. Differential effects of alendronate treatment on bone from growing osteogenesis imperfecta and wild-type mouse. *Bone*. 2005;36(1):150-158. doi:10.1016/j.bone.2004.10.006.
36. Bouxsein ML, Boyd SK, Christiansen BA, Guldberg RE, Jepsen KJ, Müller R. Guidelines for assessment of bone microstructure in rodents using micro-computed tomography. *J Bone Miner Res*. 2010;25(7):1468-1486. doi:10.1002/jbmr.141.
37. Glasson SS, Chambers MG, Van Den Berg WB, Little CB. The OARSI histopathology initiative – recommendations for histological assessments of osteoarthritis in the mouse. *Osteoarthr Cartil*. 2010;18:S17-S23. doi:10.1016/j.joca.2010.05.025.
38. Little CB, Barai A, Burkhardt D, Smith SM, Fosang AJ, Werb Z, Shah M, Thompson EW. Matrix metalloproteinase 13-deficient mice are resistant to osteoarthritic cartilage erosion but not chondrocyte hypertrophy or osteophyte development. *Arthritis Rheum*. 2009;60(12):3723-3733. doi:10.1002/art.25002.
39. Rodan GA, Seedor JG, Balena R. Preclinical pharmacology of alendronate. *Osteoporos Int*. 1993;3(S3):7-12. doi:10.1007/BF01623001.
40. Camacho NP, Raggio CL, Doty SB, Root L, Zraick V, Ilg WA, Toledano TR, Boskey AL. A controlled study of the effects of alendronate in a growing mouse model of osteogenesis imperfecta. *Calcif Tissue Int*. 2001;69(2):94-101.
41. Strassle BW, Mark L, Leventhal L, Piesla MJ, Jian Li X, Kennedy JD, Glasson SS, Whiteside GT. Inhibition of osteoclasts prevents cartilage loss and pain in a rat model of degenerative joint disease. *Osteoarthr Cartil*. 2010;18(10):1319-1328.

doi:10.1016/j.joca.2010.06.007.
42. Poulet B, Westerhof TA, Hamilton RW, Shefelbine SJ, Pitsillides AA. Spontaneous osteoarthritis in Str/ort mice is unlikely due to greater vulnerability to mechanical trauma. *Osteoarthr Cartil*. 2013;21(5):756-763. doi:10.1016/j.joca.2013.02.652.
43. Dombrecht EJ, De Tollenaere CB, Aerts K, Cos P, Schuerwegh AJ, Bridts CH, Van Offel JF, Ebo DG, Stevens WJ, De Clerck LS. Antioxidant effect of bisphosphonates and simvastatin on chondrocyte lipid peroxidation. *Biochem Biophys Res Commun*. 2006;348(2):459-464. doi:10.1016/j.bbrc.2006.07.075.
44. Sugiyama T, Meakin LB, Galea GL, Jackson BF, Lanyon LE, Ebetino FH, Russell RGG, Price JS. Risedronate does not reduce mechanical loading-related increases in cortical and trabecular bone mass in mice. *Bone*. 2011;49(1):133-139. doi:10.1016/j.bone.2011.03.775.
45. Rubin CT. Skeletal strain and the functional significance of bone architecture. *Calcif Tissue Int*. 1984;36(S1):S11-S18. doi:10.1007/BF02406128.

CHAPTER 4

COMPUTATIONAL MODELS FOR THE ANALYSIS OF LOAD-INDUCED OSTEOARTHRITIS

4.1 Introduction

Mechanical forces have been implicated in the initiation and progression of osteoarthritis (OA)[1–3]. A degenerative joint disease, OA is characterized by cartilage degradation, subchondral bone changes and osteophyte formation, leading to radiographic joint narrowing and loss of joint function[1,4–6]. Abnormal forces from joint instability due to injury[1,7], excessive physical activity[8,9] and obesity[10,11] have been associated with higher risks of OA. Studies have also suggested that moderate exercise and reduced loading may serve as beneficial treatment options for the attenuation of the disease[11–13]. In addition, tissue changes such as subchondral bone sclerosis suggest that tissue properties may also play a critical role in the joint's response to abnormal loads during disease progression[14–22].

Although several preclinical models have investigated the biological progression of the disease due to induced joint instability[23–27], few have explored the relationship between mechanical forces, tissue material properties, and OA initiation *in vivo*[17,28–30]. Instead, most studies have focused on isolating and exploring the relationship between cartilage and mechanical forces *ex vivo*[31–34]. Elucidating the joint stresses associated with tissue degeneration in OA progression *in vivo* would provide valuable knowledge regarding loads that may be detrimental to the joint, and loads that may serve as potential beneficial treatment options. Furthermore, examining how changes to the joint tissues affect joint stresses during disease would enable better understanding of the relationship between mechanical forces and OA *in vivo*.

The non-invasive tibial loading model provides a controlled mechanical setting to

examine the relationship between mechanical forces and tissue degradation during disease progression. Previous studies using this model have evaluated the biological and structural progression of the disease, which develops in response to controlled mechanical loading[35,36] with consistent joint kinematics[30]. Cyclic tibial compressive loading induced OA progression after a single loading bout[37] and after daily loading for 1, 2, and 6 weeks[35,36,38]. However, only one study to date has investigated the contact stresses in the joint associated with load-induced OA progression in this model,[29] with contact stresses reported only at the peak compressive load of 12N. Thus, contact behavior throughout each load cycle is still unknown. Furthermore, the effect of tissue material properties on joint contact stresses under loading has not been explored in this model.

In this study, we quantified the average and peak cartilage contact stresses and their spatial distribution during compressive tibial loading using experimental joint kinematics data and discrete element analysis (DEA). In addition, we evaluated the effect of changes in bone and cartilage tissue material properties on peak cartilage stresses using a simplified finite element (FE) contact model. We hypothesized that the spatial distribution and localization of highest contact stresses calculated computationally would correlate to areas of greatest tissue damage observed experimentally. We further hypothesized that differences in bone and cartilage material properties would lead to changes in stresses induced on the cartilage surface, thus providing a potential explanation of the relationship between mechanical forces, tissue properties, and OA progression in the joint.

4.2 Methods

4.2.1 Kinematic Analysis

The left knee joints of 12 adult C57Bl/6 (B6) cadaver male mice were labeled with radiopaque bone fiducial markers and subjected to compressive tibial loading from 0 to 9N as previously described[30] (Figure 4.1A). Briefly, roentgen stereophotogrammetric analysis (RSA) was performed to evaluate quasi-static joint kinematics at every 1N increment during loading. Using a custom-made calibration cage and a dental x-ray, radiographs of the labeled joint were taken at 2 planes at each increment of loading. Each joint was subjected to 3 loading trials. The exact three-dimensional location of each bone marker was then calculated. The Eulerian method for rigid body kinematics was used to quantify the absolute translation and rotation of the tibia and the relative motion of the femur to the tibia from 0 to 9N.

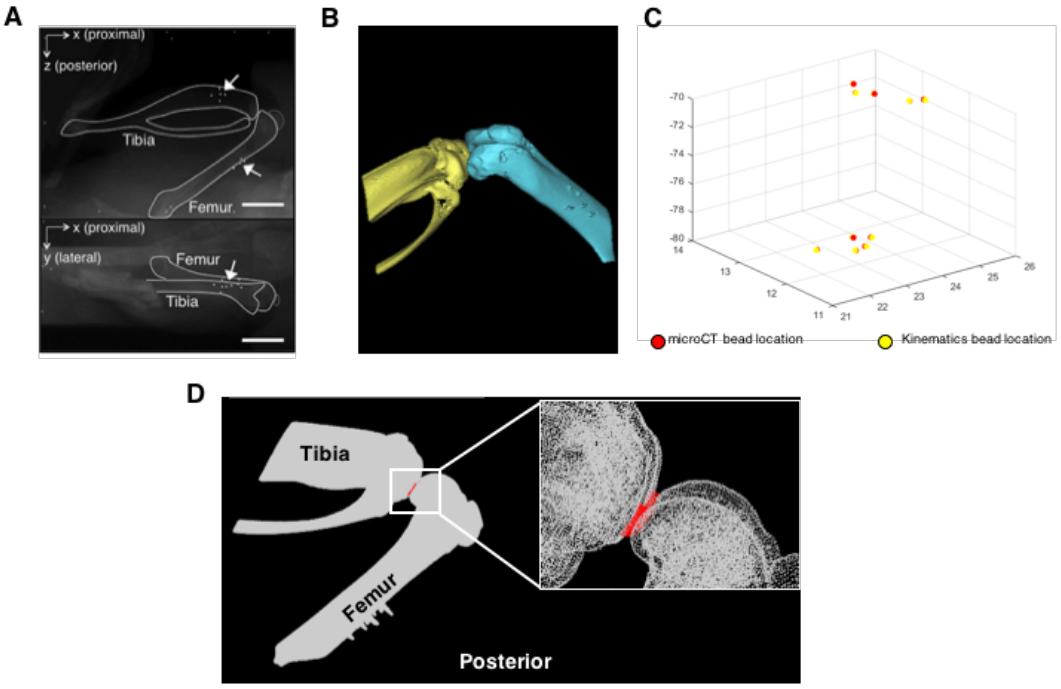

Figure 4.1 A) Knee joint kinematics was analyzed using roentgen stereophotogrammetric analysis (RSA). B) One sample was scanned via microCT, manually contoured, and C) Bead locations from RSA and microCT were matched, resulting in D) point clouds of each geometry with cartilage (red) between the two surfaces for discrete element analysis. Arrows denote beads in RSA.

4.2.2 Discrete Model Development

One labeled joint was scanned via micro computed tomography (μCT, GE eXplore CT-120) at a 25μm resolution. This joint served as the model geometry for discrete element analysis. The scan was then converted to a solid model using Materialise Mimics Research software (Plymouth, MI). The femur, tibia, and bone markers were manually contoured, resulting in three separate surface geometries (Figure 4.1B). These geometries were meshed with a triangular surface and exported as point clouds for DEA. DEA has been used extensively to study articular contact mechanics in which the articulating bone are considered rigid and the cartilage tissues are regarded as a set of individual compressive springs[39–42]. This numerical technique has been validated by experimental measurements and finite element models[41,43,44]. DEA provides a simple yet accurate framework to calculate compressive cartilage contact stresses, especially in situations for which experimental measurement techniques are difficult, as is the case here due to animal size.

Using a custom-written Matlab code, the tibia and femur were registered and aligned to RSA joint locations at 0N compressive load, as determined by the common location of each bone marker (Figure 4.1C, D). With kinematics data from RSA for all samples, DEA was conducted at every 1N increment of compressive loading, and point clouds of the tibia and femur were transformed and oriented to correct locations from 0-9N accordingly. Because the cartilage was not visualized in the microCT scan, the tissue was assumed to be a uniform 100μm thick on both the tibial and femoral surfaces. Using previously established DEA protocols[40,41,45], the elastic spring contact model was utilized to determine contact stresses in the tibial cartilage. Spring stiffness (k) and contact stress (σ) were calculated as follows:

$$k = \frac{E(1-\nu)}{(1+\nu)(1-2\nu)h} \qquad \sigma = k\delta,$$

where E is the cartilage Young's modulus, ν is Poisson's ratio, h is the assumed total cartilage thickness (200μm) and δ is the deformation in the tibial cartilage as determined by the distance between the tibial and femoral surfaces, resolved along the normal vectors on the tibial surface. Based on previous literature[46,47], the Young's modulus and Poisson's ratio of cartilage were assumed to be 6MPa and 0.47, respectively. The average forces acting on the tibial surface were also calculated by multiplying the total contact area by the average compressive stress calculated for each tibial plateau.

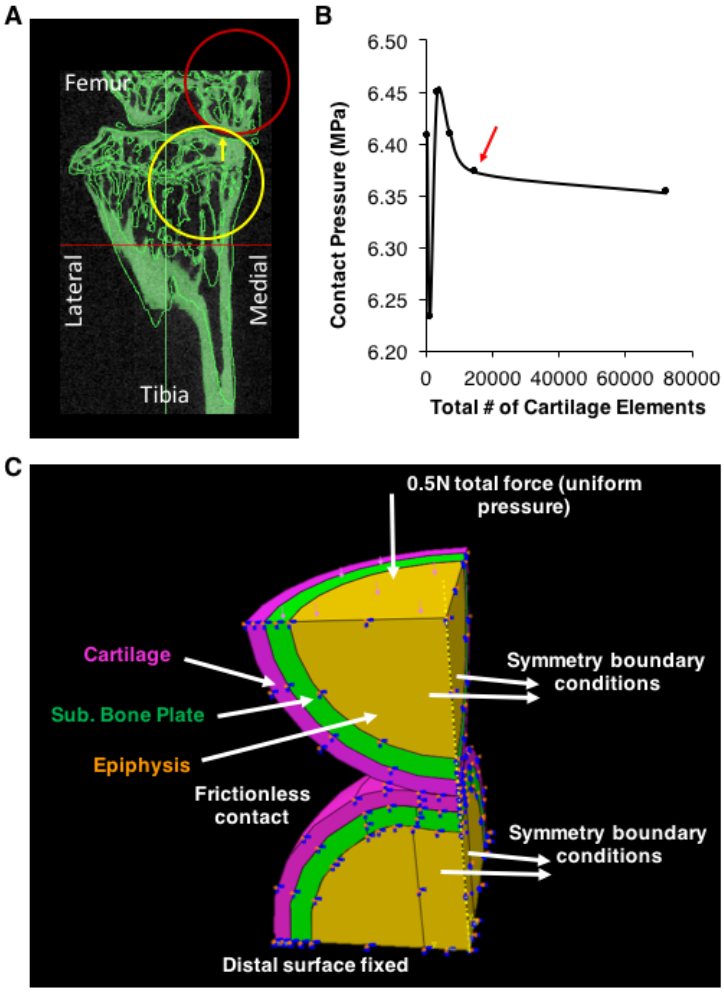

Figure 4.2 A) Tibial (yellow) and femoral (red) radii of curvature were measured on the medial aspect of the joint. In addition, the radius of curvature and depth of the tibial concavity (yellow arrow) was also measured, resulting in C) an FEA simplified geometric contact model with the noted boundary conditions. B) Mesh convergence analysis concluded that approximately 15000 cartilage elements (red arrow) were required for accurate contact pressure results.

4.2.3 Sample Measurements for Finite Element Model

A simplified FE model was developed to validate the results from the discrete element model and to conduct a parametric analysis to evaluate the effects of changing joint tissue properties on cartilage stresses during loading. Six right knee joints from adult C57Bl/6 male mice were scanned using μCT at 10μm resolution (μCT35, Scanco: 55kVp, 145μA, 600ms integration time). Each scan was converted to a solid geometry in Materialise Mimics Research software. We measured the approximate radius of curvature of the medial tibial plateau and femoral condyle by fitting circles to each surface. We also measured the radius of concavity on the tibial medial plateau and the depth of the concavity from the intercondylar eminence (Figure 4.2A). Cartilage and subchondral bone thickness measurements were obtained from Safranin O-stained histological slides and approximated for the purposes of the FE model.

4.2.4 Simple Contact Finite Element Model

Using the average geometric measurements from the samples, semi-spherical shell geometries were created with the appropriate radii for the tibial and femoral surfaces (Figure 4.2C). The tibia also included a concavity with the appropriate depth as measured from the μCT scans (Figure 4.2A). The outermost layer for each geometry was cartilage, modeled as a linear elastic tissue with a uniform thickness of 100μm, Young's Modulus of 6MPa, and Poisson's ratio of 0.47 (Table 4.1). Adjacent to the cartilage was the subchondral cortical bone layer with a uniform thickness of 130μm, Young's modulus of 18GPa, and Poisson's ratio of 0.3, material

property values obtained from the literature [48]. The rest of the each semi-spherical geometry was modeled as cancellous epiphyseal bone with Young's modulus of 568 MPa and Poisson's ratio of 0.3, as calculated using the average epiphyseal bone volume fraction in each tibia[49]. Tied constraints were modeled between both the epiphyseal and subchondral cortical layers and the cortical and cartilage layers, and frictionless contact was modeled between the tibial and femoral cartilage surfaces. To decrease computational expense and due to the symmetry of the model, only a quarter model was created, and symmetry boundary conditions were applied to appropriate surfaces (Figure 4.2C).

All parts were meshed with linear 8-node brick elements. The element size on each cartilage surface was refined during a mesh convergence analysis. A 0.5N total force was applied to the proximal surface of the cancellous and cortical bone, and the distal surface of the tibia remained fixed in all directions. Mesh convergence was conducted to determine the minimum element density on each cartilage surface that would result in the most accurate measures of contact pressures. An element density was chosen such that any further increase in element density would result in less than 1% change in resulting contact pressure and maximum principal stress. Thus, the cartilage on the tibial and femoral surfaces was meshed with approximately 8100 and 6825 elements, respectively (Figure 4.2B).

Discrete Element Analysis Validation by Finite Element Model

To validate the compressive stresses determined using DEA, the average contact forces calculated on the medial tibial plateau from 0 to 9N were applied to the simplified contact geometry. At each load, a quarter of the average contact force on the medial plateau was applied to account for the quarter geometry in the FE model. Peak contact stresses were then compared

in the two models from 0 to 9N.

4.2.5 Parametric Analysis

A parametric analysis was conducted on the simple contact FE model to examine the effects of changes in tissue properties and mass on the stresses induced on the cartilage surface. Variations in cartilage modulus and thickness, subchondral bone modulus and thickness, and epiphyseal cancellous modulus were examined (Figure 4.3, Table 4.1). Specifically, in addition to the normal geometry, altered geometries included a 50% decrease and 100% increase in cartilage and bone thicknesses and moduli. Changes in contact pressure and maximum principal stress and strain at the cartilage surface and on cortical and cancellous bone were examined.

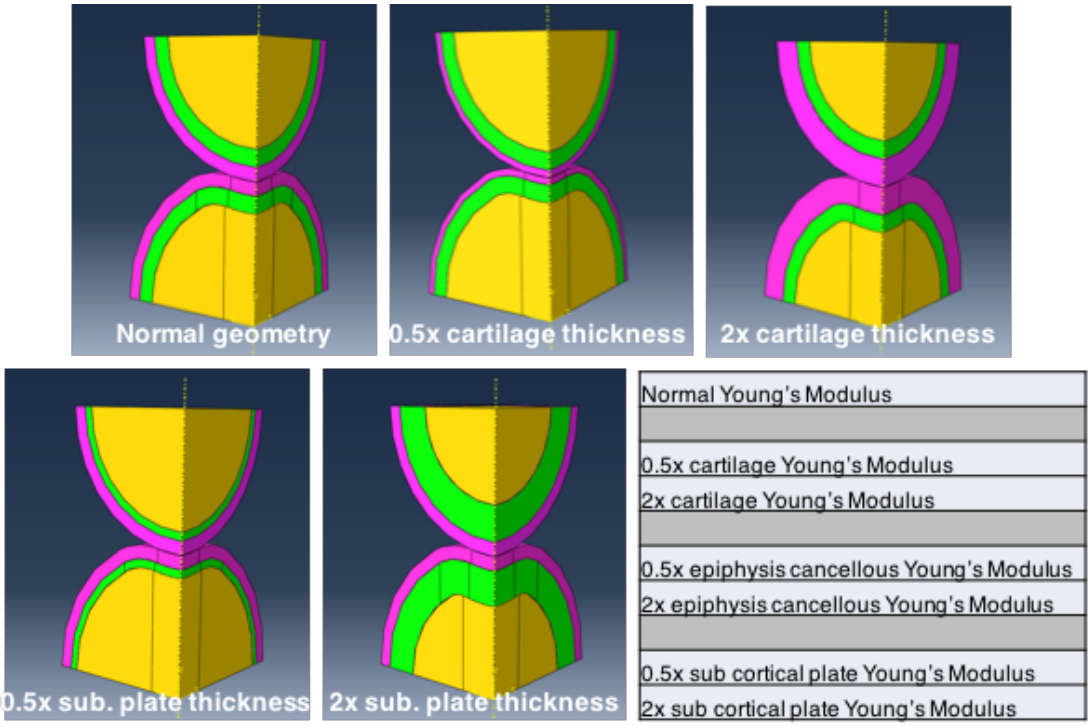

Figure 4.3 Geometric and material property values for the parametric analysis conducted on the simple contact finite element model. Cartilage layer in purple; subchondral cortical plate in green; epiphyseal geometry in yellow.

Table 4.1 Geometric and material property values for the parametric analysis conducted on the simple contact finite element model

	Cartilage			Subchondral Cortical Plate			Epiphyseal Cancellous Bone	
	Thickness (μm)	Young's Modulus (MPa)	Poisson's Ratio	Thickness (μm)	Young's Modulus (MPa)	Poisson's Ratio	Young's Modulus (MPa)	Poisson's Ratio
Normal Geometry	100	6	0.47	130	18000	0.3	568	0.3
0.5 Cartilage Thickness	50	6	0.47	130	18000	0.3	568	0.3
2x Cartilage Thickness	200	6	0.47	130	18000	0.3	568	0.3
0.5 Cartilage E	100	3	0.47	130	18000	0.3	568	0.3
2x Cartilage E	100	12	0.47	130	18000	0.3	568	0.3
0.5 Sub Plate Thickness	100	6	0.47	65	18000	0.3	568	0.3
2x Sub Plate Thickness	100	6	0.47	260	18000	0.3	568	0.3
0.5 Sub Plate E	100	6	0.47	130	9000	0.3	568	0.3
2x Sub Plate E	100	6	0.47	130	36000	0.3	568	0.3
0.5 Epi Cancellous E	100	6	0.47	130	18000	0.3	284	0.3
2x Epi Cancellous E	100	6	0.47	130	18000	0.3	1136	0.3

4.3 Results

4.3.1 Compressive Loading Results in Two Distinct Contact Behaviors

The results of the kinematics analysis of joints under loading have been published previously[30]. The tibia translated primarily anteriorly and proximally with little rotation around all axes as loading increased. In terms of relative femur to tibia motion, knee flexion increased as loading increased from 0 to 9N. Using the tibial and femoral locations from 0 to 9N, corresponding contact stresses were calculated using DEA. Due to the assumption of 100μm uniform cartilage thicknesses on the tibial and femoral surface, 0N load engendered an initial average compressive stress of 1.00MPa with a peak compressive stress of 4.60MPa on the tibial cartilage surface.

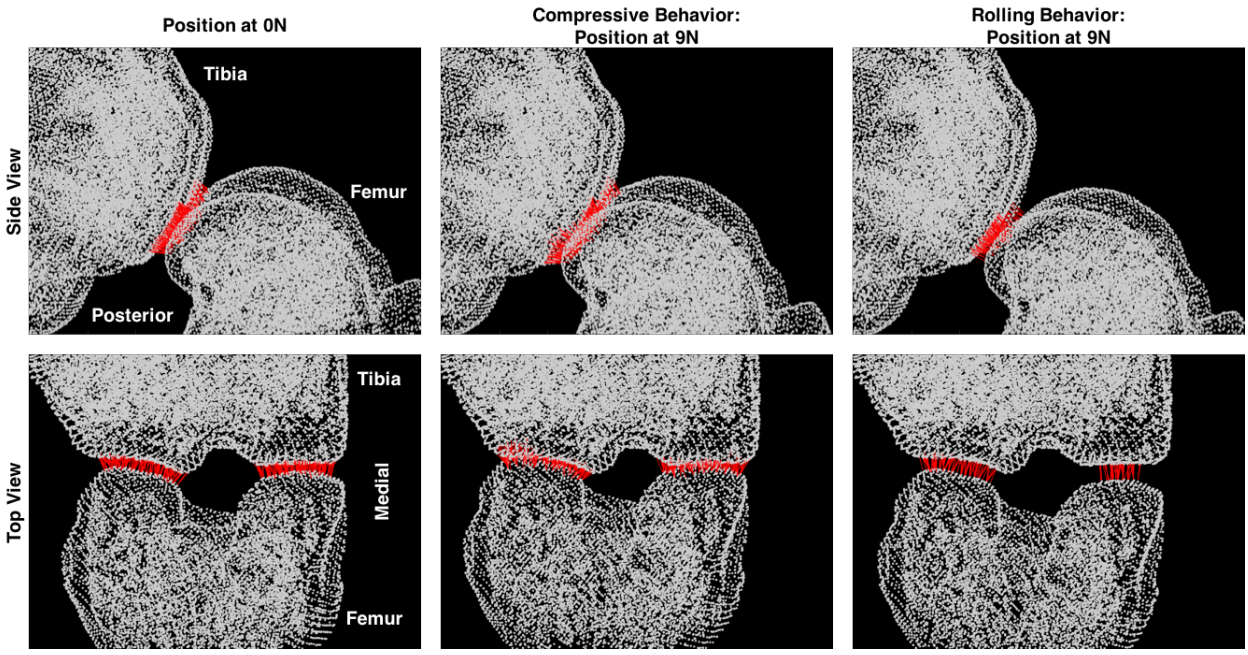

Figure 4.4 Side and top views of a trial exhibiting compressive behavior and a trial exhibiting rolling behavior as seen by comparing the 0N and 9N positions.

As tibial loading increased from 0 to 9N, two distinct behavior were observed. Regardless of individual samples, 19 out of 36 trials exhibited primarily compression of the

cartilage between the tibial and femoral surfaces as knee flexion increased with loading. In contrast, 17 trials exhibited "rolling" of the femoral surface away from the tibia as loading increased, resulting in no increased cartilage compression with load (Figure 4.4).

For trials that exhibited primarily compressive behavior, the average compressive stress increased from 1.00MPa at 0N to 2.82 ± 1.43MPa (mean ± standard deviation) at 9N, with peak compressive stress ranging from 4.60MPa to 8.98 ± 2.20MPa as the load increased (Figure 4.5A, B). Strain values averaged 2.78% (12.75% peak strain) at 0N to 7.82 ± 3.97% (24.91 ± 6.11% peak strain) at 9N (Figure 4.5C, D). The average forces acting on each tibial plateau increased to 2.19 ± 1.25 and 2.71 ± 1.37N at 9N load for the medial and lateral plateaus, respectively (Figure 4.5E). Peak contact stresses/strains occurred in the middle of each tibial plateau at 0N, and moved posteriorly, increasing in magnitude as loading increased (Figure 4.5F).

For trials exhibiting "rolling" of the femoral surface, the average compressive stress decreased as loading increased. Average stresses ranged from 1.00MPa at 0N to 0.35 ± 0.21MPa at 9N, with peak stresses of 4.60MPa and 3.57 ± 0.92MPa at 0 and 9N loads, respectively (Figure 4.6A, B). Average compressive strain values ranged from 2.78% to 0.97 ± 0.06% from 0 to 9N (Figure 4.6C). The average forces acting on each tibial plateau ranged from 1.00 to 0.33 ± 0.27N for the medial plateau and 0.78 to 0.29 ± 0.23N for the lateral plateau, as loading increased to 9N (Figure 4.6E). While peak contact stresses/strains did not increase with load, the locations of peak contact stresses moved posteriorly as loading increased from 0 to 9N (Figure 4.6F).

To ensure that the two loading behaviors were not a function of creep errors due to quasi-static kinematic measurements at every 1N increment of load, we also evaluated 5 samples that were loaded directly from 0 to 9N. Four out of five samples exhibited compressive behavior with

an average peak stress of 7.70 ± 1.83MPa at 9N, while one exhibited rolling behavior with a peak stress of 4.19MPa at 9N, thus confirming the two contact behaviors during tibial compressive loading.

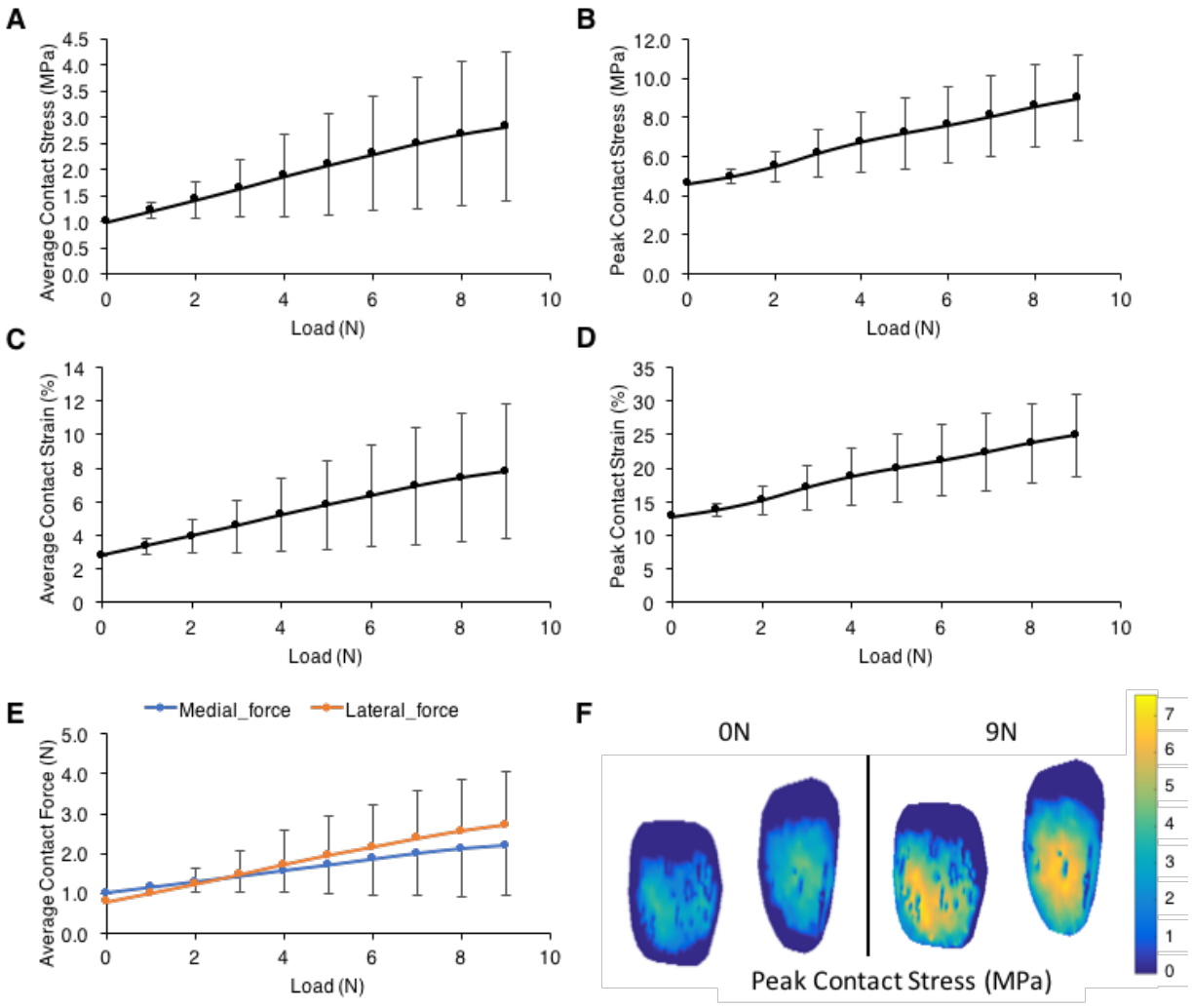

Figure 4.5 In trials exhibiting compressive behavior, A) average and B) peak contact stresses increased with load. C) Average and D) peak contact strains also increased with load. E) Contact forces increased in magnitude with load, and F) peak contact stresses translated posteriorly as loading increased.

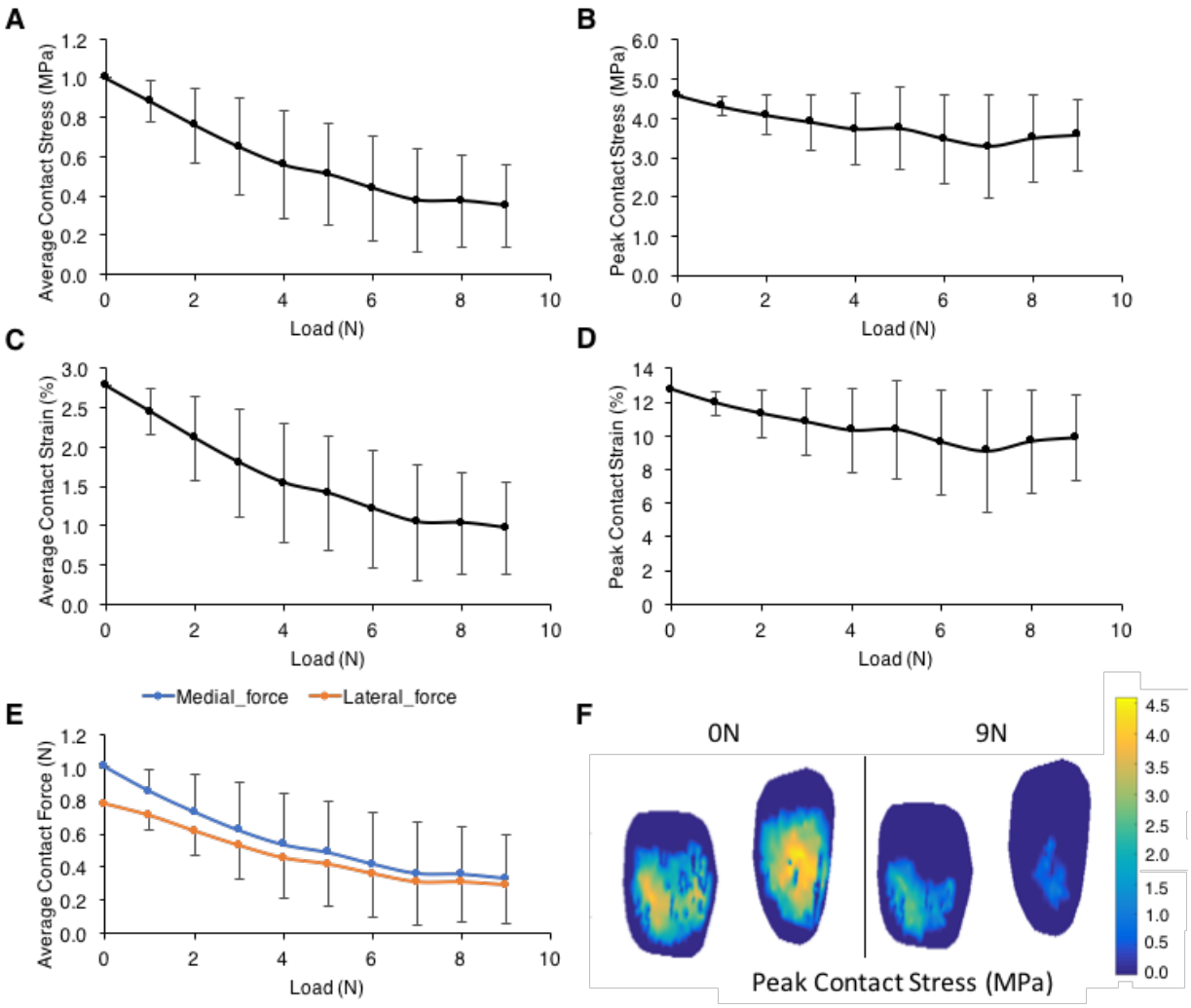

Figure 4.6 In trials exhibiting rolling behavior, A) average and B) peak contact stresses decreased with load. C) Average and D) peak contact strains also decreased with load. E) Contact forces decreased in magnitude with load, and F) peak contact stresses translated posteriorly as loading increased.

4.3.2 Simple Finite Element Contact Model Validates DEA Peak Compressive Stresses

To validate the contact results from DEA, peak loads calculated specifically from trials exhibiting compressive behavior were applied to the simple FE model. Peak compressive stresses were similar between the FE and DEA models (Figure 4.7A). The greatest difference in calculated peak compressive stresses occurred at 0N with a 21% difference between DEA and FEA results. These differences reduced as the load increased, with a minimum difference in

compressive stress of 3.6% at 8N between the two models. Such small differences in calculated stresses between DEA and FEA validate the contact results from the discrete element analysis.

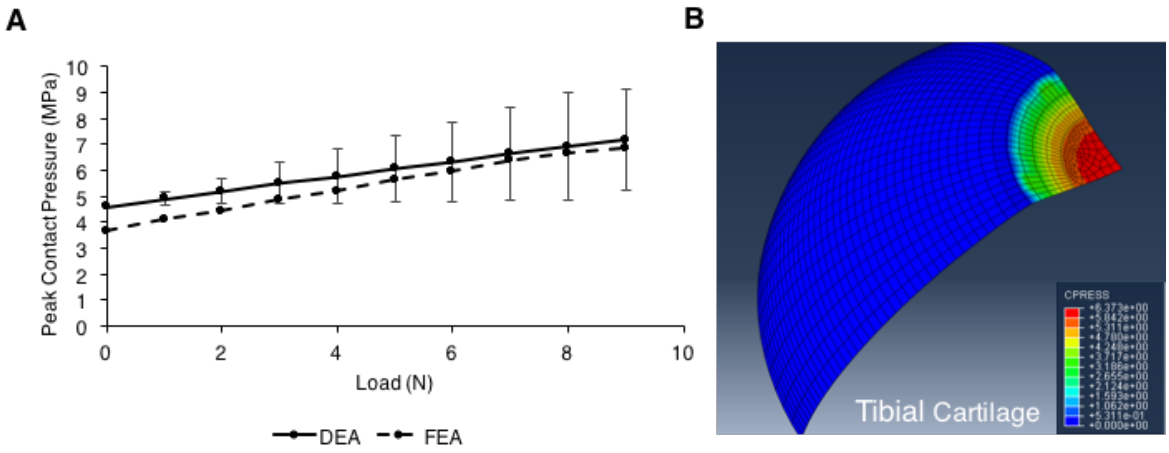

Figure 4.7 A) Peak contact pressures calculated using finite element analysis validated contact stress values determined by discrete element analysis. B) A 0.5N compressive load resulted in a peak contact stress of 6.37MPa in the middle of the tibial cartilage surface.

4.3.3 Only Cartilage Changes Affected Cartilage Contact Pressure in Simplified Finite Element Model

Parametric analyses evaluating the effects of permutations in cartilage and bone material and geometric properties on contact stresses revealed that changes to the cartilage had significant effects on contact mechanics at the joint (Figure 4.8, Table 4.2). Normal joint geometry and properties resulted in a peak contact pressure of 6.37MPa in the middle of the tibial cartilage surface (Figure 4.7B). A 50% decrease in cartilage thickness resulted in a 29% increase in contact pressure (8.20MPa), while doubled thickness led to a 23% decrease in contact pressure (4.92MPa). Furthermore, a 50% decrease in cartilage Young's modulus accounted for a 12% decrease in contact pressure, while a doubled Young's modulus resulted in a 14% increase in contact pressure. Changes in subchondral cortical and cancellous bone Young's modulus and in

cortical thickness did not significantly affect contact pressures on the cartilage surface. Differences in contact pressure with bone changes ranged from a 1.05% decrease to a 0.42% increase depending on bone material or thickness change.

Furthermore, changes in bone material properties also affected bone stresses; however, these changes affected cortical and cancellous bone stresses differently (Table 4.2). A decrease in cancellous Young's modulus led to increased peak stresses in cortical bone and decreased stresses in cancellous bone. In addition, decreased cortical Young's modulus led to decreased stresses in the cortical bone and increased stresses in the cancellous bone.

Because bone is responsive to dynamic strains values[16], we also reported strains in this study. Trends in bone strains generally followed the same patterns as bone stresses, except for changes in bone properties, for which decreased cancellous and cortical Young's moduli led to increased cancellous and cortical peak strains, respectively (Table 4.2).

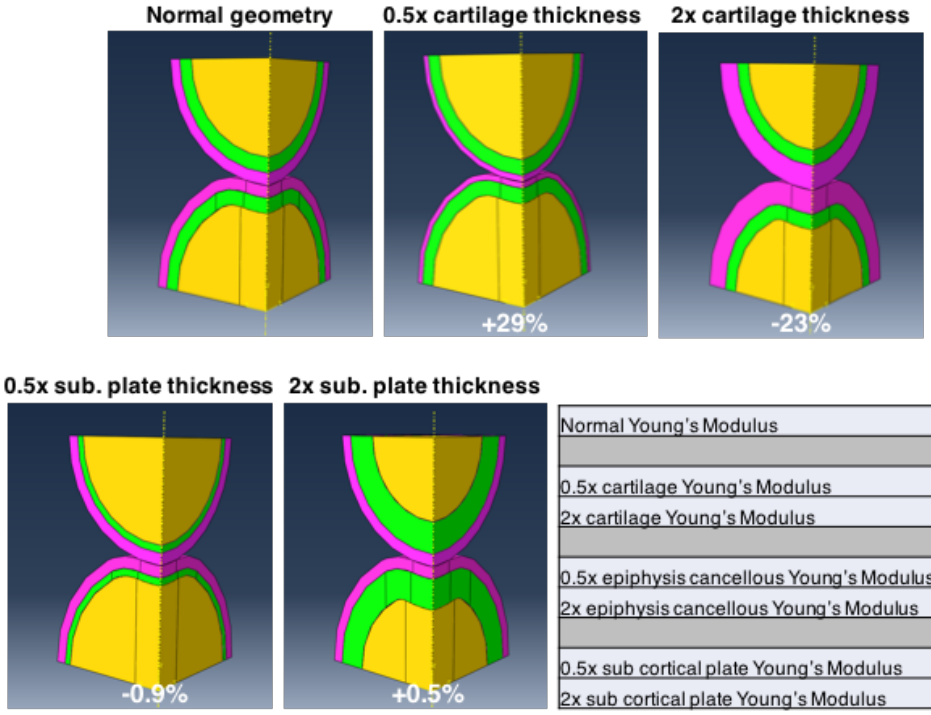

Normal Young's Modulus	---
0.5x cartilage Young's Modulus	-12%
2x cartilage Young's Modulus	+14%
0.5x epiphysis cancellous Young's Modulus	-0.2%
2x epiphysis cancellous Young's Modulus	+0.3%
0.5x sub cortical plate Young's Modulus	-0.3%
2x sub cortical plate Young's Modulus	+0.3%

Figure 4.8 Percent changes in contact pressure on cartilage surface due to changes in thicknesses and Young's moduli of joint tissues

Table 4.2 Peak contact pressure and max principal stresses and strains induced on the cartilage, subchondral plate and cancellous bone due to changes in tissue geometry or Young's modulus

	Cartilage			Subchondral Cortical Plate		Epiphyseal Cancellous Bone	
	Peak Contact Pressure (MPa)	Max Principal Stress (MPa)	Max Principal Strain (%)	Max Principal Stress (MPa)	Max Principal Strain (%)	Max Principal Stress (MPa)	Max Principal Strain (%)
Normal Geometry	6.37	-6.36	-0.39	-20.24	-8.59E-04	-2.23	-3.61E-03
0.5 Cartilage Thickness	8.20	-8.20	-0.34	-25.14	-9.59E-04	-2.73	-4.48E-03
2x Cartilage Thickness	4.92	-4.56	-0.49	-9.09	-4.93E-04	-1.54	-2.51E-03
0.5 Cartilage E	5.61	-5.59	-0.68	-18.84	-8.04E-04	-2.06	-3.32E-03
2x Cartilage E	7.24	-7.22	-0.23	-21.12	-8.73E-04	-2.35	-3.84E-03
0.5 Sub Plate Thickness	6.31	-6.29	-0.39	-20.46	-1.04E-03	-4.30	-6.59E-03
2x Sub Plate Thickness	6.40	-6.38	-0.39	-9.28	-3.35E-04	-0.64	-1.09E-03
0.5 Sub Plate E	6.35	-6.33	-0.39	-12.76	-1.17E-03	-2.94	-4.76E-03
2x Sub Plate E	6.39	-6.37	-0.39	-28.10	-5.31E-04	-1.49	-2.41E-03
0.5 Epi Cancellous E	6.36	-6.34	-0.39	-27.41	-1.04E-03	-1.48	-4.79E-03
2x Epi Cancellous E	6.39	-6.37	-0.39	-12.88	-5.95E-04	-2.96	-2.40E-03

4.4 Discussion

This study is the first to examine contact stresses in the joint under compressive loading using both discrete element and finite element analyses. We have demonstrated that the compressive tibial loading model results in two contact behaviors – a primarily compressive behavior and a femoral "rolling" behavior. In trials that exhibited compressive contact behavior, maximum contact pressure increased from 4.60MPa at 0N to approximately 9MPa at 9N. The failure or flexural strength of cartilage previously calculated in cyclic compression studies ranges between 15 and 50MPa, and depends on loading frequencies[50,51]. Although these stress values are higher than 9MPa calculated in our study, cartilage surface fibrillations have been demonstrated to occur with as little as 8MPa under static compression[52,53], or 3-7MPa over 10000 compressive cycles with an indenter[54]. Thus, the application of 9MPa over multiple bouts of 1200 compressive cycles at 4Hz is likely sufficient to induce cartilage surface damage *in vivo*. Such values may also explain the lack of macroscopic cartilage damage after a single tibial loading bout, as 1200 cycles may not be enough cycles to induce cracks on the cartilage surface. The applied contact pressure at 9N over multiple loading bouts likely leads to cartilage damage on the surface that may progress through its thickness with each additional loading bout.

Previous studies in humans[55–57] and preclinical models[45,58] have measured cartilage contact pressures in the normal knee during ambulation from 0.5 to 4MPa[59,60]. Thus, pressures exhibited in this study particularly with compressive behavior exceeded cartilage pressures measured in normal healthy tissue, also possibly explaining the cartilage damage observed *in vivo*[56,57]. These pressure values are also comparable to those reported in a FE model with similar compressive loading[29]. Using an average adult male mouse body mass of 30g, the average contact forces calculated with DEA with compressive behavior at 9N corresponded to

approximately 17 times body weight. Clinically, these forces are more than those engendered during full knee extension landing[61], vertical jumping[62], kneeling and squatting[63], activities that have been suggested to lead to increased cartilage contact pressures, injury, and potential subsequent cartilage degradation[1,7,61,64,65].

Furthermore, although contact pressures did not increase as loading increased in rolling types, peak compressive stress at 9N averaged 3.57MPa, which is within the range of normal cartilage pressures. Compressive contact forces during this behavior are approximately 2 times body weight and are comparable to those determined for normal walking in human studies[55,60]. Although shear stress was not calculated in this study, the "rolling" behavior may indicate increased shear stresses compared to the normal cartilage states, particularly in the posterior aspect of the joint. While the exact reason for the two distinct behaviors is not understood, we hypothesize that joint and animal positioning in the compressive loading device may be a potential explanation. Relative femur to tibial proximal and posterior translations were significantly different between the two contact behaviors at 9N (Figure 4.9). Since knee flexion is not restricted in this model, the relative location of the femur to the tibia at 0N is not controlled, and could cause two distinct contact behaviors. Further studies *in vivo* are needed to examine which behavior occurs during multiple loading cycles.

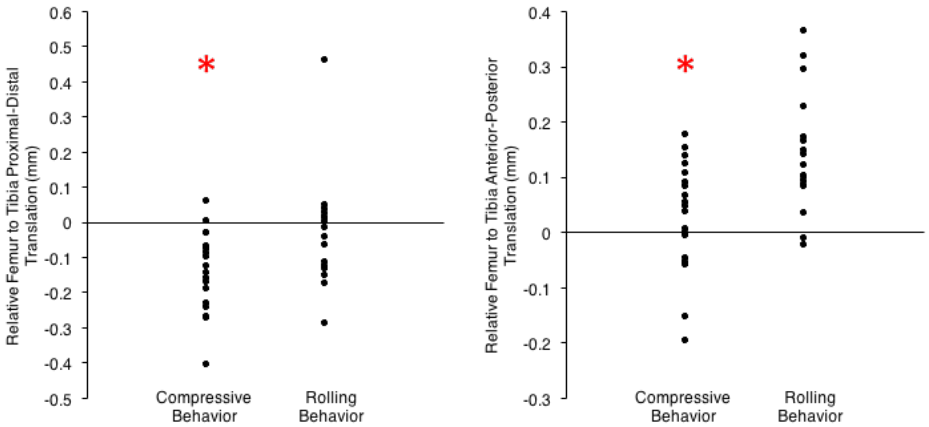

Figure 4.9 Relative femur to tibia Proximal-Distal and Anterior-Posterior translations were significantly different between compressive and rolling contact behaviors, $p<0.05$.

Despite differences in contact behaviors, in all trials the peak compressive stress location translated to the posterior aspect of the joint as loading increased from 0 to 9N. The location of peak compressive stress at 9N correlated with the area in which the most severe cartilage damage occurs in this model. Using histological scoring on Safranin O-stained slides, several studies have demonstrated that loading induces the most severe cartilage damage on the posterior aspect of the tibial plateau[36,37]. As loading increased from 0 to 9N, peak compressive stresses translated to the posterior aspect of the joint, thus confirming the correlation between highest contact stresses and most severe cartilage damage. Also of importance is that fact that contact pressures were not evenly distributed on medial and lateral surfaces, indicating varus or valgus rotation as loading increased. These rotations may produce tension in ligaments at the joint margins and could potentially explain bone formation at the enthuses of these ligaments[66,67]. Further studies are needed to examine the loads on the ligaments, confirm excessive tension on the joint margins and differentiate between the formation of osteophytes and enthesiophytes in this model.

To validate the results of the DEA model, the simplified FE contact model confirmed the contact pressures calculated during loading. The normal geometry demonstrated comparable contact pressures and stresses on the cartilage surfaces. Parametric evaluation of the effect of joint tissue changes on cartilage surfaces stresses revealed that only cartilage changes significantly affected contact pressures. Similar to previous results[35,68,69], increased cartilage thickness and reduced cartilage modulus decreased cartilage surface contact pressures. Similar to results from other computation studies[17,28], bone changes did not significantly affect cartilage contact pressures; however, they affected the peak stresses and strains engendered in the cortical

and cancellous bone.

Bone adapts to dynamic changes in applied mechanical strains[70–72]. Based on our parametric analysis, the differences in peak bone stresses and strains would result in bone adaptation *in vivo*. Therefore, although changes in bone thickness and properties may not directly affect cartilage surface stresses during loading, they may lead to changes in bone adaptation and remodeling, thus promoting changes in bone/cartilage crosstalk[73–75]. Bone remodeling has been implicated in exacerbating bone/cartilage crosstalk during OA disease progression in which molecules and cells can be easily transferred from one tissue to the other[74,75]. Thus, bone changes may play a major role by driving bone adaption, resulting in subchondral bone sclerosis, and subsequent tissue crosstalk during abnormal mechanical loading.

While the DEA and FE contact models allow us to examine the contact mechanics of the joint during loading, the use of these models to understand complex biological states have some limitations. Both models only consider compressive stresses in this study. Knee joints are subjected to rotations, shear and tensile forces and exhibit more complex stress states *in vivo*. Thus, future studies should examine the shear and tensile stress states under tibial loading. Furthermore, our discrete element analysis assumes that the bone is rigid. While our FE model eliminates for this assumption, the model is linearly elastic, which may also be inaccurate, particularly for cartilage tissue. Cartilage has been modeled extensively as a linear elastic, nearly incompressible material as it is confirmed to act as such in relatively short or instantaneous time-frames[40,76]; however, biologically, cartilage is indeed biphasic[31–33]. Further studies are needed to account for other joint motions as well as the cartilage fluid phase during longer loading durations.

Another limitation in these models is that the menisci and other soft tissues in the joint

were not considered, yet they play major roles in the mechanical stability of the joint. For instance, since the DEA did not account for the thickness of the meniscus, we are potentially underestimating the contact stresses. The use of one model geometry and a uniform cartilage thickness further exacerbates this limitation. Considering the size of the mouse joint and the limited imaging capabilities, this study nonetheless provides an initial attempt to quantify contact stress magnitudes and locations during loading. Future studies should quantify the effect of loading on other tissues in the joint using more complex, customized geometric FE models. The effects of material property changes in these tissues should also be examined as all joint tissues are affected during OA disease progression.

In conclusion, peak contact stress magnitude and location correlated with areas of severe cartilage damage during tibial compressive loading. These stress magnitudes were confirmed using both DEA and FE modeling. Unlike changes in cartilage thickness and properties, the changes in bone properties and mass did not directly affect contact stresses on the cartilage surface. However, changes in all tissues did affect stresses and strains induced on the cortical and cancellous bone. Thus, while material-related changes to the bone may not directly influence stresses on the cartilage surface, these changes may lead to differences in bone adaption, thus potentially promoting subsequent tissue crosstalk between bone and cartilage during loading. Further *in vivo* studies are needed to investigate the molecular and cellular crosstalk associated with increased strains engendered on the bone, and potential compressive loads and contact pressures that may promote cartilage health and attenuate OA progression.

4.5 REFERENCES

1. Felson DT. Osteoarthritis: New Insights. Part 1: The Disease and Its Risk Factors. *Ann Intern Med*. 2000;133(8):635. doi:10.7326/0003-4819-133-8-200010170-00016.
2. Arokoski J, Kiviranta I, Jurvelin J, Tammi M, Helminen HJ. Long-distance running causes site-dependent decrease of cartilage glycosaminoglycan content in the knee joints of beagle dogs. *Arthritis Rheum*. 1993;36(10):1451-1459. doi:10.1002/art.1780361018.
3. Lapveteläinen T, Nevalainen T, Parkkinen JJ, Arokoski J, Kiraly K, Hyttinen M, Halonen P, Helminen HJ. Lifelong moderate running training increases the incidence and severity of osteoarthritis in the knee joint of C57BL mice. *Anat Rec*. 1995;242(2):159-165. doi:10.1002/ar.1092420204.
4. Felson DT. Osteoarthritis of the Knee. *N Engl J Med*. 2006;354(8):841-848. doi:10.1056/NEJMcp051726.
5. Wieland HA, Michaelis M, Kirschbaum BJ, Rudolphi KA. Osteoarthritis - an untreatable disease? *Nat Rev Drug Discov*. 2005;4(4):331-344. doi:10.1038/nrd1693.
6. Hunter DJ, Felson DT. Osteoarthritis. *BMJ*. 2006;332(7542):639-642. doi:10.1136/bmj.332.7542.639.
7. Lohmander LS, Englund PM, Dahl LL, Roos EM. The long-term consequence of anterior cruciate ligament and meniscus injuries: osteoarthritis. *Am J Sports Med*. 2007;35(10):1756-1769. doi:10.1177/0363546507307396.
8. Kaila-Kangas L, Arokoski J, Impivaara O, Viikari-Juntura E, Leino-Arjas P, Luukkonen R, Heliövaara M. Associations of hip osteoarthritis with history of recurrent exposure to manual handling of loads over 20 kg and work participation: a population-based study of men and women. *Occup Environ Med*. 2011;68(10):734-738. doi:10.1136/oem.2010.061390.
9. Cameron KL, Hsiao MS, Owens BD, Burks R, Svoboda SJ. Incidence of physician-diagnosed osteoarthritis among active duty United States military service members. *Arthritis Rheum*. 2011;63(10):2974-2982. doi:10.1002/art.30498.
10. Felson DT, Anderson JJ, Naimark A, Walker AM, Meenan RF. Obesity and Knee Osteoarthritis. *Ann Intern Med*. 1988;109(1):18. doi:10.7326/0003-4819-109-1-18.
11. Messier SP, Loeser RF, Miller GD, Morgan TM, Rejeski WJ, Sevick MA, Ettinger WH, Pahor M, Williamson JD. Exercise and dietary weight loss in overweight and obese older adults with knee osteoarthritis: the Arthritis, Diet, and Activity Promotion Trial. *Arthritis Rheum*. 2004;50(5):1501-1510. doi:10.1002/art.20256.
12. Felson DT. Weight Loss Reduces the Risk for Symptomatic Knee Osteoarthritis in Women. *Ann Intern Med*. 1992;116(7):535. doi:10.7326/0003-4819-116-7-535.
13. Hochberg MC, Altman RD, April KT, Benkhalti M, Guyatt G, McGowan J, Towheed T, Welch V, Wells G, Tugwell P. American College of Rheumatology 2012 recommendations for the use of nonpharmacologic and pharmacologic therapies in osteoarthritis of the hand, hip, and knee. *Arthritis Care Res (Hoboken)*. 2012;64(4):465-474. doi:10.1002/acr.21596.

14. Radin E, Paul I, Rose R. Role of mechanical factors in pathogenesis of primary osteoarthritis. *Lancet*. 1972;299(7749):519-522. doi:10.1016/S0140-6736(72)90179-1.

15. Radin EL, Rose RM. Role of subchondral bone in the initiation and progression of cartilage damage. *Clin Orthop Relat Res*. 1986;(213):34-40.

16. Radin EL, Martin RB, Burr DB, Caterson B, Boyd RD, Goodwin C. Effects of mechanical loading on the tissues of the rabbit knee. *J Orthop Res*. 1984;2(3):221-234. doi:10.1002/jor.1100020303.

17. Burr DB, Schaffler MB. The Involvement of Subchondral Mineralized Tissues in Osteoarthrosis : Quantitative Microscopic Evidence. *Microsc Res Tech*. 1997;37:343-357. doi:10.1002/(SICI)1097-0029(19970515)37:4<343::AID-JEMT9>3.0.CO;2-L.

18. Burr DB. The importance of subchondral bone in the progression of osteoarthritis. *J Rheumatol Suppl*. 2004;70:77-80.

19. Li G, Yin J, Gao J, Cheng TS, Pavlos NJ, Zhang C, Zheng MH, Grynpas M, Alpert B, Katz I, Lieberman I, Pritzker K, Suri S, Walsh D, Madry H, Dijk C van, Mueller-Gerbl M, Burr D, et al. Subchondral bone in osteoarthritis: insight into risk factors and microstructural changes. *Arthritis Res Ther*. 2013;15(6):223. doi:10.1186/ar4405.

20. Kawcak CE, McIlwraith CW, Norrdin RW, Park RD, James SP. The role of subchondral bone in joint disease: a review. *Equine Vet J*. 2010;33(2):120-126. doi:10.1111/j.2042-3306.2001.tb00589.x.

21. Hayami T, Pickarski M, Zhuo Y, Wesolowski GA, Rodan GA, Duong LT. Characterization of articular cartilage and subchondral bone changes in the rat anterior cruciate ligament transection and meniscectomized models of osteoarthritis. *Bone*. 2006;38(2):234-243. doi:10.1016/j.bone.2005.08.007.

22. Botter SM, Van Osch GJVM, Clockaerts S, Waarsing JH, Weinans H, Van Leeuwen JPTM. Osteoarthritis induction leads to early and temporal subchondral plate porosity in the tibial plateau of mice: An in vivo microfocal computed tomography study. *Arthritis Rheum*. 2011;63(9):2690-2699. doi:10.1002/art.30307.

23. Glasson SS, Blanchet TJ, Morris EA. The surgical destabilization of the medial meniscus (DMM) model of osteoarthritis in the 129/SvEv mouse. *Osteoarthritis Cartilage*. 2007;15(9):1061-1069. doi:10.1016/j.joca.2007.03.006.

24. Culley KL, Dragomir CL, Chang J, Wondimu EB, Coico J, Plumb DA, Otero M, Goldring MB. Mouse models of osteoarthritis: surgical model of posttraumatic osteoarthritis induced by destabilization of the medial meniscus. *Methods Mol Biol*. 2015;1226:143-173. doi:10.1007/978-1-4939-1619-1_12.

25. Kamekura S, Hoshi K, Shimoaka T, Chung U, Chikuda H, Yamada T, Uchida M, Ogata N, Seichi A, Nakamura K, Kawaguchi H. Osteoarthritis development in novel experimental mouse models induced by knee joint instability. *Osteoarthritis Cartilage*. 2005;13(7):632-641. doi:10.1016/j.joca.2005.03.004.

26. Ma H-L, Blanchet TJ, Peluso D, Hopkins B, Morris EA, Glasson SS. Osteoarthritis severity is sex dependent in a surgical mouse model. *Osteoarthritis Cartilage*. 2007;15(6):695-700. doi:10.1016/j.joca.2006.11.005.

27. Frank CB, Beveridge JE, Huebner KD, Heard BJ, Tapper JE, O'Brien EJO, Shrive NG. Complete ACL/MCL deficiency induces variable degrees of instability in sheep with specific kinematic abnormalities correlating with degrees of early osteoarthritis. *J Orthop Res*. 2012;30(3):384-392. doi:10.1002/jor.21549.

28. Brown TD, Radin EL, Martin RB, Burr DB. Finite element studies of some juxtarticular stress changes due to localized subchondral stiffening. *J Biomech*. 1984;17(1):11-24.

29. Poulet B, Westerhof T a T, Hamilton RW, Shefelbine SJ, Pitsillides a. a. Spontaneous osteoarthritis in Str/ort mice is unlikely due to greater vulnerability to mechanical trauma. *Osteoarthr Cartil*. 2013;21(5):756-763. doi:10.1016/j.joca.2013.02.652.

30. Adebayo OO, Ko FC, Goldring SR, Goldring MB, Wright TM, van der Meulen MCH. Kinematics of meniscal- and ACL-transected mouse knees during controlled tibial compressive loading captured using roentgen stereophotogrammetry. *J Orthop Res*. 2016;(April 2016):1-23. doi:10.1002/jor.23285.

31. Ateshian GA, Warden WH, Kim JJ, Grelsamer RP, Mow VC. Finite deformation biphasic material properties of bovine articular cartilage from confined compression experiments. *J Biomech*. 30(11-12):1157-1164.

32. Lai WM, Lai WM, Mow VC. Singular Perturbation Analysis of the Nonlinear, Flow-Dependent Compressive Stress Relaxation Behavior of Articular Cartilage. *J Biomech Eng*. 1985;107(3):206. doi:10.1115/1.3138545.

33. Mow VC, Kuei SC, Lai WM, Armstrong CG. Biphasic Creep and Stress Relaxation of Articular Cartilage in Compression: Theory and Experiments. *J Biomech Eng*. 1980;102(1):73. doi:10.1115/1.3138202.

34. Wong BL, Bae WC, Gratz KR, Sah RL. Shear deformation kinematics during cartilage articulation: effect of lubrication, degeneration, and stress relaxation. *Mol Cell Biomech*. 2008;5(3):197-206.

35. Poulet B, Hamilton RW, Shefelbine S, Pitsillides AA. Characterizing a novel and adjustable noninvasive murine joint loading model. *Arthritis Rheum*. 2011;63(1):137-147. doi:10.1002/art.27765.

36. Ko FC, Dragomir C, Plumb DA, Goldring SR, Wright TM, Goldring MB, van der Meulen MCH. In vivo cyclic compression causes cartilage degeneration and subchondral bone changes in mouse tibiae. *Arthritis Rheum*. 2013;65(6):1569-1578. doi:10.1002/art.37906.

37. Ko FC, Dragomir CL, Plumb DA, Hsia AW, Adebayo OO, Goldring SR, Wright TM, Goldring MB, van der Meulen MCH. Progressive cell-mediated changes in articular cartilage and bone in mice are initiated by a single session of controlled cyclic compressive loading. *J Orthop Res*. 2016;(October 2015):n/a-n/a. doi:10.1002/jor.23204.

38. Christiansen BA, Guilak F, Lockwood KA, Olson SA, Pitsillides AA, Sandell LJ, Silva MJ, van der Meulen MCH, Haudenschild DR. Non-invasive mouse models of post-traumatic osteoarthritis. *Osteoarthritis Cartilage*. 2015;23(10):1627-1638. doi:10.1016/j.joca.2015.05.009.

39. Guess TM, Liu H, Bhashyam S, Thiagarajan G. A multibody knee model with discrete cartilage prediction of tibio - femoral contact mechanics. *Comput Methods Biomech*

Biomed Engin. 2011:1-15. doi:10.1080/10255842.2011.617004.

40. Volokh KY, Chao EYS, Armand M. On foundations of discrete element analysis of contact in diarthrodial joints. *Mol Cell Biomech*. 2007;4(2):67-73.

41. Anderson DD, Iyer KS, Segal NA, Lynch JA, Brown TD. Implementation of discrete element analysis for subject-specific, population-wide investigations of habitual contact stress exposure. *J Appl Biomech*. 2010;26(2):215-223.

42. Bei Y, Fregly BJ. *Multibody Dynamic Simulation of Knee Contact Mechanics*. Vol 26.; 2004. doi:10.1016/j.medengphy.2004.07.004.

43. Li G, Sakamoto M, Chao EYS. A comparison of different methods in predicting static pressure distribution in articulating joints. *J Biomech*. 1997;30(6):635-638. doi:10.1016/S0021-9290(97)00009-2.

44. Anderson DD, Goldsworthy JK, Li W, James Rudert M, Tochigi Y, Brown TD. Physical validation of a patient-specific contact finite element model of the ankle. *J Biomech*. 2007;40(8):1662-1669. doi:10.1016/j.jbiomech.2007.01.024.

45. Gardner-Morse M, Badger G, Beynnon B, Roemhildt M. Changes in in vitro compressive contact stress in the rat tibiofemoral joint with varus loading. *J Biomech*. 2013;46(6):1216-1220. doi:10.1016/j.jbiomech.2013.01.009.

46. Wong M, Carter DR. Theoretical stress analysis of organ culture osteogenesis. *Bone*. 1990;11(2):127-131. doi:10.1016/8756-3282(90)90060-C.

47. Beaupré GS, Stevens SS, Carter DR. Mechanobiology in the development, maintenance, and degeneration of articular cartilage. *J Rehabil Res Dev*. 37(2):145-151.

48. Rho JY, Ashman RB, Turner CH. Young's modulus of trabecular and cortical bone material: Ultrasonic and microtensile measurements. *J Biomech*. 1993;26(2):111-119. doi:10.1016/0021-9290(93)90042-D.

49. Vijayakumar V, Quenneville CE. Quantifying the regional variations in the mechanical properties of cancellous bone of the tibia using indentation testing and quantitative computed tomographic imaging. *Proc Inst Mech Eng H*. 2016;230(6):588-593. doi:10.1177/0954411916642800.

50. Sadeghi H, Espino DM, Shepherd DET. Fatigue strength of bovine articular cartilage-on-bone under three-point bending: the effect of loading frequency. *BMC Musculoskelet Disord*. 2017;18(1):142. doi:10.1186/s12891-017-1510-8.

51. Kerin AJ, Wisnom MR, Adams MA. The compressive strength of articular cartilage. *Proc Inst Mech Eng Part H J Eng Med*. 1998;212(4):273-280. doi:10.1243/0954411981534051.

52. Fick JM, Espino DM. Articular cartilage surface rupture during compression: Investigating the effects of tissue hydration in relation to matrix health. *J Mech Behav Biomed Mater*. 2011;4(7):1311-1317. doi:10.1016/j.jmbbm.2011.04.018.

53. Fick JM, Espino DM. Articular cartilage surface failure: An investigation of the rupture rate and morphology in relation to tissue health and hydration. *Proc Inst Mech Eng Part H J Eng Med*. 2012;226(5):389-396. doi:10.1177/0954411912439824.

54. Sadeghi H, Shepherd DET, Espino DM. Effect of the variation of loading frequency on

surface failure of bovine articular cartilage. *Osteoarthr Cartil*. 2015;23(12):2252-2258. doi:10.1016/j.joca.2015.06.002.

55. Fukubayashi T, Kurosawa H. The Contact Area and Pressure Distribution Pattern of the Knee: A Study of Normal and Osteoarthrotic Knee Joints. *Acta Orthpaedica Scand*. 1980;51:871-879.

56. Segal NA, Anderson DD, Iyer KS, Baker J, Torner JC, Lynch JA, Felson DT, Lewis CE, Brown TD. Baseline articular contact stress levels predict incident symptomatic knee osteoarthritis development in the MOST cohort. *J Orthop Res*. 2009;27(12):1562-1568. doi:10.1002/jor.20936.

57. Segal NA, Kern AM, Anderson DD, Niu J, Lynch J, Guermazi A, Torner JC, Brown TD, Nevitt M, Multicenter Osteoarthritis Study Group the MKOS. Elevated tibiofemoral articular contact stress predicts risk for bone marrow lesions and cartilage damage at 30 months. *Osteoarthr Cartil*. 2012;20(10):1120-1126. doi:10.1016/j.joca.2012.05.013.

58. Brown TD, Pope DF, Hale JE, Buckwalter JA, Brand RA. Effects of osteochondral defect size on cartilage contact stress. *J Orthop Res*. 1991;9(4):559-567. doi:10.1002/jor.1100090412.

59. Brand R. Joint Contact Stress: A Reasonable Surrgoate for Biological Processes? *Iowa Orthop J*. 2005;25:82-94.

60. Morrison JB. The mechanics of the knee joint in relation to normal walking. *J Biomech*. 1970;3(1):51-61. doi:10.1016/0021-9290(70)90050-3.

61. Makinejad MD, Abu Osman NA, Abu Bakar Wan Abas W, Bayat M. Preliminary analysis of knee stress in full extension landing. *Clinics (Sao Paulo)*. 2013;68(9):1180-1188. doi:10.6061/clinics/2013(09)02.

62. Cleather DJ, Goodwin JE, Bull AMJ. Hip and knee joint loading during vertical jumping and push jerking. *Clin Biomech*. 2013;28(1):98-103. doi:10.1016/j.clinbiomech.2012.10.006.

63. Nagura T, Matsumoto H, Kiriyama Y, Chaudhari A, Andriacchi TP. Tibiofemoral Joint Contact Force in Deep Knee Flexion and Its Consideration in Knee Osteoarthritis and Joint Replacement. *J Appl Biomech*. 2006;22:305-313.

64. Felson DT, Hannan MT, Naimark A, Berkeley J, Gordon G, Wilson PW, Anderson J. Occupational physical demands, knee bending, and knee osteoarthritis: results from the Framingham Study. *J Rheumatol*. 1991;18(10):1587-1592.

65. Coggon D, Croft P, Kellingray S, Barrett D, McLaren M, Cooper C. Occupational physical activities and osteoarthritis of the knee. *Arthritis Rheum*. 2000;43(7):1443-1449. doi:10.1002/1529-0131(200007)43:7<1443::AID-ANR5>3.0.CO;2-1.

66. Benjamin M, Toumi H, Ralphs JR, Bydder G, Best TM, Milz S. Where tendons and ligaments meet bone: attachment sites (’entheses’) in relation to exercise and/or mechanical load. *J Anat*. 2006;208(4):471-490. doi:10.1111/j.1469-7580.2006.00540.x.

67. Rogers J, Shepstone L, Dieppe P. Bone formers: osteophyte and enthesophyte formation are positively associated. *Ann Rheum Dis*. 1997;56(2):85-90. doi:10.1136/ARD.30.6.605.

68. Li G, Lopez O, Rubash H. Variability of a Three-Dimensional Finite Element Model Constructed Using Magnetic Resonance Images of a Knee for Joint Contact Stress Analysis. *J Biomed Eng*. 2001;123:341-346.

69. Huber-Betzer H, Brown TD, Mattheck C. Some effects of global joint morphology on local stress aberrations near imprecisely reduced intra-articular fractures. *J Biomech*. 1990;23(8):811-822. doi:10.1016/0021-9290(90)90028-2.

70. Meakin LB, Price JS, Lanyon LE. The Contribution of Experimental in vivo Models to Understanding the Mechanisms of Adaptation to Mechanical Loading in Bone. *Front Endocrinol (Lausanne)*. 2014;5:154. doi:10.3389/fendo.2014.00154.

71. Rubin C LL. Regulation of Bone Mass by Mechanical Strain Magnitude. Calcified Tissue International. file:///Users/Funmi/Downloads/Rubin Cal Tiss 1985 37 411-417.pdf. Published 1985. Accessed January 22, 2016.

72. Lynch ME, Main RP, Xu Q, Schmicker TL, Schaffler MB, Wright TM, van der Meulen MCH. Tibial compression is anabolic in the adult mouse skeleton despite reduced responsiveness with aging. *Bone*. 2011;49(3):439-446. doi:10.1016/j.bone.2011.05.017.

73. Burr DB. The importance of subchondral bone in osteoarthrosis. *Curr Opin Rheumatol*. 1998;10(3):256-262.

74. Findlay DM, Kuliwaba JS. Bone-cartilage crosstalk: a conversation for understanding osteoarthritis. *Bone Res*. 2016;4:16028. doi:10.1038/boneres.2016.28.

75. Yuan XL, Meng HY, Wang YC, Peng J, Guo QY, Wang AY, Lu SB. Bone–cartilage interface crosstalk in osteoarthritis: potential pathways and future therapeutic strategies. *Osteoarthr Cartil*. 2014;22(8):1077-1089. doi:10.1016/j.joca.2014.05.023.

76. Ateshian GA, Henak CR, Weiss JA. Toward patient-specific articular contact mechanics. *J Biomech*. 2015;48(5):779-786. doi:10.1016/j.jbiomech.2014.12.020.

CHAPTER 5

EMPOWERING EARLY MASTERY OF SPATIAL VISUALIZATION SKILLS IN UNDERREPRESENTED MINORITY ENGINEERING STUDENTS

The following chapter is published as a conference paper in the *Proceedings of the 2014 IEEE Frontiers in Education Conference (FIE)* and reprinted here with permission. The reference to the published work is:

> Adebayo O, Farrar E, Evans R, Nathans-Kelly T, McCray T. (2014) Empowering Early Mastery of Spatial Visualization Skills in Underrepresented Minority Engineering Students. *2014 IEEE Frontiers in Education Conference (FIE) Proceedings* (pp. 1-8). IEEE.

5.1 Introduction

In the College of Engineering at Cornell University, the goal of the Office of Diversity Programs in Engineering (DPE) is to support students, especially those from backgrounds traditionally underrepresented in engineering, and to provide the programing necessary to assist them in being successful. We strive to increase the retention and graduation rate of students underrepresented in higher education, often referred to as underrepresented minority students (URM), and students who are the first in their family to attend college or first generation college students (FGC). More specifically, our goal in the implementation of a grant from the National Science Foundation (NSF) and the Science, Technology, Engineering, and Mathematics Talent Expansion Program (STEP) (award: DUE #1317501) is, by the end of a five-year period, to increase the overall graduation rate of URM and FGC students from 66% to 84%. The latter is the overall graduation rate of the engineering student body at Cornell. We recognize that while the overall graduation rate from Cornell Engineering is far above the United States national

average (63%), progress could still be made by closing the gap between the graduation rates of URM and FGC students and those more traditional students. Three interventions are outlined in our grant implementation, including: a tutoring program, a summer math institute and a spatial-visualization course. In this paper, we focus on the third of those interventions of creating, effecting and researching a course to improve the spatial visualization (SV) skills of URM and FGC engineering students at Cornell.

As the range of definitions for "spatial visualization" is wide and varied, we feel compelled to define it here for our purposes. Perhaps the simplest definition is "the ability to mentally manipulate, rotate, twist, or invert pictorially presented stimuli"[1]. However, that simplest of definitions soon becomes more complicated when Voyer et al.[2], redefine it as "the ability to manipulate complex spatial information when several stages are needed to produce the correct solution." The first definition represents spatial visualization as a kind of mental exercise; the second as a response to a particular problem or project.

Our understanding gets further complicated when we consider the relation of SV skills to "spatial ability" or "representing, transforming, generating and recalling symbolic, nonlinguistic information"[3], and their relation to "spatial thinking" or "a constructive amalgam of three elements: concepts of space, tools of representation and processes of reasoning"[4]. These different terms that can mean different things are often used interchangeably. For the purposes of this paper, we would like to define SV skills more generally as *spatial intelligence*, a term that we allow to contain the ideas of spatial visualization and spatial perception, including the activities of mental rotation of objects, spatial relation between objects, and overall spatial orientation[5]. As with mastery of any set of complex skills, doing one type of activity repeatedly does not develop that mastery; instead, a variety of sub-tasks or related tasks will move you towards mastery.

Lieu and Sorby note that "you need to do a variety of tasks to develop your spatial intelligence, just as developing linguistic intelligence requires you to read, write, and listen"[5].

There exists a preponderance of evidence for three understandings in relation to the development of SV skills. First, there are at least some group differences, most specifically related to gender, and then only to particular kinds of SV skills, e.g., 3D mental rotations. The strongest explanation for these differences is dissimilar socialization processes[3-5]. Second, it is possible to reduce or even eliminate these differences through direct instruction[6-9]. Third, reducing or eliminating these differences or simply enhancing SV skills generally seems to be predictive of student success, typically defined as retention in the STEM fields[6,8,10,11].

There is an important caveat related to the third of these understandings. Currently, there is little empirical evidence, and even worse, no investigation relating to how students actually use or apply their newly-won SV skills in response to authentic engineering projects or to solve real engineering problems. In other words, while there may be some suggestive correlations that SV skills vary according to socialization, that these variances can be reduced or eliminated, and that such reductions or eliminations can lead to success; there is little if any evidence of what that success actually entails other than retention at the academic organization.

It was with all three of these understandings and this final important caveat in mind that the Engineering Communications Program (ECP), DPE, the Cornell University Engineering Success (CUES) program, and two Ph.D. graduate students from Biomedical Engineering designed and implemented an innovative active-learning, project-based course to teach URM and FGC students SV skills. While our primary aim was to improve the SV skills of those students, hoping as we suggested above to increase their overall graduation rate; we were equally (actually more) interested in developing their spatial intelligence as well as investigating exactly what that

spatial intelligence really means in response to authentic engineering projects or in solving real engineering problems.

5.2 Course Description and Research Methodologies

The cohort of students involved in this first iteration of our SV course, entitled ***Spatial Visualization/Thinking for Engineers***, were pre-registered based on their invitation to and voluntary enrollment in the Robert L. Ryan Scholars Program. Ryan Scholars are entering first-year students (median age: 18) selected based on their demonstrated potential for success in engineering, as determined by Cornell admission, but also based on the existence of a variety of risk factors that have been shown to make persistence in engineering more difficult. These factors include low resourced high school, low socioeconomic status (SES), FGC student, English as a second language, single parent household, and limited access to rigorous advanced placement math and science coursework. In the fall semester, all of the Ryan Scholars (31 students) were preregistered for the spatial visualization course regardless of their score on the Purdue Spatial Visualization test (PSVT).

Our SV course was taught weekly for 14 weeks in the fall semester of 2013 at Cornell University. In order to coordinate with the NSF ENGAGE curriculum[13], we designed the first six lectures to instill mastery of SV skills, including rotations, reflections, flat-patterns, cutting planes, combining objects, and isometric/orthographic sketching. We used the PSVT to conduct pre- and post-testing of students' ability to perform spatial visualization tasks. The pre-test was administered prior to the beginning of the course. Students then attended the six one-hour lectures, with homework assignments to provide practice and further enhancement of SV skills. The post-test was administered immediately following these lectures. The second part of the

course consisted of project work, in which students were placed in teams. Each student team had a *client* from Cornell biomedical engineering faculty. Prior to the course and in partnership with the instructors, the clients each developed a visualization request that would employ and extend students' SV skills. The clients' requests were designed to challenge the students' ability to understand, manipulate, and communicate complex SV concepts by requiring them to create clear and accurate visuals from cutting-edge engineering research data, provided by the clients. At the course conclusion, student teams were required to present their visuals in a formal, professional setting, in which the visuals they developed were evaluated by their peers, the instructors, and the clients.

As we developed the course, we became very aware of how the term *project-based learning* (PjBL) was typically used and that it held a decidedly different meaning than problem-based learning (PBL), which often includes project-based learning within its framework. Both are, like spatial intelligence, complex: they provide a focus for intellectual inquiry; they eschew a tidy problem statement or any predetermined outcome; they encourage application of knowledge rather than rote learning; they rely on student action and critical thinking; functioning in teams; they encourage hands-on work; and they facilitate learning guided by faculty serving as mentors or guides[14-22].

From the start, we deployed PjBL purposefully, incorporating outside clients and stakeholders who provided the projects for student teams. Our reasoning and our research led us to believe that having a concrete deliverable was a powerful tool for student engagement at a deep learning level. As such, we purposefully included client meetings and assessment as 2.5% and 5% of the final grade, respectively. We understood well that, while PBL may have some expected or predictable outcomes, PjBLs have no such comforts. Client interaction can bring

new and fresh constraints, freedoms or regulating factors on a team's project. The instructor often will not be able to anticipate a client simply saying "I don't like this team's approach at all," or "Can you do this all again, but this time aim for an audience of 8th graders?" In a sense, the instructors deploying PjBL have to be as agile (or more so) than the student teams working with the client. As PjBL work often does not have a pre-determined outcome or deliverable, clients can (and did) frame the deliverable with their teams variously. Projects were contingent on the client's specific need, and the projects were "real" and "authentic" because the deliverables/artifacts were going to be put into immediate use for biomedical engineering research purposes, in our case. The deliverables were to be a technical report (for academic assessment), a formal presentation where all clients and other stakeholders were present (assessed by clients and instructors alike), and the delivery of the client's requested artifact (poster, demo model, visual, etc.). The artifact needed to meet the specific stated needs of the client (which may differ from the expectations of the instructors) while also meeting the requirements of the academic unit.

We believed that this project-based course design would not only teach students SV skills, but empower them to apply these skills in real engineering contexts, thus enhancing and deepening their knowledge of spatial visualization. Furthermore, we believed that such early application of spatial visualization skills would provide relevant practice for engineering students for future school and engineering work. In addition, immediate examination of the process of applying spatial visualization skills to engineering project work would enable us to understand if and how SV skills specifically and spatial intelligence more generally enhances success in engineering.

In order to study students' development or what "success" might actually entail, we

employed two research methodologies. The first was an action research methodology in which we quite intentionally created a new design for an SV course, one that instead of relying simply on drill and demonstration to improve SV skills was more focused on active-learning and a project-based pedagogy. We adhered to the standard approach for such action research, i.e., plan, act, observe, and reflect. The data that we collected were both quantitative and qualitative in nature. For example, we used PSVT pre- and post-test results and in-class instructor observations and journals, respectively. However, we also devised ways to generate other, also valuable kinds of data: expert feedback on project results, student progress reports and project evaluations. We even required each of the student teams to create and use an e-portfolio to document their project's progress, challenges, and goals during each of week of the semester. We then used our second research methodology, "grounded theory" to code and analyze the data. By combining these two methodologies, we feel that we were able to track, and indeed, to learn about students' acquisition of SV skills and presumably spatial intelligence, their application of those skills and their ability to critically evaluate their own and others' use of spatial intelligence.

5.3 Results & Discussion

5.3.1 Students showed enhanced spatial visualization knowledge after SV lectures.

Students showed overall improvement in SV test results after attending the six one-hour lectures designed to improve SV skills. The mean score increased by 13% in the post-test as compared to the pre-test mean score of 75% (student's t-test, $p<0.05$) (Figure 5.1A). Furthermore, the spread in scores decreased, from a range of 35-100% on the pre-test to a range of 53-100% on the post-test, with 26 out of 31 students scoring higher on the post-test than the pre-test, 2 students with no change, and 3 students with a 1-question reduction in score. In

general, high scorers on the pre-test also scored highly on the post-test, and low scorers on the pre-test generally showed the largest improvement in test score (Figure 5.1B).

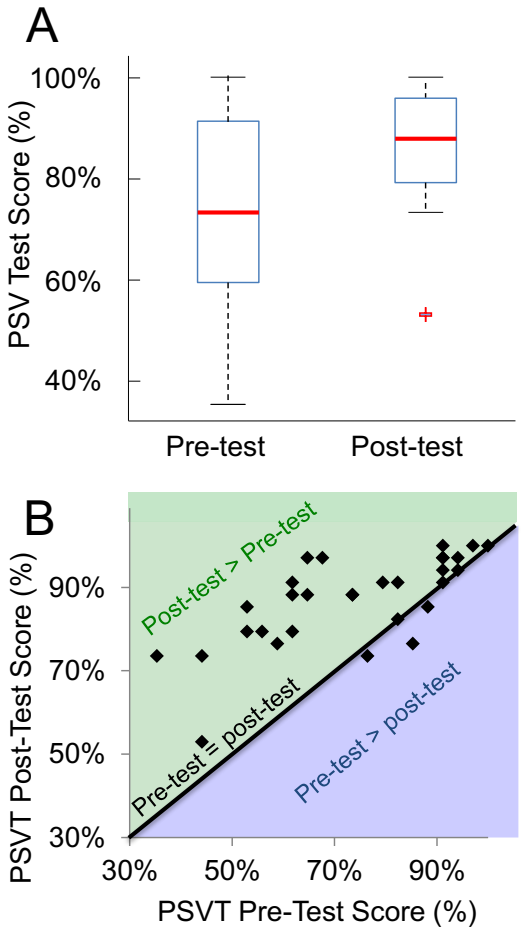

Figure 5.1 Student improvement on PSVT after 6 weeks of SV course

An initial activity identified a primary practical SV weakness: students did not know how to create visuals (in this case, a 2D drawing) to communicate complex features of a 3D object (Figure 5.2). This activity required students to draw a given 3D object, exchange drawings with a peer, and then re-construct the object drawn by their peer. During the activity, instructors observed students attempting to create a drawing of these features in a number of ways. Some students used labeled "front, back, side" views. Some drew isometric sketches of their object, but failed to capture details that were "hidden" from the perspective they chose (Figure 5.2, arrows).

Still others used shading, annotations, or distortions (dashed boxes) in their drawing to communicate complex surfaces or details that would be hidden using standard isometric views. The students then exchanged their "visual" with a peer. Uniformly, the students declared themselves unable to recreate the object sketched by their peer's drawing, revealing to both instructors and the students the need for clear, understandable ways of creating visuals in order to have success in this simple "engineering"

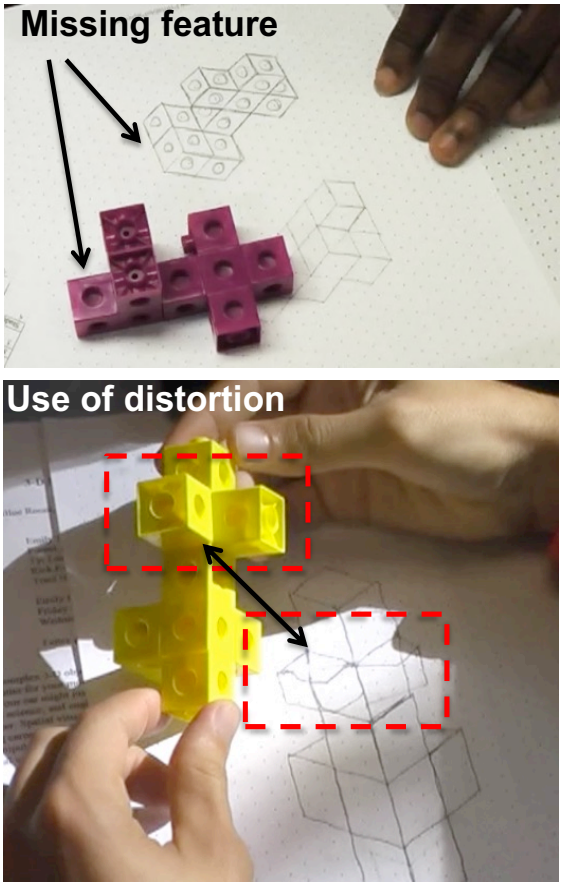

Figure 5.2 Week 1 activity to reveal and evaluate student use of SV

This activity was later compared to student performance in their final project and their ability to create a visual, representing a complex engineering concept, in a manner that could be understood by others. Based on expert feedback from biomedical researchers as well as peer

evaluations, each student group was able to successfully create a spatial visual that explained their engineering topic in an understandable way. The student group shown in Figure 5.3 transformed 2-D images into a 3-D visual that also communicated change over time (Figure 5.3, purple to orange boxes) and successfully interpreted the meaning of their visual within the context of biomedical engineering (Figure 5.3, orange to red boxes).

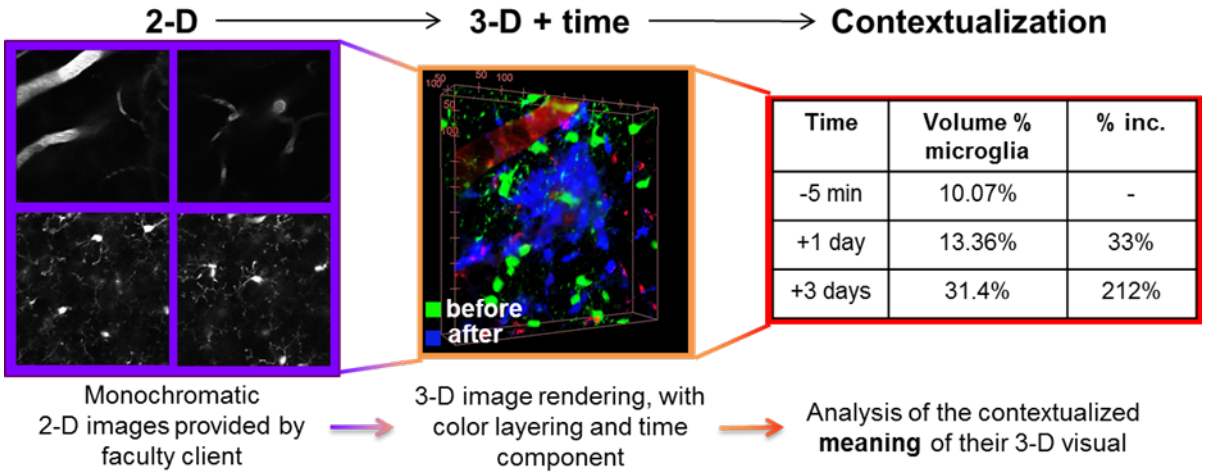

Figure 5.3 Progression of student SV use in project development

Furthermore, we gathered evidence of SV mastery by asking students to identify SV use in the final project presentations by their peers. Each student was required to observe the project presentations given by their peers (eight presentations total) and to record what he or she felt demonstrated "use of SV" in each presentation. Student responses were compared to instructors' evaluations of the presentations and judged to be accurate observations of SV, though often described in variable language. The most common student response was *views*, which encompassed student identification of a number of SV ideas, including *3D views*, *multiple views*, and *front/side/back views*. Students also frequently used *orthogonal*, *isometric*, and *3D* to describe SV use in their peers' presentations. Seven students identified use of *cutting planes* in the presentations, which were also referred to as *slices* or *sections*. The ability of students to

accurately identify explicit uses of SV in the presentations of their peers is evidence of their enhanced knowledge of SV skills and language.

Two things struck us as particularly interesting about students' evaluations of their peers presentations: identification of technology as SV use and identification of SV using language ***not taught by instructors***. First, many students identified use of different software programs as a SV technique. Throughout the course, we taught students how to use several software programs to create "visuals" for their faculty clients. These included ImageJ®, an open source image processing platform developed by the NIH, MATLAB®, developed by MathWorks and licensed by Cornell University, and SolidworksTM®, also licensed by Cornell University. Up to eight students identified use of these programs as explicit use of SV, suggesting that students could "read" their peers' presentations, evaluate what software was used, and identify that software use as inherently a SV technique. This reveals a fascinating "behind the scenes" look at what qualified as "SV" in the minds of our students. Secondly, students also used words that were not explicitly defined as "SV" within the course to describe SV use in their peers' presentations. These vocabulary items included *kymograph*, *image stacks*, *angles*, *volume calculations*, *depth*, *vector geometr*y, *interpolation*, *simulation*, *surface plot*, *multiple dimensions*, and *scaling*. These words were observed by instructors to arise from work on the SV projects, including dialogue with faculty clients, discussion with instructors, teamwork with peers, and the inherent challenge of their project that extended their application and understanding of SV.

5.3.2 Students applied SV knowledge in an engineering context, iteratively.

While the direct mastery of the spatial visualization knowledge was quite evident in the test scores and student language, the use and application of said knowledge in an engineering

context proved more difficult to interpret. Using analysis of student progress reports and instructor journals, we were able to examine the evolution of student SV knowledge throughout the course. First, we observed that students needed to be able to mentally visualize their project's problem statement before they could begin the process of visual creation. This mental visualization arose either through previous familiarity with the topic, or through analogy with a familiar reference. For example, one student team was tasked with creating a visual of a cell and its nucleus moving through an "obstacle course". These students used the analogy of a marble (nucleus) within a balloon (the cell) being squeezed through a ring (obstacle course) as an initial mental visualization of the problem (Figure 5.4). This group was able to quickly begin applying SV skills to their creation of a visual for their client.

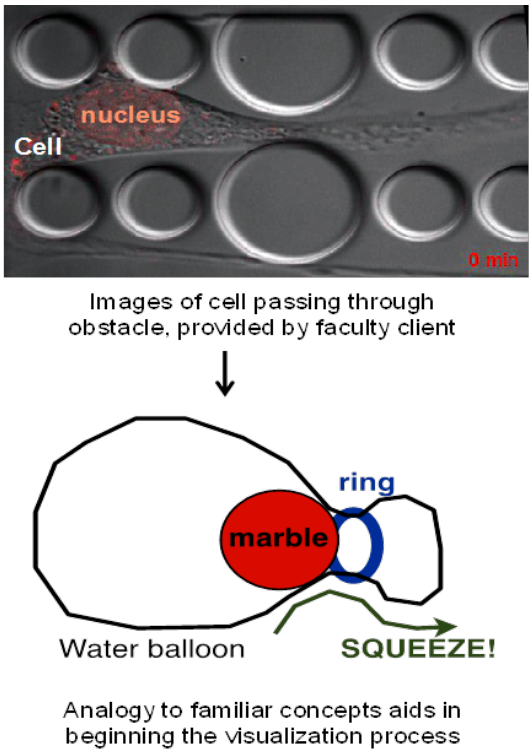

Figure 5.4 Example of SV project data (upper) with corresponding visualization of the project's context (lower)

As a counter-example, a separate team of students was asked to create a visual of microglia cells migrating in the brain. These students struggled to find an analogy to this that they could understand, due to lack of background information on the topic and the difficulty of understanding the images provided to them by their client. Progress in this team was slow and they were unable to articulate how they could use SV skills in this context. Eventually, the instructors were able to identify this "road-block" and assist the team in developing an understanding of the microglia in the brain (Figure 5.5). After the students understood the nature of microglia and their role in the human brain, they were immediately able to apply SV skills such as isometric views, cutting planes, and rotations in pursuing their goal of creating a visual that effectively captured microglia movement for their client.

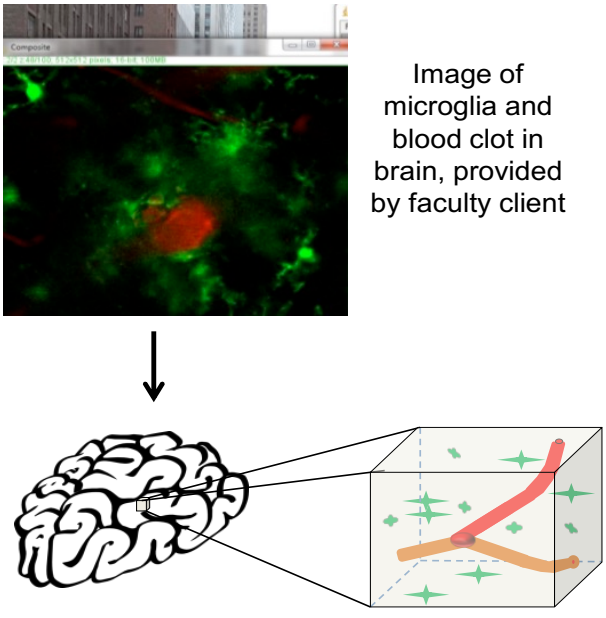

Figure 5.5 Example of SV project data (upper) with corresponding visualization of the project's context (lower)

For all student project teams, achieving a solid mental visualization of their given concept

preceded their ability to begin meaningful work in visual creation for their projects. Once they understood the context of their visualization project, only then were they able to use assistive visual tools such as MATLAB®, ImageJ®, and SolidWorks® to begin creating their representative visuals. Students were able to use these tools appropriately and in a meaningful way, due to their recent knowledge of spatial visualization. Armed with the language and knowledge of SV terms, students easily manipulated visual tools to create 3D models, 2D representations, frames, cutting planes of objects and isometric views of various objects integral to their engineering concept. This knowledge allowed the students to not only manipulate visual tools, but actually to begin to interpret, examine and further their understanding of their engineering concept. For instance, it was only after the students studying microglia migration had created an isometric view of their data, that they began to truly understand migration of these cells, learning that they needed to account for the shape and density of certain microglia.

Essentially, SV skills not only allowed students to utilize visual tools more appropriately, but also facilitated further understanding of complex engineering concepts. A deeper understanding of these engineering concepts then empowered students to create more appropriate spatial visuals to represent their given topic. This iterative process thus enabled students to not only gain a deeper understanding of engineering concepts through SV knowledge, but also strengthened their use and ultimate creation of appropriate, meaningful visuals to explain these concepts. Furthermore, this cycle empowered students with a level of mastery to then critically analyze their own and others' visual representations of the engineering concepts.

5.3.3 Students gained a level of mastery to critique their own and others' use of SV.

Throughout the duration of the project, students were able to use their mastery of SV to

critically evaluate their use of visuals in explaining their engineering concept. From "trying to decide which software would be best to accomplish [the] task" to discovering that a set of data was missing some images, students were able to expertly debate which visual was most appropriate for their goal of easily explaining their concept to others. For instance, one groups, tasked with the challenge of visually representing the concept of brain machines, started with visual simulations in MATLAB®, before ultimately deciding to simplify the visual by creating a physical 3D visual of the brain. Perhaps more importantly, students were also able to use their knowledge to critique other's use of SV.

Students were asked to identify strengths and weaknesses in the final project presentations given by their peers. Interestingly, students often identified higher-order SV uses that were not included in the original ENGAGE curriculum as strengths. For example, one student identified "Good step-wise process" in reference to a team's use of visuals that captured different points in *time* to communicate the nature of a complex 3D concept. This was expressed by a different student as, "Nice visual of putting together the images from 2D different times." This extension of SV skills from multiple dimensions in space to include the time component shows how the project stimulates contextualization of SV reasoning. The ability to create and read visuals that incorporate multiple dimensions across time is an important component of engineering course work and an unexpected benefit of the SV projects.

Students perceived contextualization as critical to the efficacy of the visual presented by each team. Having worked on their own projects to capture and communicate a complex engineering idea by careful combination of SV skills with scientific data, they were highly critical of how well their peers achieved this aim. Students praised projects that were "easy to follow" with "good data backup." The students could "read" the visuals created by their peers

and decide, as experts, whether or not that visual was effective in communicating its technical message. Criticisms most often focused not on the clarity or technical strategy of the visuals used, but on how those visuals were explained within the context of the project.

Students reacted very negatively to presentations that failed to accurately or effectively contextualize their visuals. Criticisms of contextualization included, "They should have given info first and then shown the visual," and "A little more background to help understand relevance." The students critically evaluated not just the technical aspects of a visual, but how well it communicated a complex, contextualized engineering concept. It is evident that students attained a level of mastery that enabled them to not only analyze their own use of visuals throughout their project, but also appropriately critique and evaluate their peers' use of SV in explaining other engineering concepts.

5.4 Conclusions

Like other studies, student post-test results and use of language demonstrated evidence of improved SV skills by direct instruction[6-9]. However, the novelty of this project-based course lies in the understanding of how students used SV skills within engineering applications and its implications for success and retention in engineering programs. While there is little doubt about the relevance of SV in engineering contexts, the way in which students applied such skills within their projects reflects a more complicated link than previously hypothesized. Before the process of SV application could begin, students had to first understand or mentally visualize their given engineering concept. This process is extremely important to note, as students are unable to use SV appropriately without first visually grasping the engineering concept. The engineering concept after being "thrown on the mind's screen" can only then be "observed and manipulated

by the mind's eye"[23]. The process of "observation and manipulation" here can specifically be described as students applying SV knowledge within the context of their projects. Such a process was iterative, as students used their SV skills to not simply create their visuals but also to further inform their understanding of their engineering concepts. Deeper understanding of said concepts then allowed students to delve into examining their use of SV skills, empowering them with the mastery to critically analyze theirs and other's choices of SV techniques. The use of a project-based course, not only enhanced SV skills but more importantly, enabled mastery of such skills by deepening the practice of SV application within engineering contexts. Students will inevitably be faced with many visuals throughout their engineering careers, and the use and knowledge of SV will be extremely important. This course empowered students with SV tools and challenged them to practice the ways in which they can use those tools to interpret and analyze visuals to aid in their understanding of engineering concepts. The expectation is that the enhanced spatial knowledge gained in this course will be helpful to students in their future educational careers; however examination of this hypothesis should be the subject of future investigations.

5.5 REFERENCES

1. M.G. McGee, "Human spatial abilities: Psychometric studies and environmental, genetic, hormonal, and neurological influences," Psychological Bulletin, vol. 86, pp. 889-918, 1979.
2. D. Voyer, S. Voyer and M.P. Bryden, "Magnitude of sex differences in spatial abilities: A meta-analysis and consideration of critical variables." Psychological Bulletin, vol. 117, no. 2, pp. 250-270, 1995.
3. M.C. Linn and A.C. Petersen, "Emergence and characterization of gender differences in spatial abilities: A meta-analysis." Child Development, vol. 56, pp. 1479-1498, 1985.
4. National Research Council, Learning to think spatially. Washington, D.C.: The National Academies Press, 2006.
5. D. Lieu and S.A. Sorby, The fundamentals of visualization, modeling, and graphics for engineering design. Delmar, Cengage Learning, Clifton Park, NY, 2009.
6. S.A. Sorby and B.J. Baartmans, "The development and assessment of a course for 3-D spatial visualization skills of first year engineering students." Journal of Engineering Education, vol. 89, no. 3, pp. 301-307, July 2000.
7. N. Martin-Dorta, J.L. Saorin, and M. Contero, "Development of a fast remedial course to improve the spatial abilities of engineering students." Journal of Engineering Education, vol. 97, no. 4, pp. 505-513, October 2008.
8. S.A. Sorby, "Educational research in developing 3-D spatial skills for engineering students." International Journal of Science Education, vol. 31, no. 3, pp. 459-480, February 2009.
9. N.S. Newcombe and M. Stieff, "Six Myths about Spatial Thinking." International Journal of Science Education, vol. 34, no. 6, pp. 955-971, July 2011.
10. S. Hsi, M.C. Linn and J.E. Bell, "The role of spatial reasoning in engineering and the design of spatial instruction." Journal of Engineering Education, vol. 86, no. 2, pp.151-158. 1997.
11. S.A. Sorby, "Developing 3-D spatial visualization skills." Engineering Design Graphics Journal, vol. 63, no. 2, pp. 21-32 Spring 1999.
12. S. Strong and R. Smith, "Spatial visualization: Fundamentals and trends in engineering graphics." Journal of Industrial Technology, vol. 18, no. 1, pp.1-6, January 2001.
13. ENGAGE Learning, National Science Foundation. Retrieved from http://www.engageengineering.org/ , 2014.
14. R. Donnelly and M. Fitzmaurice, "Collaborative project-based learning and problem-based learning in higher education: A consideration of tutor and student roles in learner-focused strategies," in Emerging Issues in the Practice of University Learning and Teaching, 2005, pp. 87-98.
15. J. R. Savery, "Overview of problem-based learning; Definitions and Distinctions," The Interdisciplinary J of Problem-based Learning, vol. 1, no. 1, pp 9-20, Spring 2006.
16. Y. V. Zastavker, M. Ong, and L. Page, "Women in Engineering: Exploring the effects of project-based learning in a first-year undergraduate engineering program," 36th ASEE/IEEE Frontiers in Education Conference, session S3G-1, October 2006.
17. C.W. Swan, K.G. Paterson, and A.R. Bielefeldt, "Measuring the impacts of project-based service learning in engineering education," 39th ASEE/IEEE Frontiers in Education Conference, session M3B-1, October 2009.

18. S. Barge, Principles of Problem and Project Based Learning: The Aalborg PBL Model (AalborgUniversity), http://www.en.aau.dk/About+Aalborg+University/The+Aalborg+model+for+problem+based+learning+(PBL)/ .
19. D. Bedard, C. Lison, D. Dalle, D. Cote, and N. Boutin, "Problem-based and project-based learning in engineering and medicine: Determinants of students' engagement and persistance," Interdisciplinary J of Problem-based Learning, vol. 6, no. 2, pp 7-30.
20. G. Pleiss, M. Perry, Y.V. Zastavker, "Student self-efficacy in introductory project-based learning courses," 2012 Frontiers in Education Conference, pp. 1-6, October 2012.
21. B. Galand, M. Frenay, and B. Raucent, "Effectiveness of problem-based learning in engineering education: A comparative study on three levels of knowledge structure," International J of Engineering Education, vol. 28, no. 4, pp. 939-947, 2012.
22. K-H. Tseng, C-C. Chang, S-J. Lou, W-P. Chen, "Attitudes towards science technology, engineering, and mathematics (STEM) in a project-based learning (PjBL) environment," Int J Technol Des Edu, vol. 23, pp. 87-102, 2013.
23. E. Ferguson, Engineering and the Mind's Eye. Cambridge, MA: The MIT Press, 1992

CHAPTER 6

SUMMARY AND DISCUSSION

6.1 Summary

The objective of this work was to characterize the biomechanical pathway of OA development in the murine tibial loading model. Abnormal mechanical forces, such as those induced from joint instability due to injury[1,2], obesity[3,4], or excessive physical force[5,6] have been hypothesized to play a major role in disease initiation. Many preclinical models of OA have focused on the use of injury to induce disease and characterized OA progression biologically[7–12]. However, confounding factors such as joint inflammation and difficulty in measuring joint mechanics have prevented studies from distinguishing the exact role of mechanical forces in OA initiation[13]. Furthermore, the role of tissue material properties in the joint in response to abnormal mechanical forces during disease progression has not been fully characterized. The non-invasive tibial loading model provides a controlled platform that enables the simultaneous analyses of bone and cartilage tissues in response to a consistent and controlled mechanical stimulus. Thus, we can elucidate the relationships between mechanical forces, joint tissue properties, and OA development.

6.1.1 Kinematics of Meniscal- and ACL-Transected Mouse Knees during Controlled Tibial Compressive Loading Captured Using Roentgen Stereophotogrammetry

Although abnormal mechanical forces play a role in OA initiation[1,14,15], the exact etiology of disease development is unknown. The non-invasive tibial loading model[16] provides a controlled platform without confounding factors such as surgical insult[17] to examine the relationship between joint motion and OA progression. The model has been previously

established to induce OA progression following a single bout[18] or after 1, 2, and 6 weeks of daily loading[16,19]. This compressive loading recapitulates hallmark features of OA including cartilage degradation and thinning, subchondral bone changes, and osteophyte formation[16,20]. Although the biological and structural features of load-induced OA have been characterized in this model, the exact joint kinematics leading to disease initiation was previously unknown.

In this study, the kinematics of intact knee joints were characterized and compared to the kinematics of ACL- and meniscal-transected joints. Using roentgen stereophotogrammetric analysis (RSA), the kinematics of intact and injuries knee joints were characterized under tibial compressive loading[21]. ACL-transected joints immediately dislocated, whereas intact and meniscal-transected joints exhibited similar and consistent joint kinematics with compressive loading. Tibial loading induced a proximal and anterior translation of the tibia and increased flexion of the knee as compression increased from 0 to 9N. This study confirmed that the tibial loading model induced controlled and consistent joint kinematics in conjunction with OA progression, and thus could serve as an excellent model through which to elucidate the relationship between joint mechanics and OA development.

6.1.2 Role of Subchondral Bone Properties and Changes in Development of Load-Induced Osteoarthritis in Mice

The role of the subchondral bone in OA initiation and progression has been long debated[22–28]. While some hypothesize that subchondral bone stiffness plays a major role in the biomechanical progression of disease[23–25], others believe that subchondral bone remodeling may drive increased bone-cartilage crosstalk leading to disease initiation[26–30]. Clinical evidence of subchondral bone sclerosis[20,31], in addition to preclinical evidence of temporal changes in bone

mass during OA progression[10,32], make the subchondral bone an attractive target for potential therapeutics. For example, clinical studies have explored the use of bisphosphonates to inhibit bone remodeling with the objective of attenuating OA severity[33,34]. While these treatments reduced bone remodeling, they did not slow radiographic joint space narrowing in OA patients. Although post-traumatic preclinical studies[35–38] have shown promising efficacy of bisphosphonate treatment in attenuating OA, inflammation due to surgery confounds and limits clinical comparisons. The tibial loading model[16] provides a controlled, non-invasive platform in which to examine the role of subchondral bone remodeling and properties on OA progression and severity.

In this study, we used the bisphosphonate, alendronate, to inhibit bone remodeling, and examined two mouse strains with different subchondral bone mass and properties[39]. Adult male B6 (low subchondral bone mass) and FVB (high subchondral bone mass) mice were separated into daily alendronate- and vehicle-treatment groups. The left limb of each mouse was subjected to daily tibial loading for 1, 2, and 6 weeks. Although FVB mice had higher subchondral bone mass, OA progression was less severe with loading compared to B6 mice. ALN treatment generally prevented age-related reductions in cancellous bone mass; however, treatment did not prevent load-induced bone changes. ALN treatment exacerbated OA severity of B6 mice, but attenuated OA in FVB mice. Unlike previous hypotheses, lower subchondral bone mass and stiffness did not correlate with reduced OA severity, and ALN treatment did not necessarily attenuate OA progression. We hypothesize that these data may result from the use of two mouse strains with different bone and cartilage homeostasis. Despite our contrasting results to previous studies, bone properties may play a role in OA progression through changes in bone turnover rather than intrinsic bone mass and stiffness.

6.1.3 Computational Models for the Analysis of Load-Induced Osteoarthritis

To fully elucidate the role of mechanical forces in OA development and to enable potential comparisons to the clinical case, the contact mechanics of the joint must be characterized. While knee contact mechanics have been measured clinically in many activities and with OA disease progression[40–46], preclinical studies on joint mechanics in relation to OA are limited. Specifically, in the mouse, few studies have examined joint mechanics, due its small size, and the difficulty in measuring *in vivo* contact pressures[47,48]. Computational models can serve as a great tool to characterize the joint contact mechanics for situations in which *in vivo* experimental measurements are difficult. In addition, validated models enable us to examine the role of tissue material properties and changes on load-induced OA more effectively and faster than can be done experimentally.

To this end, we examined the joint contact mechanics during tibial compressive loading using a discrete element model. Using kinematics data from cadaveric studies from 0-9N compressive loads as inputs, we characterized the contact pressures on the tibial cartilage surface. As loading increased, the peak contact pressures were sufficient to induce fibrillations on the cartilage surfaces, and the areas of peak contact pressures computationally correlated with areas of highest cartilage damage experimentally; thus, confirming a direct relationship between mechanical forces and OA initiation. Although the movement of the contact areas was not examined in this study, we also hypothesize that in conjunction with load magnitude, sliding velocity during loading may also correlate with areas of highest cartilage damage.

In addition, we developed a simple finite element contact model and conducted a

parametric analysis to examine the effects of alterations in tissue material properties and geometry on contact pressures. Only changes in cartilage properties and geometry affected cartilage pressures. However, changes in both cortical and cancellous bone and cartilage resulted in significant changes in stresses/strains induced in the bone. Thus, while changing bone properties may not directly affect contact pressure, changes to any tissue in the joint could alter the stresses engendered in the bone, thus inducing subsequent bone adaptation. Such bone remodeling has been suggested to play a key role in bone-cartilage crosstalk in the initiation and development of OA[29], and opportunity for future studies using this model. We have directly correlated mechanical stimulus induced by tibial loading to the area of biological changes observed in the joint and examined the role of cartilage and bone tissue properties on contact pressures. Ultimately, these results not only confirm the role of mechanical forces on OA initiation and progression, but also begin to elucidate the role of each joint tissue on disease development.

6.1.4 Strengths of This Work

A major strength of the tibial loading model in understanding the relationship between mechanical forces and OA development is the lack of confounding inflammatory responses observed in post-traumatic models[10,11,13]. The use of a non-invasive, mechanical stimulus to induce OA lends itself well to studies aimed at distinguishing the role of mechanical forces in disease initiation. Joint kinematics in this model has been characterized and demonstrated to be consistent and controlled[21]. Furthermore, analysis of contact mechanics suggests that areas of highest mechanical stress correlate with areas of greatest joint damage. Future studies can thus explore and fully characterize potential mechanical treatment options such as more moderate

loads that may be beneficial for cartilage and joint health *in vivo*.

In addition, the use of the tibial loading model allows the simultaneous analysis of all the tissues in the joint. Selective targeting of joint tissues, such as bone or cartilage, by using drugs or genetic mouse models is possible, and can facilitate better understanding of the role of each tissue in mechanical loading in a healthy and diseased joint. Furthermore, because OA has been shown to affect the whole joint, the model can enable both examination of specific joint tissues, and whole-joint evaluation of disease progression, thus improving understanding of the biomechanical pathology of osteoarthritis.

Another strength of this work is the use of computational models to characterize joint mechanics. Due to the small size of the mouse, *in vivo* experimental characterization of joint mechanics is difficult. Discrete element models have been used extensively to characterize contact pressures in articulating surfaces[49–52], and provide an accurate platform with which to examine the relationship between mechanics and biology in OA progression. Furthermore, the use of finite element modeling enables customized analysis to each joint geometry, thus furthering our understanding of mechanobiology of OA in both the preclinical and clinical settings.

6.1.5 Limitations of This Work

Although this work is one of the first to explore the relationship between mechanical forces and OA pathology, these studies have several limitations. First, the characterization of joint kinematics in this model was conducted on cadaver mice. While this work provides a foundation in understanding joint kinematics with tibial loading, tissue material changes, particularly in the cartilage due to its viscoelastic behavior[53], may have occurred due to animal

death. Thus, the true motion of the joint in vivo may be different than characterized. Furthermore, only one cycle of loading was characterized in this study; however, in our *in vivo* studies, one bout of loading was composed of 1200 cycles. The kinematics of the joint could change with subsequent loading cycles. Thus, while the kinematics in cadaveric studies are useful in understanding joint mechanics, evaluating true kinematics *in vivo* requires analyses with live animals over multiple load cycles.

The use of two mouse strains to distinguish the role of subchondral bone properties in the initiation of OA introduces a confounding factor due to potential differences in mouse metabolism and bone homeostasis. Results from our finite element parametric analysis suggest that although differences in subchondral bone properties may not directly affect contact pressures, they may play a role in rates of bone remodeling and adaptation to load. Although we did not measure rates of bone remodeling in this work, the use of two mouse strains may have masked any evidence of differences in bone remodeling rates due to differences in subchondral bone properties. Furthermore, ALN was used to inhibit bone remodeling, and its effect may have been intrinsically different between the two mouse strains. Therefore, interpretations of the effect of ALN on each mouse strain should be considered carefully, as the conclusions may depend on the baseline rate of bone remodeling in each mouse strain or differences in bone response to treatment. Future studies should consider this limitation with an experimental design controlling for, or at least report differences in, baseline bone homeostasis.

In addition, the use of cadaveric studies to characterize joint kinematics and contact mechanics in healthy limbs only considers the joint at the initiation of loading. Previous studies have demonstrated that the joint geometry changes as daily loading continues[16,19]. Osteophyte formation in addition to cartilage and bone changes alter joint geometry, and could lead to

significant changes in joint kinematics. Clinically, such geometric changes lead to reduced joint functionality and contact mechanics[20]. Thus, understanding the joint kinematics and contact mechanics not only at the start of a loading study but as OA progresses would provide key knowledge regarding the mechanism through which mechanical forces initiate and progress the disease *in vivo.*

Lastly, although the use of the mouse provides many key advantages in understanding OA pathology, limitations exist in the comparison to the human case. Elucidating the relationship between the joint mechanical environment and the onset of OA in the mouse will provide significant knowledge of the biomechanical mechanism of disease; however, clinical implications should be interpreted carefully. Unlike the human knee, the mouse knee is naturally flexed, and any comparisons of joint contact mechanics may not necessarily be directly applicable to the clinical scenario. Although mouse gait has been previously characterized,[54–57] the contact pressures induced in the knee during normal gait are unknown. Therefore, developing an accurate biological meaning of the calculated contact pressures may be difficult and should be interpreted carefully.

6.2 Future Work

This thesis provides a foundation for characterizing joint mechanics in the mouse knee in relation to the onset and progression of osteoarthritis, and thus can be used to launch additional work to further our knowledge of the role of mechanical forces in OA development. The integration of experimental with computational studies will advance our understanding of load-induced OA in mouse, while simultaneously enabling interpretations of and comparisons to the clinical case.

6.2.1 Characterization of Contact Mechanics during OA Progression

As previously described, our study only used measurements from the healthy tibia and femur to create computational models and analyze joint kinematics and contact mechanics at the start of loading. Although these data provide an estimate of joint kinematics and contact mechanics, joint mechanics *in vivo* and during OA progression is unknown. The proposed future study would be comprehensive, utilizing both experimental and computational techniques to understand the biomechanics of OA induction longitudinally *in vivo.*

To characterize joint kinematics *in vivo*, mice would be subjected to tibial loading for 1, 2, or 6 weeks, like previous studies[16]. Prior to the final loading bout in the each duration group, the tibia and femur in each joint will be labelled with radiopaque markers for roentgen stereophotogrammetric analysis, and the joint can also be injected with nanoparticle contrast agents[58] to visualize the cartilage and meniscus. The final loading bout for duration would be conducted within an *in vivo* microCT[59], and the positions of the joint at 0 and 9N would be analyzed for each cycle. The kinematics can thus be characterized from the first to the final cycle for each loading duration. These data would allow us to not only understand the joint kinematics over the course of multiple loading cycles, but also provide knowledge about the changes in kinematics as OA progresses.

Once the *in vivo* joint kinematics have been characterized after 1, 2, and 6 weeks of OA progression, similar computational models as in Chapter 4 can be developed to elucidate contact mechanics. Visualization of the cartilage and menisci using nanoparticles would enable a more appropriate approximation of localized tissue thickness and a customized computational

geometry for each joint. This increased complexity of the computational model would allow for a more accurate evaluation of stresses and strains in the cartilage and bone, during each loading bout, and as OA progresses from 1 to 6 weeks. These data would provide valuable information about the changes in joint kinematics during OA progression and a viable platform through which to develop biomechanical therapies for disease treatment.

6.2.2 Changes in Chondrocyte Homeostasis in Load-Induced Osteoarthritis

In addition to a more complex *in vivo* study to confirm our *ex vivo* results, future work should investigate the mechanobiology of OA progression in the cartilage and bone, and their interactions. Tibial loading does not induce structural cartilage damage initially, but rather initiates a cell-mediated process through which OA develops[18]. Although changes in chondrocyte homeostasis with loading have been examined *in vitro*[60–62], the effect of loading *in vivo* is unknown. Future studies should focus on understanding the genetic and molecular changes in the chondrocyte with loading. Immunohistochemical staining of chondrocytes after a single load bout can be used to analyze cell viability, hypertrophy (Type X Collagen)[63], and apoptosis (Caspase 3)[18]. Genetic changes can also be examined using real-time PCR[64] to isolate chondrocytes and determine genes that are up- or down- regulated with loading. This study would enable potential future genetic therapies to prevent or treat OA.

To further enable the potential development of treatments and better elucidate the role of chondrocyte changes in OA progression, genetic mouse models could then be utilized. These models would investigate the role of inhibiting chondrocyte genetic changes in attenuating OA. Conditional knockout models, using the Col2a1 promoter (cre/loxP system)[65,66], could be developed for specific genes based on the chondrocyte genetic analysis previously described. For

example, studies have implicated ADAMTS5 in the cartilage degradation as OA progresses[67]. Studies have demonstrated effective attenuation of OA in ADAMTS5 knockout mice in injury models[66]. The biological and mechanical effect of genetic knockouts, such as ADAMTS5, should be investigated in the tibial loading model in which the joint mechanical environment can be more precisely measured. These studies would increase the knowledge of mechanobiology of cartilage degradation during OA progression, and the relationship between mechanical forces and chondrocyte changes during disease development.

6.2.3 Role of Subchondral Bone Microdamage in Load-Induced Osteoarthritis

An understanding of bone changes with loading would also improve the knowledge of cartilage-bone crosstalk in load-induced OA. Changes in cartilage-bone crosstalk is hypothesized to result from increased bone turnover due to microdamage from loading[27,29,30]. In the tibial model, loading does not induce overt macroscopic damage to the subchondral bone; however, osteoarthritic bone changes contribute to the initiation and progression of OA. Burr *et al.*[27,29,30] have hypothesized that abnormal loads associated with OA may initiate microcracks or microdamage in the subchondral cancellous bone leading to increased bone turnover. However, most studies investigating the subchondral bone have utilized post-traumatic models that limit the ability to distinguish surgical trauma from OA-induced changes. Using the tibial loading model, studies can investigate whether microdamage is present and correlate areas of microcracks with increased bone turnover to understand the role of microcracks in cartilage-bone crosstalk. Specifically, mice could be subjected to a single loading bout, injected with calcein,[68] and analyzed using bone histomorphometry[69], after 1, and 2 weeks post-loading. Joints could also be stained with lead uranyl acetate and sectioned using serial milling to visualize

microcracks in the cancellous bone after a single bout of loading[70,71]. Locations of high bone turnover and microcracks could be examined to see if they co-localize after a single compressive loading bout. In addition to investigating the co-localization of microcracks and bone turnover, cartilage-bone crosstalk can be analyzed by examining whether areas of high bone turnover underlie areas of the most severe cartilage degradation. Understanding the relationship between microdamage, bone turnover, and cartilage-bone crosstalk may provide insight to the mechanobiology of OA progression leading to potential clinical treatment options.

6.3 Synthesis of This Work

Taken together, the results of this work suggest that *in vivo* tibial loading induces controlled and consistent kinematics in the healthy mouse knee joint. These controlled motions induce contact pressures on the cartilage surface, that may not directly lead to cartilage damage, but rather initiate a cell-mediated response to loading[18]. Changes in the stresses engendered on the subchondral bone are also evident and may explain potential changes in bone remodeling as OA progresses. Our experimental and computational results suggest that although subchondral bone mass and stiffness may change as the disease progresses, increased bone mass and stiffness may not be sufficient to exacerbate or explain increased cartilage damage and OA severity. Instead, consistent joint motions through tibial compressive loading induce bone adaptation[72], and the magnitude of bone changes may depend on baseline subchondral bone properties. Thus, although subchondral bone properties may play a role in load-induced OA development, our results suggest that changes to subchondral bone remodeling with load may better explain the disease severity. The tibial loading model results in consistent joint motions and instability, leading to changes in the contact pressures and stresses induced on the cartilage and bone. These

stresses initiate a cell-mediated process through which cartilage and bone adapt, leading to the onset and progression of OA. This work presents an initial step in understanding the mechanobiology of OA. Future studies can build on this work, furthering our knowledge of osteoarthritis and leading to the potential development of therapeutics.

6.4 REFERENCES

1. Felson DT. Osteoarthritis: New Insights. Part 1: The Disease and Its Risk Factors. *Ann Intern Med*. 2000;133(8):635. doi:10.7326/0003-4819-133-8-200010170-00016.
2. Lohmander LS, Englund PM, Dahl LL, Roos EM. The long-term consequence of anterior cruciate ligament and meniscus injuries: osteoarthritis. *Am J Sports Med*. 2007;35(10):1756-1769. doi:10.1177/0363546507307396.
3. Felson DT, Anderson JJ, Naimark A, Walker AM, Meenan RF. Obesity and Knee Osteoarthritis. *Ann Intern Med*. 1988;109(1):18. doi:10.7326/0003-4819-109-1-18.
4. Messier SP, Loeser RF, Miller GD, Morgan TM, Rejeski WJ, Sevick MA, Ettinger WH, Pahor M, Williamson JD. Exercise and dietary weight loss in overweight and obese older adults with knee osteoarthritis: the Arthritis, Diet, and Activity Promotion Trial. *Arthritis Rheum*. 2004;50(5):1501-1510. doi:10.1002/art.20256.
5. Kaila-Kangas L, Arokoski J, Impivaara O, Viikari-Juntura E, Leino-Arjas P, Luukkonen R, Heliövaara M. Associations of hip osteoarthritis with history of recurrent exposure to manual handling of loads over 20 kg and work participation: a population-based study of men and women. *Occup Environ Med*. 2011;68(10):734-738. doi:10.1136/oem.2010.061390.
6. Cameron KL, Hsiao MS, Owens BD, Burks R, Svoboda SJ. Incidence of physician-diagnosed osteoarthritis among active duty United States military service members. *Arthritis Rheum*. 2011;63(10):2974-2982. doi:10.1002/art.30498.
7. McErlain DD, Appleton CTG, Litchfield RB, Pitelka V, Henry JL, Bernier SM, Beier F, Holdsworth DW. Study of subchondral bone adaptations in a rodent surgical model of OA using in vivo micro-computed tomography. *Osteoarthr Cartil*. 2008;16(4):458-469. doi:10.1016/j.joca.2007.08.006.
8. Pond MJ, Nuki G. Experimentally-induced osteoarthritis in the dog. *Ann Rheum Dis*. 1973;32(4):387-388.
9. Kamekura S, Hoshi K, Shimoaka T, Chung U, Chikuda H, Yamada T, Uchida M, Ogata N, Seichi A, Nakamura K, Kawaguchi H. Osteoarthritis development in novel experimental mouse models induced by knee joint instability. *Osteoarthritis Cartilage*. 2005;13(7):632-641. doi:10.1016/j.joca.2005.03.004.
10. Hayami T, Pickarski M, Zhuo Y, Wesolowski GA, Rodan GA, Duong LT. Characterization of articular cartilage and subchondral bone changes in the rat anterior cruciate ligament transection and meniscectomized models of osteoarthritis. *Bone*. 2006;38(2):234-243. doi:10.1016/j.bone.2005.08.007.
11. Glasson SS, Blanchet TJ, Morris EA. The surgical destabilization of the medial meniscus (DMM) model of osteoarthritis in the 129/SvEv mouse. *Osteoarthritis Cartilage*. 2007;15(9):1061-1069. doi:10.1016/j.joca.2007.03.006.
12. Culley KL, Dragomir CL, Chang J, Wondimu EB, Coico J, Plumb DA, Otero M, Goldring MB. Mouse models of osteoarthritis: surgical model of posttraumatic osteoarthritis induced by destabilization of the medial meniscus. *Methods Mol Biol*. 2015;1226:143-173. doi:10.1007/978-1-4939-1619-1_12.
13. Christiansen BA, Guilak F, Lockwood KA, Olson SA, Pitsillides AA, Sandell LJ, Silva MJ, van der Meulen MCH, Haudenschild DR. Non-invasive mouse models of post-traumatic osteoarthritis. *Osteoarthr Cartil*. 2015;23(10):1627-1638. doi:10.1016/j.joca.2015.05.009.

14. Arokoski J, Kiviranta I, Jurvelin J, Tammi M, Helminen HJ. Long-distance running causes site-dependent decrease of cartilage glycosaminoglycan content in the knee joints of beagle dogs. *Arthritis Rheum*. 1993;36(10):1451-1459. doi:10.1002/art.1780361018.
15. Lapveteläinen T, Nevalainen T, Parkkinen JJ, Arokoski J, Kiraly K, Hyttinen M, Halonen P, Helminen HJ. Lifelong moderate running training increases the incidence and severity of osteoarthritis in the knee joint of C57BL mice. *Anat Rec*. 1995;242(2):159-165. doi:10.1002/ar.1092420204.
16. Ko FC, Dragomir C, Plumb DA, Goldring SR, Wright TM, Goldring MB, van der Meulen MCH. In vivo cyclic compression causes cartilage degeneration and subchondral bone changes in mouse tibiae. *Arthritis Rheum*. 2013;65(6):1569-1578. doi:10.1002/art.37906.
17. Christiansen BA, Guilak F, Lockwood KA, Olson SA, Pitsillides AA, Sandell LJ, Silva MJ, van der Meulen MCH, Haudenschild DR. Non-invasive mouse models of post-traumatic osteoarthritis. *Osteoarthritis Cartilage*. 2015;23(10):1627-1638. doi:10.1016/j.joca.2015.05.009.
18. Ko FC, Dragomir CL, Plumb DA, Hsia AW, Adebayo OO, Goldring SR, Wright TM, Goldring MB, van der Meulen MCH. Progressive cell-mediated changes in articular cartilage and bone in mice are initiated by a single session of controlled cyclic compressive loading. *J Orthop Res*. 2016;(October 2015):n/a-n/a. doi:10.1002/jor.23204.
19. Poulet B, Hamilton RW, Shefelbine S, Pitsillides AA. Characterizing a novel and adjustable noninvasive murine joint loading model. *Arthritis Rheum*. 2011;63(1):137-147. doi:10.1002/art.27765.
20. Wieland HA, Michaelis M, Kirschbaum BJ, Rudolphi KA. Osteoarthritis - an untreatable disease? *Nat Rev Drug Discov*. 2005;4(4):331-344. doi:10.1038/nrd1693.
21. Adebayo OO, Ko FC, Goldring SR, Goldring MB, Wright TM, van der Meulen MCH. Kinematics of meniscal- and ACL-transected mouse knees during controlled tibial compressive loading captured using roentgen stereophotogrammetry. *J Orthop Res*. 2016;(April 2016):1-23. doi:10.1002/jor.23285.
22. Li G, Yin J, Gao J, Cheng TS, Pavlos NJ, Zhang C, Zheng MH, Grynpas M, Alpert B, Katz I, Lieberman I, Pritzker K, Suri S, Walsh D, Madry H, Dijk C van, Mueller-Gerbl M, Burr D, et al. Subchondral bone in osteoarthritis: insight into risk factors and microstructural changes. *Arthritis Res Ther*. 2013;15(6):223. doi:10.1186/ar4405.
23. Radin E, Paul I, Rose R. Role of mechanical factors in pathogenesis of primary osteoarthritis. *Lancet*. 1972;299(7749):519-522. doi:10.1016/S0140-6736(72)90179-1.
24. Radin EL, Rose RM. Role of subchondral bone in the initiation and progression of cartilage damage. *Clin Orthop Relat Res*. 1986;(213):34-40.
25. Radin EL, Martin RB, Burr DB, Caterson B, Boyd RD, Goodwin C. Effects of mechanical loading on the tissues of the rabbit knee. *J Orthop Res*. 1984;2(3):221-234. doi:10.1002/jor.1100020303.
26. Burr DB, Schaffler MB. The Involvement of Subchondral Mineralized Tissues in Osteoarthrosis : Quantitative Microscopic Evidence. *Microsc Res Tech*. 1997;37:343-357. doi:10.1002/(SICI)1097-0029(19970515)37:4<343::AID-JEMT9>3.0.CO;2-L.
27. Burr DB. The importance of subchondral bone in osteoarthrosis. *Curr Opin Rheumatol*. 1998;10(3):256-262.
28. Kawcak CE, McIlwraith CW, Norrdin RW, Park RD, James SP. The role of subchondral bone in joint disease: a review. *Equine Vet J*. 2010;33(2):120-126. doi:10.1111/j.2042-3306.2001.tb00589.x.

29. Burr DB. The importance of subchondral bone in the progression of osteoarthritis. *J Rheumatol Suppl*. 2004;70:77-80.
30. Brown TD, Radin EL, Martin RB, Burr DB. Finite element studies of some juxtarticular stress changes due to localized subchondral stiffening. *J Biomech*. 1984;17(1):11-24.
31. Lawrence RC, Helmick CG, Arnett FC, Deyo RA, Felson DT, Giannini EH, Heyse SP, Hirsch R, Hochberg MC, Hunder GG, Liang MH, Pillemer SR, Steen VD, Wolfe F. Estimates of the prevalence of arthritis and selected musculoskeletal disorders in the United States. *Arthritis Rheum*. 1998;41(5):778-799. doi:10.1002/1529-0131(199805)41:5<778::AID-ART4>3.0.CO;2-V.
32. Botter SM, Van Osch GJVM, Clockaerts S, Waarsing JH, Weinans H, Van Leeuwen JPTM. Osteoarthritis induction leads to early and temporal subchondral plate porosity in the tibial plateau of mice: An in vivo microfocal computed tomography study. *Arthritis Rheum*. 2011;63(9):2690-2699. doi:10.1002/art.30307.
33. Spector TD, Conaghan PG, Buckland-Wright JC, Garnero P, Cline GA, Beary JF, Valent DJ, Meyer JM, Dixon T, Shaw M, Ebrahim S, Dieppe P, Millar W, Melzer D, Guralnik J, Brock D, Quam J, Michet C, et al. Effect of risedronate on joint structure and symptoms of knee osteoarthritis: results of the BRISK randomized, controlled trial [ISRCTN01928173]. *Arthritis Res Ther*. 2005;7(3):R625. doi:10.1186/ar1716.
34. Bingham CO, Buckland-Wright JC, Garnero P, Cohen SB, Dougados M, Adami S, Clauw DJ, Spector TD, Pelletier JP, Raynauld JP, Strand V, Simon LS, Meyer JM, Cline GA, Beary JF. Risedronate decreases biochemical markers of cartilage degradation but does not decrease symptoms or slow radiographic progression in patients with medial compartment osteoarthritis of the knee: Results of the two-year multinational knee osteoarthritis st. *Arthritis Rheum*. 2006;54(11):3494-3507. doi:10.1002/art.22160.
35. Muehleman C, Green J, Williams JM, Kuettner KE, Thonar EJ-MA, Sumner DR. The effect of bone remodeling inhibition by zoledronic acid in an animal model of cartilage matrix damage. *Osteoarthr Cartil*. 2002;10(3):226-233. doi:10.1053/joca.2001.0506.
36. Hayami T, Pickarski M, Wesolowski GA, Mclane J, Bone A, Destefano J, Rodan GA, Duong LT. The role of subchondral bone remodeling in osteoarthritis: Reduction of cartilage degeneration and prevention of osteophyte formation by alendronate in the rat anterior cruciate ligament transection model. *Arthritis Rheum*. 2004;50(4):1193-1206. doi:10.1002/art.20124.
37. Myers SL, Brandt KD, Burr DB, O'Connor BL, Albrecht M. Effects of a bisphosphonate on bone histomorphometry and dynamics in the canine cruciate deficiency model of osteoarthritis. *J Rheumatol*. 1999;26(12):2645-2653.
38. Siebelt M, Waarsing JH, Groen HC, Müller C, Koelewijn SJ, de Blois E, Verhaar JAN, de Jong M, Weinans H. Inhibited osteoclastic bone resorption through alendronate treatment in rats reduces severe osteoarthritis progression. *Bone*. 2014;66:163-170. doi:10.1016/j.bone.2014.06.009.
39. Wergedal JE, Sheng MH-C, Ackert-Bicknell CL, Beamer WG, Baylink DJ. Genetic variation in femur extrinsic strength in 29 different inbred strains of mice is dependent on variations in femur cross-sectional geometry and bone density. *Bone*. 2005;36(1):111-122. doi:10.1016/j.bone.2004.09.012.
40. Donahue T, Hull M, Rashid M, Jacobs C. A Finite Element Model of the Human Knee Joint for the Study of Tibio-Femoral Contact. *J Biomed Eng*. 2002;124(273-280).
41. Fukubayashi T, Kurosawa H. The Contact Area and Pressure Distribution Pattern of the

Knee: A Study of Normal and Osteoarthrotic Knee Joints. *Acta Orthpaedica Scand*. 1980;51:871-879.
42. Segal NA, Anderson DD, Iyer KS, Baker J, Torner JC, Lynch JA, Felson DT, Lewis CE, Brown TD. Baseline articular contact stress levels predict incident symptomatic knee osteoarthritis development in the MOST cohort. *J Orthop Res*. 2009;27(12):1562-1568. doi:10.1002/jor.20936.
43. Segal NA, Kern AM, Anderson DD, Niu J, Lynch J, Guermazi A, Torner JC, Brown TD, Nevitt M, Multicenter Osteoarthritis Study Group the MKOS. Elevated tibiofemoral articular contact stress predicts risk for bone marrow lesions and cartilage damage at 30 months. *Osteoarthr Cartil*. 2012;20(10):1120-1126. doi:10.1016/j.joca.2012.05.013.
44. Makinejad MD, Abu Osman NA, Abu Bakar Wan Abas W, Bayat M. Preliminary analysis of knee stress in full extension landing. *Clinics (Sao Paulo)*. 2013;68(9):1180-1188. doi:10.6061/clinics/2013(09)02.
45. Cleather DJ, Goodwin JE, Bull AMJ. Hip and knee joint loading during vertical jumping and push jerking. *Clin Biomech*. 2013;28(1):98-103. doi:10.1016/j.clinbiomech.2012.10.006.
46. Nagura T, Matsumoto H, Kiriyama Y, Chaudhari A, Andriacchi TP. Tibiofemoral Joint Contact Force in Deep Knee Flexion and Its Consideration in Knee Osteoarthritis and Joint Replacement. *J Appl Biomech*. 2006;22:305-313.
47. Poulet B, Westerhof T a T, Hamilton RW, Shefelbine SJ, Pitsillides a. a. Spontaneous osteoarthritis in Str/ort mice is unlikely due to greater vulnerability to mechanical trauma. *Osteoarthr Cartil*. 2013;21(5):756-763. doi:10.1016/j.joca.2013.02.652.
48. Das Neves Borges P, Forte AE, Vincent TL, Dini D, Marenzana M. Rapid, automated imaging of mouse articular cartilage by microCT for early detection of osteoarthritis and finite element modelling of joint mechanics. *Osteoarthr Cartil*. 2014;22(10):1419-1428. doi:10.1016/j.joca.2014.07.014.
49. Guess TM, Liu H, Bhashyam S, Thiagarajan G. A multibody knee model with discrete cartilage prediction of tibio - femoral contact mechanics. *Comput Methods Biomech Biomed Engin*. 2011:1-15. doi:10.1080/10255842.2011.617004.
50. Volokh KY, Chao EYS, Armand M. On foundations of discrete element analysis of contact in diarthrodial joints. *Mol Cell Biomech*. 2007;4(2):67-73.
51. Anderson DD, Iyer KS, Segal NA, Lynch JA, Brown TD. Implementation of discrete element analysis for subject-specific, population-wide investigations of habitual contact stress exposure. *J Appl Biomech*. 2010;26(2):215-223.
52. Bei Y, Fregly BJ. *Multibody Dynamic Simulation of Knee Contact Mechanics*. Vol 26.; 2004. doi:10.1016/j.medengphy.2004.07.004.
53. Mow VC, Kuei SC, Lai WM, Armstrong CG. Biphasic Creep and Stress Relaxation of Articular Cartilage in Compression: Theory and Experiments. *J Biomech Eng*. 1980;102(1):73. doi:10.1115/1.3138202.
54. Clarke K., Still J. Gait Analysis in the Mouse. *Physiol Behav*. 1999;66(5):723-729. doi:10.1016/S0031-9384(98)00343-6.
55. Ferland CE, Laverty S, Beaudry F, Vachon P. Gait analysis and pain response of two rodent models of osteoarthritis. *Pharmacol Biochem Behav*. 2011;97(3):603-610. doi:10.1016/j.pbb.2010.11.003.
56. Cendelín J, Voller J, Vožeh F. Ataxic gait analysis in a mouse model of the olivocerebellar degeneration. *Behav Brain Res*. 2010;210(1):8-15.

doi:10.1016/j.bbr.2010.01.035.
57. Wooley CM, Sher RB, Kale A, Frankel WN, Cox GA, Seburn KL. Gait analysis detects early changes in transgenic SOD1(G93A) mice. *Muscle Nerve*. 2005;32(1):43-50. doi:10.1002/mus.20228.
58. Ashton JR, West JL, Badea CT. In vivo small animal micro-CT using nanoparticle contrast agents. *Front Pharmacol*. 2015;6:256. doi:10.3389/fphar.2015.00256.
59. Buie HR, Campbell GM, Klinck RJ, MacNeil JA, Boyd SK. Automatic segmentation of cortical and trabecular compartments based on a dual threshold technique for in vivo micro-CT bone analysis. *Bone*. 2007;41(4):505-515. doi:10.1016/j.bone.2007.07.007.
60. Lee JH, Fitzgerald JB, Dimicco MA, Grodzinsky AJ. Mechanical Injury of Cartilage Explants Causes Specific Time-Dependent Changes in Chondrocyte Gene Expression. *ARTHRITIS Rheum*. 2005;52(8):2386-2395. doi:10.1002/art.21215.
61. Wehland M, Aleshcheva G, Schulz H, Saar K, Hübner N, Hemmersbach R, Braun M, Ma X, Frett T, Warnke E, Riwaldt S, Pietsch J, Corydon TJ, Infanger M, Grimm D. Differential gene expression of human chondrocytes cultured under short-term altered gravity conditions during parabolic flight maneuvers. 2012. doi:10.1186/s12964-015-0095-9.
62. Villanueva I, Weigel CA, Bryant SJ. Cell-matrix interactions and dynamic mechanical loading influence chondrocyte gene expression and bioactivity in PEG-RGD hydrogels. *Acta Biomater*. 2009;5(8):2832-2846. doi:10.1016/j.actbio.2009.05.039.
63. Von Der Mark K, Kirsch T, Nerlich A, Kuss A, Weseloh G, Glückert K, Stöss H. Type x collagen synthesis in human osteoarthritic cartilage. indication of chondrocyte hypertrophy. *Arthritis Rheum*. 1992;35(7):806-811. doi:10.1002/art.1780350715.
64. Martin I, Jakob M, Schäfer D, Dick W, Spagnoli G, Heberer M. Quantitative analysis of gene expression in human articular cartilage from normal and osteoarthritic joints. *Osteoarthr Cartil*. 2001;9(2):112-118. doi:10.1053/joca.2000.0366.
65. Roughley P. Creating conditional knockout mice for OA research. *Osteoarthr Cartil*. 2013;21(1):S7. doi:10.1016/j.joca.2012.09.015.
66. Glasson SS, Askew R, Sheppard B, Carito B, Blanchet T, Ma H-L, Flannery CR, Peluso D, Kanki K, Yang Z, Majumdar MK, Morris EA. Deletion of active ADAMTS5 prevents cartilage degradation in a murine model of osteoarthritis. *Nature*. 2005;434(7033):644-648. doi:10.1038/nature03369.
67. Goldring MB, Marcu KB. Cartilage homeostasis in health and rheumatic diseases. *Arthritis Res Ther*. 2009;11(3):224. doi:10.1186/ar2592.
68. Melville KM, Kelly NH, Khan SA, Schimenti JC, Ross FP, Main RP, van der Meulen MCH. Female Mice Lacking Estrogen Receptor-Alpha in Osteoblasts Have Compromised Bone Mass and Strength. *J Bone Miner Res*. 2014;29(2):370-379. doi:10.1002/jbmr.2082.
69. Dempster DW, Compston JE, Drezner MK, Glorieux FH, Kanis JA, Malluche H, Meunier PJ, Ott SM, Recker RR, Parfitt AM. Standardized nomenclature, symbols, and units for bone histomorphometry: a 2012 update of the report of the ASBMR Histomorphometry Nomenclature Committee. *J Bone Miner Res*. 2013;28(1):2-17. doi:10.1002/jbmr.1805.
70. SLYFIELD Jr. CR, NIEMEYER KE, TKACHENKO EV, TOMLINSON RE, STEYER GG, PATTHANACHAROENPHON CG, KAZAKIA GJ, WILSON DL, HERNANDEZ CJ. Three-dimensional surface texture visualization of bone tissue through epifluorescence-based serial block face imaging. *J Microsc*. 2009;236(1):52-59. doi:10.1111/j.1365-2818.2009.03204.x.

71. Lambers FM, Bouman AR, Rimnac CM, Hernandez CJ, Tang S. Microdamage Caused by Fatigue Loading in Human Cancellous Bone: Relationship to Reductions in Bone Biomechanical Performance. Roeder RK, ed. *PLoS One*. 2013;8(12):e83662. doi:10.1371/journal.pone.0083662.
72. Lynch ME, Main RP, Xu Q, Schmicker TL, Schaffler MB, Wright TM, van der Meulen MCH. Tibial compression is anabolic in the adult mouse skeleton despite reduced responsiveness with aging. *Bone*. 2011;49(3):439-446. doi:10.1016/j.bone.2011.05.017.

APPENDIX A: CHAPTER 2 DATA

Absolute tibial motion measured by roentgen stereophotogrammetric analysis:

Animal	Group	Limb	Trial	Load	X (mm)	Y (mm)	Z (mm)	x-ro (deg)	y-ro (deg)	z-ro (deg)
ACLT1	ACL	L	1	0	0.000	0.000	0.000	0.000	0.000	0.000
ACLT1	ACL	L	1	1	-0.003	0.053	-0.012	-0.926	-0.100	0.409
ACLT1	ACL	L	1	2	-0.003	0.100	-0.027	-1.680	-0.149	0.824
ACLT1	ACL	L	1	3	0.011	0.113	-0.027	-1.781	-0.234	1.103
ACLT1	ACL	L	1	4	0.033	0.035	0.025	-0.297	-0.520	1.050
ACLT1	ACL	L	1	5	0.077	-0.031	0.004	0.430	-0.265	0.810
ACLT1	ACL	L	1	6	0.103	0.004	-0.048	0.272	0.137	1.293
ACLT1	ACL	L	1	7	0.134	0.036	-0.116	-0.846	0.550	1.338
ACLT1	ACL	L	1	8	0.167	0.000	-0.129	-1.168	0.534	0.884
ACLT1	ACL	L	1	9	0.208	-0.061	-0.145	-1.233	0.608	0.245
ACLT1	ACL	L	2	0	0.000	0.000	0.000	0.000	0.000	0.000
ACLT1	ACL	L	2	1	-0.030	0.108	0.066	-0.082	-0.532	1.421
ACLT1	ACL	L	2	2	-0.060	0.200	0.128	-0.086	-1.035	2.719
ACLT1	ACL	L	2	3	-0.053	0.240	0.103	-0.172	-0.829	3.494
ACLT1	ACL	L	2	4	-0.041	0.229	0.087	-0.423	-0.812	3.672
ACLT1	ACL	L	2	5	0.005	0.160	0.022	-0.629	-0.344	3.247
ACLT1	ACL	L	2	6	0.039	0.115	-0.017	-0.090	0.055	3.177
ACLT1	ACL	L	2	7	0.108	0.019	-0.121	0.289	0.995	2.453
ACLT1	ACL	L	2	8	0.180	-0.082	-0.247	0.258	2.098	1.584
ACLT1	ACL	L	2	9	0.254	-0.183	-0.393	-0.068	3.330	0.666
ACLT1	ACL	L	3	0	0.000	0.000	0.000	0.000	0.000	0.000
ACLT1	ACL	L	3	1	0.004	0.043	0.040	0.030	-0.290	0.603
ACLT1	ACL	L	3	2	0.012	0.093	0.051	-0.170	-0.353	1.208
ACLT1	ACL	L	3	3	0.040	0.115	-0.001	-0.177	0.177	1.580
ACLT1	ACL	L	3	4	0.081	0.134	-0.129	-0.597	1.273	1.771
ACLT1	ACL	L	3	5	0.115	0.072	-0.174	0.260	1.722	1.477
ACLT1	ACL	L	3	6	0.152	0.001	-0.220	0.537	1.943	0.893
ACLT1	ACL	L	3	7	0.193	-0.064	-0.282	1.026	2.386	0.431
ACLT1	ACL	L	3	8	0.189	0.044	-0.276	0.626	2.055	1.434
ACLT1	ACL	L	3	9	0.175	0.174	-0.260	0.314	1.659	2.674
ACLT2	ACL	L	1	0	0.000	0.000	0.000	0.000	0.000	0.000
ACLT2	ACL	L	1	1	0.025	-0.011	-0.013	-0.262	0.150	0.072
ACLT2	ACL	L	1	2	0.051	-0.026	-0.027	-0.494	0.298	0.109
ACLT2	ACL	L	1	3	0.064	-0.015	-0.038	-0.021	0.146	0.946

ACLT2	ACL	L	1	4	0.075	-0.008	-0.072	0.129	0.148	1.487
ACLT2	ACL	L	1	5	0.109	-0.027	-0.148	-0.158	0.797	1.208
ACLT2	ACL	L	1	6	0.139	-0.053	-0.203	0.099	1.407	0.934
ACLT2	ACL	L	1	7	0.170	-0.068	-0.254	0.294	1.948	0.783
ACLT2	ACL	L	1	8	0.180	-0.060	-0.265	0.291	1.845	1.127
ACLT2	ACL	L	1	9	0.195	-0.053	-0.284	0.068	1.824	1.367
ACLT2	ACL	L	2	0	0.000	0.000	0.000	0.000	0.000	0.000
ACLT2	ACL	L	2	1	0.000	-0.028	0.036	0.775	-0.302	0.473
ACLT2	ACL	L	2	2	-0.002	-0.057	0.075	1.543	-0.670	0.942
ACLT2	ACL	L	2	3	0.037	-0.090	0.021	1.768	0.024	1.073
ACLT2	ACL	L	2	4	0.061	-0.089	-0.020	1.722	0.373	1.478
ACLT2	ACL	L	2	5	0.072	-0.047	-0.053	1.619	0.525	2.316
ACLT2	ACL	L	2	6	0.096	-0.071	-0.089	1.951	0.797	2.242
ACLT2	ACL	L	2	7	0.115	-0.080	-0.121	1.634	0.908	2.076
ACLT2	ACL	L	2	8	0.157	-0.122	-0.186	1.706	1.542	1.535
ACLT2	ACL	L	2	9	0.198	-0.152	-0.257	1.652	2.198	1.106
ACLT2	ACL	L	3	0	0.000	0.000	0.000	0.000	0.000	0.000
ACLT2	ACL	L	3	1	0.013	-0.003	-0.011	-0.893	-0.145	-0.082
ACLT2	ACL	L	3	2	0.024	-0.013	-0.015	-1.543	-0.313	-0.146
ACLT2	ACL	L	3	3	0.030	0.001	-0.029	-1.700	-0.311	0.436
ACLT2	ACL	L	3	4	0.043	-0.001	-0.052	-1.663	-0.211	0.783
ACLT2	ACL	L	3	5	0.029	0.039	-0.054	-1.573	-0.554	1.713
ACLT2	ACL	L	3	6	0.045	0.030	-0.083	-1.820	-0.532	1.678
ACLT2	ACL	L	3	7	0.048	0.076	-0.118	-2.141	-0.514	2.417
ACLT2	ACL	L	3	8	0.063	0.064	-0.117	-0.856	-0.242	3.018
ACLT2	ACL	L	3	9	0.084	0.050	-0.127	0.274	0.149	3.517
ACLT3	ACL	L	1	0	0.000	0.000	0.000	0.000	0.000	0.000
ACLT3	ACL	L	1	1	0.026	-0.032	-0.028	0.031	0.211	-0.228
ACLT3	ACL	L	1	2	0.046	-0.064	-0.048	0.097	0.275	-0.461
ACLT3	ACL	L	1	3	0.063	-0.089	-0.053	-0.139	0.059	-0.904
ACLT3	ACL	L	1	4	0.082	-0.108	-0.065	-0.148	-0.044	-1.121
ACLT3	ACL	L	1	5	0.111	-0.105	-0.099	-0.341	0.223	-1.082
ACLT3	ACL	L	1	6	0.134	-0.113	-0.116	-0.625	0.233	-1.249
ACLT3	ACL	L	1	7	0.164	-0.128	-0.116	-0.873	0.007	-1.628

ACLT3	ACL	L	1	8	0.218	-0.133	-0.129	-1.041	0.101	-1.839
ACLT3	ACL	L	1	9	0.274	-0.140	-0.140	-1.194	0.150	-2.089
ACLT3	ACL	L	2	0	0.000	0.000	0.000	0.000	0.000	0.000
ACLT3	ACL	L	2	1	0.024	-0.006	-0.022	0.107	0.498	0.437
ACLT3	ACL	L	2	2	0.052	-0.008	-0.053	0.241	1.117	0.970
ACLT3	ACL	L	2	3	0.063	-0.084	-0.040	0.591	0.804	0.392
ACLT3	ACL	L	2	4	0.068	-0.146	-0.023	0.668	0.187	-0.226
ACLT3	ACL	L	2	5	0.079	-0.142	-0.036	0.319	-0.021	-0.137
ACLT3	ACL	L	2	6	0.120	-0.075	-0.109	0.213	0.855	1.032
ACLT3	ACL	L	2	7	0.153	-0.027	-0.169	0.244	1.465	1.815
ACLT3	ACL	L	2	8	0.175	-0.040	-0.201	0.381	1.606	1.717
ACLT3	ACL	L	2	9	0.196	-0.056	-0.233	0.467	1.729	1.569
ACLT3	ACL	L	3	0	0.000	0.000	0.000	0.000	0.000	0.000
ACLT3	ACL	L	3	1	0.040	0.080	-0.085	-0.115	1.299	1.534
ACLT3	ACL	L	3	2	0.074	0.145	-0.161	-0.299	2.411	2.790
ACLT3	ACL	L	3	3	0.091	0.102	-0.161	-0.444	2.119	2.314
ACLT3	ACL	L	3	4	0.099	0.051	-0.154	-0.397	1.619	1.750
ACLT3	ACL	L	3	5	0.105	0.031	-0.159	-0.166	1.327	1.722
ACLT3	ACL	L	3	6	0.119	0.054	-0.185	-0.281	1.419	2.116
ACLT3	ACL	L	3	7	0.149	0.100	-0.239	-0.804	1.967	2.683
ACLT3	ACL	L	3	8	0.178	0.083	-0.257	-0.724	2.000	2.584
ACLT3	ACL	L	3	9	0.205	0.058	-0.271	-0.646	1.928	2.328
DMM1	DMM	R	1	0	0.000	0.000	0.000	0.000	0.000	0.000
DMM1	DMM	R	1	1	0.039	0.070	-0.008	0.078	0.191	1.031
DMM1	DMM	R	1	2	0.072	0.119	-0.018	0.330	0.397	1.791
DMM1	DMM	R	1	3	0.094	0.147	-0.007	0.381	0.461	2.080
DMM1	DMM	R	1	4	0.118	0.167	0.008	0.515	0.451	2.246
DMM1	DMM	R	1	5	0.148	0.176	-0.001	0.756	0.630	2.338
DMM1	DMM	R	1	6	0.184	0.190	-0.025	1.132	1.051	2.571
DMM1	DMM	R	1	7	0.215	0.233	-0.009	1.405	0.963	3.087
DMM1	DMM	R	1	8	0.246	0.295	0.025	0.678	0.749	3.401
DMM1	DMM	R	1	9	0.271	0.349	0.065	-0.085	0.407	3.579
DMM1	DMM	R	3	0	0.000	0.000	0.000	0.000	0.000	0.000
DMM1	DMM	R	3	1	0.041	0.007	-0.010	0.006	0.143	0.310
DMM1	DMM	R	3	2	0.079	0.009	-0.015	0.042	0.211	0.552
DMM1	DMM	R	3	3	0.090	-0.049	-0.030	0.405	0.279	0.003

DMM1	DMM	R	3	4	0.098	-0.077	-0.039	0.854	0.208	-0.279
DMM1	DMM	R	3	5	0.124	-0.059	-0.075	1.986	0.251	0.222
DMM1	DMM	R	3	6	0.159	0.040	-0.072	1.860	0.135	1.337
DMM1	DMM	R	3	7	0.188	0.089	-0.071	1.192	0.099	1.637
DMM1	DMM	R	3	8	0.224	0.124	-0.103	0.589	0.459	1.648
DMM1	DMM	R	3	9	0.263	0.147	-0.147	0.275	0.908	1.575
DMM2	DMM	R	1	0	0.000	0.000	0.000	0.000	0.000	0.000
DMM2	DMM	R	1	1	0.008	-0.046	-0.004	0.448	-0.429	-0.156
DMM2	DMM	R	1	2	0.020	-0.079	-0.006	0.815	-0.883	-0.100
DMM2	DMM	R	1	3	0.042	-0.069	-0.024	0.317	-0.873	0.017
DMM2	DMM	R	1	4	0.043	-0.089	-0.020	-0.177	-1.221	-0.345
DMM2	DMM	R	1	5	0.051	-0.114	-0.033	-0.317	-1.230	-0.680
DMM2	DMM	R	1	6	0.051	-0.148	-0.040	-0.306	-1.467	-1.132
DMM2	DMM	R	1	7	0.099	-0.091	-0.084	-0.646	-1.032	-0.416
DMM2	DMM	R	1	8	0.157	-0.041	-0.151	-1.292	-0.206	0.150
DMM2	DMM	R	1	9	0.219	0.021	-0.221	-2.246	0.763	0.782
DMM2	DMM	R	2	0	0.000	0.000	0.000	0.000	0.000	0.000
DMM2	DMM	R	2	1	0.036	0.021	-0.040	-0.054	0.543	0.710
DMM2	DMM	R	2	2	0.068	0.035	-0.076	-0.031	0.987	1.328
DMM2	DMM	R	2	3	0.082	0.032	-0.084	-0.271	1.076	1.436
DMM2	DMM	R	2	4	0.106	0.035	-0.106	0.033	1.310	1.780
DMM2	DMM	R	2	5	0.153	0.076	-0.163	0.299	2.093	2.677
DMM2	DMM	R	2	6	0.181	0.094	-0.205	0.557	2.431	3.154
DMM2	DMM	R	2	7	0.206	0.127	-0.224	0.449	2.464	3.673
DMM2	DMM	R	2	8	0.198	0.104	-0.185	-0.409	1.918	2.923
DMM2	DMM	R	2	9	0.199	0.095	-0.159	-1.159	1.575	2.429
DMM2	DMM	R	3	0	0.000	0.000	0.000	0.000	0.000	0.000
DMM2	DMM	R	3	1	-0.002	-0.006	-0.007	-1.593	0.778	-0.888
DMM2	DMM	R	3	2	0.008	0.002	-0.022	-3.072	1.673	-1.433
DMM2	DMM	R	3	3	0.031	0.015	-0.046	-2.935	1.973	-0.957
DMM2	DMM	R	3	4	0.053	0.029	-0.049	-2.466	1.687	-0.195
DMM2	DMM	R	3	5	0.069	0.015	-0.084	-1.684	1.699	0.045
DMM2	DMM	R	3	6	0.110	0.055	-0.131	-1.492	2.167	0.772

DMM2	DMM	R	3	7	0.126	0.058	-0.150	-1.356	2.346	0.621
DMM2	DMM	R	3	8	0.156	0.078	-0.188	-1.294	2.733	0.713
DMM2	DMM	R	3	9	0.181	0.087	-0.228	-1.271	3.168	0.586
DMM3	DMM	R	1	0	0.000	0.000	0.000	0.000	0.000	0.000
DMM3	DMM	R	1	1	-0.015	-0.104	-0.016	1.148	-0.198	-0.785
DMM3	DMM	R	1	2	-0.029	-0.211	-0.042	2.336	-0.322	-1.599
DMM3	DMM	R	1	3	-0.026	-0.229	-0.035	2.113	-0.354	-1.835
DMM3	DMM	R	1	4	-0.002	-0.175	-0.024	1.731	-0.355	-1.252
DMM3	DMM	R	1	5	0.020	-0.187	-0.069	2.292	-0.067	-1.159
DMM3	DMM	R	1	6	0.046	-0.194	-0.125	3.136	0.360	-1.029
DMM3	DMM	R	1	7	0.078	-0.129	-0.142	2.990	0.713	-0.393
DMM3	DMM	R	1	8	0.140	-0.062	-0.229	3.043	1.789	0.301
DMM3	DMM	R	1	9	0.198	0.003	-0.315	2.865	2.886	0.868
DMM3	DMM	R	2	0	0.000	0.000	0.000	0.000	0.000	0.000
DMM3	DMM	R	2	1	0.013	-0.022	-0.022	-0.315	0.340	-0.172
DMM3	DMM	R	2	2	0.027	-0.027	-0.033	-1.052	0.649	-0.275
DMM3	DMM	R	2	3	0.057	0.031	-0.034	-1.451	0.716	0.543
DMM3	DMM	R	2	4	0.074	0.034	-0.052	-1.085	0.752	0.880
DMM3	DMM	R	2	5	0.086	0.019	-0.075	-0.252	0.745	1.062
DMM3	DMM	R	2	6	0.108	0.027	-0.113	0.342	0.954	1.332
DMM3	DMM	R	2	7	0.137	0.045	-0.164	0.306	1.411	1.439
DMM3	DMM	R	2	8	0.174	0.073	-0.218	0.088	1.964	1.703
DMM3	DMM	R	2	9	0.206	0.098	-0.265	-0.385	2.485	1.838
DMM3	DMM	R	3	0	0.000	0.000	0.000	0.000	0.000	0.000
DMM3	DMM	R	3	1	-0.046	-0.070	0.065	-0.843	-0.721	-1.008
DMM3	DMM	R	3	2	-0.087	-0.130	0.127	-1.749	-1.377	-1.922
DMM3	DMM	R	3	3	-0.082	-0.204	0.091	-1.006	-1.283	-2.268
DMM3	DMM	R	3	4	-0.045	-0.227	0.012	-0.147	-0.667	-2.035
DMM3	DMM	R	3	5	-0.029	-0.218	-0.003	-0.588	-0.470	-2.097
DMM3	DMM	R	3	6	0.007	-0.173	-0.032	-1.232	0.032	-1.759

DMM3	DMM	R	3	7	0.079	-0.033	-0.066	-2.667	0.773	-0.464
DMM3	DMM	R	3	8	0.146	0.115	-0.101	-4.686	1.573	0.731
DMM3	DMM	R	3	9	0.210	0.268	-0.138	-7.015	2.344	1.887
DMM4	DMM	R	1	0	0.000	0.000	0.000	0.000	0.000	0.000
DMM4	DMM	R	1	1	0.020	0.007	-0.045	1.176	0.026	0.224
DMM4	DMM	R	1	2	0.034	0.007	-0.090	2.322	0.027	0.310
DMM4	DMM	R	1	3	0.081	0.108	-0.082	0.895	0.354	1.288
DMM4	DMM	R	1	4	0.095	0.102	-0.126	0.441	0.983	0.918
DMM4	DMM	R	1	5	0.090	0.064	-0.158	0.357	1.365	0.124
DMM4	DMM	R	1	6	0.100	0.031	-0.218	1.601	1.518	-0.351
DMM4	DMM	R	1	7	0.134	0.082	-0.234	1.208	1.710	-0.121
DMM4	DMM	R	1	8	0.194	0.171	-0.297	0.669	2.655	0.501
DMM4	DMM	R	1	9	0.251	0.255	-0.366	0.147	3.658	1.075
DMM4	DMM	R	2	0	0.000	0.000	0.000	0.000	0.000	0.000
DMM4	DMM	R	2	1	0.036	0.025	-0.060	0.774	0.563	0.718
DMM4	DMM	R	2	2	0.065	0.038	-0.114	1.664	0.990	1.245
DMM4	DMM	R	2	3	0.087	0.051	-0.120	1.555	1.147	1.561
DMM4	DMM	R	2	4	0.098	0.037	-0.151	2.262	1.265	1.512
DMM4	DMM	R	2	5	0.104	0.041	-0.169	2.544	1.306	1.589
DMM4	DMM	R	2	6	0.121	0.064	-0.198	2.829	1.456	2.025
DMM4	DMM	R	2	7	0.158	0.137	-0.187	2.334	1.353	3.092
DMM4	DMM	R	2	8	0.178	0.145	-0.227	2.465	1.718	3.072
DMM4	DMM	R	2	9	0.194	0.142	-0.270	2.563	2.125	2.827
DMM4	DMM	R	3	0	0.000	0.000	0.000	0.000	0.000	0.000
DMM4	DMM	R	3	1	0.006	-0.026	-0.022	0.109	0.252	-0.471
DMM4	DMM	R	3	2	0.007	-0.064	-0.050	0.258	0.581	-1.129
DMM4	DMM	R	3	3	0.012	-0.125	-0.107	1.044	0.940	-1.906
DMM4	DMM	R	3	4	0.022	-0.170	-0.162	1.652	1.278	-2.542
DMM4	DMM	R	3	5	0.076	-0.100	-0.193	1.118	1.722	-1.699
DMM4	DMM	R	3	6	0.121	-0.035	-0.227	1.075	1.962	-0.881
DMM4	DMM	R	3	7	0.144	-0.024	-0.279	1.563	2.203	-0.830
DMM4	DMM	R	3	8	0.179	0.014	-0.343	1.907	2.576	-0.420
DMM4	DMM	R	3	9	0.221	0.068	-0.412	2.035	3.140	0.158

DMM1	DMM	L	1	0	0.000	0.000	0.000	0.000	0.000	0.000
DMM1	DMM	L	1	1	0.013	-0.042	0.015	2.479	0.202	0.680
DMM1	DMM	L	1	2	0.025	-0.062	0.015	3.941	0.308	1.266
DMM1	DMM	L	1	3	0.058	-0.017	-0.052	1.224	-0.041	1.039
DMM1	DMM	L	1	4	0.099	-0.015	-0.113	0.497	0.188	1.086
DMM1	DMM	L	1	5	0.150	-0.095	-0.136	3.088	1.064	1.218
DMM1	DMM	L	1	6	0.178	-0.129	-0.167	4.210	1.449	1.387
DMM1	DMM	L	1	7	0.212	-0.216	-0.178	5.849	1.550	0.933
DMM1	DMM	L	1	8	0.240	-0.214	-0.224	5.460	1.595	0.837
DMM1	DMM	L	1	9	0.271	-0.210	-0.276	5.040	1.724	0.759
DMM1	DMM	L	2	0	0.000	0.000	0.000	0.000	0.000	0.000
DMM1	DMM	L	2	1	0.060	0.082	-0.092	-2.055	0.644	0.753
DMM1	DMM	L	2	2	0.114	0.166	-0.185	-4.391	1.106	1.502
DMM1	DMM	L	2	3	0.149	0.297	-0.323	-8.431	1.235	2.539
DMM1	DMM	L	2	4	0.189	0.178	-0.234	-4.069	1.401	3.026
DMM1	DMM	L	2	5	0.255	0.065	-0.219	-0.763	2.203	3.056
DMM1	DMM	L	2	6	0.320	-0.113	-0.162	4.111	2.842	2.799
DMM1	DMM	L	2	7	0.351	-0.016	-0.249	0.915	2.615	3.068
DMM1	DMM	L	2	8	0.394	0.035	-0.319	-1.033	2.676	3.126
DMM1	DMM	L	2	9	0.447	0.080	-0.405	-3.113	2.923	3.072
DMM1	DMM	L	3	0	0.000	0.000	0.000	0.000	0.000	0.000
DMM1	DMM	L	3	1	0.035	0.018	-0.084	-0.816	0.978	0.466
DMM1	DMM	L	3	2	0.058	0.060	-0.170	-2.174	1.743	1.143
DMM1	DMM	L	3	3	0.057	0.100	-0.203	-2.833	1.812	2.165
DMM1	DMM	L	3	4	0.054	0.124	-0.206	-2.600	1.704	3.121
DMM1	DMM	L	3	5	0.092	0.006	-0.139	0.417	1.711	2.816
DMM1	DMM	L	3	6	0.130	-0.058	-0.149	1.811	2.180	2.774
DMM1	DMM	L	3	7	0.167	-0.038	-0.238	1.219	3.133	3.070
DMM1	DMM	L	3	8	0.183	-0.007	-0.298	1.054	3.785	3.663
DMM1	DMM	L	3	9	0.207	-0.005	-0.345	1.388	4.468	3.937
DMM2	DMM	L	1	0	0.000	0.000	0.000	0.000	0.000	0.000
DMM2	DMM	L	1	1	0.043	-0.064	-0.005	0.889	0.383	0.156
DMM2	DMM	L	1	2	0.089	-0.130	-0.017	1.746	0.884	0.241
DMM2	DMM	L	1	3	0.135	-0.176	-0.044	1.912	1.278	0.524
DMM2	DMM	L	1	4	0.162	-0.161	-0.105	0.245	1.424	1.176
DMM2	DMM	L	1	5	0.197	-0.178	-0.141	-0.527	1.530	1.565
DMM2	DMM	L	1	6	0.257	-0.253	-0.174	-0.642	1.720	1.081
DMM2	DMM	L	1	7	0.313	-0.286	-0.228	-0.892	2.564	1.541
DMM2	DMM	L	1	8	0.386	-0.335	-0.296	-1.131	3.659	1.705

DMM2	DMM	L	1	9	0.475	-0.419	-0.354	-0.652	4.940	1.351
DMM2	DMM	L	2	0	0.000	0.000	0.000	0.000	0.000	0.000
DMM2	DMM	L	2	1	0.103	-0.100	-0.061	0.436	1.132	-0.917
DMM2	DMM	L	2	2	0.189	-0.173	-0.126	0.509	2.130	-1.415
DMM2	DMM	L	2	3	0.285	-0.315	-0.156	0.712	2.063	-2.910
DMM2	DMM	L	2	4	0.337	-0.346	-0.213	0.259	2.332	-2.533
DMM2	DMM	L	2	5	0.386	-0.337	-0.329	-1.309	3.253	-1.727
DMM2	DMM	L	2	6	0.427	-0.339	-0.414	-1.974	4.092	-0.880
DMM2	DMM	L	2	7	0.480	-0.376	-0.485	-2.316	4.756	-0.645
DMM2	DMM	L	2	8	0.509	-0.343	-0.583	-4.140	5.315	0.383
DMM2	DMM	L	2	9	0.543	-0.327	-0.679	-5.877	5.850	1.182
DMM2	DMM	L	3	0	0.000	0.000	0.000	0.000	0.000	0.000
DMM2	DMM	L	3	1	-0.012	0.059	-0.076	-1.882	-0.302	1.274
DMM2	DMM	L	3	2	-0.018	0.100	-0.150	-3.409	-0.497	2.408
DMM2	DMM	L	3	3	0.002	0.083	-0.223	-3.718	0.129	3.262
DMM2	DMM	L	3	4	0.069	0.028	-0.320	-3.769	1.524	3.336
DMM2	DMM	L	3	5	0.103	0.012	-0.413	-5.000	1.727	3.768
DMM2	DMM	L	3	6	0.168	-0.065	-0.466	-5.734	1.386	3.142
DMM2	DMM	L	3	7	0.191	-0.078	-0.537	-7.335	0.788	3.675
DMM2	DMM	L	3	8	0.311	-0.153	-0.714	-8.302	2.848	3.413
DMM2	DMM	L	3	9	0.413	-0.221	-0.863	-9.147	4.446	3.334
DMM3	DMM	L	1	0	0.000	0.000	0.000	0.000	0.000	0.000
DMM3	DMM	L	1	1	0.043	-0.027	-0.005	0.210	0.157	-0.031
DMM3	DMM	L	1	2	0.080	-0.045	-0.012	0.369	0.272	0.156
DMM3	DMM	L	1	3	0.112	-0.029	-0.029	-0.123	0.061	0.637
DMM3	DMM	L	1	4	0.138	-0.008	-0.043	-0.019	-0.012	1.282
DMM3	DMM	L	1	5	0.194	-0.027	-0.078	0.320	0.340	0.869
DMM3	DMM	L	1	6	0.237	-0.046	-0.111	1.220	0.762	0.923
DMM3	DMM	L	1	7	0.270	-0.063	-0.140	1.725	0.639	0.860
DMM3	DMM	L	1	8	0.308	-0.086	-0.169	2.286	0.221	0.444
DMM3	DMM	L	1	9	0.345	-0.104	-0.206	2.577	-0.201	0.042
DMM3	DMM	L	2	0	0.000	0.000	0.000	0.000	0.000	0.000
DMM3	DMM	L	2	1	0.032	-0.014	-0.026	-0.360	-0.190	-0.362

DMM3	DMM	L	2	2	0.065	-0.034	-0.048	-0.665	-0.421	-0.841
DMM3	DMM	L	2	3	0.112	-0.057	-0.081	-0.289	0.093	-1.038
DMM3	DMM	L	2	4	0.125	-0.037	-0.108	-0.653	-0.102	-0.379
DMM3	DMM	L	2	5	0.144	-0.016	-0.145	-0.953	-0.092	0.221
DMM3	DMM	L	2	6	0.174	-0.016	-0.181	-0.610	0.157	0.566
DMM3	DMM	L	2	7	0.228	-0.040	-0.225	-0.241	0.624	0.033
DMM3	DMM	L	2	8	0.303	-0.070	-0.300	-0.184	1.520	-0.923
DMM3	DMM	L	2	9	0.380	-0.105	-0.381	-0.111	2.507	-1.968
DMM3	DMM	L	3	0	0.000	0.000	0.000	0.000	0.000	0.000
DMM3	DMM	L	3	1	-0.010	0.033	-0.010	-0.405	-0.847	0.884
DMM3	DMM	L	3	2	-0.023	0.066	-0.022	-0.738	-1.653	1.850
DMM3	DMM	L	3	3	-0.010	0.064	-0.038	-0.772	-2.178	2.076
DMM3	DMM	L	3	4	0.026	0.031	-0.052	-0.276	-2.252	1.771
DMM3	DMM	L	3	5	0.041	0.031	-0.068	0.269	-2.322	2.291
DMM3	DMM	L	3	6	0.024	0.055	-0.083	0.699	-2.661	3.644
DMM3	DMM	L	3	7	0.053	0.041	-0.119	0.823	-2.549	3.597
DMM3	DMM	L	3	8	0.068	0.058	-0.149	0.608	-2.775	4.022
DMM3	DMM	L	3	9	0.078	0.083	-0.180	0.376	-3.018	4.622
DMM4	DMM	L	1	0	0.000	0.000	0.000	0.000	0.000	0.000
DMM4	DMM	L	1	1	0.058	-0.064	-0.029	0.705	0.624	-0.696
DMM4	DMM	L	1	2	0.104	-0.106	-0.056	1.181	1.088	-1.082
DMM4	DMM	L	1	3	0.124	-0.113	-0.056	1.814	1.036	-0.740
DMM4	DMM	L	1	4	0.138	-0.113	-0.044	2.855	0.900	-0.110
DMM4	DMM	L	1	5	0.176	-0.116	-0.078	2.839	1.143	-0.244
DMM4	DMM	L	1	6	0.196	-0.091	-0.115	2.690	1.324	0.030
DMM4	DMM	L	1	7	0.222	-0.064	-0.175	2.249	1.708	0.153
DMM4	DMM	L	1	8	0.242	-0.059	-0.209	2.475	2.019	0.464
DMM4	DMM	L	1	9	0.262	-0.052	-0.245	2.506	2.293	0.769
DMM4	DMM	L	2	0	0.000	0.000	0.000	0.000	0.000	0.000
DMM4	DMM	L	2	1	0.031	-0.056	-0.007	0.924	0.295	-0.521
DMM4	DMM	L	2	2	0.056	-0.101	-0.014	1.601	0.472	-0.915

DMM4	DMM	L	2	3	0.070	-0.075	-0.062	0.600	0.635	-0.540
DMM4	DMM	L	2	4	0.080	-0.049	-0.095	0.087	0.736	0.128
DMM4	DMM	L	2	5	0.103	-0.042	-0.127	-0.318	0.867	0.373
DMM4	DMM	L	2	6	0.106	-0.035	-0.120	0.234	0.614	0.893
DMM4	DMM	L	2	7	0.125	-0.038	-0.140	0.914	0.803	1.159
DMM4	DMM	L	2	8	0.148	-0.032	-0.171	0.935	1.117	1.327
DMM4	DMM	L	2	9	0.171	-0.022	-0.203	0.909	1.414	1.552
DMM4	DMM	L	3	0	0.000	0.000	0.000	0.000	0.000	0.000
DMM4	DMM	L	3	1	0.032	-0.016	-0.028	0.556	0.710	0.363
DMM4	DMM	L	3	2	0.063	-0.033	-0.058	1.114	1.425	0.674
DMM4	DMM	L	3	3	0.089	-0.043	-0.081	1.601	1.838	1.116
DMM4	DMM	L	3	4	0.112	-0.053	-0.102	1.911	1.991	1.393
DMM4	DMM	L	3	5	0.134	-0.038	-0.131	2.025	2.215	1.751
DMM4	DMM	L	3	6	0.159	-0.029	-0.171	1.668	2.304	1.539
DMM4	DMM	L	3	7	0.185	-0.023	-0.215	1.097	2.518	1.288
DMM4	DMM	L	3	8	0.210	-0.020	-0.270	0.532	3.030	1.301
DMM4	DMM	L	3	9	0.236	-0.020	-0.325	0.155	3.638	1.381

Relative femur to tibia motion as measured by roentgen stereophotogrammetry:

Animal	Group	Limb	Trial	Load	X (mm)	Y (mm)	Z (mm)	x-ro (deg)	y-ro (deg)	z-ro (deg)
ACLT1	ACL	L	1	0	0.000	0.000	0.000	0.000	0.000	0.000
ACLT1	ACL	L	1	1	0.000	-0.101	-0.014	0.485	0.084	0.781
ACLT1	ACL	L	1	2	0.034	-0.203	-0.004	0.728	-0.350	1.579
ACLT1	ACL	L	1	3	-0.001	-0.205	-0.038	0.923	-0.180	1.620
ACLT1	ACL	L	1	4	-0.076	-0.157	-0.146	-0.638	0.726	2.034
ACLT1	ACL	L	1	5	-0.116	-0.027	-0.138	-0.371	0.335	2.105
ACLT1	ACL	L	1	6	-0.112	-0.071	-0.087	-0.574	-0.661	2.057
ACLT1	ACL	L	1	7	-0.092	-0.167	-0.019	-0.545	-1.929	1.513
ACLT1	ACL	L	1	8	-0.112	-0.206	-0.035	-1.430	-2.162	0.693
ACLT1	ACL	L	1	9	-0.145	-0.177	-0.048	-1.878	-2.389	0.091
ACLT1	ACL	L	2	0	0.000	0.000	0.000	0.000	0.000	0.000
ACLT1	ACL	L	2	1	-0.019	-0.089	-0.100	0.048	0.969	0.855
ACLT1	ACL	L	2	2	-0.034	-0.172	-0.196	-0.129	1.836	1.419
ACLT1	ACL	L	2	3	-0.030	-0.292	-0.194	-1.416	1.277	1.166
ACLT1	ACL	L	2	4	-0.010	-0.346	-0.193	-2.122	0.699	1.020
ACLT1	ACL	L	2	5	-0.008	-0.240	-0.125	-1.617	-0.540	0.683
ACLT1	ACL	L	2	6	0.014	-0.077	-0.075	-0.788	-1.760	1.058
ACLT1	ACL	L	2	7	-0.015	-0.053	0.011	-2.014	-3.299	0.568
ACLT1	ACL	L	2	8	-0.149	-0.046	0.077	-3.044	-3.840	0.231
ACLT1	ACL	L	2	9	-0.290	-0.037	0.163	-3.762	-4.497	1.138
ACLT1	ACL	L	3	0	0.000	0.000	0.000	0.000	0.000	0.000
ACLT1	ACL	L	3	1	-0.018	-0.132	-0.061	-0.865	0.313	1.022
ACLT1	ACL	L	3	2	-0.022	-0.277	-0.084	-1.596	0.230	2.048
ACLT1	ACL	L	3	3	-0.070	-0.358	-0.059	-2.258	-0.222	2.599
ACLT1	ACL	L	3	4	-0.052	-0.358	0.069	-2.060	-2.086	2.055
ACLT1	ACL	L	3	5	-0.081	-0.321	0.100	-3.353	-2.751	1.864
ACLT1	ACL	L	3	6	-0.098	-0.222	0.126	-3.257	-3.363	1.846
ACLT1	ACL	L	3	7	-0.138	-0.100	0.157	-2.949	-4.015	2.260
ACLT1	ACL	L	3	8	-0.126	-0.147	0.126	-2.316	-3.888	2.553
ACLT1	ACL	L	3	9	-0.125	-0.248	0.083	-2.210	-3.485	2.902
ACLT2	ACL	L	1	0	0.000	0.000	0.000	0.000	0.000	0.000
ACLT2	ACL	L	1	1	-0.016	-0.041	-0.016	-0.269	-0.444	0.118
ACLT2	ACL	L	1	2	-0.045	-0.071	-0.032	-0.505	-0.780	0.287
ACLT2	ACL	L	1	3	-0.106	-0.054	-0.059	-0.611	-0.399	0.217
ACLT2	ACL	L	1	4	-0.056	-0.050	-0.043	-0.471	-1.385	0.823
ACLT2	ACL	L	1	5	-0.025	-0.020	0.021	0.155	-3.066	0.629

ACLT2	ACL	L	1	6	-0.037	-0.017	0.043	-0.308	-4.231	0.114
ACLT2	ACL	L	1	7	-0.059	-0.015	0.059	-0.826	-5.313	0.753
ACLT2	ACL	L	1	8	-0.043	-0.031	0.044	-0.764	-5.786	0.164
ACLT2	ACL	L	1	9	-0.033	-0.034	0.036	-0.367	-6.328	0.282
ACLT2	ACL	L	2	0	0.000	0.000	0.000	0.000	0.000	0.000
ACLT2	ACL	L	2	1	-0.066	-0.016	-0.083	-1.670	0.906	0.789
ACLT2	ACL	L	2	2	-0.126	-0.019	-0.165	-3.159	1.828	1.597
ACLT2	ACL	L	2	3	-0.172	0.008	-0.135	-3.832	0.890	2.529
ACLT2	ACL	L	2	4	-0.210	-0.051	-0.129	-4.763	0.384	2.907
ACLT2	ACL	L	2	5	-0.217	-0.087	-0.123	-4.451	0.147	1.913
ACLT2	ACL	L	2	6	-0.255	-0.017	-0.112	-3.940	-0.032	1.484
ACLT2	ACL	L	2	7	-0.242	0.007	-0.094	-3.122	-0.653	1.137
ACLT2	ACL	L	2	8	-0.240	-0.012	-0.052	-4.031	-2.067	1.997
ACLT2	ACL	L	2	9	-0.233	-0.045	-0.002	-4.844	-3.552	2.755
ACLT2	ACL	L	3	0	0.000	0.000	0.000	0.000	0.000	0.000
ACLT2	ACL	L	3	1	-0.056	-0.036	-0.024	0.394	0.495	0.499
ACLT2	ACL	L	3	2	-0.115	-0.065	-0.055	0.542	1.046	1.013
ACLT2	ACL	L	3	3	-0.129	-0.082	-0.054	0.680	0.899	0.810
ACLT2	ACL	L	3	4	-0.089	-0.020	-0.021	1.291	-0.088	0.939
ACLT2	ACL	L	3	5	-0.047	-0.022	-0.027	2.004	-0.086	0.643
ACLT2	ACL	L	3	6	-0.020	0.000	-0.001	2.682	-0.653	1.153
ACLT2	ACL	L	3	7	0.020	-0.069	0.025	2.634	-1.422	1.796
ACLT2	ACL	L	3	8	0.009	0.034	0.024	2.626	-1.787	2.742
ACLT2	ACL	L	3	9	-0.001	0.112	0.034	2.316	-2.396	3.351
ACLT3	ACL	L	1	0	0.000	0.000	0.000	0.000	0.000	0.000
ACLT3	ACL	L	1	1	0.013	-0.047	0.030	-1.064	-0.897	0.665
ACLT3	ACL	L	1	2	0.032	-0.109	0.055	-2.316	-1.655	1.226
ACLT3	ACL	L	1	3	0.050	-0.085	0.053	-2.208	-2.093	1.921
ACLT3	ACL	L	1	4	0.052	-0.093	0.040	-2.582	-2.458	2.388
ACLT3	ACL	L	1	5	0.061	-0.112	0.061	-2.657	-3.471	2.363
ACLT3	ACL	L	1	6	0.102	-0.078	0.078	-1.914	-4.601	1.946
ACLT3	ACL	L	1	7	0.105	-0.088	0.075	-2.152	-5.166	2.567
ACLT3	ACL	L	1	8	0.074	-0.116	0.086	-2.751	-5.936	3.577
ACLT3	ACL	L	1	9	0.037	-0.140	0.093	-3.394	-6.610	4.766
ACLT3	ACL	L	2	0	0.000	0.000	0.000	0.000	0.000	0.000
ACLT3	ACL	L	2	1	-0.022	0.003	0.017	-0.064	-0.678	0.433
ACLT3	ACL	L	2	2	-0.042	-0.002	0.043	-0.219	-1.526	0.988
ACLT3	ACL	L	2	3	-0.055	0.019	0.010	-1.542	-1.326	0.307
ACLT3	ACL	L	2	4	-0.031	0.058	-0.014	-2.051	-1.252	1.254

ACLT3	ACL	L	2	5	-0.039	0.069	-0.022	-1.600	-1.237	1.324
ACLT3	ACL	L	2	6	-0.043	0.033	0.042	-1.126	-2.721	0.023
ACLT3	ACL	L	2	7	-0.087	-0.011	0.069	-1.320	-3.334	0.665
ACLT3	ACL	L	2	8	-0.103	-0.038	0.085	-2.201	-3.753	0.569
ACLT3	ACL	L	2	9	-0.117	-0.066	0.101	-3.144	-4.175	0.287
ACLT3	ACL	L	3	0	0.000	0.000	0.000	0.000	0.000	0.000
ACLT3	ACL	L	3	1	-0.022	-0.095	0.077	-0.292	-1.536	1.030
ACLT3	ACL	L	3	2	-0.040	-0.172	0.144	-0.544	-2.872	1.727
ACLT3	ACL	L	3	3	-0.060	-0.129	0.123	-0.532	-2.638	0.769
ACLT3	ACL	L	3	4	-0.087	-0.105	0.087	-0.891	-2.019	0.074
ACLT3	ACL	L	3	5	-0.079	-0.099	0.070	-1.275	-2.035	0.133
ACLT3	ACL	L	3	6	-0.045	-0.100	0.093	-0.789	-2.866	0.684
ACLT3	ACL	L	3	7	-0.041	-0.136	0.137	-0.339	-3.996	1.277
ACLT3	ACL	L	3	8	-0.037	-0.098	0.144	-0.343	-4.585	1.140
ACLT3	ACL	L	3	9	-0.044	-0.052	0.141	-0.402	-4.916	0.678
DMM1	DMM	R	1	0	0.000	0.000	0.000	0.000	0.000	0.000
DMM1	DMM	R	1	1	0.052	-0.065	0.033	0.024	-1.184	1.195
DMM1	DMM	R	1	2	0.107	-0.133	0.070	-0.461	-2.337	1.997
DMM1	DMM	R	1	3	0.131	-0.180	0.066	-0.678	-2.971	2.783
DMM1	DMM	R	1	4	0.145	-0.192	0.058	-0.925	-3.428	2.853
DMM1	DMM	R	1	5	0.137	-0.139	0.067	-0.465	-4.067	3.592
DMM1	DMM	R	1	6	0.053	-0.135	0.066	-0.734	-4.153	3.949
DMM1	DMM	R	1	7	-0.003	-0.231	0.027	-1.588	-3.979	5.050
DMM1	DMM	R	1	8	-0.002	-0.338	-0.022	-1.523	-4.387	5.391
DMM1	DMM	R	1	9	0.014	-0.427	-0.074	-1.285	-4.787	5.631
DMM1	DMM	R	3	0	0.000	0.000	0.000	0.000	0.000	0.000
DMM1	DMM	R	3	1	-0.031	0.051	-0.027	0.530	-0.009	0.059
DMM1	DMM	R	3	2	-0.092	0.122	-0.069	1.312	0.389	0.366
DMM1	DMM	R	3	3	-0.178	0.262	-0.106	2.233	1.062	0.882
DMM1	DMM	R	3	4	-0.218	0.219	-0.127	0.796	1.381	0.471
DMM1	DMM	R	3	5	-0.238	0.115	-0.113	-1.628	1.199	0.657
DMM1	DMM	R	3	6	-0.284	0.044	-0.143	-1.514	1.336	1.224
DMM1	DMM	R	3	7	-0.256	0.059	-0.159	-0.127	0.548	1.789
DMM1	DMM	R	3	8	-0.158	-0.091	-0.102	-1.298	-1.401	1.147
DMM1	DMM	R	3	9	-0.053	-0.250	-0.019	-2.986	-3.560	0.750
DMM2	DMM	R	1	0	0.000	0.000	0.000	0.000	0.000	0.000
DMM2	DMM	R	1	1	0.044	-0.010	-0.002	-1.250	-0.378	0.255
DMM2	DMM	R	1	2	0.078	-0.030	-0.007	-2.342	-0.660	0.248
DMM2	DMM	R	1	3	0.045	0.001	-0.006	-1.574	-0.813	0.490

DMM2	DMM	R	1	4	-0.004	0.111	-0.039	0.128	-0.111	0.643
DMM2	DMM	R	1	5	-0.019	0.189	-0.040	1.052	-0.250	0.752
DMM2	DMM	R	1	6	0.033	0.174	-0.040	0.809	-0.771	0.595
DMM2	DMM	R	1	7	0.028	0.071	-0.007	0.805	-1.894	0.410
DMM2	DMM	R	1	8	0.049	0.005	0.076	1.493	-3.893	1.299
DMM2	DMM	R	1	9	0.065	-0.068	0.166	2.500	-6.062	2.208
DMM2	DMM	R	2	0	0.000	0.000	0.000	0.000	0.000	0.000
DMM2	DMM	R	2	1	-0.001	-0.048	0.044	-0.176	-1.048	0.666
DMM2	DMM	R	2	2	0.016	-0.095	0.087	-0.506	-2.120	1.350
DMM2	DMM	R	2	3	0.045	-0.130	0.089	-0.933	-2.945	1.228
DMM2	DMM	R	2	4	0.062	-0.147	0.108	-1.634	-3.816	1.554
DMM2	DMM	R	2	5	0.027	-0.179	0.147	-2.113	-4.946	2.181
DMM2	DMM	R	2	6	0.064	-0.190	0.198	-2.465	-6.350	2.542
DMM2	DMM	R	2	7	-0.015	-0.149	0.186	-1.337	-6.105	3.157
DMM2	DMM	R	2	8	0.034	-0.091	0.146	-0.013	-6.745	2.126
DMM2	DMM	R	2	9	0.090	-0.070	0.123	0.863	-7.785	1.277
DMM2	DMM	R	3	0	0.000	0.000	0.000	0.000	0.000	0.000
DMM2	DMM	R	3	1	0.054	-0.074	0.011	0.903	-1.419	0.254
DMM2	DMM	R	3	2	0.090	-0.159	0.030	1.867	-2.856	0.019
DMM2	DMM	R	3	3	0.098	-0.195	0.050	1.745	-3.596	1.165
DMM2	DMM	R	3	4	0.022	-0.177	0.006	1.715	-2.741	2.261
DMM2	DMM	R	3	5	-0.054	-0.148	-0.012	1.015	-2.218	2.571
DMM2	DMM	R	3	6	-0.148	-0.163	-0.008	0.988	-2.334	3.214
DMM2	DMM	R	3	7	-0.172	-0.194	-0.025	0.370	-2.736	2.819
DMM2	DMM	R	3	8	-0.153	-0.260	-0.001	-0.304	-4.009	3.172
DMM2	DMM	R	3	9	-0.126	-0.311	0.027	-0.860	-5.378	3.399
DMM3	DMM	R	1	0	0.000	0.000	0.000	0.000	0.000	0.000
DMM3	DMM	R	1	1	0.056	0.026	0.002	-2.306	-0.442	0.557
DMM3	DMM	R	1	2	0.111	0.059	0.016	-4.587	-1.061	1.241
DMM3	DMM	R	1	3	0.116	0.088	-0.004	-4.190	-1.146	1.200
DMM3	DMM	R	1	4	0.073	0.023	-0.040	-3.977	-0.815	0.379
DMM3	DMM	R	1	5	0.081	0.089	0.005	-3.703	-1.575	0.161
DMM3	DMM	R	1	6	0.070	0.093	0.042	-4.828	-2.434	0.351
DMM3	DMM	R	1	7	0.037	0.029	0.032	-4.918	-3.011	0.386
DMM3	DMM	R	1	8	0.014	-0.039	0.103	-5.016	-4.810	0.818
DMM3	DMM	R	1	9	0.005	-0.100	0.179	-4.812	-6.814	2.098
DMM3	DMM	R	2	0	0.000	0.000	0.000	0.000	0.000	0.000
DMM3	DMM	R	2	1	-0.031	0.038	0.013	0.592	-0.147	0.514
DMM3	DMM	R	2	2	-0.081	0.074	0.012	1.742	0.002	0.978

DMM3	DMM	R	2	3	-0.126	0.016	-0.008	2.297	0.184	0.571
DMM3	DMM	R	2	4	-0.196	-0.037	-0.034	1.172	0.758	0.661
DMM3	DMM	R	2	5	-0.224	-0.083	-0.054	-0.725	0.743	0.040
DMM3	DMM	R	2	6	-0.259	-0.061	-0.045	-1.064	0.483	0.051
DMM3	DMM	R	2	7	-0.225	0.026	0.017	0.609	-1.059	0.781
DMM3	DMM	R	2	8	-0.172	-0.024	0.056	0.504	-3.103	1.550
DMM3	DMM	R	2	9	-0.116	-0.083	0.087	0.431	-5.135	2.092
DMM3	DMM	R	3	0	0.000	0.000	0.000	0.000	0.000	0.000
DMM3	DMM	R	3	1	0.079	0.082	-0.060	1.063	0.221	0.545
DMM3	DMM	R	3	2	0.107	0.161	-0.129	2.209	1.103	1.172
DMM3	DMM	R	3	3	0.120	0.256	-0.091	1.827	0.546	1.902
DMM3	DMM	R	3	4	0.058	0.233	-0.046	0.282	0.130	1.694
DMM3	DMM	R	3	5	0.009	0.184	-0.071	-0.024	0.264	2.010
DMM3	DMM	R	3	6	-0.080	0.101	-0.090	-0.292	0.190	2.621
DMM3	DMM	R	3	7	-0.111	-0.009	-0.061	1.712	-1.209	0.885
DMM3	DMM	R	3	8	-0.089	-0.125	-0.017	4.231	-3.509	1.082
DMM3	DMM	R	3	9	-0.064	-0.248	0.029	6.966	-5.844	3.010
DMM4	DMM	R	1	0	0.000	0.000	0.000	0.000	0.000	0.000
DMM4	DMM	R	1	1	0.075	0.034	0.085	-0.490	-1.333	0.716
DMM4	DMM	R	1	2	0.136	0.069	0.161	-1.082	-2.462	1.221
DMM4	DMM	R	1	3	0.087	-0.035	0.119	-0.044	-3.068	2.183
DMM4	DMM	R	1	4	0.074	-0.053	0.121	-0.041	-4.065	1.891
DMM4	DMM	R	1	5	0.079	-0.035	0.098	-0.552	-4.858	1.021
DMM4	DMM	R	1	6	0.084	-0.015	0.110	-2.237	-5.631	0.716
DMM4	DMM	R	1	7	0.003	-0.056	0.033	-2.544	-5.670	0.391
DMM4	DMM	R	1	8	-0.058	-0.087	0.041	-1.595	-7.016	1.362
DMM4	DMM	R	1	9	-0.113	-0.109	0.058	-0.583	-8.470	2.322
DMM4	DMM	R	2	0	0.000	0.000	0.000	0.000	0.000	0.000
DMM4	DMM	R	2	1	-0.043	-0.017	0.050	-0.877	-0.601	0.258
DMM4	DMM	R	2	2	-0.072	-0.021	0.097	-1.852	-1.109	0.401
DMM4	DMM	R	2	3	-0.093	-0.048	0.089	-2.013	-1.388	0.755
DMM4	DMM	R	2	4	-0.087	-0.034	0.109	-2.722	-1.808	0.880
DMM4	DMM	R	2	5	-0.077	-0.070	0.104	-3.465	-2.145	1.174
DMM4	DMM	R	2	6	-0.105	-0.108	0.090	-3.933	-2.282	1.899
DMM4	DMM	R	2	7	-0.158	-0.189	0.035	-3.721	-2.099	2.977
DMM4	DMM	R	2	8	-0.163	-0.155	0.052	-3.299	-2.908	3.171
DMM4	DMM	R	2	9	-0.155	-0.101	0.080	-2.757	-3.918	3.091
DMM4	DMM	R	3	0	0.000	0.000	0.000	0.000	0.000	0.000
DMM4	DMM	R	3	1	0.000	0.058	-0.010	0.059	-0.625	0.653

DMM4	DMM	R	3	2	0.006	0.125	-0.013	0.070	-1.360	1.490
DMM4	DMM	R	3	3	0.014	0.219	0.006	-0.585	-2.289	2.489
DMM4	DMM	R	3	4	-0.008	0.280	-0.001	-1.273	-2.893	3.227
DMM4	DMM	R	3	5	-0.081	0.187	-0.047	-1.304	-3.479	2.356
DMM4	DMM	R	3	6	-0.108	0.107	-0.059	-1.484	-4.349	1.165
DMM4	DMM	R	3	7	-0.113	0.078	-0.050	-2.182	-5.235	0.676
DMM4	DMM	R	3	8	-0.119	0.072	-0.007	-2.095	-6.343	0.003
DMM4	DMM	R	3	9	-0.137	0.045	0.037	-1.947	-7.578	0.764
DMM1	DMM	L	1	0	0.000	0.000	0.000	0.000	0.000	0.000
DMM1	DMM	L	1	1	-0.018	0.097	-0.040	-1.793	-0.139	0.686
DMM1	DMM	L	1	2	-0.027	0.174	-0.060	-2.609	-0.299	1.118
DMM1	DMM	L	1	3	-0.033	0.223	0.006	1.157	-0.532	0.703
DMM1	DMM	L	1	4	-0.026	0.197	0.045	1.566	-1.631	0.429
DMM1	DMM	L	1	5	-0.052	0.234	0.032	-1.372	-3.010	0.705
DMM1	DMM	L	1	6	-0.046	0.243	0.033	-2.498	-4.034	1.259
DMM1	DMM	L	1	7	-0.065	0.356	0.000	-3.782	-4.774	0.765
DMM1	DMM	L	1	8	-0.070	0.315	-0.010	-3.677	-5.516	0.963
DMM1	DMM	L	1	9	-0.068	0.275	-0.006	-3.564	-6.474	1.046
DMM1	DMM	L	2	0	0.000	0.000	0.000	0.000	0.000	0.000
DMM1	DMM	L	2	1	-0.080	-0.071	0.050	2.059	-0.163	0.578
DMM1	DMM	L	2	2	-0.140	-0.149	0.110	4.395	-0.352	1.172
DMM1	DMM	L	2	3	-0.131	-0.302	0.235	8.468	-1.094	2.384
DMM1	DMM	L	2	4	-0.082	-0.225	0.148	3.479	-2.138	2.600
DMM1	DMM	L	2	5	-0.056	-0.141	0.133	-0.397	-3.790	2.432
DMM1	DMM	L	2	6	-0.114	0.031	0.027	-5.318	-4.304	2.419
DMM1	DMM	L	2	7	-0.091	-0.076	0.098	-1.906	-4.781	3.090
DMM1	DMM	L	2	8	-0.021	-0.144	0.196	-0.389	-6.333	2.794
DMM1	DMM	L	2	9	0.049	-0.212	0.317	1.150	-8.188	2.310
DMM1	DMM	L	3	0	0.000	0.000	0.000	0.000	0.000	0.000
DMM1	DMM	L	3	1	-0.046	-0.011	0.071	0.532	-1.087	0.304
DMM1	DMM	L	3	2	-0.078	-0.042	0.145	1.605	-2.011	0.501
DMM1	DMM	L	3	3	-0.075	-0.083	0.143	1.691	-2.462	0.527
DMM1	DMM	L	3	4	-0.082	-0.115	0.102	1.107	-2.532	0.065
DMM1	DMM	L	3	5	-0.093	-0.062	0.004	-2.565	-2.830	0.168
DMM1	DMM	L	3	6	-0.080	-0.078	0.005	-4.396	-3.824	0.609
DMM1	DMM	L	3	7	-0.026	-0.126	0.116	-4.334	-6.068	0.785
DMM1	DMM	L	3	8	-0.044	-0.087	0.152	-3.639	-6.994	0.945
DMM1	DMM	L	3	9	-0.076	-0.008	0.175	-3.300	-7.875	0.829
DMM2	DMM	L	1	0	0.000	0.000	0.000	0.000	0.000	0.000

DMM2	DMM	L	1	1	0.014	0.015	-0.016	-1.851	-1.764	1.546
DMM2	DMM	L	1	2	0.025	0.040	-0.022	-3.553	-3.671	3.068
DMM2	DMM	L	1	3	-0.042	0.054	-0.059	-4.275	-4.361	4.042
DMM2	DMM	L	1	4	-0.069	0.041	-0.047	-2.474	-5.085	4.276
DMM2	DMM	L	1	5	-0.071	0.022	-0.063	-1.791	-6.099	4.165
DMM2	DMM	L	1	6	-0.072	0.028	-0.098	-2.424	-7.632	5.362
DMM2	DMM	L	1	7	-0.056	0.009	-0.107	-3.096	-9.989	5.915
DMM2	DMM	L	1	8	-0.116	0.030	-0.130	-2.940	-11.583	6.166
DMM2	DMM	L	1	9	-0.191	0.112	-0.154	-2.987	-13.415	6.876
DMM2	DMM	L	2	0	0.000	0.000	0.000	0.000	0.000	0.000
DMM2	DMM	L	2	1	-0.057	-0.034	-0.041	-1.892	-2.302	1.042
DMM2	DMM	L	2	2	-0.103	-0.092	-0.077	-3.307	-4.423	1.533
DMM2	DMM	L	2	3	-0.098	0.231	-0.051	0.565	-5.828	1.312
DMM2	DMM	L	2	4	-0.101	0.276	-0.095	1.657	-7.603	2.126
DMM2	DMM	L	2	5	-0.106	0.220	-0.084	2.572	-10.035	3.159
DMM2	DMM	L	2	6	-0.049	0.226	-0.040	3.644	-12.856	3.135
DMM2	DMM	L	2	7	-0.036	0.241	-0.026	4.156	-14.836	3.321
DMM2	DMM	L	2	8	-0.011	0.137	-0.007	4.766	-16.637	3.296
DMM2	DMM	L	2	9	0.003	0.045	0.005	5.203	-18.346	3.535
DMM2	DMM	L	3	0	0.000	0.000	0.000	0.000	0.000	0.000
DMM2	DMM	L	3	1	0.069	-0.099	0.069	1.272	-1.091	0.400
DMM2	DMM	L	3	2	0.125	-0.170	0.134	2.344	-2.235	0.737
DMM2	DMM	L	3	3	0.126	-0.183	0.169	2.086	-4.105	0.060
DMM2	DMM	L	3	4	0.048	-0.059	0.210	3.609	-6.239	0.636
DMM2	DMM	L	3	5	0.032	-0.098	0.207	4.423	-7.576	1.054
DMM2	DMM	L	3	6	-0.005	-0.084	0.155	4.799	-8.285	2.294
DMM2	DMM	L	3	7	0.036	-0.109	0.143	6.157	-9.492	2.398
DMM2	DMM	L	3	8	0.022	-0.026	0.261	7.712	-13.931	3.943
DMM2	DMM	L	3	9	0.025	0.069	0.364	9.554	-17.986	5.340
DMM3	DMM	L	1	0	0.000	0.000	0.000	0.000	0.000	0.000
DMM3	DMM	L	1	1	-0.022	0.020	0.024	0.044	-0.722	0.927
DMM3	DMM	L	1	2	-0.044	0.036	0.048	0.203	-1.365	2.142
DMM3	DMM	L	1	3	-0.065	0.038	0.070	1.141	-1.688	3.477
DMM3	DMM	L	1	4	-0.061	0.069	0.083	1.806	-2.365	4.981

DMM3	DMM	L	1	5	-0.081	0.003	0.131	0.641	-3.331	4.339
DMM3	DMM	L	1	6	-0.107	-0.076	0.182	-1.498	-4.043	3.017
DMM3	DMM	L	1	7	-0.120	-0.041	0.194	-1.807	-4.639	2.927
DMM3	DMM	L	1	8	-0.148	0.039	0.166	-1.503	-5.217	3.111
DMM3	DMM	L	1	9	-0.177	0.102	0.146	-1.133	-5.764	3.013
DMM3	DMM	L	2	0	0.000	0.000	0.000	0.000	0.000	0.000
DMM3	DMM	L	2	1	0.045	0.096	0.036	1.580	-0.760	0.355
DMM3	DMM	L	2	2	0.097	0.186	0.074	3.013	-1.539	0.644
DMM3	DMM	L	2	3	0.069	0.215	0.098	2.490	-2.527	0.142
DMM3	DMM	L	2	4	0.090	0.184	0.121	2.502	-3.022	0.070
DMM3	DMM	L	2	5	0.099	0.163	0.144	2.881	-3.755	0.624
DMM3	DMM	L	2	6	0.051	0.116	0.142	2.322	-4.354	1.321
DMM3	DMM	L	2	7	-0.049	0.115	0.132	1.565	-4.969	0.198
DMM3	DMM	L	2	8	-0.234	-0.035	0.110	-1.276	-5.505	3.378
DMM3	DMM	L	2	9	-0.405	-0.198	0.107	-4.306	-6.476	7.060
DMM3	DMM	L	3	0	0.000	0.000	0.000	0.000	0.000	0.000
DMM3	DMM	L	3	1	0.109	-0.251	0.033	-3.965	-0.482	3.556
DMM3	DMM	L	3	2	0.230	-0.515	0.086	-8.003	-1.104	6.599
DMM3	DMM	L	3	3	0.280	-0.704	0.130	-11.347	-1.670	9.288
DMM3	DMM	L	3	4	0.213	-0.628	0.105	-11.367	-1.738	9.911
DMM3	DMM	L	3	5	0.263	-0.621	0.140	-12.127	-2.699	10.014
DMM3	DMM	L	3	6	0.362	-0.771	0.194	-14.527	-3.417	9.816
DMM3	DMM	L	3	7	0.405	-0.875	0.254	-16.275	-4.768	10.263
DMM3	DMM	L	3	8	0.434	-0.858	0.275	-15.899	-5.465	9.917
DMM3	DMM	L	3	9	0.460	-0.866	0.295	-15.885	-6.038	9.763
DMM4	DMM	L	1	0	0.000	0.000	0.000	0.000	0.000	0.000
DMM4	DMM	L	1	1	-0.053	0.059	0.016	-0.700	-0.750	0.762
DMM4	DMM	L	1	2	-0.085	0.100	0.034	-1.222	-1.435	1.363
DMM4	DMM	L	1	3	-0.049	0.100	0.042	-1.933	-2.049	1.029
DMM4	DMM	L	1	4	-0.040	0.127	0.024	-2.811	-2.303	0.631
DMM4	DMM	L	1	5	-0.101	0.127	0.024	-2.933	-2.539	1.046
DMM4	DMM	L	1	6	-0.108	0.136	0.044	-2.643	-3.005	1.131
DMM4	DMM	L	1	7	-0.094	0.103	0.099	-2.265	-3.966	0.982
DMM4	DMM	L	1	8	-0.089	0.036	0.122	-3.064	-4.683	0.486
DMM4	DMM	L	1	9	-0.100	-0.045	0.139	-3.773	-5.191	0.039

DMM4	DMM	L	2	0	0.000	0.000	0.000	0.000	0.000	0.000
DMM4	DMM	L	2	1	-0.054	0.124	-0.003	-0.091	-0.157	0.221
DMM4	DMM	L	2	2	-0.093	0.231	0.000	-0.038	-0.287	0.442
DMM4	DMM	L	2	3	-0.061	0.149	0.056	0.415	-1.001	0.332
DMM4	DMM	L	2	4	-0.023	0.105	0.093	0.571	-1.722	0.250
DMM4	DMM	L	2	5	-0.023	0.085	0.111	0.533	-2.247	0.609
DMM4	DMM	L	2	6	-0.001	0.092	0.095	0.108	-2.383	0.057
DMM4	DMM	L	2	7	-0.008	0.110	0.099	-0.083	-2.781	0.930
DMM4	DMM	L	2	8	0.002	0.196	0.133	1.478	-3.533	2.276
DMM4	DMM	L	2	9	0.015	0.291	0.171	3.192	-4.307	3.629
DMM4	DMM	L	3	0	0.000	0.000	0.000	0.000	0.000	0.000
DMM4	DMM	L	3	1	-0.095	0.020	-0.024	-0.617	-0.179	0.086
DMM4	DMM	L	3	2	-0.194	0.035	-0.049	-1.309	-0.304	0.096
DMM4	DMM	L	3	3	-0.224	0.074	-0.052	-1.281	-0.799	0.883
DMM4	DMM	L	3	4	-0.187	0.070	-0.022	-1.610	-1.637	1.314
DMM4	DMM	L	3	5	-0.178	0.031	0.000	-2.371	-2.269	0.964
DMM4	DMM	L	3	6	-0.211	-0.026	0.010	-2.972	-2.443	0.198
DMM4	DMM	L	3	7	-0.227	-0.034	0.035	-2.350	-2.928	0.193
DMM4	DMM	L	3	8	-0.234	-0.109	0.079	-2.324	-3.736	0.197
DMM4	DMM	L	3	9	-0.244	-0.180	0.123	-2.525	-4.603	0.611

APPENDIX B: CHAPTER 3 DATA

Epiphyseal bone morphological metrics in the tibia as measured by microCT:

ID	Strain	Limb	Duration	Treatment	BV/TV	Tb. Th (mm)	Tb. Sp	TMD (mgHA/cm3)
A35	B6	Left	1 week	Veh	0.2696	0.0540	0.1900	991.5860
A35	B6	Right	1 week	Veh	0.3299	0.0585	0.1906	982.9260
A36	B6	Left	1 week	Veh	0.3270	0.0558	0.1761	991.0000
A36	B6	Right	1 week	Veh	0.3271	0.0561	0.1677	1007.7330
A37	B6	Left	1 week	Veh	0.3044	0.0567	0.1606	999.1390
A37	B6	Right	1 week	Veh	0.3015	0.0536	0.1715	991.7810
A38	B6	Left	1 week	Veh	0.3050	0.0551	0.1800	1002.4590
A38	B6	Right	1 week	Veh	0.3238	0.0561	0.1737	999.4640
A39	B6	Left	1 week	Veh	0.3015	0.0546	0.2018	973.8110
A39	B6	Right	1 week	Veh	0.3154	0.0580	0.1787	1007.9290
A40	B6	Left	1 week	Veh	0.2774	0.0509	0.1848	982.9910
A40	B6	Right	1 week	Veh	0.3078	0.0528	0.1837	993.3440
B49	B6	Left	1 week	Aln	0.3153	0.0560	0.1834	1002.0040
B49	B6	Right	1 week	Aln	0.3106	0.0542	0.1814	1002.1990
B50	B6	Left	1 week	Aln	0.2013	0.0460	0.2047	988.0050
B50	B6	Right	1 week	Aln	0.1506	0.0417	0.2140	979.2150
B51	B6	Left	1 week	Aln	0.3263	0.0569	0.1777	992.9530
B51	B6	Right	1 week	Aln	0.3157	0.0591	0.1905	996.0780
B52	B6	Left	1 week	Aln	0.2898	0.0559	0.1914	980.1270
B52	B6	Right	1 week	Aln	0.3184	0.0601	0.1825	1022.5136
B53	B6	Left	1 week	Aln	0.2909	0.0539	0.1844	967.4950
B53	B6	Right	1 week	Aln	0.2877	0.0534	0.1885	981.6240
B54	B6	Left	1 week	Aln	0.2517	0.0507	0.1969	994.1250
B54	B6	Right	1 week	Aln	0.2975	0.0560	0.1873	1022.3830
C63	B6	Left	2 week	Veh	0.2710	0.0538	0.1772	979.5410
C63	B6	Right	2 week	Veh	0.3099	0.0575	0.1802	993.3440
C64	B6	Left	2 week	Veh	0.3039	0.0600	0.1758	981.0385
C64	B6	Right	2 week	Veh	0.2651	0.0540	0.1903	1001.8080
C65	B6	Left	2 week	Veh	0.2282	0.0532	0.2061	959.4870
C65	B6	Right	2 week	Veh	0.2961	0.0548	0.1951	1005.8450
C66	B6	Left	2 week	Veh	0.3210	0.0606	0.1818	1002.9807
C66	B6	Right	2 week	Veh	0.2729	0.0513	0.1853	1006.9520
C67	B6	Left	2 week	Veh	0.2265	0.0507	0.1934	949.7850
C67	B6	Right	2 week	Veh	0.2965	0.0556	0.1811	987.6140

D75	B6	Left	2 week	Aln	0.2423	0.0517	0.2086	956.2310
D75	B6	Right	2 week	Aln	0.2793	0.0531	0.1892	989.2420
D76	B6	Left	2 week	Aln	0.3427	0.0578	0.1881	981.3640
D76	B6	Right	2 week	Aln	0.2539	0.0474	0.1843	975.1780
D77	B6	Left	2 week	Aln	0.3336	0.0576	0.1712	990.6090
D77	B6	Right	2 week	Aln	0.2557	0.0478	0.1951	1000.5060
D78	B6	Left	2 week	Aln	0.2410	0.0532	0.1862	970.1650
D78	B6	Right	2 week	Aln	0.2554	0.0496	0.1798	1001.7430
D79	B6	Left	2 week	Aln	0.2099	0.0458	0.2069	958.5750
D79	B6	Right	2 week	Aln	0.2419	0.0509	0.2065	990.2840
D80	B6	Left	2 week	Aln	0.2327	0.0525	0.2101	972.1830
D80	B6	Right	2 week	Aln	0.2386	0.0498	0.2112	1006.2360
D81	B6	Left	2 week	Aln	0.2471	0.0522	0.1911	970.7510
D81	B6	Right	2 week	Aln	0.2914	0.0512	0.1874	998.6180
E06	B6	Left	6 week	Veh	0.2844	0.0571	0.1767	957.2730
E06	B6	Right	6 week	Veh	0.2491	0.0519	0.2179	987.8750
E07	B6	Left	6 week	Veh	0.3188	0.0697	0.1840	986.8330
E07	B6	Right	6 week	Veh	0.2692	0.0524	0.1854	1009.9470
E08	B6	Left	6 week	Veh	0.2611	0.0632	0.2060	977.2620
E08	B6	Right	6 week	Veh	0.2604	0.0519	0.1832	1005.9750
E09	B6	Left	6 week	Veh	0.2425	0.0599	0.1987	965.7370
E09	B6	Right	6 week	Veh	0.2308	0.0489	0.2091	1007.8640
E10	B6	Left	6 week	Veh	0.1941	0.0495	0.1950	937.2840
E10	B6	Right	6 week	Veh	0.2831	0.0533	0.1845	989.7630
E13	B6	Left	6 week	Veh	0.3875	0.0672	0.1348	979.5410
E13	B6	Right	6 week	Veh	0.2595	0.0523	0.1923	1000.7660
F18	B6	Left	6 week	Aln	0.3818	0.0653	0.1521	999.4650
F18	B6	Right	6 week	Aln	0.3064	0.0579	0.1848	1019.8440
F19	B6	Left	6 week	Aln	0.3048	0.0595	0.1753	973.9410
F19	B6	Right	6 week	Aln	0.3437	0.0574	0.1749	1023.4900
F20	B6	Left	6 week	Aln	0.3085	0.0566	0.1637	965.0210
F20	B6	Right	6 week	Aln	0.3292	0.0564	0.1750	992.9530
F21	B6	Left	6 week	Aln	0.3095	0.0600	0.1748	966.2580
F21	B6	Right	6 week	Aln	0.3213	0.0558	0.1891	1018.8670
F26	B6	Left	6 week	Aln	0.2881	0.0545	0.1938	966.3880
F26	B6	Right	6 week	Aln	0.3270	0.0542	0.1840	1011.7050
F27	B6	Left	6 week	Aln	0.3910	0.0721	0.1775	978.0440
F27	B6	Right	6 week	Aln	0.3349	0.0577	0.1738	1022.0570
G32	FVB	Left	1 week	Veh	0.3534	0.0576	0.1618	1029.1540

G32	FVB	Right	1 week	Veh	0.3514	0.0580	0.1626	1030.5870
G33	FVB	Left	1 week	Veh	0.3326	0.0567	0.1693	1040.6140
G33	FVB	Right	1 week	Veh	0.3502	0.0581	0.1639	1031.8240
G34	FVB	Left	1 week	Veh	0.3444	0.0559	0.1643	1035.5350
G34	FVB	Right	1 week	Veh	0.3468	0.0565	0.1549	1034.0380
G35	FVB	Left	1 week	Veh	0.3711	0.0561	0.1482	1035.6650
G35	FVB	Right	1 week	Veh	0.3712	0.0570	0.1527	1053.4400
G36	FVB	Left	1 week	Veh	0.4010	0.0609	0.1727	1038.9865
G36	FVB	Right	1 week	Veh	0.4121	0.0571	0.1339	1041.4600
G37	FVB	Left	1 week	Veh	0.3597	0.0571	0.1560	1022.5780
G37	FVB	Right	1 week	Veh	0.3646	0.0577	0.1522	1029.285
H40	FVB	Left	1 week	Aln	0.3145	0.0527	0.1784	1018.1510
H40	FVB	Right	1 week	Aln	0.3403	0.0584	0.1641	1030.3260
H41	FVB	Left	1 week	Aln	0.3276	0.0582	0.172	1024.922
H41	FVB	Right	1 week	Aln	0.3465	0.0586	0.1628	1052.659
H42	FVB	Left	1 week	Aln	0.3394	0.0588	0.1596	1025.899
H42	FVB	Right	1 week	Aln	0.3708	0.0583	0.1542	1052.724
H49	FVB	Left	1 week	Aln	0.2682	0.0471	0.173	981.494
H49	FVB	Right	1 week	Aln	0.3582	0.0579	0.159	1050.511
H51	FVB	Left	1 week	Aln	0.3666	0.0625	0.1599	1025.5737
H51	FVB	Right	1 week	Aln	0.347	0.0581	0.1634	1031.108
H52	FVB	Left	1 week	Aln	0.3279	0.0566	0.1612	1022.904
H52	FVB	Right	1 week	Aln	0.3437	0.0559	0.1666	1026.42
J53	FVB	Left	2 week	Veh	0.3031	0.0515	0.1674	1025.573
J53	FVB	Right	2 week	Veh	0.3664	0.0567	0.16	1045.562
J54	FVB	Left	2 week	Veh	0.2525	0.051	0.1847	1021.797
J54	FVB	Right	2 week	Veh	0.3463	0.059	0.1716	1056.631
J55	FVB	Left	2 week	Veh	0.2583	0.053	0.1743	997.706
J55	FVB	Right	2 week	Veh	0.3427	0.0582	0.1754	1052.594
J56	FVB	Left	2 week	Veh	0.3364	0.0548	0.1663	1023.946
J56	FVB	Right	2 week	Veh	0.3392	0.0621	0.1758	1064.3143
J57	FVB	Left	2 week	Veh	0.2461	0.0466	0.1737	1006.301
J57	FVB	Right	2 week	Veh	0.3782	0.0623	0.1656	1064.3794
J58	FVB	Left	2 week	Veh	0.3265	0.0553	0.1612	1032.931
J58	FVB	Right	2 week	Veh	0.3638	0.0594	0.1679	1060.212
K66	FVB	Left	2 week	Aln	0.3157	0.0513	0.1675	1031.498
K66	FVB	Right	2 week	Aln	0.3504	0.0561	0.1563	1052.268
K68	FVB	Left	2 week	Aln	0.4063	0.0604	0.1513	1036.3821
K68	FVB	Right	2 week	Aln	0.3473	0.0564	0.1638	1043.023

K75	FVB	Left	2 week	Aln	0.2782	0.0503	0.1675	989.242
K75	FVB	Right	2 week	Aln	0.3683	0.0597	0.1617	1063.598
K76	FVB	Left	2 week	Aln	0.3896	0.0574	0.1502	1046.148
K76	FVB	Right	2 week	Aln	0.3943	0.0593	0.1522	1052.724
K77	FVB	Left	2 week	Aln	0.3267	0.0604	0.1666	1040.484
K77	FVB	Right	2 week	Aln	0.4137	0.0615	0.1666	1059.0404
K78	FVB	Left	2 week	Aln	0.4326	0.0628	0.1422	1052.334
K78	FVB	Right	2 week	Aln	0.3974	0.061	0.1522	1061.9053
L01	FVB	Left	6 week	Veh	0.3261	0.056	0.1774	1022.709
L01	FVB	Right	6 week	Veh	0.3252	0.059	0.1723	1052.789
L02	FVB	Left	6 week	Veh	0.1859	0.0471	0.2009	985.531
L02	FVB	Right	6 week	Veh	0.3209	0.0576	0.1798	1045.692
L03	FVB	Left	6 week	Veh	0.3081	0.0565	0.173	1028.503
L03	FVB	Right	6 week	Veh	0.2921	0.0578	0.1775	1044.651
L04	FVB	Left	6 week	Veh	0.3952	0.0638	0.1276	1028.3735
L04	FVB	Right	6 week	Veh	0.371	0.0614	0.1685	1048.2972
L11	FVB	Left	6 week	Veh	0.2998	0.0557	0.1666	1023.75
L11	FVB	Right	6 week	Veh	0.2688	0.0523	0.1814	1032.931
M15	FVB	Left	6 week	Aln	0.3301	0.0517	0.1565	1004.022
M15	FVB	Right	6 week	Aln	0.3545	0.0602	0.163	1041.1351
M18	FVB	Left	6 week	Aln	0.3124	0.06	0.1516	1032.2802
M18	FVB	Right	6 week	Aln	0.3704	0.0602	0.1639	1043.9348
M19	FVB	Left	6 week	Aln	0.3398	0.0519	0.1578	1029.675
M19	FVB	Right	6 week	Aln	0.3461	0.0577	0.1635	1060.603
M20	FVB	Left	6 week	Aln	0.3473	0.0551	0.154	1037.619
M20	FVB	Right	6 week	Aln	0.3187	0.0567	0.1858	1060.603
M21	FVB	Left	6 week	Aln	0.2924	0.0487	0.1581	1023.36
M21	FVB	Right	6 week	Aln	0.3773	0.0603	0.1629	1045.8882
M24	FVB	Left	6 week	Aln	0.3481	0.0564	0.1587	1014.374
M24	FVB	Right	6 week	Aln	0.3688	0.0578	0.1692	1061.123
M25	FVB	Left	6 week	Aln	0.3249	0.053	0.1652	1031.433
M25	FVB	Right	6 week	Aln	0.3568	0.0603	0.1643	1060.7333

Subchondral Cortical Bone Morphology in the tibia measured by microCT:

ID	Strain	Limb	Duration	Treatment	avg thickness (mm)	avg TMD (mgHA/cm3)
A35	B6	Left	1 week	Veh	0.1495	921.82095
A35	B6	Right	1 week	Veh	0.1330	895.4187
A36	B6	Left	1 week	Veh	0.1305	909.64535
A36	B6	Right	1 week	Veh	0.1260	909.05935
A37	B6	Left	1 week	Veh	0.1350	890.56805
A37	B6	Right	1 week	Veh	0.1280	888.8751
A38	B6	Left	1 week	Veh	0.1235	902.28785
A38	B6	Right	1 week	Veh	0.1270	902.353
A39	B6	Left	1 week	Veh	0.1395	886.10795
A39	B6	Right	1 week	Veh	0.1425	921.91855
A40	B6	Left	1 week	Veh	0.1320	888.5171
A40	B6	Right	1 week	Veh	0.1410	896.26515
B49	B6	Left	1 week	Aln	0.1465	922.0814
B49	B6	Right	1 week	Aln	0.1260	917.6539
B50	B6	Left	1 week	Aln	0.1005	851.95775
B50	B6	Right	1 week	Aln	0.0930	824.44875
B51	B6	Left	1 week	Aln	0.1505	926.86695
B51	B6	Right	1 week	Aln	0.1340	900.0741
B52	B6	Left	1 week	Aln	0.1340	898.3161
B52	B6	Right	1 week	Aln	0.1375	899.32535
B53	B6	Left	1 week	Aln	0.1390	894.99555
B53	B6	Right	1 week	Aln	0.1295	906.87815
B54	B6	Left	1 week	Aln	0.1165	888.41935
B54	B6	Right	1 week	Aln	0.1270	898.28355
C63	B6	Left	2 week	Veh	0.1195	885.7499
C63	B6	Right	2 week	Veh	0.1250	906.09675
C64	B6	Left	2 week	Veh	0.1430	883.37335
C64	B6	Right	2 week	Veh	0.1210	875.3974
C65	B6	Left	2 week	Veh	0.1250	849.5812
C65	B6	Right	2 week	Veh	0.1330	915.668
C66	B6	Left	2 week	Veh	0.1350	883.6338
C66	B6	Right	2 week	Veh	0.1260	897.14415
C67	B6	Left	2 week	Veh	0.1135	808.56185
C67	B6	Right	2 week	Veh	0.1390	900.6601
D75	B6	Left	2 week	Aln	0.1105	826.95545

D75	B6	Right	2 week	Aln	0.1290	887.80085
D76	B6	Left	2 week	Aln	0.1345	909.15695
D76	B6	Right	2 week	Aln	0.1140	876.30895
D77	B6	Left	2 week	Aln	0.1350	877.0577
D77	B6	Right	2 week	Aln	0.1195	890.3076
D78	B6	Left	2 week	Aln	0.1305	859.7384
D78	B6	Right	2 week	Aln	0.1280	896.4605
D79	B6	Left	2 week	Aln	0.1180	832.58745
D79	B6	Right	2 week	Aln	0.1235	872.4349
D80	B6	Left	2 week	Aln	0.1300	880.67125
D80	B6	Right	2 week	Aln	0.1250	907.75705
D81	B6	Left	2 week	Aln	0.1190	846.9117
D81	B6	Right	2 week	Aln	0.1225	891.4796
E06	B6	Left	6 week	Veh	0.0930	818.10045
E06	B6	Right	6 week	Veh	0.1245	886.6614
E07	B6	Left	6 week	Veh	0.1285	835.51745
E07	B6	Right	6 week	Veh	0.1195	886.9544
E08	B6	Left	6 week	Veh	0.1005	821.9094
E08	B6	Right	6 week	Veh	0.1295	894.377
E09	B6	Left	6 week	Veh	0.1290	868.78875
E09	B6	Right	6 week	Veh	0.1155	899.6834
E10	B6	Left	6 week	Veh	0.0830	786.16395
E10	B6	Right	6 week	Veh	0.1260	884.2849
E13	B6	Left	6 week	Veh	0.1250	845.6746
E13	B6	Right	6 week	Veh	0.1285	880.86655
F18	B6	Left	6 week	Aln	0.1250	869.3421
F18	B6	Right	6 week	Aln	0.1265	893.5956
F19	B6	Left	6 week	Aln	0.1010	800.87885
F19	B6	Right	6 week	Aln	0.1250	911.92415
F20	B6	Left	6 week	Aln	0.1140	820.50955
F20	B6	Right	6 week	Aln	0.1250	881.42005
F21	B6	Left	6 week	Aln	0.0945	794.30275
F21	B6	Right	6 week	Aln	0.1335	910.3289
F26	B6	Left	6 week	Aln	0.1095	856.02715
F26	B6	Right	6 week	Aln	0.1285	908.4082
F27	B6	Left	6 week	Aln	0.1150	822.5931
F27	B6	Right	6 week	Aln	0.1330	911.07775
G32	FVB	Left	1 week	Veh	0.1220	918.4677
G32	FVB	Right	1 week	Veh	0.1305	950.20895

G33	FVB	Left	1 week	Veh	0.1295	926.6716
G33	FVB	Right	1 week	Veh	0.1330	962.5798
G34	FVB	Left	1 week	Veh	0.1230	934.6476
G34	FVB	Right	1 week	Veh	0.1290	948.3207
G35	FVB	Left	1 week	Veh	0.1255	911.8916
G35	FVB	Right	1 week	Veh	0.1345	951.83665
G36	FVB	Left	1 week	Veh	0.1295	935.72195
G36	FVB	Right	1 week	Veh	0.1295	945.71635
G37	FVB	Left	1 week	Veh	0.1245	937.12175
G37	FVB	Right	1 week	Veh	0.1200	932.98725
H40	FVB	Left	1 week	Aln	0.1215	907.36645
H40	FVB	Right	1 week	Aln	0.1300	931.68505
H41	FVB	Left	1 week	Aln	0.1330	908.01755
H41	FVB	Right	1 week	Aln	0.1340	959.87775
H42	FVB	Left	1 week	Aln	0.1290	910.329
H42	FVB	Right	1 week	Aln	0.1420	961.7009
H51	FVB	Left	1 week	Aln	0.1405	920.0304
H51	FVB	Right	1 week	Aln	0.1395	942.49335
H52	FVB	Left	1 week	Aln	0.1270	909.84065
H52	FVB	Right	1 week	Aln	0.1345	931.3921
J53	FVB	Left	2 week	Veh	0.1230	902.5483
J53	FVB	Right	2 week	Veh	0.1290	955.5479
J54	FVB	Left	2 week	Veh	0.1290	914.56115
J54	FVB	Right	2 week	Veh	0.1345	951.6739
J55	FVB	Left	2 week	Veh	0.1140	871.3931
J55	FVB	Right	2 week	Veh	0.1400	949.65545
J56	FVB	Left	2 week	Veh	0.1250	908.6035
J56	FVB	Right	2 week	Veh	0.1310	945.8791
J57	FVB	Left	2 week	Veh	0.1200	885.39175
J57	FVB	Right	2 week	Veh	0.1390	968.08165
J58	FVB	Left	2 week	Veh	0.1250	898.38125
J58	FVB	Right	2 week	Veh	0.1410	964.37035
K66	FVB	Left	2 week	Aln	0.1330	916.83995
K66	FVB	Right	2 week	Aln	0.1360	960.7893
K68	FVB	Left	2 week	Aln	0.1340	924.8811
K68	FVB	Right	2 week	Aln	0.1445	951.8041
K75	FVB	Left	2 week	Aln	0.1160	861.6917
K75	FVB	Right	2 week	Aln	0.1355	944.9024
K76	FVB	Left	2 week	Aln	0.1410	927.15995

K76	FVB	Right	2 week	Aln	0.1445	968.79785
K77	FVB	Left	2 week	Aln	0.1365	906.78045
K77	FVB	Right	2 week	Aln	0.1425	982.01515
K78	FVB	Left	2 week	Aln	0.1495	939.43315
K78	FVB	Right	2 week	Aln	0.1530	975.3739
L01	FVB	Left	6 week	Veh	0.1330	910.394
L01	FVB	Right	6 week	Veh	0.1245	921.62555
L02	FVB	Left	6 week	Veh	0.1010	827.24845
L02	FVB	Right	6 week	Veh	0.1290	929.1132
L03	FVB	Left	6 week	Veh	0.1275	895.6467
L03	FVB	Right	6 week	Veh	0.1325	929.69925
L04	FVB	Left	6 week	Veh	0.1280	915.5052
L04	FVB	Right	6 week	Veh	0.1290	945.42335
L11	FVB	Left	6 week	Veh	0.1010	893.00975
L11	FVB	Right	6 week	Veh	0.1205	907.75705
M15	FVB	Left	6 week	Aln	0.1230	891.31675
M15	FVB	Right	6 week	Aln	0.1265	937.6101
M18	FVB	Left	6 week	Aln	0.1200	886.79165
M18	FVB	Right	6 week	Aln	0.1325	951.6414
M19	FVB	Left	6 week	Aln	0.1230	913.68215
M19	FVB	Right	6 week	Aln	0.1265	950.24145
M20	FVB	Left	6 week	Aln	0.1285	914.8216
M20	FVB	Right	6 week	Aln	0.1260	936.959
M21	FVB	Left	6 week	Aln	0.1155	877.0903
M21	FVB	Right	6 week	Aln	0.1305	932.6617
M24	FVB	Left	6 week	Aln	0.1300	892.52135
M24	FVB	Right	6 week	Aln	0.1305	962.77515
M25	FVB	Left	6 week	Aln	0.1170	903.03665
M25	FVB	Right	6 week	Aln	0.1325	935.94975

Cartilage histological scores, local thickness measurements and osteophyte maturity and size measured on Safranin O stained slides.

ID	Strain	Limb	Duration	Treatment	Sum histo. Score	Avg Post. Th. (mm)	Avg Mid. Th. (mm)	Avg Ant. Th (mm)	Osteo. Mat	Osteo. Size
A35	B6	Left	1 week	Veh	10.5	0.118	0.113	0.095	1	0.078
A35	B6	Right	1 week	Veh	2	0.081	0.102	0.124	0	0.000
A36	B6	Left	1 week	Veh	6	0.122	0.111	0.081	1	0.137
A36	B6	Right	1 week	Veh	0	0.084	0.103	0.123	0	0.000
A37	B6	Left	1 week	Veh	7	0.115	0.103	0.090	1	0.204
A37	B6	Right	1 week	Veh						
A38	B6	Left	1 week	Veh	2.5	0.095	0.091	0.075	1	0.112
A38	B6	Right	1 week	Veh	1	0.101	0.116	0.095	0	0.000
A39	B6	Left	1 week	Veh	12.5	0.082	0.109	0.107	1	0.174
A39	B6	Right	1 week	Veh						
A40	B6	Left	1 week	Veh	9	0.110	0.127	0.083	1	0.066
A40	B6	Right	1 week	Veh	0	0.096	0.112	0.101	0	0.000
B49	B6	Left	1 week	Aln	12	0.114	0.118	0.069	1	0.092
B49	B6	Right	1 week	Aln	0.5	0.096	0.119	0.086	0	0.000
B50	B6	Left	1 week	Aln	5	0.103	0.106	0.082	1	0.128
B50	B6	Right	1 week	Aln	1	0.101	0.109	0.109	0	0.000
B51	B6	Left	1 week	Aln	14	0.096	0.110	0.096	1	0.084
B51	B6	Right	1 week	Aln	2	0.079	0.109	0.099	0	0.000
B52	B6	Left	1 week	Aln	10	0.129	0.110	0.098	1	0.061
B52	B6	Right	1 week	Aln	2	0.087	0.118	0.107	0	0.000
B53	B6	Left	1 week	Aln	11	0.116	0.128	0.111	1	0.157
B53	B6	Right	1 week	Aln	0	0.082	0.125	0.108	0	0.000
B54	B6	Left	1 week	Aln	5.5	0.106	0.120	0.090	1	0.103
B54	B6	Right	1 week	Aln	1	0.085	0.100	0.102	0	0.000
C63	B6	Left	2 week	Veh	8.5	0.116	0.126	0.112	2	0.305
C63	B6	Right	2 week	Veh	3	0.081	0.098	0.101	0	0.000
C64	B6	Left	2 week	Veh	9.5	0.112	0.120	0.093	2	0.408
C64	B6	Right	2 week	Veh	2.5	0.086	0.108	0.113	0	0.000
C65	B6	Left	2 week	Veh	15	0.107	0.121	0.104	2	0.399
C65	B6	Right	2 week	Veh	6	0.080	0.114	0.109	0	0.000
C66	B6	Left	2 week	Veh	13.5	0.121	0.107	0.088	2	0.242
C66	B6	Right	2 week	Veh	2.5	0.067	0.116	0.129	0	0.000

C67	B6	Left	2 week	Veh	8	0.120	0.129	0.083	2	0.271
C67	B6	Right	2 week	Veh	1	0.097	0.090	0.117	0	0.000
D75	B6	Left	2 week	Aln	8	0.123	0.098	0.096	2	0.386
D75	B6	Right	2 week	Aln	2	0.105	0.110	0.103	0	0.000
D76	B6	Right	2 week	Aln	2	0.095	0.113	0.094	0	0.000
D76	B6	Left	2 week	Aln	4	0.092	0.119	0.112	1	0.132
D77	B6	Left	2 week	Aln	8.5	0.113	0.105	0.087	1	0.388
D77	B6	Right	2 week	Aln	0.5	0.080	0.096	0.098	0	0.000
D78	B6	Left	2 week	Aln	5.5	0.109	0.122	0.088	1	0.322
D78	B6	Right	2 week	Aln	1.5	0.087	0.117	0.094	0	0.000
D79	B6	Left	2 week	Aln	18	0.114	0.103	0.085	2	0.322
D79	B6	Right	2 week	Aln	0.5	0.077	0.109	0.102	0	0.000
D80	B6	Left	2 week	Aln	7	0.136	0.119	0.090	2	0.434
D80	B6	Right	2 week	Aln	0	0.102	0.107	0.106	0	0.000
D81	B6	Right	2 week	Aln	0	0.107	0.111	0.103	0	0.000
D81	B6	Left	2 week	Aln	6.5	0.090	0.114	0.094	2	0.383
E06	B6	Left	6 week	Veh	13	0.121	0.099	0.094	3	0.886
E06	B6	Right	6 week	Veh	2	0.068	0.109	0.100	0	0.000
E07	B6	Left	6 week	Veh	4	0.096	0.112	0.109	3	0.319
E07	B6	Right	6 week	Veh	1	0.071	0.120	0.108	0	0.000
E08	B6	Right	6 week	Veh	1.5	0.079	0.093	0.106	0	0.000
E08	B6	Left	6 week	Veh	19	0.077	0.091	0.096	2	0.746
E09	B6	Left	6 week	Veh	5.5	0.107	0.125	0.094	3	0.293
E09	B6	Right	6 week	Veh	4	0.072	0.102	0.107	0	0.000
E10	B6	Left	6 week	Veh	17	0.097	0.126	0.104	3	0.979
E10	B6	Right	6 week	Veh	4	0.084	0.110	0.092	0	0.000
E13	B6	Left	6 week	Veh	13	0.105	0.124	0.103	3	0.501
E13	B6	Right	6 week	Veh	2	0.094	0.114	0.117	0	0.000
F18	B6	Left	6 week	Aln					2	1.018
F18	B6	Right	6 week	Aln	1	0.113	0.105	0.086	0	0.000
F19	B6	Left	6 week	Aln	15.5	0.128	0.109	0.092	2	0.459
F19	B6	Right	6 week	Aln	0	0.075	0.092	0.089	0	0.000
F20	B6	Right	6 week	Aln	0	0.132	0.115	0.105	0	0.000
F20	B6	Left	6 week	Aln	13.5	0.082	0.101	0.133	2	0.375
F21	B6	Left	6 week	Aln	16.5	0.125	0.106	0.110	2	0.705
F21	B6	Right	6 week	Aln	1.5	0.083	0.101	0.120	0	0.000
F26	B6	Left	6 week	Aln						
F26	B6	Right	6 week	Aln	0	0.114	0.104	0.095	0	0.000
F27	B6	Left	6 week	Aln	33	0.114	0.104	0.082	2	0.552

F27	B6	Right	6 week	Aln	0	0.064	0.096	0.123	0	0.000
G32	FVB	Left	1 week	Veh	9	0.116	0.156	0.128	0	0.000
G32	FVB	Right	1 week	Veh	0.5	0.103	0.125	0.116	0	0.000
G33	FVB	Left	1 week	Veh	10.5	0.117	0.142	0.135	1	0.135
G33	FVB	Right	1 week	Veh	3	0.090	0.124	0.134	0	0.000
G34	FVB	Left	1 week	Veh	14	0.148	0.163	0.098	1	0.053
G34	FVB	Right	1 week	Veh	5	0.145	0.166	0.132	0	0.000
G35	FVB	Left	1 week	Veh	9	0.108	0.149	0.132	1	0.105
G35	FVB	Right	1 week	Veh	1.5	0.096	0.137	0.141	0	0.000
G36	FVB	Left	1 week	Veh	10.5	0.121	0.136	0.096	1	0.084
G36	FVB	Right	1 week	Veh	1	0.105	0.152	0.126	0	0.000
G37	FVB	Left	1 week	Veh	1	0.147	0.159	0.106	1	0.083
G37	FVB	Right	1 week	Veh	1	0.126	0.119	0.135	0	0.000
H40	FVB	Left	1 week	Aln	2.5	0.159	0.132	0.105	1	0.109
H40	FVB	Right	1 week	Aln	5	0.111	0.144	0.129	0	0.000
H41	FVB	Right	1 week	Aln	4	0.138	0.128	0.082	0	0.000
H41	FVB	Left	1 week	Aln	3	0.099	0.147	0.087	1	0.074
H42	FVB	Right	1 week	Aln	1	0.128	0.158	0.104	0	0.000
H42	FVB	Left	1 week	Aln	4	0.107	0.147	0.138	1	0.114
H49	FVB	Right	1 week	Aln	1	0.145	0.139	0.094	0	0.000
H49	FVB	Left	1 week	Aln	7	0.147	0.139	0.117	1	0.109
H51	FVB	Right	1 week	Aln	0.5	0.121	0.155	0.109	0	0.000
H51	FVB	Left	1 week	Aln	6	0.142	0.150	0.138	1	0.218
H52	FVB	Left	1 week	Aln	5	0.142	0.139	0.131	1	0.074
H52	FVB	Right	1 week	Aln	0	0.149	0.143	0.110	0	0.000
J53	FVB	Right	2 week	Veh	0	0.128	0.127	0.115	0	0.000
J53	FVB	Left	2 week	Veh	12	0.094	0.129	0.139	1	0.107
J54	FVB	Right	2 week	Veh	0.5	0.133	0.145	0.111	0	0.000
J54	FVB	Left	2 week	Veh	4	0.095	0.147	0.126	1	0.158
J55	FVB	Left	2 week	Veh	6	0.101	0.146	0.132	2	0.220
J55	FVB	Right	2 week	Veh	1	0.100	0.136	0.139	0	0.000
J56	FVB	Left	2 week	Veh	11	0.161	0.131	0.090	1	0.203
J56	FVB	Right	2 week	Veh	1	0.100	0.161	0.146	0	0.000
J57	FVB	Left	2 week	Veh	10	0.158	0.148	0.101	2	0.194
J57	FVB	Right	2 week	Veh	2	0.091	0.151	0.158	0	0.000
J58	FVB	Left	2 week	Veh	15	0.134	0.141	0.103	2	0.163
J58	FVB	Right	2 week	Veh	2	0.111	0.149	0.119	0	0.000
K66	FVB	Right	2 week	Aln	0	0.151	0.166	0.115	0	0.000
K66	FVB	Left	2 week	Aln	10	0.106	0.150	0.152	1	0.183

K68	FVB	Left	2 week	Aln	4.5	0.100	0.146	0.114	1	0.188
K68	FVB	Right	2 week	Aln	2	0.079	0.103	0.139	0	0.000
K75	FVB	Left	2 week	Aln	11	0.085	0.149	0.136	1	0.224
K75	FVB	Right	2 week	Aln						
K76	FVB	Left	2 week	Aln	0.5	0.098	0.145	0.130	2	0.281
K76	FVB	Right	2 week	Aln						
K77	FVB	Left	2 week	Aln	4.5	0.136	0.135	0.106	1	0.135
K77	FVB	Right	2 week	Aln	4	0.097	0.149	0.123	0	0.000
K78	FVB	Left	2 week	Aln	0.5	0.112	0.159	0.154	1	0.201
K78	FVB	Right	2 week	Aln	3.5	0.084	0.151	0.156	0	0.000
L01	FVB	Left	6 week	Veh	11	0.102	0.143	0.137	2	0.390
L01	FVB	Right	6 week	Veh	2	0.094	0.136	0.141	0	0.000
L02	FVB	Left	6 week	Veh	15	0.096	0.125	0.146	2	0.343
L02	FVB	Right	6 week	Veh						
L03	FVB	Left	6 week	Veh	0.5	0.143	0.150	0.114	2	0.255
L03	FVB	Right	6 week	Veh	2	0.098	0.123	0.146	0	0.000
L04	FVB	Right	6 week	Veh	0	0.119	0.145	0.124	0	0.000
L04	FVB	Left	6 week	Veh	2.5	0.093	0.129	0.101	1	0.349
L11	FVB	Left	6 week	Veh	12	0.106	0.148	0.143	2	0.471
L11	FVB	Right	6 week	Veh	1	0.093	0.135	0.134	0	0.000
M15	FVB	Left	6 week	Aln	12	0.117	0.160	0.122	1	0.161
M15	FVB	Right	6 week	Aln	2	0.101	0.140	0.127	0	0.000
M18	FVB	Left	6 week	Aln	8.5	0.123	0.152	0.124	1	0.381
M18	FVB	Right	6 week	Aln	3.5	0.109	0.144	0.136	0	0.000
M19	FVB	Left	6 week	Aln	4.5	0.122	0.157	0.111	2	0.413
M19	FVB	Right	6 week	Aln	1.5	0.100	0.142	0.118	0	0.000
M20	FVB	Left	6 week	Aln						
M20	FVB	Right	6 week	Aln	2	0.106	0.140	0.145	0	0.000
M21	FVB	Left	6 week	Aln	6	0.120	0.157	0.143	2	0.388
M21	FVB	Right	6 week	Aln	2.5	0.125	0.136	0.122	0	0.000
M24	FVB	Left	6 week	Aln	11	0.129	0.144	0.136	2	0.453
M24	FVB	Right	6 week	Aln	6.5	0.100	0.153	0.144	0	0.000
M25	FVB	Left	6 week	Aln	8	0.132	0.132	0.112	1	0.430
M25	FVB	Right	6 week	Aln	0	0.103	0.146	0.133	0	0.000

APPENDIX C: CHAPTER 4 DATA

Average compressive stress (MPa) for all trials calculated using discrete element analysis:

Load (N)	kinematics_beadsA01_1.xlsx	kinematics_beadsA01_2.xlsx	kinematics_beadsA01_3.xlsx	kinematics_beadsA02_1.xlsx	kinematics_beadsA02_2.xlsx	kinematics_beadsA02_3.xlsx
0	1.00E+00	1.00E+00	1.00E+00	1.00E+00	1.00E+00	1.00E+00
1	9.49E-01	1.00E+00	8.88E-01	1.23E+00	1.13E+00	1.15E+00
2	8.80E-01	9.97E-01	7.76E-01	1.44E+00	1.26E+00	1.31E+00
3	8.22E-01	9.73E-01	6.70E-01	1.70E+00	1.37E+00	1.44E+00
4	7.55E-01	9.64E-01	5.58E-01	1.94E+00	1.49E+00	1.59E+00
5	6.81E-01	9.30E-01	4.42E-01	2.17E+00	1.60E+00	1.72E+00
6	6.18E-01	9.07E-01	3.55E-01	2.41E+00	1.71E+00	1.87E+00
7	5.58E-01	8.78E-01	2.66E-01	2.69E+00	1.80E+00	2.02E+00
8	5.00E-01	8.44E-01	1.94E-01	2.97E+00	1.89E+00	2.19E+00
9	4.41E-01	8.18E-01	1.40E-01	3.25E+00	1.97E+00	2.33E+00
Load (N)	kinematics_beadsA03_1.xlsx	kinematics_beadsA03_2.xlsx	kinematics_beadsA03_3.xlsx	kinematics_beadsA04_1.xlsx	kinematics_beadsA04_2.xlsx	kinematics_beadsA04_3.xlsx
0	1.00E+00	1.00E+00	1.00E+00	1.00E+00	1.00E+00	1.00E+00
1	1.12E+00	9.37E-01	1.22E+00	1.12E+00	8.24E-01	1.13E+00
2	1.19E+00	8.50E-01	1.44E+00	1.23E+00	6.25E-01	1.28E+00
3	1.27E+00	7.57E-01	1.65E+00	1.33E+00	4.41E-01	1.43E+00
4	1.34E+00	6.70E-01	1.89E+00	1.42E+00	2.68E-01	1.56E+00
5	1.38E+00	6.02E-01	2.13E+00	1.50E+00	1.48E-01	1.71E+00
6	1.42E+00	5.16E-01	2.36E+00	1.58E+00	6.91E-02	1.86E+00
7	1.45E+00	4.44E-01	2.60E+00	1.66E+00	1.89E-02	2.01E+00
8	1.45E+00	3.81E-01	2.80E+00	1.73E+00	No contact	2.16E+00
9	1.48E+00	3.13E-01	3.04E+00	1.77E+00	No contact	2.30E+00
Load (N)	kinematics_beadsA05_1.xlsx	kinematics_beadsA05_2.xlsx	kinematics_beadsA05_3.xlsx	kinematics_beadsACLT1_1.xlsx	kinematics_beadsACLT1_2.xlsx	kinematics_beadsACLT1_3.xlsx
0	1.00E+00	1.00E+00	1.00E+00	1.00E+00	1.00E+00	1.00E+00
1	1.35E+00	8.94E-01	1.28E+00	1.25E+00	8.98E-01	9.96E-01
2	1.73E+00	7.84E-01	1.58E+00	1.51E+00	7.55E-01	9.57E-01
3	2.15E+00	6.67E-01	1.87E+00	1.78E+00	6.47E-01	9.22E-01
4	2.59E+00	5.74E-01	2.21E+00	2.04E+00	5.31E-01	8.74E-01

5	3.07E+00	4.82E-01	2.59E+00	2.32E+00	4.44E-01	8.23E-01
6	3.66E+00	4.04E-01	2.97E+00	2.64E+00	3.58E-01	7.62E-01
7	4.25E+00	3.18E-01	3.36E+00	2.96E+00	3.02E-01	6.60E-01
8	4.81E+00	2.59E-01	3.72E+00	3.29E+00	2.47E-01	5.83E-01
9	5.34E+00	2.10E-01	4.08E+00	3.59E+00	2.08E-01	5.03E-01
Load (N)	kinematics_beadsACLT2_1.xlsx	kinematics_beadsACLT2_2.xlsx	kinematics_beadsACLT2_3.xlsx	kinematics_beadsACLT3_1.xlsx	kinematics_beadsACLT3_2.xlsx	kinematics_beadsACLT3_3.xlsx
0	1.00E+00	1.00E+00	1.00E+00	1.00E+00	1.00E+00	1.00E+00
1	1.21E+00	1.24E+00	9.17E-01	6.83E-01	8.35E-01	9.01E-01
2	1.43E+00	1.48E+00	8.30E-01	4.11E-01	6.72E-01	8.05E-01
3	1.64E+00	1.70E+00	7.42E-01	1.80E-01	5.29E-01	6.88E-01
4	1.87E+00	1.95E+00	6.57E-01	6.67E-02	4.01E-01	5.93E-01
5	2.12E+00	2.19E+00	5.80E-01	2.71E-02	2.87E-01	5.08E-01
6	2.39E+00	2.48E+00	5.08E-01	7.16E-03	1.91E-01	4.21E-01
7	2.66E+00	2.72E+00	4.52E-01	9.61E-04	1.22E-01	3.46E-01
8	2.91E+00	2.95E+00	4.02E-01	No contact	7.14E-02	2.75E-01
9	3.15E+00	3.17E+00	3.64E-01	No contact	3.60E-02	2.14E-01
Load (N)	kinematics_beadsDMM1_1.xlsx	kinematics_beadsDMM1_2.xlsx	kinematics_beadsDMM1_3.xlsx	kinematics_beadsDMM2_1.xlsx	kinematics_beadsDMM2_2.xlsx	kinematics_beadsDMM2_3.xlsx
0	1.00E+00	1.00E+00	1.00E+00	1.00E+00	1.00E+00	1.00E+00
1	1.34E+00	9.59E-01	1.04E+00	1.69E+00	1.33E+00	8.77E-01
2	1.66E+00	9.09E-01	1.07E+00	2.51E+00	1.61E+00	6.97E-01
3	1.99E+00	8.59E-01	1.10E+00	3.44E+00	1.87E+00	5.13E-01
4	2.32E+00	8.15E-01	1.15E+00	4.48E+00	2.10E+00	3.52E-01
5	2.59E+00	7.63E-01	1.19E+00	5.22E+00	2.31E+00	2.05E-01
6	2.78E+00	7.12E-01	1.23E+00	5.64E+00	2.46E+00	8.73E-02
7	2.90E+00	6.59E-01	1.27E+00	6.22E+00	2.61E+00	2.02E-02
8	2.93E+00	6.05E-01	1.29E+00	6.59E+00	2.67E+00	1.32E-03
9	2.78E+00	5.48E-01	1.32E+00	6.51E+00	2.70E+00	No contact
Load (N)	kinematics_beadsDMM3_1.xlsx	kinematics_beadsDMM3_2.xlsx	kinematics_beadsDMM3_3.xlsx	kinematics_beadsDMM4_1.xlsx	kinematics_beadsDMM4_2.xlsx	kinematics_beadsDMM4_3.xlsx
0	1.00E+00	1.00E+00	1.00E+00	1.00E+00	1.00E+00	1.00E+00
1	1.00E+00	9.01E-01	5.99E-01	1.05E+00	8.58E-01	1.24E+00

2	9.84E-01	7.78E-01	2.83E-01	1.09E+00	7.23E-01	1.47E+00
3	9.45E-01	6.88E-01	8.99E-02	1.12E+00	5.89E-01	1.67E+00
4	8.87E-01	6.12E-01	1.54E-02	1.16E+00	4.81E-01	1.90E+00
5	8.29E-01	5.48E-01	No contact	1.19E+00	3.89E-01	2.15E+00
6	7.67E-01	5.01E-01	No contact	1.23E+00	3.17E-01	2.37E+00
7	6.94E-01	4.81E-01	No contact	1.25E+00	2.77E-01	2.61E+00
8	6.14E-01	4.65E-01	No contact	1.29E+00	2.44E-01	2.83E+00
9	5.32E-01	4.43E-01	No contact	1.32E+00	2.15E-01	3.00E+00